Metal Complexes with Non-innocent *N*-donor Ligands: Molecular and Electronic Structures, Reactivity, and Application

Dissertation

zur

Erlangung des Doktorgrades

der Naturwissenschaften

(Dr. rer. nat.)

dem

Fachbereich Chemie

der Philipps-Universität Marburg

vorgelegt von

Marat M. Khusniyarov

aus

Petropawlowsk-Kamtschatskiy

Russland

Marburg an der Lahn

2006

Vom Fachbereich Chemie

der Philipps-Universität Marburg als Dissertation am *09.06.2006* angenommen.

Erstgutachter: Prof. Dr. J. Sundermeyer

Zweitgutachter: Prof. Dr. M. Bröring

Tag der mündlichen Prüfung am *30.06.2006*

to my wife Maria

Chemistry is just Physics
of valence electrons

Articles published:

- **M. M. Khusniyarov**, K. Harms, J. Sundermeyer;

  New Highly Fluorinated Phenazine Derivatives: Correlation between Crystal Structure and NMR Spectroscopy.

  J. Fluorine Chem. **2006**, *127*, 200–204.

- **M. M. Khusniyarov**, K. Harms, O. Burghaus, J. Sundermeyer;

  Molecular and Electronic Structures of Homoleptic Nickel and Cobalt Complexes with Non-innocent Bulky Diimine Ligands Derived from Fluorinated 1,4-Diaza-1,3-butadien (DAD) and Bis(arylimino)acenaphthene (BIAN).

  Eur. J. Inorg. Chem. **2006**, article online.

- **M. M. Khusniyarov**, K. Harms, J. Sundermeyer, B. Sarkar, W. Kaim, J. van Slageren, C. Duboc, J. Fiedler;

  A Series of Metal Complexes with the Non-Innocent *N*,*N*'-Bis(pentafluorophenyl)-*o*-phenylenediamine: Twisted Geometry as a Tuner for Electronic Structure.

  Manuscript in preparation.

Report:

- **M. M. Khusniyarov**;

  Late Transition Metal Complexes with Non-innocent Nitrogen Ligands.

  "Aktuelle Themen aus der Anorganischen Chemie", Fachbereich Chemie der Philipps-Universität, Marburg, 9th February, **2006**.

Acknowledgements

I would like to acknowledge everyone who extended their support and help during the course of this work. My deep sense of gratitude goes to:

- Prof. Dr. Jörg Sundermeyer for a great opportunity to perform my PhD work in his research group and for this interesting research topic.
- Dr. Klaus Harms for all X-ray structures he determined.
- Gertraud Geiseler for her patience by searching for good crystals among dark powder in dark solutions.
- Dr. Xiulan Xie for her interesting NMR lectures and for her help by my first steps on working with NMR spectrometers.
- The whole NMR department for measurements of NMR spectra on high frequency spectrometers and for assistance by my independent measurements.
- Dr. Olaf Burghaus for recording of EPR spectra, their simulation, and interesting discussions about spins, ZFS, etc.
- P. Clemens for SQUID measurements and great interest in magnetic properties of my complexes.
- Dr. Steinbach for his understanding of my problems regarding mass spectrometry and help on working with MALDI spectrometer.
- The whole mass department for recording of numerous mass spectra for me.
- Prof. Dr. Martin Bröring for opportunity to perform UV-vis measurements at his research group and for his consent to be the second referee for this work.
- Prof. Dr. Wolfgang Kaim and Dr. Biprajit Sarkar (Stuttgart University) for their interest in part of the present work and fruitful collaboration (physicochemical investigation of complexes in Chapter I).
- Alex Petrov for his introduction of synthetic chemistry to me and interesting discussions about chemistry and more, as well as for a nice time in and outside the laboratory.
- Dr. Alexey Merkoulov for his fruitful discussions concerning physical chemistry and spectroscopy.
- Irene Barth for her assistance in searching for every possible glasses, equipments, etc. in our big laboratory.

- Daniel Gaess, Jan Döring, and Hans-Peter Keller for their helpful suggestions concerning the gramatical correctness of my dissertation.
- All present and past PhD students/postdocs I worked with: Alex, Alexey and Katya, Andreas, Daniel, Denis, Jan, Matthias, Nuri, Ralf, Thomas, Udo, Wael for their help if I needed and a nice time in the lab and sometimes out of there.
- All my old and new friends I found in Germany, because of them I was not alone there.
- My wife Maria, without her this dissertation would not have been possible.

Table of Contents

CHAPTER III

Molecular and electronic structures of homoleptic nickel and cobalt complexes with non-innocent bulky diimine ligands derived from fluorinated 1,4-diaza-1,3-butadien (DAD) and bis(arylimino)acenaphthene (BIAN).

CHAPTER IV

Ethylene polymerization with new bis(arylimino)acenaphthene (BIAN) complexes of iron and copper activated with MAO.

CHAPTER V

Synthesis and characterization of phthalocyanines of alkaline earth metals.

List of Abbreviations

Ac	acetyl
acac	acetylacetonate
Ar	aromatic substituent
av.	average
B	base
bpy	2,2'-bipyridine
Bu	butyl
Cp	cyclopentadienyl
CT	charge ransfer
CV	cyclic voltammetry
Cy	cyclohexyl
DFT	density function theory
Dip	2,6-diisopropyl
DME	dimethoxyethane
DMF	*N,N*-dimethylformamide
DMSO	dimethyl sulfoxide
EI	electron ionization
EPR	electron paramagnetic resonance
ESI	electrospray ionization
Et	ethyl
^{F}Ar	fluorinated (partly or completely) aromatic substituents
^{F}Ph	pentafluorophenyl
HOMO	highest occupied molecular orbital
HS	high-spin
IL	intra-ligand
IR	infrared
LLCT	ligand-to-ligand charge transfer
LLIVCT	ligand-to-ligand intervalence charge transfer
LMCT	ligand-to-metal charge transfer
LS	low-spin
LUMO	lowest unoccupied molecular orbital
M.p.	melting point
m/z	mass-to-charge ratio

MALDI	matrix-assisted laser desorption/ionization
MAO	methylaluminoxane
Me	methyl
MLCT	metal-to-ligand charge transfer
M_n	number-average molecular weight
MO	molecular orbital
MS	mass spectrometry
M_w	weight-average molecular weight
NIR	near ultraviolet
NMR	nuclear magnetic resonance
OTf	trifluoromethanesulfonate
OTTLE	optically transparent thin-layer electrode/electrochemical
PE	polyethylene
Ph	phenyl
Pr	propyl
py	pyridine
SQUID	superconducting quantum interface device
THF	tetrahydrofuran
TIP	temperature-independent paramagnetism
TLC	thin layer chromatography
TMS	tetramethylsilane
TOF	time of flight
Ts	tosyl
UV-vis	ultraviolet-visible spectrophotometry
ZFS	zero-field splitting

Ligands used in this work:

H_2BPPD	*N*,*N*′-bis(pentafluorophenyl)-*o*-phenylenediamine
^{F}DAD	*N*,*N*′-bis(pentafluorophenyl)-2,3-dimethyl-1,4-diaza-1,3-butadiene
^{F}BIAN	bis[*N*-{3,5-bis(trifluoromethyl)phenyl}imino]acenaphthene
Dip-BIAN	bis[*N*-{2,6-bis(isopropyl)phenyl}imino]acenaphthene
H_2Pc	metal-free phthalocyanine
18-CR-6	18-crown-6 (1,4,7,10,13,16-hexaoxacyclooctadecan)
DB18-CR-6	dibenzo-18-crown-6 (2,3,11,12-dibenzo-1,4,7,10,13,16-hexaoxacyclooctadeca-2,11-diene)

List of compounds synthesized with their numbers:

[$Ni^{II}(BPPD)_2$]	**(1)**
[$Pd^{II}(BPPD)_2$]	**(2)**
[$Co(BPPD)_2$]	**(3)**
[$Cu^{II}(BPPD)_2$]	**(4)**
[$Fe^{III}(BPPD)_2$]	**(5)**
1,2,2,3,4-pentafluoro-10-(2,3,4,5,6-pentafluorophenyl)-2,10-dihydrophenazine	**(6)**
1,3,4-trifluoro-10-(2,3,4,5,6-pentafluorophenyl)-2(10H)-phenazinone	**(7)**
[$Ni^{II}(^{F}DAD)_2$]	**(8)**
[$Co^{II}(^{F}DAD)_2$]	**(9)**
[$Ni^{II}(^{F}BIAN)_2$]	**(10)**
[$Co^{I}(^{F}BIAN)_3$]	**(11)**
[$Cu^{II}(^{F}BIAN)Cl_2$]	**(12)**
[Cu^{II}(Dip-BIAN)Cl_2]	**(13)**
[Fe^{II}(Dip-BIAN)Cl_2]	**(14)**
[Fe^{III}(Dip-BIAN)Cl_3]	**(15)**
[PcCa]	**(16)**
[PcSr]	**(17)**
[PcBa]	**(18)**
[PcBa(18-CR-6)]	**(19)**
[PcBa(DB18-CR-6)]	**(20)**

☙ Zusammenfassung ❧

Die vorliegende Arbeit umfasst Komplexe der späten Übergangsmetalle der Gruppen VIII–XI und der Erdalkalimetalle, die *non-innocent* *N*-Donor-Liganden enthalten. Die Typen von redox-aktiven Liganden, die in dieser Arbeit verwendet werden, umfassen *o*-Phenylendiamin Derivate (Kapitel I und II), 1,4-Diaza-1,3-butadien Derivate (DAD, Kapitel III), Derivate von Bis(*N*-arylimino)acenaphthen (BIAN, Kapitel III und IV) und unsubstituiertes Phthalocyanin. Während Kapitel I–III auf grundlegende Studien an Komplexen der späten Übergangsmetalle mit *non-innocent* Liganden eingehen, umfassen Kapitel IV und V potentielle Anwendungen solcher Komplexe. Die in dieser Arbeit erhaltenen Ergebnisse werden der Reihenfolge der Kapitel entsprechend wie folgt zusammengefasst.

Kapitel I.

Eine Reihe homoleptischer Komplexe [M(BPPD)$_2$] (M =Ni (**1**), Pd (**2**), Co (**3**), Cu (**4**), Fe (**5**)) mit einem neuen *non-innocent* Liganden *N*,*N*'-Bis(pentafluorphenyl)-*o*-phenylendiamin (H_2BPPD) wurde synthetisiert. Die *physikalischen* (*spektroskopishen*) Oxidationszustände des Liganden und der Metallatome in den Komplexen **1**, **2**, **4** und **5** wurden durch Röntgenstrukturanalyse bei niedrigen Temperaturen anhand einer Bindungslängenanalyse bestimmt. Die Komplexe **1**, **2** und **4** bestehen aus zweiwertigen Metallionen und je zwei π-radikalischen Anionen $(BPPD)^{1-}$.

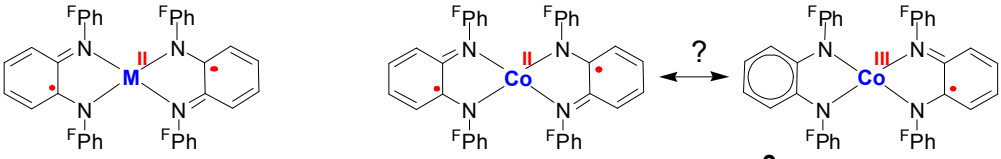

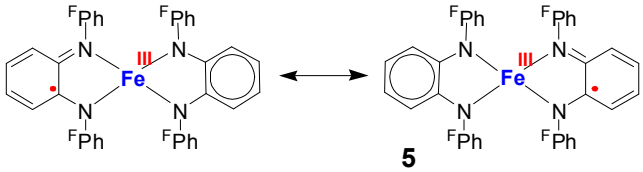

Der einzigartige vierfachkoordinierte Eisenkomplex **5** enthält ein Eisen(III) Zentrum, ein π-radikalisches Anion $(BPPD)^{1-}$ und ein geschlossenschaliges Dianion $(BPPD)^{2-}$. Der Komplex **5** benimmt sich wie ein Klasse III Gemischtvalenz-System mit Elektronendelokalisierung über beide Liganden. Das Oxidationszustandmuster des Kobaltkomplexes **3** ist noch nicht eindeutig bestimmt, da das Ligandbindungsmuster von **3** einen Zustand zwischen **1** (**2**, **4**) und **5** einnimmt.

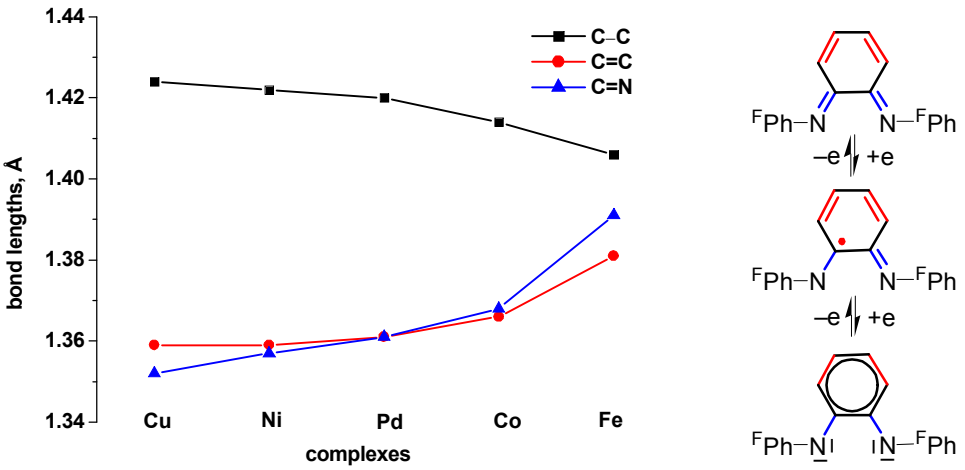

Abbildung 1. Die charakteristischen durchschnittlichen Bindungsabstände in den Komplexen [M(BPPD)$_2$].

Die sterisch anspruchsvollen *N*-C_6F_5 Substituenten zwingen die Komplexe **1** und **3** – **5**, eine stark verzerrt-tetraedrische (*twisted*) Geometrie anzunehmen. Dies stellt einen auffallenden Kontrast zu den ausschließlich planaren Komplexen der bereits bekannten o-Phenylendiamin Derivate dar. Infolge des verglichen mit 3d-Metallen großen Ionenradius des Palladiums, nimmt der Komplex **2** eine quadratisch planare, deutlich weniger verdrillte Konfiguration an.

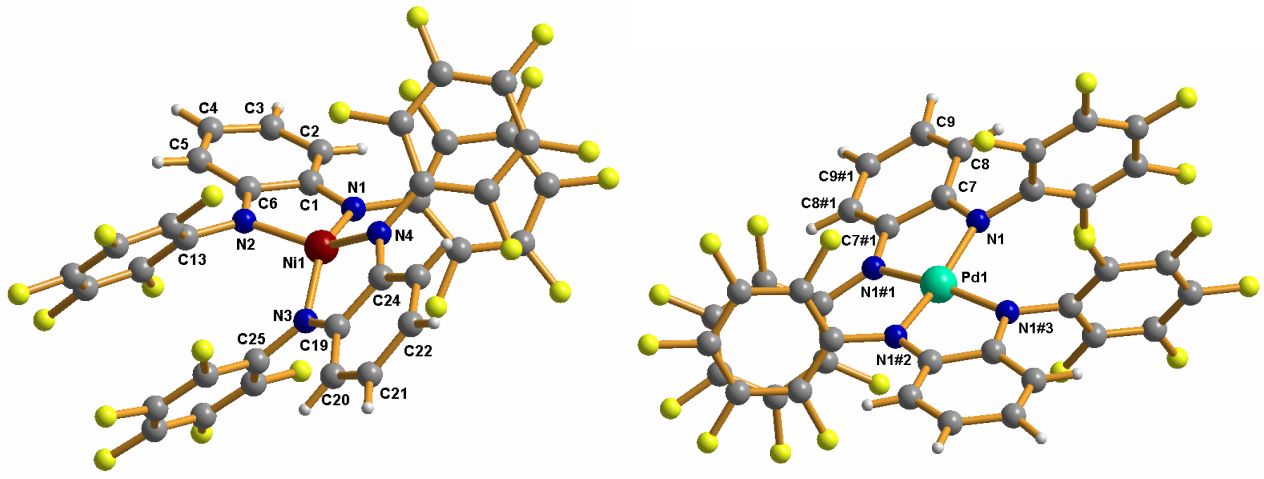

Abbildung 2. Kristallstrukturen des stark verdrillten Komplexes **1** (53.7(1)º zwischen den NCCN-Ebenen) und des weniger verzerrten Komplexes **2** (22.4(2)º).

Die elektronischen Strukturen der Komplexe **1** – **4** und einige ihrer benachbarten kationischen und anionischen Redoxzustände wurden durch EPR- und UV-Vis-NIR Spektroelektrochemie (in Kooperation mit Prof. Kaim, Stuttgart) untersucht. Die verdrillte Konfiguration der Komplexe verursacht beträchtliche Änderungen in ihren elektronischen Strukturen verglichen mit den bekannten ausschließlich planaren Komplexen, während die stark elektonziehenden *N*-C_6F_5 Gruppen die Redoxeigenschaften der Komplexe stark beeinflussen. Die verdrehte Ligandenanordnung kann mit Ni^{II}, Fe^{III} und Co^{II}(?) zu *high-spin* Zuständen in den entsprechenden Komplexen führen. Die Superaustausch-Wechselwirkungen zwischen den

entfernten radikalischen Liganden sind nicht so ausgeprägt wie in den planaren Komplexen. Dies führt zu einem ligand-zentrierten Spingrundzustand im angenähert tetraedrischen Cu^{II} Komplex und nicht zu einem metall-zentrierten Spingrundzustand wie in den planaren Analoga.

Kapitel II.

Die Reaktivität der Komplexe [M(BPPD)$_2$] (M = Fe, Co, Ni, Pd, Cu; H_2BPPD = *N*,*N*′-bis(pentafluorphenyl)-*o*-phenylendiamin) **1** – **5** wurde ausführlich untersucht. Die homoleptischen Komplexe **1** – **5** zeigen nicht die Fähigkeit zur Koordination eines beliebigen zusätzlichen Liganden in der Addition, oxidativen Addition oder oxidativen Alkylierung/Arylierung. Diese Inertheit wird sterischen Faktoren zugeschrieben, weil steisch anspruchsvolle perfluorirte Phenylringe das Metallzentrum effektiv abschirmen und eine Zunahme der Koordinationszahl verhindern.

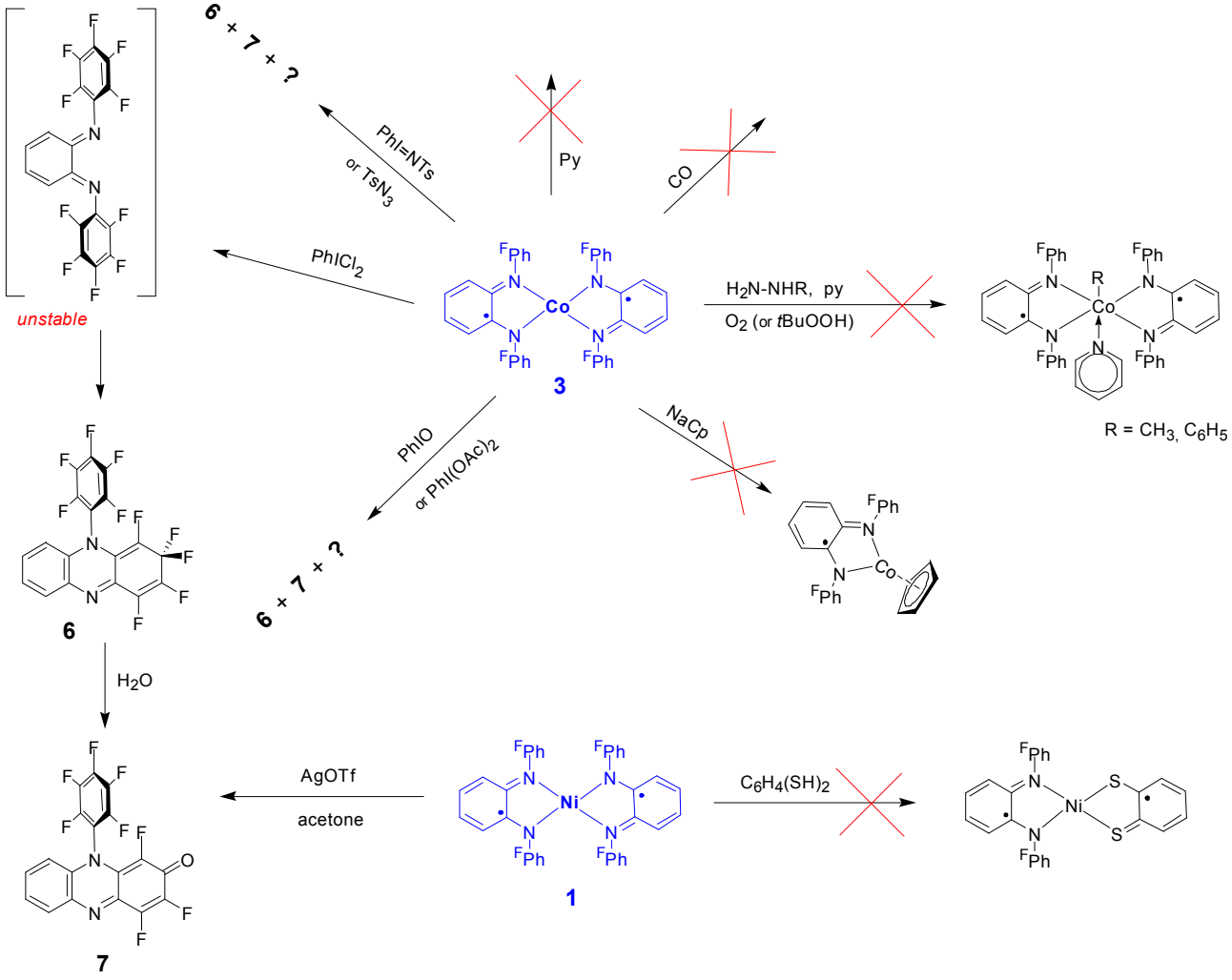

Abbildung 3. Reaktivität von [M(BPPD)$_2$] Komplexen.

Die Oxidation des redoxaktiven Liganden wird bei Reaktion der Komplexe mit Silbertriflat oder Iodosyldichlorid $PhICl_2$ beobachtet. Mono-kationische Komplexe sind nicht stabil und erleiden

eine Dekomplexierung und Folgereaktionen, die auf die Bildung von Phenazinderivaten als Produkte einer intramolekularen nucleophilen Reaktion hinauslaufen. Ein Mechanismus für diese Reaktion wurde vorgeschlagen.

Oxidation von $[Co(BPPD)_2]$ mit $PhICl_2$ ergab das Phenazin Derivat **6**, das sich durch Hydrolyse zum substituierten Phenazinon **7** überführen läßt. Dasselbe Phenazinon **7** wurde in der Reaktion von $[Ni(BPPD)_2]$ mit Silbertriflat in Azeton erhalten. Die organischen Verbindungen Phenazin **6** und Phenazinon **7** wurden in reiner Form isoliert und ausführlich mittels Massenspektrometrie, NMR-, IR-, UV-Vis Spektroskopie, Elementar- und Röntgenstrukturanalyse charakterisiert. ^{1}H, ^{19}F NMR Spektroskopie und Röntgenstrukturanalyse bestätigen, dass F13 und H3 in **6** und **7** dem Anisotropie-Effekt der nahe liegenden C_6F_5-Ringe unterliegen. Phenazin/Phenazinon Derivate haben zahlreiche Anwendungen, weshalb weitere Untersuchung ihrer physikochemischen und medizinischen Eigenschaften vielversprechend sein können.

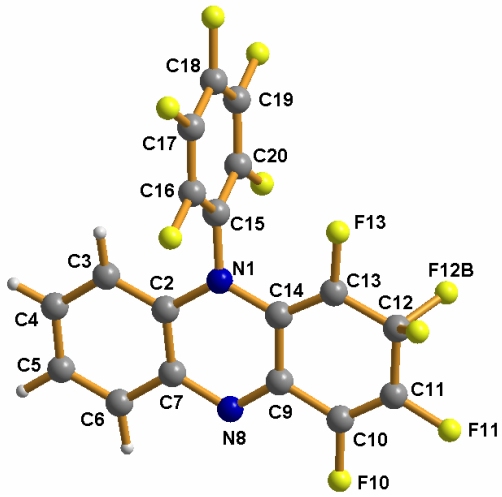

Abbildung 4. Molekulare Struktur von Phenazin Derivat **6**.

Kapitel III.

Diimin Komplexe mit sterisch anspruchsvollen fluorierten *N*-Substituenten $[Ni^{II}(^{F}DAD)_2]$ **8** und $[Co^{II}(^{F}DAD)_2]$ **9** (^{F}DAD – *N,N'*-bis(pentafluorphenyl)-2,3-dimethyl-1,4-diaza-1,3-butadien) sowie Diimin Komplexe mit erweitertem π-System $[Ni^{II}(^{F}BIAN)_2]$ **10** und $[Co^{I}(^{F}BIAN)_3]$ **11** ($^{F}BIAN$ – bis[*N*-{3,5-bis(trifluormethyl)phenyl}imino]acenaphthen) wurden synthetisiert. Verbindung **11** stellt den ersten bekannten Komplex mit drei Bis(imino)acenaphthen-Liganden dar, während **10** der erste späte Übergangsmetallkomplex mit zwei BIAN Liganden ist.

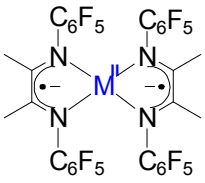

$[Ni^{II}(^{F}DAD)_2]$ **8**
$[Co^{II}(^{F}DAD)_2]$ **9**

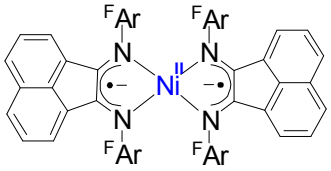

$[Ni^{II}(^{F}BIAN)_2]$ **10**

$^{F}Ar = 3,5\text{-}(CF_3)_2C_6H_3$

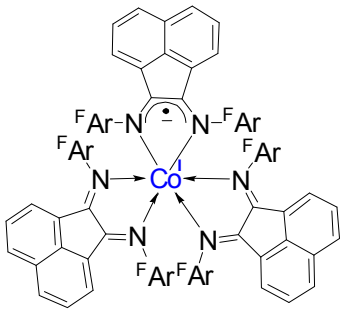

$[Co^{I}(^{F}BIAN)_3]$ **11**

Sowohl BIAN als auch DAD sind *non-innocent* Liganden und können in drei Redox-Zuständen vorliegen: neutrales Diimin L^0, π-Radikal Anion L^{1-} und geschlossenschaliges Dianion L^{2-}. Die *physikalischen (spektroskopischen)* Oxidationszustände des Liganden und der Metalle in den Komplexen **8** – **11** wurden durch Röntgenstrukturanalyse bei niedrigen Temperaturen (193 K) ermittelt. Anhand einer Bindungslängenanalyse wurde gezeigt, dass die Komplexe **8** – **10** die zweiwertigen Metallionen Ni^{II} d^8 und Co^{II} d^7 mit Paaren von radikal-anionischen Liganden enthalten, während der einzigartige Komplex **11** am besten als ein Kobalt(I) Komplex mit zwei neutralen $(^{F}BIAN)^0$ und einem radikalischen $(^{F}BIAN)^{1-}$ Liganden beschrieben werden kann.

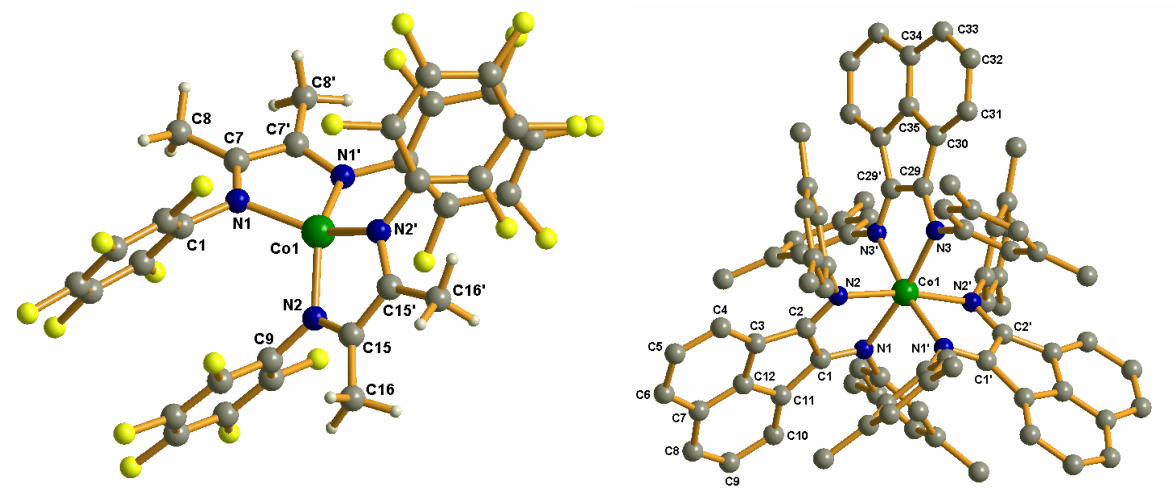

Abbildung 5. Molekulare Struktur von $[Co^{II}(^{F}DAD)_2]$ **9** (links) und $[Co^{I}(^{F}BIAN)_3]$ **11** (rechts). Fluor and Wasserstoffatome in der Struktur **11** werden der Übersichtlichkeit halber weggelassen.

Die elektronischen Strukturen der paramagnetischen Kobaltkomplexe **9** und **11** wurden durch SQUID und X-Band EPR-Spektroskopie untersucht. Beide Komplexe besitzen einen Dublettgrundzustand, wobei sich die Elektrondichte größtenteils in d-Orbitalen des Metalls befindet. Der Dublett–Quartett Energieabstand von 159 cm^{-1} wurde für **11** gefunden, indem man magnetische Suszeptibilitätsdaten an das Modell zweier magnetischer Zentren mit isotropischer Austauschwechselwirkung anpasste. Die entsprechende Spin-Hamiltonian wird in Abb. 6 gezeigt.

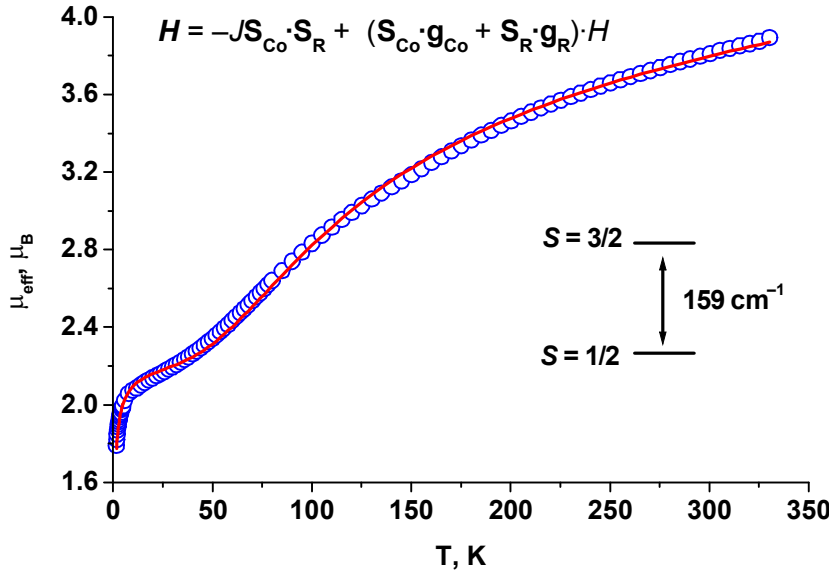

Abbildung 6. Temperaturabhängigkeit des effektiven magnetischen Moments von **11**.

Die EPR Spektroskopie offenbart, dass Komplex **11** in Lösung teilweise dissoziiert nach

$$[Co(BIAN)_3] \rightleftharpoons [Co(BIAN)_2] + BIAN$$

Die elektronischen Strukturen von $[Ni^{II}(^{F}DAD)_2]$ und $[Ni^{II}(^{F}BIAN)_2]$ sowie bekannten strukturell charakterisierten Komplexen $[Ni(DAD)_2]$ haben gezeigt, dass sie aus einem zweiwertigen Nickel d^8 und einem Paar radikal-anionischer Liganden bestehen. Die verzerrt-tetraedrische Geometrie dieser Komplexe impliziert ein *high-spin* Ni^{II} ($S_{Ni} = 1$) Zentrum, weshalb der beobachtete Diamagnetismus der intramolekularen antiferromagnetischen Kopplung des Metallspins mit Spins der zwei π-radikalischen Liganden zugeschrieben wird.

Kapitel IV.

Vier neue Komplexe von Eisen und Kupfer mit sterisch anspruchsvollen BIAN Liganden wurden synthetisiert.

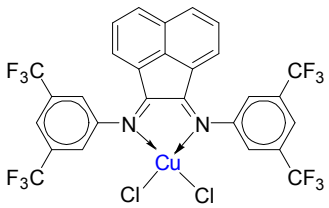

$[Cu^{II}(^{F}BIAN)Cl_2]$ **12**

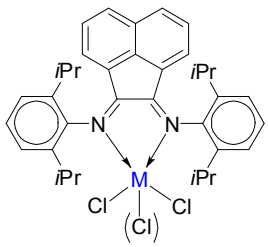

$[Cu^{II}(Dip\text{-}BIAN)Cl_2]$ **13**

$[Fe^{II}(Dip\text{-}BIAN)Cl_2]$ **14**

$[Fe^{III}(Dip\text{-}BIAN)Cl_3]$ **15**

Die Komplexe **12** – **15** wurden mittels Massenspektrometrie, UV-Vis-, IR Spektroskopie und Elementaranalyse charakterisiert. *High-spin* Zustände der Eisenkomplexe $[Fe^{II}(Dip\text{-}BIAN)Cl_2]$ (S = 2) und $[Fe^{III}(Dip\text{-}BIAN)Cl_3]$ (S = 5/2) wurden durch Messung der magnetischen Suszeptibilität in

Lösung (Evans Methode) festgestellt. Die Kristallstruktur von [Cu^{II}(Dip-BIAN)Cl_2] wurde gelöst. Die Wasserstoffatome zweier Chloroform-Moleküle sind im nahen H…Cl-Kontakt mit zwei Chloratomen des Komplexes in dem Gitter, wie in Abbildung 7 gezeigt.

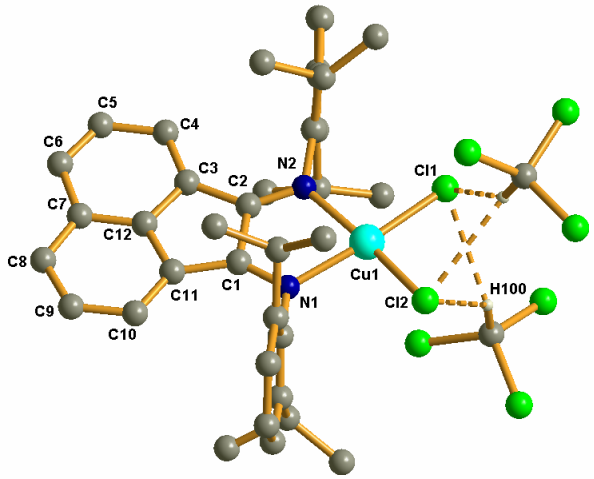

Abbildung 7. Molekulare Struktur von **13** mit zwei Chloroform Molekülen. Alle Wasserstoffatome außer denjenigen von Chloroform Molekülen werden nicht gezeigt.

Nach der Aktivierung mit MAO wurden die Komplexe als Katalysatoren in der Ethylenpolymerisation getestet. Die Eisenkomplexe **14** und **15** sind fähig, Ethylen mit niedriger Aktivität (~3 kg PE/mol_{cat}·h·atm) zu polymerisieren, während die Kupferkomplexe **12** und **13** keine Katalysatoren für die Ethylenpolymerisation darstellen. Die niedrige Aktivität der Eisenkomplexe **14** und **15** und die Inaktivität der Kupferkomplexe **12** und **13** sind eher mit elektronischen als mit sterischen Gründen zu erklären. Keines der für die Komplexe **12** – **15** denkbaren aktiven Zentren folgt der von Gibson postulierten "14-Elektronen-Regel" für hoch-aktive Katalysatoren für die Polymerisation von α-Olefinen.

Kapitel V.

Drei Erdalkaliphthalocyanine [PcM] (M = Ca, Sr, Ba) **16** – **18** und zwei Komplexe mit Kronenethern [PcBa(18-CR-6)] **19** und [PcBa(DB18-CR-6)] **20** wurden dargestellt**.** Die letzten offenbaren bessere Löslichkeiten verglichen mit dem Vorgängerkomplex **18**.

Für die Synthese von **16** sind zwei Wege verfügbar, nämlich ausgehend von metallischem Calcium oder von wasserfreiem $CaCl_2$. Im Gegensatz dazu lieferte nur der Einsatz von metallischem Strontium und Barium die Zielkomplexe **17** und **18**. Der Einsatz der Chloride des Strontiums und Bariums führte nicht zu Metallophthalocyaninen. Dies wurde der niedrigen Löslichkeit von $SrCl_2$ und $BaCl_2$ im Reaktionsmedium (siedendes 1-Pentanol) zugeschrieben. Niedrige Konzentrationen von Ba^{2+} und Sr^{2+} in alkoholischer Lösung führen überwiegend zur Bildung von metallfreiem PcH_2.

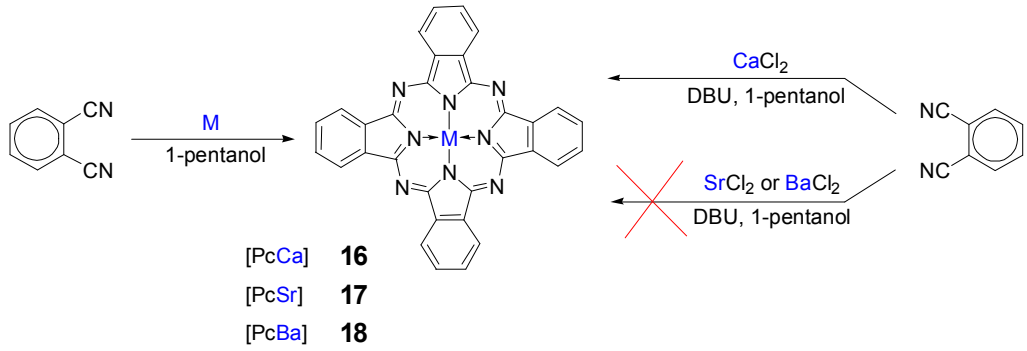

Obwohl einige Referenzen bezüglich [PcCa] und [PcBa] in älterer Literatur gefunden wurden, waren diese Komplexe nie in reiner Form synthetisiert und charakterisiert worden. In dieser Arbeit wurden alle Komplexe **16** – **20** mittels Massenspektrometrie, NMR-, IR-, UV-Vis Spektroskopie und Elementaranalyse ausführlich charakterisiert. In den MALDI-TOF Spektren von **16** – **18** wurden Signale von $[PcM_2]^+$ Ionen entdeckt. Dieses kann auf die Bildung von Kettenstrukturen in den Kristallstrukturen dieser Komplexe hinweisen.

Die vorläufigen Ergebnisse der Feststellung der Kristallpackungen von **16**–**18** durch Röntgenstrukturanalyse zeigen, dass zwei Moleküle von [PcBa] eine dimere Untereinheit $[PcBa]_2$ einer kolumnar gestapelten Anordnung darstellen. Die ausschließlich entlang der *c* Achse im Kristall ausgerichteten Doppeldecker $[PcBa]_2$ bilden aber keine eindimensionale Kettenstruktur. So wird die in der Abbildung 8 gezeigte Kristallpackung von **18** am besten als eine "unterbrochene Kette" beschrieben. Weitere Kristallisationsversuche, um die Kettenstruktur zu erhalten, sind reizvoll.

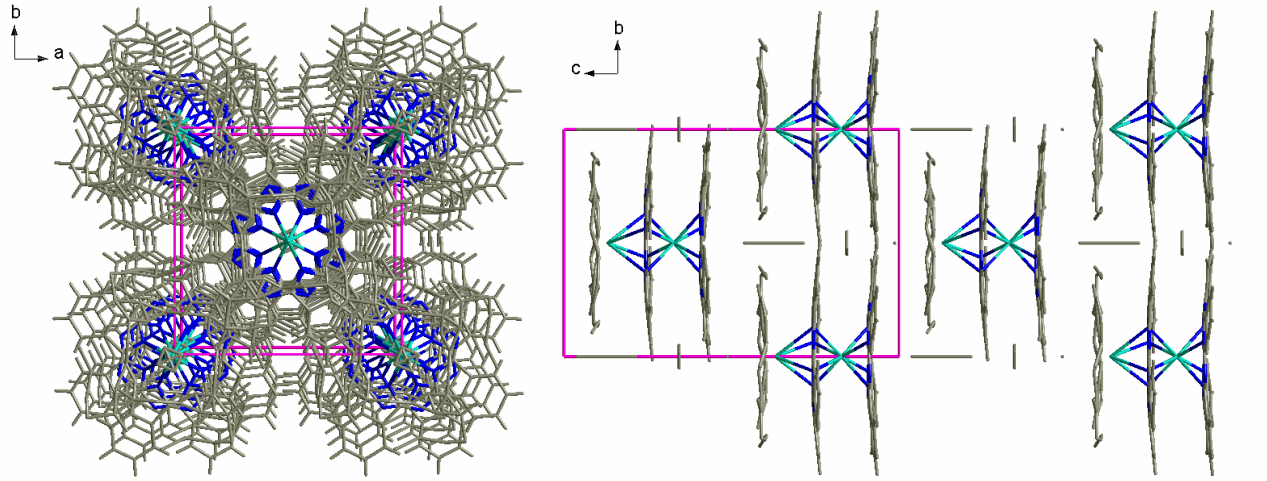

Abbildung 8. Die Kristallpackung von **18** zeigt eine Anordnung als "unterbrochene Kette"; fehlgeordnete Donoratome des Lösungsmittels terminieren als dritte Koordinationsebene jede kolumnare Untereinheit.

Die Komplexe **19** und **20** sind 1:1 Komplexe des entsprechenden Kronenethers an Phthalocyaninatobarium **18**, wie durch ^{1}H NMR Spektroskopie gezeigt wurde. Doppeldecker (*Sandwich*) Strukturen werden für Komplexe **19** und **20** vorgeschlagen.

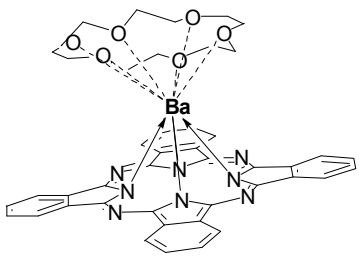

[PcBa(18-CR-6)] **19**

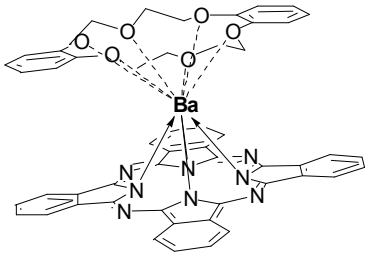

[PcBa(DB18-CR-6)] **20**

Eine weitere Untersuchung der physikalisch-chemischen Eigenschaften der Komplexe **16** – **18** ist vielversprechend angesichts ihres Potentials in pseudo-eindimensionalen halb-/leitenden Materialen.

☙ General Introduction ❧

Numerous *non-innocent* ligands are known at present, their number is increasing each year: new types of ligands are being synthesized and already known ligands are shown to be *non-innocent*.[1] The discussion of the types of *non-innocent* ligands will be restricted to *N*-donor ligands.

Before we start to discuss the term "*non-innocent ligand*", it is necessary to introduce two terms: *formal oxidation state* and *physical* or *spectroscopic oxidation state*. These two terms are, at first sight, very similar but not identical. The *formal oxidation state* of a given metal ion in a mononuclear coordination compound is commonly defined by "the charge remaining on the metal after all ligands have been removed in their normal, closed-shell configuration – that is with their electron pair".[2] For example, the *formal oxidation state* of the iron in a neutral $[Fe(acac)_3]$ (acac = acetylacetonato) is +3, because when calculating the *formal oxidation state* one removes three acac ligands as usual in their closed-shell anionic form leaving the charge +3 on the metal.

On the other hand, it is sometimes possible to determine the electronic configuration of the metal in the complex directly by various spectroscopic methods. To determine the oxidation state of the metal in iron complexes, for example, it is usual practice to apply ^{57}Fe Mössbauer spectroscopy. By knowing the electronic configuration of the metal in the complex, one can immediately calculate the oxidation state of the metal ion. In 1969 Jörgensen suggested that the oxidation state of the metal ion, which is determined from its known electronic configuration, should be specified as the *physical* or the *spectroscopic oxidation state*.[3] A Mössbauer spectrum[4] recorded on $[Fe(acac)_3]$ confirms the *physical oxidation state* of iron to be +3.

Although both, the *formal* and the *physical oxidation state* of the iron in our example $[Fe(acac)_3]$ were shown to be the same, it is not always the case. In 1966 Balch and Holm reported the reaction of nickel chloride with *o*-phenylenediamine in aqueous ammonia resulting in the formation of a neutral complex with the "brutto" formula $[Ni(C_6H_4(NH)_2)_2]$.[5] Which structure corresponds to the given "brutto" formula and which oxidation state has the metal in this complex?

Let us first apply the rules for determining the *formal oxidation state* of the nickel. Two "classical" structures can be drawn for this complex.

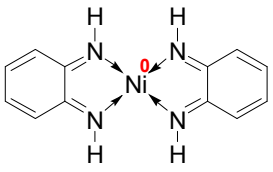

A

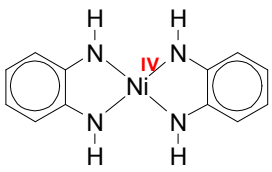

B

Structure **A** comprises two *o*-benzoquinonediimine neutral ligands, while structure **B** consists of two *o*-phenylenediamido(2–) dianions. Both ligands are "normal" closed-shell ligands. After removing the ligands in their closed-shell form, we obtain the *formal oxidation state* of the nickel. For structure **A** the *formal oxidation state* of the nickel is zero, while for structure **B** we obtain the unusually high *formal oxidation state* +4 (!). Certainly we can speculate that the complex contains two types of the ligand: one *o*-benzoquinonediimine and one *o*-phenylenediamido(2–), but several methods, including single crystal X-ray analysis,[6] confirm that the two ligands are identical.

On the other hand, it was shown by various spectroscopic methods and DFT calculations that the electronic configuration of nickel in $[Ni(C_6H_4(NH)_2)_2]$ and related complexes is d^8 and consequently the *physical oxidation state* is +2.[7] It is important to note that the *formal oxidation state* of the nickel determined to be 0 or +4, depending on the proposed structure, does not agree with the *physical oxidation state* being +2. Both *formal* and *physical oxidation states* are often used as synonyms, which they are not. In some areas of coordination chemistry, this practice leads to considerable confusion.[8]

The term *formal oxidation state* is widely used in academic literature as well as in textbooks. This leads to absurd descriptions of some rather air stable complexes, in which the central metal is assumed to be in an unusually high or unusually low oxidation state, as already mentioned for $[Ni(C_6H_4(NH)_2)_2]$. To avoid such misleading descriptions, it is recommended to switch from the *formal oxidation state* to the *physical oxidation state*, particularly when an unusual oxidation state of the metal is observed or when it is already known that some of the ligands in the complex under investigation are *non-innocent*.

Let us come back to the term *non-innocent*, as it is generally used in coordination chemistry. We take example $[Ni(C_6H_4(NH)_2)_2]$ discussed above. If the "real", that is *physical*, oxidation state of the nickel is +2 and two coordinated ligands are identical, then both *o*-phenylenediamine-derived ligands should possess the charge –1. Both ligands in electronic structures **A** and **B** shown above are in their closed-shell forms, while the +2 oxidation state of the nickel forces the two ligands to be open-shell radical monoanions (electronic structure **C**).

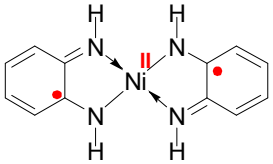

C

Such an electronic structure of $[Ni(C_6H_4(NH)_2)_2]$ was proposed by Balch and Holm in 1966[5] and was recently fully confirmed by Wieghardt.[7]

Ligands that have several, at least two, different oxidation states available at common redox potentials are called *non-innocent*. Since two redox forms of such ligands are associated through a

one electron oxidation-reduction process, one redox form of the ligands is "normal" closed-shell, and the other one is therefore open-shell radical. Three redox forms of an *o*-phenylenediamine derived ligand and their relationship are shown in Figure 1.

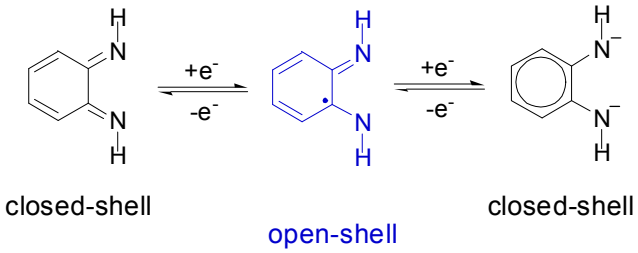

Figure 1. Different redox states of the *o*-phenylenediamine derived ligand.

While "non-innocence" of the dioxygen molecule does not give reason to any doubt and the sequence $O_2 \rightarrow O_2^{\bullet -} \rightarrow O_2^{2-}$ can be found in advanced textbooks, the use and application of the term "*non-innocent*" towards large systems seems to occur reluctantly. Instead, many coordination chemists still prefer to operate with closed-shell ligands and π-back donation schemes, even when the closed-shell terminology is not appropriate any more. Despite of it the number of articles, in which the term "*non-innocent*" is used, is increasing every year. Statistics for the last fifteen years is shown in Diagram 1.

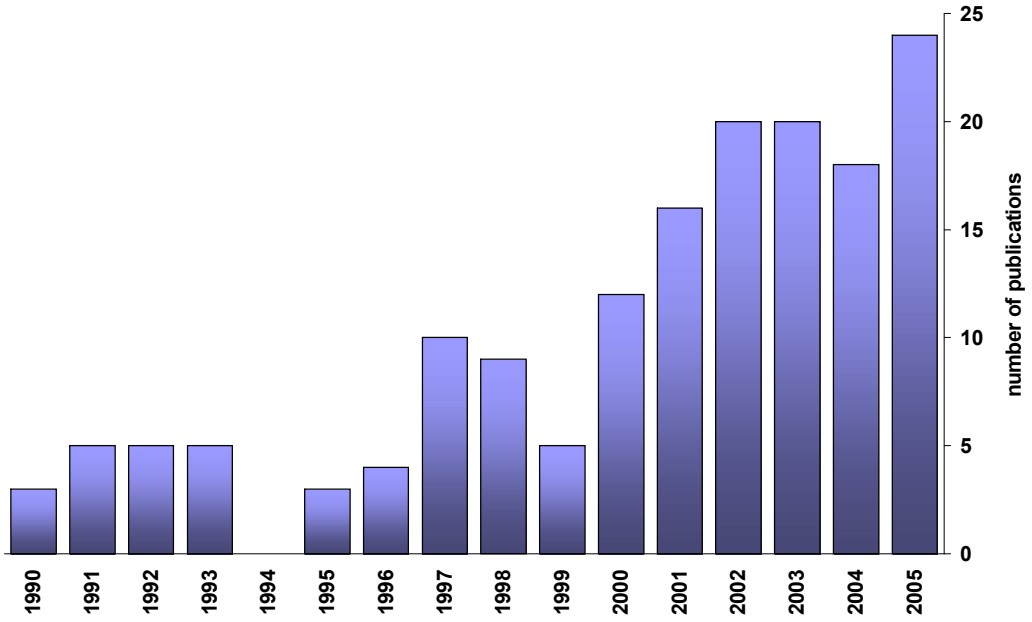

Diagram 1. Number of publications using the term "*non-innocent*".

"Number of publications" in Diagram 1 is the number of articles, in which titles and/or abstracts phrases "*noninnocent*", "*non-innocent*" or "*non innocent*" are used. The data was acquired from the *SciFinder Scholar* database.

Complexes of late transition metals with *non-innocent* ligands are of particular interest with regard to their electronic structures. Since late transition metals commonly have several oxidation

states available, ambiguity of oxidation state determination may arise with transition metal coordinated to the *non-innocent* ligand. Let us consider aniline derived ligands, which are shown to be *non-innocent*.[9] When aniline is deprotonated and attached to the transition metal M, for which at least two oxidation states +n and +(n–1) are available, two electronic states related to each other via a ligand-to-metal charge transfer process can be proposed.

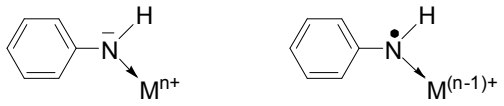

D **E**

In structure **D**, the metal ion M^{n+} is coordinated by an anilido $(PhNH)^-$ ligand. This structure represents a common amido complex. However, in structure **E**, one electron is transferred from the anilido ligand to the metal so that the metal with oxidation state +(n–1) is coordinated by an anilino radical (PhNH). The question is, are we able to distinguish between these two valence isomers.

Different spectroscopic methods such as EPR, resonance Raman, X-ray absorption (XAS), UV-vis, Mössbauer, etc. can by applied to determine the *physical oxidation state* of the metal and the ligand. Often several spectroscopic methods are needed to solve the problem, since one chosen spectroscopy may deliver ambiguous results when applied to such complex potential multispin systems.

Recently Wieghardt et al.[8] and earlier Carugo et al.[10] have shown that oxidation state of the *non-innocent* ligand(s) and consequently the metal can be established by high-quality X-ray structure determination. It is possible because different redox forms of the *non-innocent* ligand have distinctly differing bond distance patterns. The changes in bond distances of the *non-innocent* ligand in different redox forms can be predicted by MO considerations. As an example, the frontier orbitals calculated for *o*-benzoquinonediimine $(bqdi)^0$ are shown in Figure 2.

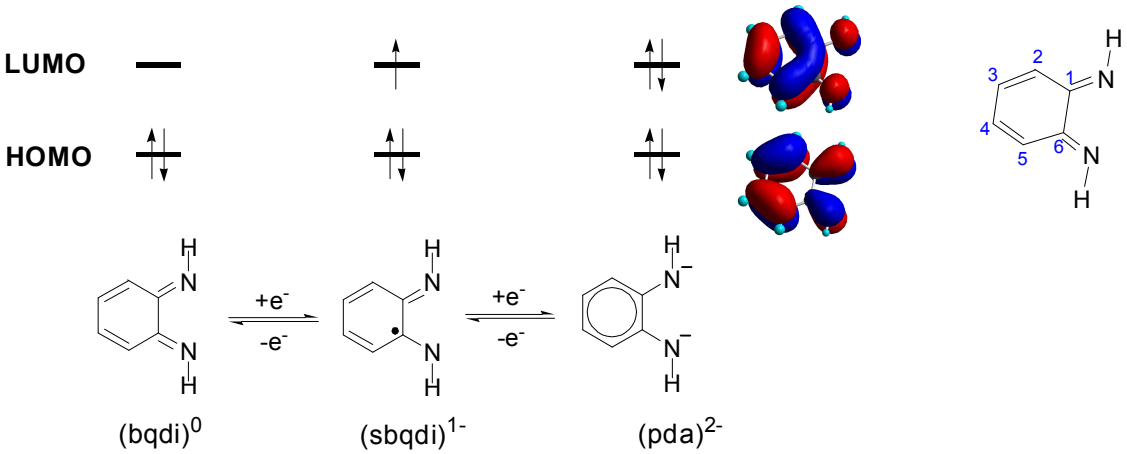

Figure 2. Frontier orbitals of *o*-phenylenediamine derived ligands based on semi-empirical calculations (MOPAC, PM3 performed in *CS Chem3D Ultra 7.0*).

Both HOMO and LUMO in $(bqdi)^0$ are π-orbitals. The filled HOMO results in the double bond character of C2–C3, C4–C5, and two C–N bonds forming a quinoid type structure. Two-electron reduction of $(bqdi)^0$ results in filling of the $(bqdi)^0$ LUMO and formation of the *o*-phenylenediamido dianion $(pda)^{2-}$. It is clearly shown in Figure 2 that LUMO has antibonding character with respect to C2–C3, C4–C5, and two C–N bonds, but bonding character with respect to C1–C2, C1–C6, C5–C6, and C3–C4 bonds. Thus, the reduction of $(bqdi)^0$ to $(pda)^{2-}$ is accompanied by the loss of the quinoid type structure, lengthening of C2–C3, C4–C5, and two C–N bonds and shortening of the other four C–C bonds. Actually, all six carbon–carbon bonds become almost equivalent and could be compared to those in benzene.[7] When the LUMO is only half filled, as in the radical intermediate *o*-benzosemiquinonediiminato $(sbqdi)^{1-}$, the bond lengths are between those of $(bqdi)^0$ and $(pda)^{2-}$. This trend is general and it remains valid regardless of the substituents in the ring or at the nitrogen atoms.

Thus, having several "standard" structures where the oxidation state of the ligand is unambiguously determined, we are allowed to determine the oxidation state of the ligand in a new complex by comparing its bond distance pattern with that of the "standards".

Besides the already mentioned *o*-phenylenediamine derived ligands,[11] well known 1,4-diaza-1,3-butadien (DAD) derived ligands[12] are *non-innocent*, too (Figure 3). This class of ligands has received most attention in complexes used in the polymerization of α-olefins.[13] Although the DAD ligands in catalyst precursors are always in their closed-shell diimine form, they probably change their oxidation state after *in situ* activation. Naturally occurring macrocyclic porphyrins[14] and their artificial analogues tetrabenzotetraazaporphyrins (or more conventional, phthalocyanines)[15] are found in different redox forms in metal complexes as well. The non-innocent nature of phthalocyanines has found its application in the construction of pseudo-one-dimensional semi-/conductors.[16] Bis(arylimino)acenaphthene (BIAN) ligands are related to the DAD family, they possess an extended π-system compared to DAD ligands. They received most attention in the polymerization of α-olefins similar to the DAD complexes. Investigation of its non-innocence has started only recently and the radical $(BIAN)^{1-}$ and the closed-shell dianion $(BIAN)^{2-}$ are found in complexes.[17]

Chelating ligands 2,2'-bipyridine and 1,10-phenanthroline are *non-innocent* ligands too, but their high lying HOMOs makes it more difficult to reduce them to the radical anionic species. Recently, Wieghardt has shown that aniline derived[9] as well as phenol derived[1c] ligands are *non-innocent* and their anilinato and phenolato anions, respectively, can be oxidized to neutral radical ligands. Very recently Büttner et al.[18] has reported on the synthesis and characterization of complex $[Rh^{I}(trop_2N)(bpy)]^{+}(OTf)^{-}$ with aminyl radical $trop_2N^{\cdot}$ (trop –

5-H-dibenzo[a,d]cycloheptene-5-yl) stabilized by Rh^{I} center. This complex is the first example of stable compound containing one-electron oxidized aliphatic amide – aminyl radical.

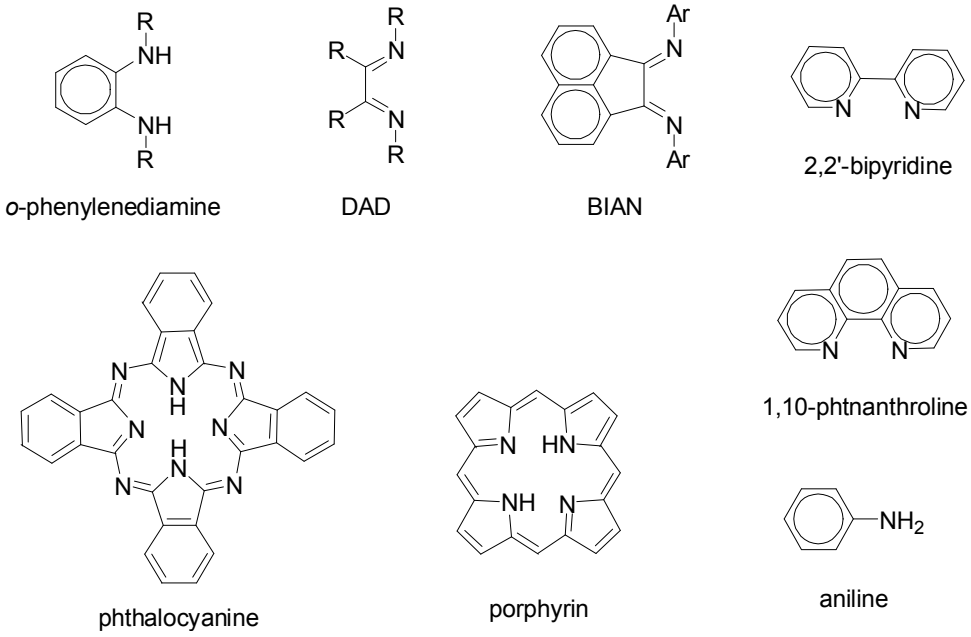

Figure 3. Several examples of *non-innocent N*-donor ligands.

Instead of listing all known *non-innocent N*-donor ligands we discuss features rendering ligands *non-innocent*. First of all, almost all above-mentioned *non-innocent* ligands have a π-system or a system of conjugated double bonds including the *N*-donor atom(s). Secondly, a *non-innocent* ligand in its oxidized form should possess a low-lying LUMO to allow its reduction at accessible potentials, and *vice versa,* such a ligand in its reduced form should have a high-lying HOMO to allow its oxidation. Any ligand satisfying with these requirements may be *non-innocent* and attention should be given to transition metal complexes with such ligands regarding the determination of the oxidation state of the ligand and the metal.

The following Chapters are dedicated to complexes with *non-innocent N*-donor ligands:

- Chapter I and II – *o*-phenylenediamine derived ligands,
- Chapter III – DAD and BIAN ligands,
- Chapter IV – BIAN ligands,
- Chapter V – phthalocyanines.

References.

[1] a) M. D. Ward, J. A. McCleverty, *J. Chem. Soc., Dalton Trans.* **2002**, 275–288; b) A. Vlček Jr., *Coord. Chem. Rev.* **2002**, *230*, 225–242; c) P. Chaudhuri, K. Wieghardt, *Prog. Inorg. Chem.* **2001**, *50*, 151–216. d) C. G. Pierpont, *Coord. Chem. Rev.* **2001**, *216–217*, 99–125. e) M. M. Conradie, J. Conradie, A. Ghosh, *J. Inorg. Biochem.* **2006**, *100*, 620–626.

[2] L. S. Hegedus, *Transition Metals in the Synthesis of Complex Organic Molecules*; University Science Books: Mill Valley, CA, **1994**, p. 3.

[3] C. K. Jörgensen, *Oxidation Numbers and Oxidation States*, Springer: Heidelberg, Germany, **1969**.

[4] L. M. Epstein, *J. Chem. Phys.* **1962**, *36*, 2731–2737.

[5] A. L. Balch, R. H. Holm, *J. Am. Chem. Soc.* **1966**, 5201–5209.

[6] G. S. Hall, R. H. Soderberg, *Inorg. Chem.* **1968**, *7*, 2300–2303.

[7] a) D. Herebian, E. Bothe, F. Neese, T. Weyhermüller, K. Wieghardt, *J. Am. Chem. Soc.* **2003**, *125*, 9116–9128. b) V. Bachler, G. Olbrich, F. Neese, K. Wieghardt, *Inorg. Chem.* **2002**, *41*, 4179–4193. c) D. Herebian, K. E. Wieghardt, F. Neese *J. Am. Chem. Soc.* **2003**, *125*, 10997–11005.

[8] P. Chaudhuri, C. N. Verani, E. Bill, E. Bothe, T. Weyhermüller, K. Wieghardt *J. Am. Chem. Soc.* **2001**, *123*, 2213–2223.

[9] F. N. Penkert, T. Weyhermüller, E. Bill, P. Hildebrandt, S. Lecomte, K. Wieghardt, *J. Am. Chem. Soc.* **2000**, *122*, 9663–9673.

[10] O. Carugo, K. Djinović, M. Rizzi, C. B. Castellani, *J. Chem. Soc., Dalton Trans.* **1991**, 1551–1555.

[11] A. Mederos, S. Domínguez, R. Hernández-Molina, J. Sanchiz, F. Brito, *Coord. Chem. Rev.* **1999**, *193–195*, 913–939.

[12] G. van Koten, K. Vrieze, *Adv. Organomet. Chem.* **1982**, *21*, 151–239.

[13] S. D. Ittel, L. K. Johnson, M. Brookhart, *Chem. Rev.* **2000,** *100*, 1169–1203.

[14] a) K. M. Smith, M. G. H. Vicente, Product Class 8: Porphyrins and Related Compounds, in *Science of Synthesis* **2004**, *17*, 1081–1235. b) F.-P. Montforts, M. Glasenapp-Breiling, D. Kusch, Porphyrines and Realted Compounds, in *Houben-Weyl* **1997**, *E 9d*, 577–716. c) K. M. Kadish, K. M. Smith, R. Guilard, Eds., *The Porphyrin Handbook*, Academic: Boston, MA **2000**; Vols. 1–10. d) K. M. Smith, Ed., *Porphyrins and Metalloporphyrins*, Elsevier: Amsterdam, **1975**.

[15] a) N. B. McKeown, Product Class 9: Phthalocyanines and Related Compounds, in *Science of Synthesis* **2004**, *17*, 1237–1368. b) M. Hanack, H. Heckmann, R. Polley, Phthalocyanines and Related Compounds, in *Houben-Weyl* **1997**, *E 9d*, 717–842. c) C. C. Leznoff, A. B. P. Lever, *Phthalocyanines: Properties and Applications*, VCH: New York, **1989–1996**, volumes 1–4. d) N. B. McKeown, *Phthalocyanine, Materials: Synthesis, Structure and Function*, Cambridge University Press: Cambridge, UK, **1998**.

[16] M. Hanack, M. Lang, *Adv. Mater.* **1994**, *6*, 819–833.

[17] a) I. L. Fedushkin, A. A. Skatova, V. A. Chudakova, V. K. Cherkasov, S. Dechert, H. Schumann, *Russ. Chem. Bull., Int. Ed.* **2004**, *53*, 2142–2147. b) I. L. Fedushkin, A. A. Skatova, V. A. Chudakova, G. K. Fukin, S. Dechert, H. Schumann, *Eur. J. Inorg. Chem.* **2003**, 3336–3346.

[18] T. Büttner, J. Geier, G. Frison, J. Harmer, C. Calle, A. Schweiger, H. Schönberg, H. Grützmacher, *Science* **2005**, *307*, 235–238.

☙ Chapter I ❧

A series of metal complexes with non-innocent ligand *N*,*N*′-bis(pentafluorophenyl)-*o*-phenylenediamine: twisted geometry as a tuner for electronic structure.

Abstract.

A series of homoleptic complexes of the new non-innocent ligand *N*,*N*′-bis(pentafluorophenyl)-*o*-phenylenediamine (H_2BPPD), namely $[Ni^{II}(^{F}sbqdi)_2]$ (**1**), $[Pd^{II}(^{F}sbqdi)_2]$ (**2**), $[Co^{II}(^{F}sbqdi)_2] \leftrightarrow [Co^{III}(^{F}pda)(^{F}sbqdi)]$ (**3**), $[Cu^{II}(^{F}sbqdi)_2]$ (**4**), and $[Fe^{III}(^{F}pda)(^{F}sbqdi)]$ (**5**) was synthesized. Herein $(^{F}pda)^{2-}$ represents doubly deprotonated H_2BPPD, and $(^{F}sbqdi)^{1-}$ the radical anion which is formed by one-electron oxidation of $(^{F}pda)^{2-}$. Oxidation states of ligands and metals in complexes **1**, **2**, **4**, and **5** were determined by single crystal X-ray crystallography performed at low temperatures. Complex **5** represents the first monomeric iron complex containing two *o*-phenylenediamine derived ligands, whereas complex **4** is the first such copper(II) complex where both *o*-phenylenediamine derived ligands are shown to be present in monoanionic radical form. The bulky *N*-C_6F_5 substituents force the complexes **1** and **3–5** to adopt heavily distorted tetrahedral (twisted) structures, which is in striking contrast to strictly planar *o*-phenylenediamine derived complexes reported previously. Electronic structures of the neutral compounds **1**–**4** and of some of their cationic and/or anionic neighboring redox states were probed using EPR and UV-vis-NIR spectroelectrochemistry. Twisted geometry of the complexes results in considerable changes in their electronic structures compared to the planar complexes, whereas the strong electron withdrawing *N*-C_6F_5 groups have a great influence on redox properties.

Introduction.

ortho-Phenylenediamine (H_2pda) and its derivatives are classical examples of non-innocent *N*-donor ligands.[1] They can serve as monodentate or bidentate ligands[2] and they can form complexes in the doubly deprotonated dianionic form $(pda)^{2-}$, which in turn can be oxidized to *o*-benzosemiquinonediiminato radical monoanions $(sbqdi)^{1-}$ and to neutral *o*-benzoquinonediimine $(bqdi)^{0}$ ligands. Different such forms and oxidation states are summarized in Scheme 1.

Complexes containing derivatives of H_2pda reveal interesting electronic properties and can undergo series of electron transfer reactions.[3] Many of these electron transfer processes take place not at the metal but at the ligand(s), demonstrating the non-innocent nature of the latter.[4] Recently such complexes received considerable attention with respect to revision and reinterpretation of their crystal[5] and electronic[6] structures, to the investigation of their reactivity,[7] and to detailed theoretical studies aimed at understanding the nature of these potential multispin systems.[6,8]

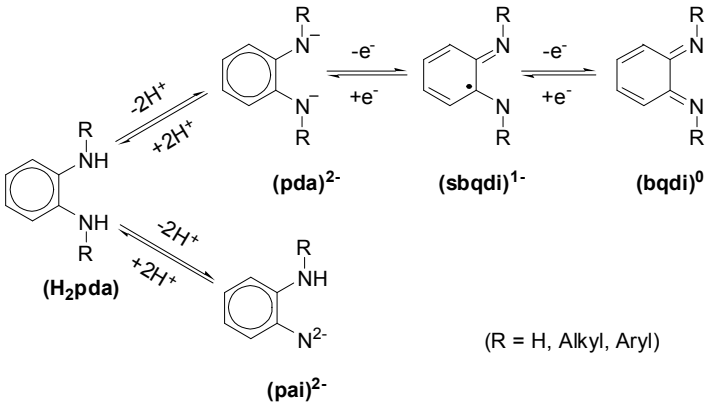

Scheme 1. Different forms and oxidation states of *o*-phenylenediamine derived ligands.

Determination of metal and ligand oxidation states in late transition metal complexes with non-innocent ligands is difficult when the oxidation state of the metal is highly variable. For example, a neutral complex $[Co(^1lig)_2]$[9,10] (Fig. 1) may be formulated as $[Co^{II}(^1sbqdi)_2]$, $[Co^{III}(^1sbqdi)(^1pda)]$ or as a corresponding Co^0, Co^I or Co^{IV} complex with the appropriate set of oxidized or reduced ligands. Wieghardt et al.[11] have shown that in such a case the oxidation state of the metal and of the non-innocent ligand can be assigned on the basis of single-crystal X-ray structure analyses, because $(pda)^{2-}$, $(sbqdi)^{1-}$, and $(bqdi)^0$ have distinctly different bond distance patterns (Fig. 2). Since the difference of bond lengths is in the order of a few pm, accurate crystal structure analyses at low temperatures are required to assign oxidation states of the metal and of the ligand(s) with sufficient confidence.

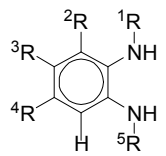

$^1R=^2R=^3R=^4R=^5R$ = H	$^1H_2$pda
$^1R=^3R=^4R=^5R$ = H, ^2R = OH	$^2H_2$pda
$^2R=^3R=^4R$ = H, $^1R=^5R$ = *n*-Pr	$^3H_2$pda
$^1R=^3R=^5R$ = H, $^2R=^4R$ = *t*-Bu	$^4H_2$pda
$^1R=^2R=^3R=^4R$ = H, ^5R = Ph	$^5H_2$pda
^2R = H, $^3R=^4R$ = NHPh, $^1R=^5R$ = Ph	$^6H_2$pda
$^2R=^3R=^4R=^5R$ = H, ^1R = c-Hex	$^7H_2$pda
$^2R=^3R=^4R$ = H, $^1R=^5R$ = SO_2CH_3	$^8H_2$pda

Figure 1. Substituted *o*-phenylenediamines and designation thereof.

As shown in Scheme 1, the parent H_2pda can be doubly deprotonated to form two different dianions: *o*-phenyleneaminoimido $(pai)^{2-}$ and *o*-phenylenediamido $(pda)^{2-}$. Monodentate $(pai)^{2-}$ has been observed in $[Re^V(^2pai)Cl_3(PPh_3)_2]$[12] and bidentate $(pda)^{2-}$ has been found in

$[Ti^{IV}(^{3}pda)ClCp]$[13] and $(Et_4N)_2[W(CO)_3(^{1}pda)]\cdot(^{1}H_2pda)$.[14] The oxidation of $(pda)^{2-}$ results in the formation of two new species: One-electron oxidation of $(pda)^{2-}$ gives the open-shell *o*-benzosemiquinonediiminato radical monoanion $(sbqdi)^{1-}$, and two-electron oxidation gives the closed-shell neutral *o*-benzoquinonediimine $(bqdi)^{0}$. The radical anion $(sbqdi)^{1-}$ can be found in $[Ni^{II}(^{4}sbqdi)_2]$,[5] $[M^{II}(^{5}sbqdi)_2]$[5,15] (M = Ni, Pd, Pt), $[Co^{III}(^{1}sbqdi)_2(py)]Cl$,[16] $[Co^{III}(^{1}sbqdi)_2(PPh_3)](ClO_4)$,[17] $[Co^{III}(^{5}sbqdi)_2(py)](OAc)$,[15] $[Co^{III}(^{1}sbqdi)_2Cl]$,[9] and $[Co^{III}(^{5}sbqdi)_2I]$.[6] The $(bqdi)^{0}$ form of the ligand is well represented by X-ray structure determination of $[Fe^{II}(^{1}bqdi)(CN)_4](Me_2\text{-}DABCO)$,[18] $[Cu^{I}(^{6}bqdi)(PPh_3)_2](BF_4)$,[19] $[Ru^{II}(^{1}bqdi)(PPh_3)_2(MeCN)_2](PF_6)_2$,[20] $[Ru^{II}(^{1}bqdi)(PPh_3)_2Cl_2]$,[21] $[Ru^{II}(^{1}bqdi)(L)(H_2O)](PF_6)_2$,[22] $[Ru^{II}(^{1}bqdi)I(L)](PF_6)$[22] (L = 1,4,7-trimethyl-1,4,7-triazacyclononane), and $[Ru^{II}(^{5}bqdi)(bpy)_2](PF_6)_2$.[15] These studies clearly demonstrated how intraligand bond lengths vary in a systematic manner if $(pda)^{2-}$, $(sbqdi)^{1-}$ and neutral $(bqdi)^{0}$ are compared.

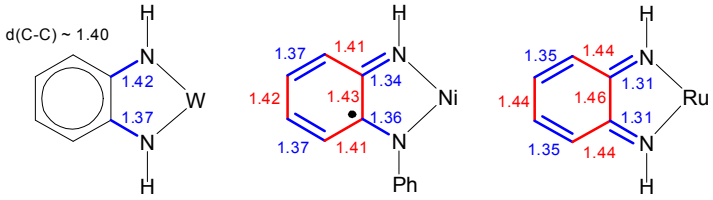

Figure 2. Characteristic bond distances of *o*-phenylenediamine-derived ligands in different oxidation states: $(Et_4N)_2[W(CO)_3(^{1}pda)]$ (left),[14] $[Ni^{II}(^{5}sbqdi)_2]$ (center),[5] $[Ru^{II}(^{1}bqdi)(PPh_3)_2(MeCN)_2](PF_6)_2$ (right).[20]

In 1966 Balch and Holm[3] reported the synthesis and properties of a series of the neutral binary complexes of the type $[M(^{1}lig)_2]$, where M = Ni, Pd, Pt, Co. Structures of nickel[23] and cobalt[9] complexes were determined later showing planar geometry. Herebian et al.[5] showed that the diamagnetic planar complexes $[M(^{4}lig)_2]$ and $[M(^{5}lig)_2]$ (M = Ni, Pd, Pt) are best described as containing a divalent d^8 metal ion and two antiferromagnetically coupled radical anions (singlet diradical species). This interpretation was confirmed by density functional theory (DFT) calculations.[8] The electronic structure of planar $[Co(lig)_2]$ complexes is still a matter of debate with respect to the presence of Co^{II} versus Co^{III}.[6] All structurally characterized complexes of the general formula $[M(lig)_2]$ were found to be strictly planar, except for two copper complexes $[Cu^{I}(^{7}bqdi)_2]Cl$ and $(HNEt_3)_2[Cu(^{8}lig)_2]$, which adopt distorted tetrahedral geometry.[24]

As displayed in Figure 1, the so far investigated *o*-phenylenediamine-type ligands typically contain H or electron-releasing *N*-substituents such as alkyl, rendering the ligand more electron-rich than the corresponding catecholato analogues. By substituting both oxygen atoms {O} with the electronically similar but sterically much more demanding *N*-pentafluorophenyl groups $\{NC_6F_5\}$ we anticipated to create a new non-innocent ligand of similar electron donor/acceptor ability but much increased space requirement in comparison to the catecholato/*o*-quinone ligands.

Herein we present a series of the new complexes $[M(BPPD)_2]$,[25] where M is Ni, Pd, Co, Cu or Fe, based on the new *N*,*N*′-bis(pentafluorophenyl)-*o*-phenylenediamine ($H_2BPPD = {}^{F}H_2pda$). As a consequence of the steric situation a significant deviation from MN_4 planarity is observed for all of these complexes. Assignments of the oxidation states of the ligands and of the metals along with the electronic properties of these complexes are reported in the following, based on crystal structure, electrochemistry, magnetism and spectroscopy (UV-vis-NIR, EPR).

Results and Discussion.

Synthesis and Characterization.

The common synthesis of $[M(lig)_2]$ complexes is performed by aerobic oxidation of the H_2pda ligand in the presence of metal salt and aqueous ammonia[3] or triethylamine[5] as bases. In our experiments, the use of triethylamine for the synthesis of **1** led to low yields and to the necessity to purify the product in the presence of large amounts of unreacted ligand. Therefore, *n*-butyllithium was employed as a base to give the best results. The general synthetic procedure for complexes **1**–**4** involves a double deprotonation of the ligand with *n*-butyllithium under anaerobic conditions, the addition of the appropriate anhydrous metal salt, and slow complexation, followed by oxidation with pure oxygen.

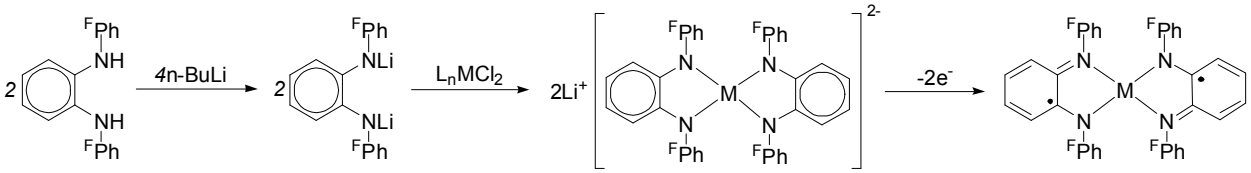

Scheme 2. Synthesis strategy.

Complexes **1** and **2** are diamagnetic at room temperature showing sharp resonance signals in the proton and ^{19}F NMR spectra. As solids they are stable in contact with air, and toluene solutions can be kept for at least 2 d. Complexes **3** and **4** are paramagnetic at room temperature (see below). As solids complexes **3** and **4** are stable in contact with air, but after 1 d in non-dried solvents they start to decompose, showing a set of colored spots on the TLC plate.

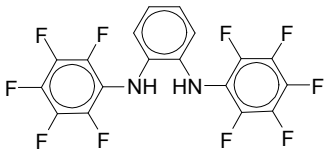

H_2BPPD = ^{F}H_2pda
(this work)

$[Ni^{II}(^Fsbqdi)_2]$ (**1**) $[Co(BPPD)_2]$ (**3**)
$[Pd^{II}(^Fsbqdi)_2]$ (**2**) $[Cu^{II}(^Fsbqdi)_2]$ (**4**)
$[Fe^{III}(^Fsbqdi)(^Fpda)]$ (**5**)

Chart 1. The ligand H_2BPPD and complexes derived thereof.

Complex **5** was prepared employing equivalent amounts of anhydrous iron trichloride as oxidant, since the target complex is very oxygen sensitive and undergoes irreversible oxidation to give an undefined paramagnetic solid. The paramagnetic iron complex is unstable on exposure to air.

Our attempts to oxidize **3** with chloroform, tetrachloromethane or iodine to generate a five-coordinated cobalt(III) species failed. When the strong oxidizing agent $PhICl_2$ was used, decomplexation of cobalt and formation of a new fluorinated phenazine derivative, an isomer of oxidized ligand $(^{F}bqdi)^{0}$, was observed that is reported elsewhere.[26]

The purity of **1** and **2** was confirmed by ^{1}H and ^{19}F NMR spectroscopy. Complexes **3**, **4** and **5** were recrystallized to give analytically pure samples. The composition of all synthesized complexes is in excellent agreement with the results of high-resolution mass spectra. Elemental analyses show generally slightly higher values for nitrogen content and slightly lower for carbon. This is typical for C–F containing compounds. In order to assign oxidation states of the metals and the ligands the structures of the complexes **1**–**5** have been determined by X-ray crystallography at low temperatures.

Crystal Structures.

Table 1 contains the crystallographic data and Table 2 summarizes important bond lengths of the complexes. The structure of the nickel complex **1** consists of two doubly deprotonated one-electron oxidized radical anion ligands attached to the four-coordinated nickel(II) (Fig. 3). From a comparison of the C–C and C–N bond distances of the ligands in **1** with corresponding bonds of the complexes reported previously (Fig. 2), it is evident that both ligands in **1** are in the radical monoanion $(^{F}sbqdi)^{1-}$ form. The C–N bond length at average (av.) 1.357(5) Å along with a quinonoid type bond pattern of the six-membered ring with two short C=C bonds at av. 1.359(6) Å and four longer C–C bonds at av. 1.422(6) Å are in good agreement with the presence of two radical monoanions $(^{F}sbqdi)^{1-}$ in **1**. It is important to note that observed bond lengths are accurate within ± 0.018 Å (3σ). This allows us to determine the oxidation state of the ligand. Since the whole complex possesses zero charge, the physical (or spectroscopic)[27] oxidation state of Ni is +II with d^{8} electronic configuration.

Table 1. Crystallographic Data for **1**·(C_6H_{14}), **2**·4(C_4H_8O), **3**·2(C_4H_8O), **4**·(C_6H_{14}) and **5**·($C_4H_{10}O$)

	1·(C_6H_{14})	**2**· 4(C_4H_8O)	**3**·2(C_4H_8O)	**4**·(C_6H_{14})	**5**·($C_4H_{10}O$)
chem. formula	$C_{42}H_{22}F_{20}N_4Ni$	$C_{52}H_{40}F_{20}N_4O_4Pd$	$C_{44}H_{24}CoF_{20}N_4O_2$	$C_{42}H_{22}CuF_{20}N_4$	$C_{40}H_{18}F_{20}FeN_4O$
crystal size, mm	0.22 x 0.15 x 0.14	0.27 x 0.15 x 0.02	0.34 x 0.18 x 0.07	0.14 x 0.11 x 0.05	0.33 x 0.21 x 0.02
Fw	1021.35	1271.28	1079.60	1026.18	1006.43
space group	C 2/c (No. 15)	F ddd (No. 70)	C 2/c (No. 15)	C 2/c (No. 15)	P 2_1/n (No. 14)
a, Å	58.619(3)	15.0923(14)	59.292(3)	59.219(3)	8.6433(11)
b, Å	15.3293(6)	19.2020(14)	15.3580(4)	15.3696(8)	28.148(2)
c, Å	8.6322(4)	35.566(3)	8.6688(3)	8.5864(5)	15.3298(18)
β, °	97.288(3)		97.952(9)	97.394(4)	92.910(9
V, Å^3	7694.1(6)	10307.1(15)	7818.0(5)	7750.1(8)	3724.8(7)
Z	8	8	8	8	4
T, K	193	193	193	193	123
ρ calc., g cm^{-3}	1.763	1.638	1.834	1.759	1.795
μ(MoKα), cm^{-1}	6.42	4.83	5.84	7.00	5.48
refl. collected /θ_{max}	42127/25	16959/25	48100/25	39191/25	32048/23
unique refl./I>2σ(I)	6752/4779	2200/1643	6888/4681	6754/4456	5181/2937
no. params/restraints	636/1	193/0	583/0	641/61	597
R1[a]/goodnes of fit[b]	0.0576/1.064	0.0496/1.005	0.0454/0.942	0.0398/0.928	0.0672/0.990
wR2[c] (unique refl.)	0.1477	0.1189	0.1218	0.0996	0.1283

[a] Observation criterion: I>2σ(I). R1=Σ||F_0|–|F_c||/Σ|F_0|. [b] Goodness of fit (GoF)=[Σ{w(F_0^2–F_c^2)^2}/(n–p)]$^{1/2}$. [c] wR2=[Σ{w(F_0^2–F_c^2)^2}/Σ{w(F_0^2}^{2}]$^{1/2}$, where w=1/σ^2(F_0^2)+(aP)^2+bP and P=(F_0^2+2F_c^2)/3.

Table 2. Selected bond lengths [Å] of complexes **1**–**5**.

	[Pd^{II}(^{F}sbqdi)$_2$] (**2**)		[Ni^{II}(^{F}sbqdi)$_2$] (**1**)	[Co(BPPD)$_2$] (**3**)	[Cu^{II}(^{F}sbqdi)$_2$] (**4**)	[Fe^{III}(^{F}sbqdi)(^{F}pda)] (**5**)
N1–Pd1	1.993(3)	M1–N1	1.910(3)	1.912(2)	1.945(2)	1.896(5)
		M1–N2	1.902(3)	1.903(2)	1.947(3)	1.896(6)
		M1–N3	1.897(3)	1.900(2)	1.945(3)	1.893(5)
		M1–N4	1.888(3)	1.905(2)	1.941(3)	1.884(5)
C7–C8	1.405(6)	C1–C2	1.427(6)	1.416(4)	1.426(4)	1.418(8)
C9–C9#1	1.432(9)	C3–C4	1.415(7)	1.402(5)	1.413(5)	1.415(10)
		C5–C6	1.409(6)	1.392(4)	1.417(4)	1.385(9)
C7–C7#1	1.436(7)	C1–C6	1.421(6)	1.427(4)	1.440(4)	1.430(9)
		C19–C20	1.426(6)	1.415(4)	1.432(4)	1.425(8)
		C21–C22	1.424(8)	1.410(5)	1.405(6)	1.369(10)
		C23–C24	1.420(6)	1.425(4)	1.426(5)	1.408(9)
		C19–C24	1.437(6)	1.423(4)	1.436(5)	1.398(10)
C8–C9	1.361(6)	C2–C3	1.358(6)	1.369(4)	1.360(5)	1.377(10)
		C4–C5	1.359(6)	1.360(4)	1.359(5)	1.379(8)
		C20–C21	1.349(7)	1.375(5)	1.349(5)	1.386(9)
		C22–C23	1.370(6)	1.358(5)	1.367(5)	1.382(9)
C7–N1	1.361(5)	C1–N1	1.353(5)	1.365(3)	1.350(4)	1.379(8)
		C6–N2	1.366(5)	1.374(3)	1.348(4)	1.397(7)
		C19–N3	1.352(5)	1.372(3)	1.352(4)	1.386(8)
		C24–N4	1.358(5)	1.361(4)	1.358(4)	1.402(8)

Two essentially planar NCCN-chelate ligands[28] are twisted with respect to each other forming a dihedral angle of 53.7(1)˚, whereas almost all structurally characterized complexes of the type [Ni(lig)$_2$] are known to adopt a nearly planar geometry. A similar twisted geometry as for **1** was reported by tom Dieck et al. for a related nickel complex [Ni(DAD)$_2$] bearing two sterically demanding *N,N´*-bis(2,6-dimethylphenyl)diazadiene ligands.[29] This complex, doubtfully formulated as a Ni(0) compound with two closed-shell DAD ligands, reveals a dihedral angle between the two diimine planes of 44.5˚.

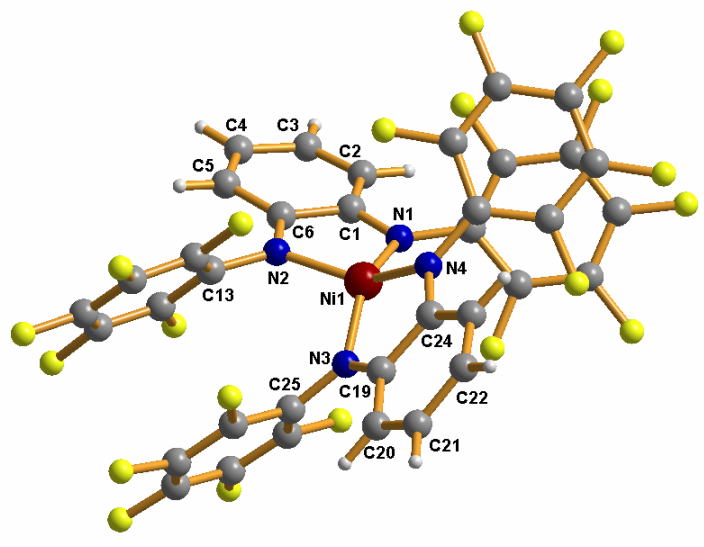

Figure 3. Molecular structure of heavily twisted **1.**

We attribute the considerable distortion from planarity in **1** to the repulsive interaction between the bulky C_6F_5 groups engaged in intramolecular C_6F_5/C_6F_5 stacking (Fig. 3). Two pairs of the perfluorinated phenyl rings in *syn* position are nearly coplanar with interplanar angles of 2.1(2)° and 5.2(2)°. The distances[30] between these C_6F_5 rings are 3.20 and 3.28 Å. If we assume that complex **1** adopts a planar geometry without great changes in bond distances and angles, a simple geometrical consideration then reveals that the coplanar C_6F_5 rings would be forced to a face-to-face distance of approximately 2.87 Å. Recently, Lorenzo et al.[31] have shown by DFT calculations that the energy minimum for the gas phase dimer $(C_6F_6)_2$ in face-to-face configuration is reached when the interplanar distance is 3.31–3.37 Å. Assuming that the energy minima for the pair C_6F_5/C_6F_5 in **1** and the calculated pair $(C_6F_6)_2$ are reached at the close distances we would expect very strong repulsion between two pairs of C_6F_5 rings in the hypothetical planar **1**.

As a consequence of the repulsion of the four C_6F_5 substituents a distortion of the complex in the direction of a tetrahedron as well as synchronous rotation of the phenyl rings provide the sufficient increase of the C_6F_5/C_6F_5 distances. The molecular structure of **1** reveals the interplanar C_6F_5/C_6F_5 distances at 3.20 and 3.28 Å which is in excellent agreement with the distances of 3.23 and 3.32 Å between C_6F_5 rings engaged in intramolecular stacking in the sandwich complex

bis[η^5-1,2,4-tris(pentafluorophenyl)cyclopentadienyl]iron(II)[32] and with distances 3.23–3.27 Å in complexes $[M^{II}(^{F}DAD)_2]$[33] (M = Co, Ni; ^{F}DAD – radical anion of *N,N′*-bis(pentafluorophenyl)-2,3-dimethyl-1,4-diaza-1,3-butadiene). Summarizing, the twisted geometry of **1** is determined by repulsion forces between the two pairs of the perfluorinated rings. On the other hand, the π/π effect of the perfluorinated phenyl rings on the ligand bond pattern must be small since the C_6F_5 rings form dihedral angles in the range of 51.1(2) – 55.4(2)° with the corresponding NCCN planes.

The molecular structure of the palladium complex **2** differs significantly from that of **1** (Fig. 4). The molecular structure of **2** possesses D_2 symmetry in the crystal and shows less deviation from planarity in comparison with **1**. The dihedral angle formed by the two NCCN planes is only 22.4(2)°. We ascribe this trend towards planarity to the longer bond distances Pd–N at 1.993(3) Å in comparison with Ni–N (av. 1.900(3) Å). This contributes to holding the perfluorinated phenyl rings at a sufficient distance even without great deformation from the planar configuration. The rings in *syn* position are nearly coplanar with a dihedral angle of 3.3(2)°. The interplanar distance C_6F_5/C_6F_5 is 3.21 Å, closely resembling the interplanar distance in **1**. As a consequence of increased planarity the perfluorophenyl rings form larger angles of 73.6(2)° with the central ligand plane.

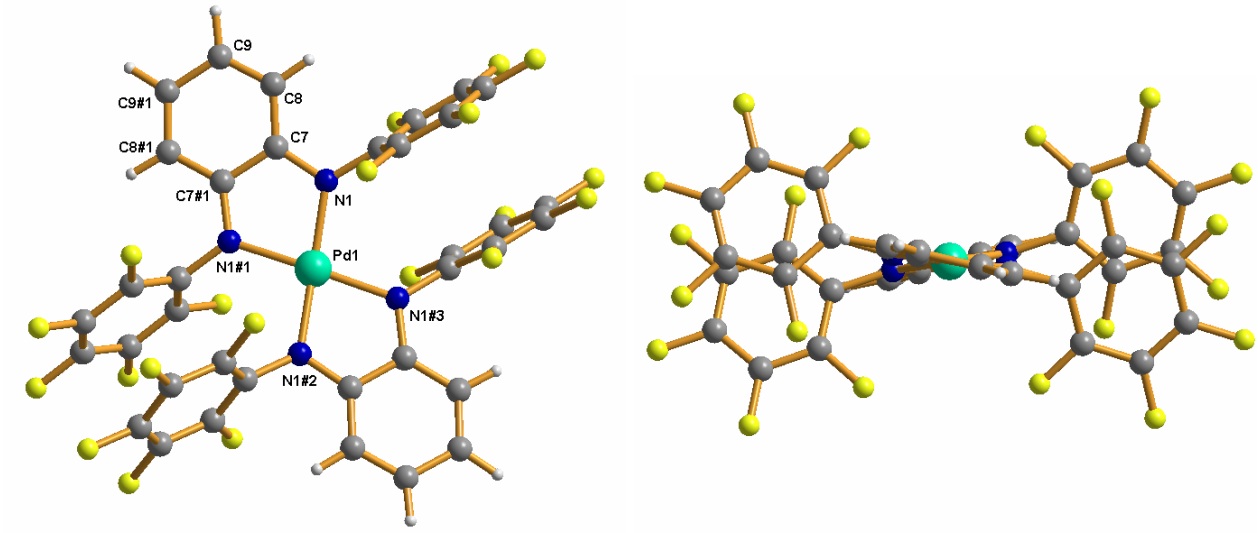

Figure 4. Molecular structures of slightly twisted **2**.

The crystal structure of **2** shows C–N bond lengths of 1.361(5) Å, along with a characteristic quinonoid type distortion of the six-membered ring with two short C=C bonds at 1.361(6) Å and four longer C–C bonds at av. 1.420(7) Å. Taking into account the accuracy of bond length determination (± 0.018 Å) we identify both ligands as $(^{F}sbqdi)^{1-}$ radical monoanions and the metal as Pd^{II} (electronic configuration d^8).

The crystal structure of the cobalt complex **3** closely resembles that of **1** (Fig. 5). Two nearly planar NCCN entities form an interplanar angle of 54.0(1)° whereas the pairs of the perfluorinated phenyl rings are almost coplanar with dihedral angles of 2.2(2)° and 5.2(1)° with respect to each other, and in the range of 50.7(1) – 55.6(1)° with respect to the NCCN planes.

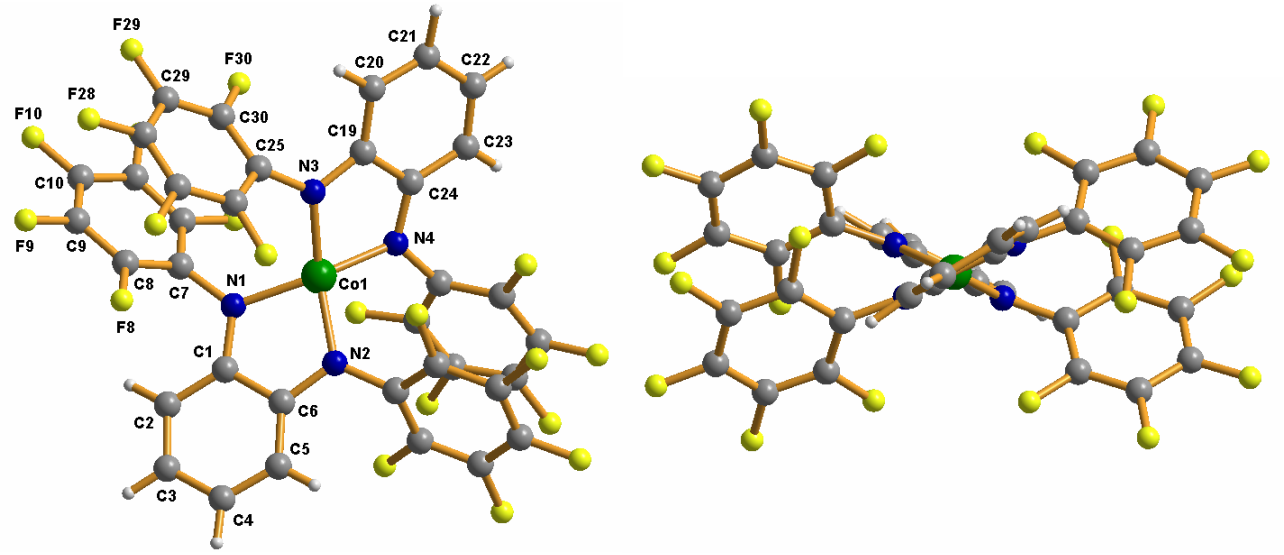

Figure 5. Molecular structures of **3** showing a highly twisted geometry.

The most interesting feature of the cobalt complex **3** is the bond pattern within the ligands. At first sight it closely resembles the bond patterns observed in complexes **1**, **2** and **4** (*vide infra*). The C–N bonds show partly double bond character with an average length of 1.368(3) Å while the six-membered rings reveal a quinonoid type distortion with two short C=C bonds at av. 1.366(5)° and four longer C–C bonds at av. 1.414(4)°. This bond pattern suggests that the two ligands are in the radical monoanion form (^{F}sbqdi)$^{1-}$. Taking into account the electroneutrality of the complex, the oxidation state of the central atom would be Co^{II} (d^7) (Fig. 6, form **A**) with a possible high-spin/low-spin alternative (high-spin configuration favored for a distorted tetrahedral structure)[6].

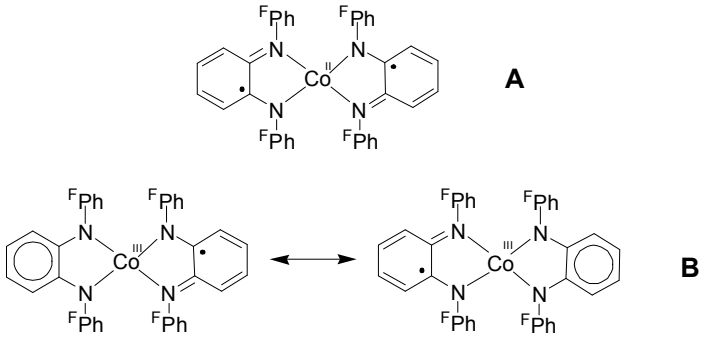

Figure 6. Two different electronic structures of [Co(BPPD)$_2$].

On detailed inspection, however, slight differences in the bond lengths of **3** when compared with those of complexes **1**, **2** or **4** are noted. The average C–C bond length in **3** is slightly shorter in

comparison to that of **1**, whereas the C=C and C=N distances are slightly longer. The most conspicuous changes are observed for the C=N bond distances: av. 1.368(3) Å in complex **3** versus av. 1.357(5) Å in complex **1**. We realize that such small changes can be explained simply by the standard uncertainties from the crystal structure determinations, however, the fact that we observe an apparent shortening of the C–C bonds along with simultaneous lengthening of C=C and C=N bonds can be rationalized by assuming fractional changes in the oxidation states of the ligands and, by implication, of the metal. Complex **3** could then also be formulated as containing two forms of the ligand: one radical monoanion $(^{F}sbqdi)^{1-}$ and one closed-shell dianion $(^{F}pda)^{2-}$, connected by a four-coordinated high-spin Co^{III} (d^6) ion (Fig. 6, form **B**). Experimentally, both ligands reveal the same bond pattern within the error limits, and it may thus be assumed that the ligand "mixed valency" is averaged to give the observed structural equivalency of the two ligands. Contributions from $(^{F}pda)^{2-}$ would then account for the changes observed in the structure of **3**.

In such a case it is reasonable to expect the bond lengths to be average between those of an aromatic dianion and the corresponding radical monoanion, as was suggested in a recent work of Bill et al.[6] dealing with the problem of determination of spin and oxidation states in cobalt complexes with non-innocent ligands. Accurate calculations of the bond lengths for a complex **B** would require two accurately determined reference structures representative for radical monoanion and aromatic dianion. Since the bond lengths vary slightly with the ligand substituents and the geometry of the complex (see, for example, two related well-resolved structures $[Ni(^{1}L_{N,O})_2]$[6] and $[Pd(^{2}L_{N,O})(bpy)]PF_6$,[34] where $^{1}L_{N,O}$ is a doubly deprotonated one-electron oxidized form of 2-(2-trifluoromethyl)anilino-4,6-di-*tert*-butylphenol and $^{2}L_{N,O}$ is a doubly deprotonated one-electron oxidized form of 2-anilino-4,6-di-*tert*-butylphenol), a structure containing the aromatic dianion $(^{F}pda)^{2-}$ would be required for correct comparison. Since complexes of $(^{F}pda)^{2-}$ are not known so far we are not able to distinguish between forms **A** and **B** on the basis of the crystal structure. Our attempts to prepare extremely sensitive $[AsPh_4]_2[Co^{II}(^{F}pda)_2]$ and to grow crystals suitable for X-ray structure analysis have thus far failed.

Complex **4** represents the first structurally characterized four-coordinated copper complex containing two *o*-phenylenediamine derived ligands. Complexes of *o*-semiquinones and *o*-semiquinonemonoimines are known, however.[11,35] The oxidation states of the two ligands along with the oxidation state of the metal (+II, implying d^9 electronic configuration) were unambiguously assigned on the basis of the bond length pattern. The crystal structure of **4** resembles that of **1** or **3**, showing the presence of two almost planar ligand backbones and a twisted configuration around the metal center with a dihedral angle of 53.9(1)°. A structurally characterized Cu^{I} complex containing two *o*-benzoquinonediimine ligands $[Cu^{I}(^{7}bqdi)_2]Cl$[24a] showed distorted tetrahedral geometry around the metal with an interplanar angle of 84.6(4)°.

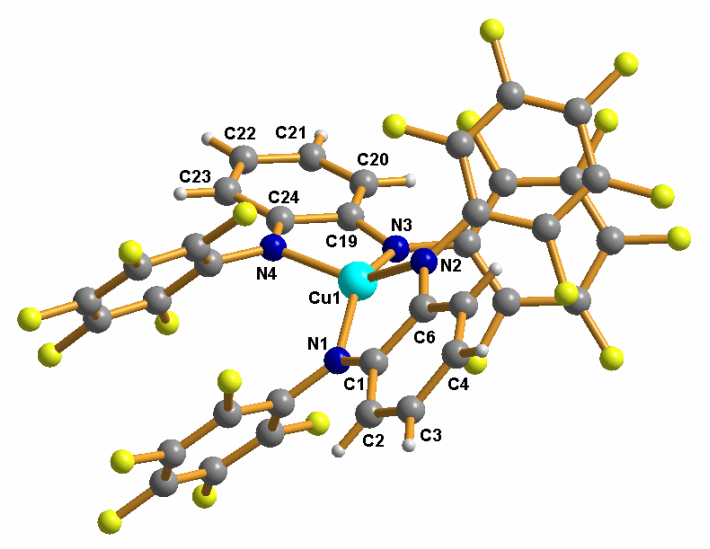

Figure 7. The molecular structure of copper complex **4**.

To the best of our knowledge complex **5** represents the first structurally characterized four-coordinated iron complex with two *o*-phenylenediamine derived ligands (Fig. 8). Very recently, Chlopek et al.[36] have reported the synthesis of a diamagnetic dimer $[Fe^{III}(^{5}sbqdi)(^{5}pda)]_2$, but no crystallographic data were reported. The molecular structure of **5** differs significantly from those of complexes **1**–**4**. Following the trend observed for the cobalt complex **3**, the formal C–C single bonds become shorter while simultaneously the formal double bonds C=C and C=N become longer. These effects in the crystal structure of **5** are more distinct than those of the cobalt complex **3**.

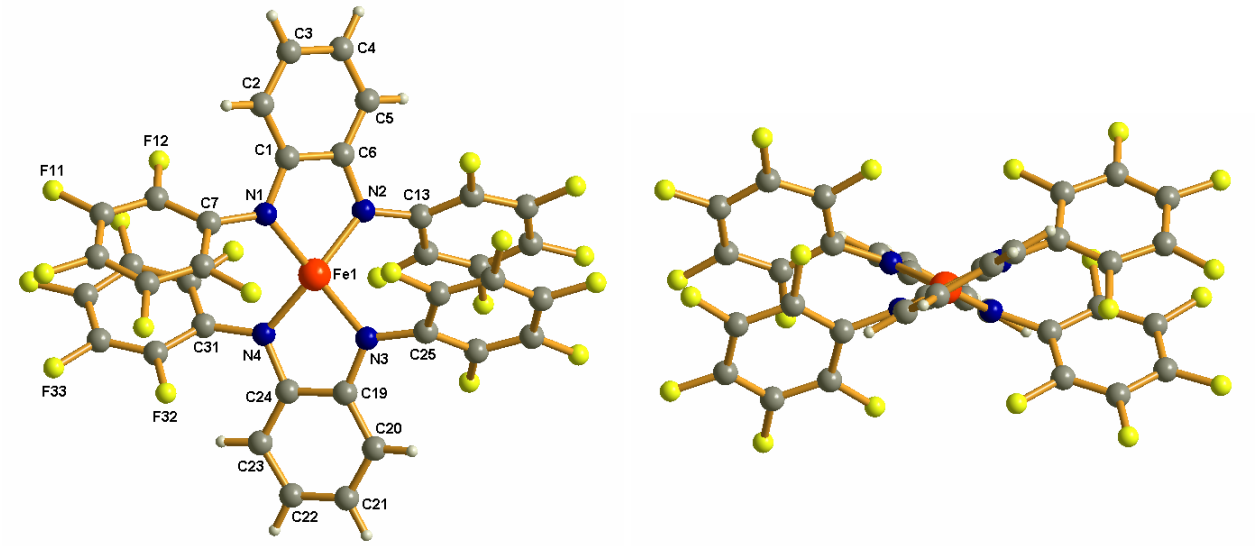

Figure 8. The molecular structure of iron complex **5**.

The bond distance patterns of the two chelated ligands are the same within the limits of the standard deviation. The C–C bonds are found at av. 1.406(9) Å (1.422(6) Å in the nickel complex **1**), the formal double bonds C=C and C=N are av. 1.381(9) and av. 1.391(8) Å, respectively

(1.359(6) and 1.357(5) Å in **1**). While the assignment of integer oxidation states of the ligands in the cobalt complex **3** is difficult (*vide supra*), we have a better access to the oxidation states of the ligands in **5**: All bond lengths in **5** are right in between those in known $(pda)^{2-}$ and $(sbqdi)^{1-}$ structures (see Fig. 2). The iron complex **5** thus contains both types of the ligand, $(^{F}sbqdi)^{1-}$ and $(^{F}pda)^{2-}$, and the equivalence of the two ligands in the crystal structure may be rationalized as electron delocalization over both ligands. According to electroneutrality of the complex we then assign the oxidation state of +III to Fe (d^5 electronic configuration).

The iron complex **5** shows twisted geometry around the metal center, which would be compatible with a high-spin configuration. The dihedral angle between the two NCCN planes of 54.0(2)° is close to that of complexes **1**, **3** or **4**. Two pairs of C_6F_5 rings in *syn* positions are nearly coplanar to each other, forming dihedral angles of 2.0(3) and 4.1(3)°. The interplanar distances between two pairs of C_6F_5 rings are 3.22 and 3.26 Å.

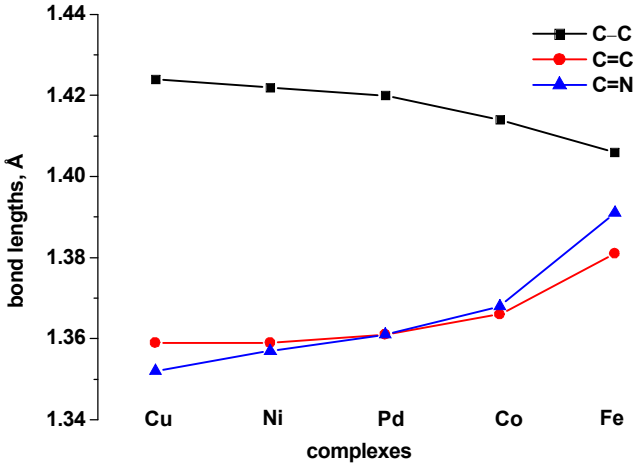

Figure 9. Characteristic averaged bond lengths in the complexes $[M(BPPD)_2]$: formally C–C bonds (black), C=C bonds (red), and C=N bonds (blue).

Summarizing the structural results, the complexes **1**–**5** contain pairs of H_2BPPD derived ligands which are largely equivalent within each complex. In complexes **1**, **2** and **4**, the oxidation state of both ligands was unambiguously determined to be –1, which renders these complexes to be described as $[Ni^{II}(^{F}sbqdi)_2]$ (**1**), $[Pd^{II}(^{F}sbqdi)_2]$ (**2**) and $[Cu^{II}(^{F}sbqdi)_2]$ (**4**). In the iron complex **5**, the bond lengths differ significantly from the corresponding distances of the above mentioned complexes (Fig. 9). Complex **5** is thus best described as $[Fe^{III}(^{F}sbqdi)(^{F}pda)]$, behaving as a Class III mixed-valence system with electron delocalization over both ligands: $[Fe^{III}(^{F}sbqdi)(^{F}pda)] \leftrightarrow [Fe^{III}(^{F}pda)(^{F}sbqdi)]$. The bond parameters of the cobalt complex **3** display intermediate values between those of complex **1** and **5** (Fig. 9), which renders an assignment of integer oxidation states most difficult. The distortion from square-planar coordination geometry is obviously the result of repulsion between the C_6F_5 moieties, favoring the assumed high-spin configurations in **3** and **5**. The

palladium complex **2** experiences less distortion from planarity as a result of longer M–N distances in comparison with those involving the first row transition elements (Table 3).

Table 3. Dihedral angles ω [°] between NCCN planes of the ligands in [M(BPPD)$_2$] complexes **1**–**5**.

Complex	**1**	**2**	**3**	**4**	**5**
Metal	Ni	Pd	Co	Cu	Fe
ω, °	53.7(1)	22.4(2)	54.0(1)	53.9(1)	54.0(2)

Spectroelectrochemistry, EPR and Magnetism. *(in collabor. with Prof. W. Kaim[37], Stuttgart)*

The oxidation state assignments based on the structural results could be confirmed and specified using additional information from electrochemistry, spectroscopy (UV-vis-NIR, EPR), and magnetism. Certain neighboring oxidation states of the compounds **1** – **4** were studied by means of spectroelectrochemistry (UV-vis-NIR and EPR coupled with CV). Such investigations of the iron complex **5** were difficult because of its high sensitivity in solution. Representative EPR and UV-vis-NIR spectra from spectroelectrochemical measurements are shown in Figures 10 – 17, whereas Tables 4 and 5 summarize redox potentials and absorption data, respectively.

All four compounds **1** – **4** could be reversibly reduced in two one-electron steps under cyclic voltammetry conditions. The first oxidation processes were irreversible in case of **1**, **3** and **4**, but reversible in case of the more planar palladium complex **2**. The first and the second reduction potentials are remarkably similar (Table 4) that is a first indication for ligand-based processes. Much less negative reduction potentials for **1** – **4** are observed compared to the previously reported ^{4}H$_2$pda and ^{5}H$_2$pda analogues.[5] In the first approximation this can be ascribed to stabilization of the LUMO by electron withdrawing *N*-C$_6$F$_5$ groups.[38] Irreversibility of the oxidation processes is in accord with our unsuccessful attempts to generate cationic complexes chemically.[26] Oxidation of **1** and **3** with AgOTf and PhIO, respectively, led to decomposition of the complexes and isolation of phenazine derivatives as isomers of oxidized ligand (^{F}bqdi)^0.[26]

Table 4. Redox potentials from cyclic voltammetry[a]

Comp.	$E_{1/2}$(red1)[b]	$E_{1/2}$(red2)[b]	$E_{1/2}$(ox1)
1	–0.48	–1.00	0.56[c]
2	–0.42	–1.01	0.61
3	–0.37	–1.06	0.27[c]
4	–0.40	–0.89	0.12[c]

[a] Potentials in V vs. $FeCp_2^{+/0}$; measurements in acetonitrile / 0.1 M Bu_4NPF_6.
[b] Reversible reduction processes (ΔE = 60 – 80 mV).
[c] Anodic peak potentials for irreversible oxidation.

Starting with the electronic spectra of the diamagnetic nickel complex **1**, it shows a typical intense absorption band in the near infrared[5,8] which is assigned to a ligand-to-ligand charge transfer (LLCT) transition.

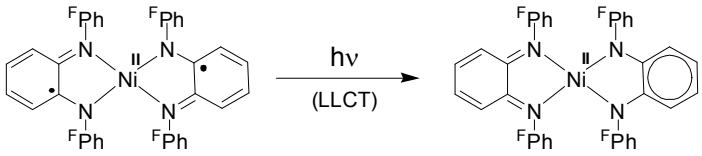

Such spin and dipole allowed transitions have been discussed in detail for planar singlet diradical compounds ([M^{II}(^{4}sbqdi)$_2$], [M^{II}(^{5}sbqdi)$_2$], M = Ni, Pd, Pt)[5,8] where the metal d^8 center ensures interaction between redox-active *o*-benzosemiquinonediiminato(1–) ligands. Apparently, this type of NIR band occurs also for system **1**, which exhibits considerable twisting between the *o*-benzosemiquinonediiminato(1–) backbones. However, the intensity of this band (1.5×10^4 $dm^3 \cdot cm^{-1} \cdot mol^{-1}$) is lower compared to the square planar complexes reported by Wieghardt ($4.1 – 5.8 \times 10^4$ $dm^3 \cdot cm^{-1} \cdot mol^{-1}$).[5]

It was possible to study the reversible one-electron reduction **1** → **1**$^-$ under the conditions of OTTLE spectroelectrochemistry, that is requiring stability for at least 1 min. A broad band at lower energies (Fig. 10, Tab. 5) was produced upon reduction. This was assigned to a ligand-to-ligand intervalence charge transfer (LLIVCT) transition between the dianionic and the monoanionic forms of the ligand.[5,8]

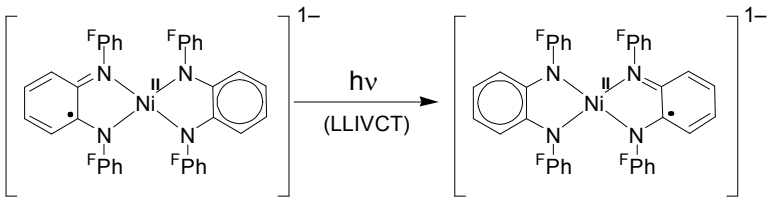

Although the structure of this mixed-valence (with respect to the redox ligands) intermediate [Ni^{II}(^{F}pda)(^{F}sbqdi)]$^-$ is not known, we suppose that it cannot become planar because of steric reasons. EPR experiments showed only a single line centered at $g = 1.97$ which broadens but does not show individual g components at 110 K. Such a signal would still be compatible with a semiquinone-type radical in the monoanion **1**$^-$. The deviation from $g = 2$ to lower values indicates low-lying excited states with non-zero angular momentum[39] which may be attributed to interactions of the radical ligand with non-planar nickel(II) close to the low-spin/high-spin transition (LS is preferred in planar, but HS – in tetrahedral complexes) and/or the dianionic co-ligand.

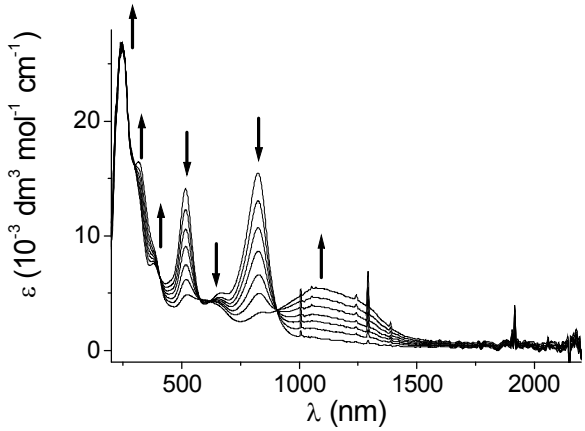

Figure 10. UV-vis-NIR spectroelectrochemical response of the transition **1** → **1**$^{-}$ in CH_3CN/0.1 M Bu_4NPF_6.

Table 5. Absorption data[a] from spectroelectrochemistry[b]

Compound	$\lambda_{max}(\varepsilon)$[a]
1	824(15400), 660(5000), 515(14100), 378(7600), 303sh, 246(26200)
1^{-}	1060(5500), 830sh, 660sh, 524(4900), 387(8800), 318(16500), 244(26900)
2	895(14200), 688sh, 572sh, 335(4900), 265(14600), 232(14400)
2^{-}	1483(10500), 895(1100), 666(1700), 390(2800), 254sh, 238(18800)
2^{2-}	1486(5100), 667(1000), 613sh, 558sh, 370(4300), 253sh, 240(19900)
2^{+}	1830(7700), 1332sh, 907(1000), 485(4800), 295(11100), 229(13800)
3	1030(3900), 778(10700), 468sh, 425(10800), 310(17800), 254sh, 225(33500)
3^{-}	2050(1900), 755sh, 667(5700), 478sh, 320(21900), 251sh, 232(36700)
3^{2-}	680(1300), 340(27500), 233(36200)
4	1150(5500), 905(3600), 680sh, 600(8300), 515sh, 369(17400), 263sh, 237(21400)
4^{-}	1975(3900), 1151(1900), 705(8100), 570(6100), 373(18500), 268sh, 237(20400)
4^{+}	997(9200), 713(9500), 587(10100), 510(9000), 407(11200), 236(26800)

[a] Wavelengths in nm, molar extinction coefficients in $dm^3\ mol^{-1}\ cm^{-1}$.
[b] In CH_3CN/0.1 M Bu_4NPF_6, except for **4**^{n} (CH_2Cl_2/0.1 M Bu_4NPF_6).

The less twisted (*vide supra*) palladium complex **2** also exhibits diamagnetism and an LLCT absorption band at 895 nm (Fig. 11). One-electron reduction results in formation of a radical species with g_{iso} = 2.020. The rhombic signal with $g_1 - g_3$ = 0.103 is observed on temperature lowering to 110 K (Fig. 12). Significant *g* splitting is ascribed to the much higher spin-orbit coupling constant of Pd^{II} (1600 cm^{-1}) vs. Ni^{II} (630 cm^{-1})[40] and has been observed similarly for square planar *o*-benzosemiquinonemono- and diiminato(1–) complexes of Pd.[5,41] The observed anisotropy indicates that the SOMO in **2**$^{-}$ has some metal character.[5]

Since the palladium complex **2** is much more planar compared to the nickel complex **1**, better π/π overlap is expected for **2**. As a consequence the LLIVCT transition for [Pd(^{F}pda)(^{F}sbqdi)]$^{-}$ occurs as an intense band at about 1500 nm. On further reduction **2**$^{-}$ → **2**$^{2-}$

LLIVCT absorption band diminishes (Fig. 11). One-electron oxidation **2** → **2**$^{+}$ occurs reversibly in the spectroelectrochemical experiment and results in the appearance of an intense long-wavelength band at about 1830 nm. This band is assigned to an LLIVCT process involving the monoanionic *o*-benzosemiquinonediiminato(1–) radical donor and the neutral *o*-benzoquinonediimine acceptor in [Pd(^{F}sbqdi)(^{F}bqdi)]$^{+}$.

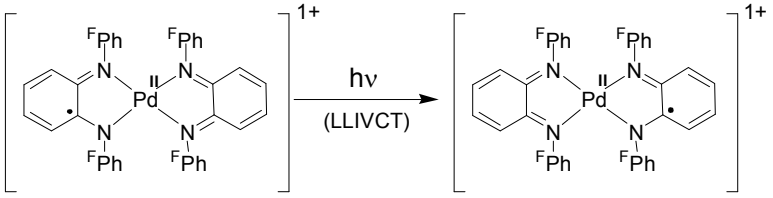

Such NIR bands and their assignment were described recently in a similar way for corresponding *o*-benzosemiquinonemonoiminato(1–) complexes of palladium(II).[41]

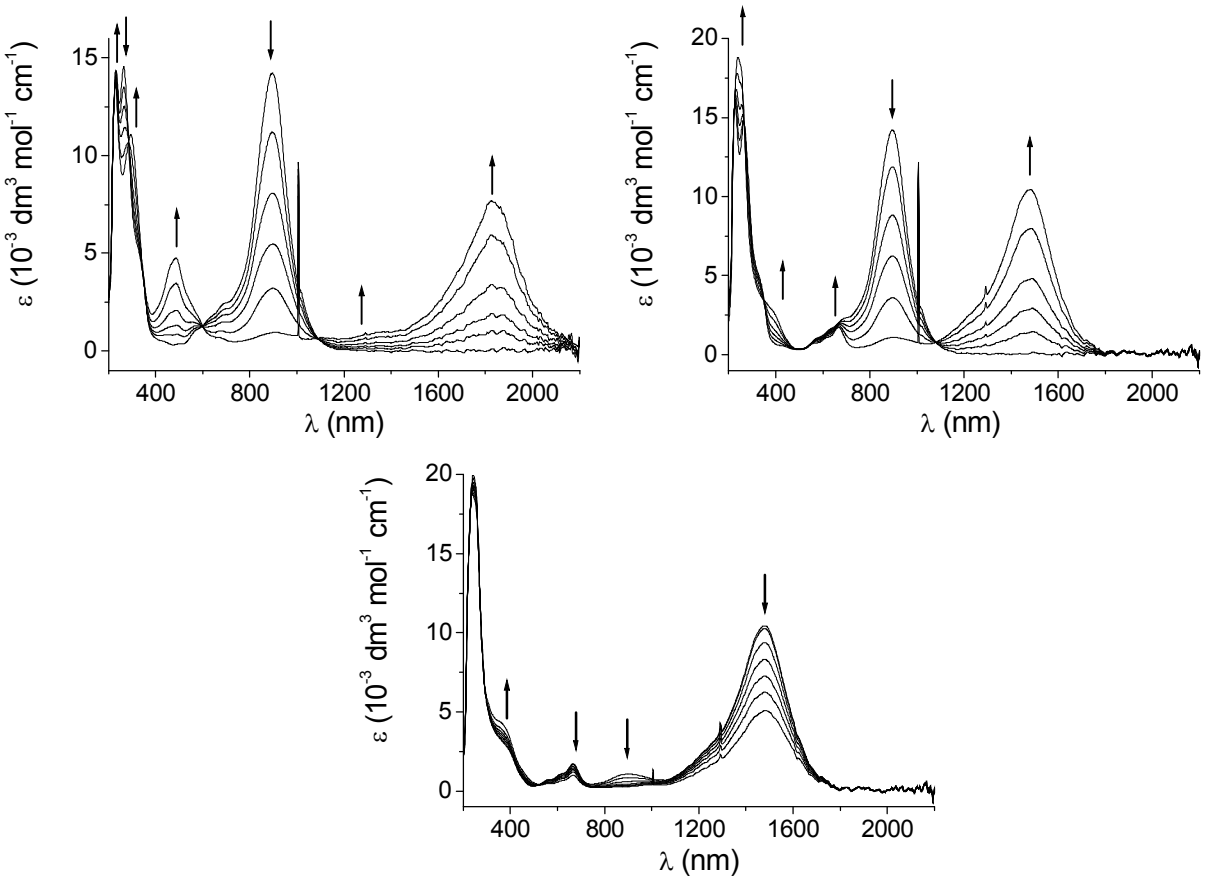

Figure 11. UV-vis-NIR spectroelectrochemical response of the transitions **2** → **2**$^{+}$ (top left), **2** → **2**$^{-}$ (top right), **2**$^{-}$ → **2**$^{2-}$ (bottom) in CH_3CN/0.1 M Bu_4NPF_6.

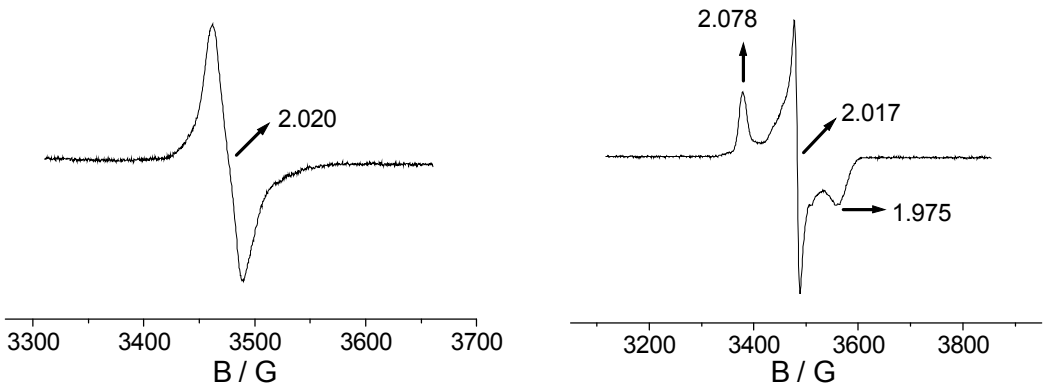

Figure 12. EPR spectra of *in situ* generated $\mathbf{2}^{-}$ in CH_3CN/0.1 M Bu_4NPF_6 at 298 K (left) and 110 K (right).

The cobalt complex **3** is paramagnetic with slightly temperature-dependent effective magnetic moment (μ_{eff}) decreasing from 2.67 μ_B at 300 K to 2.54 μ_B measured at 6 K (Fig. 13). At temperatures below 6 K the abrupt decreasing of μ_{eff} is observed that could be explained by the presence of intermolecular antiferromagnetic interactions in the solid **3**. Both electronic structures proposed on the base of bond lengths analysis: $[Co^{II}(^{F}sbqdi)_2] \leftrightarrow [Co^{III}(^{F}sbqdi)(^{F}pda)]$ are evidently odd-electron systems. The behavior of μ_{eff} observed for **3** can be ascribed to the strong antiferromagnetic coupling within the system resulting in the doublet ground state (S = 1/2) populated at the whole temperature range (2 – 300 K). The strong deviation of μ_{eff} from the spin-only value 1.73 μ_B is probably due to a large orbital momentum or the strong mixing of the ground state with low lying excited states with non-zero orbital momentum by spin-orbit coupling. The large orbital momentum together with the results of EPR spectroscopy (*vide infra*) are indicative of the predominantly metal-located spin density.

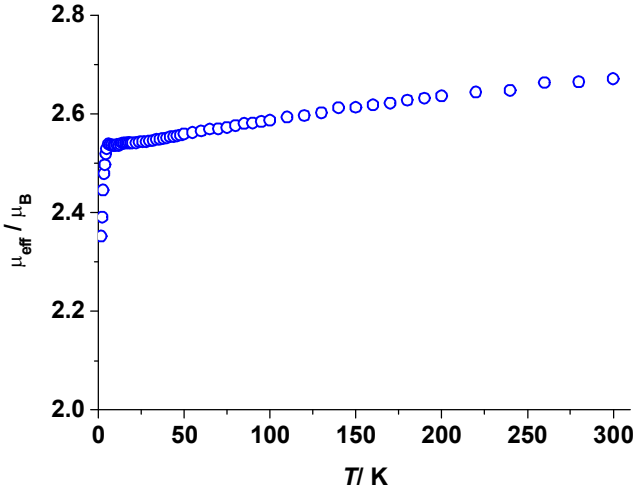

Figure 13. Temperature dependence of the effective magnetic moment of **3** measured at the field of 1 T.

This allows us to propose the following electronic structures for the ground state of **3**: a high-spin Co^{II} coupled antiferromagnetically with two radical ligands (↓/↑↑↑/↓), a low-spin Co^{II}

with two radicals coupled antiferromagnetically with each other (↑/↑/↓), and a high-spin Co^{III} coupled antiferromagnetically with one radical ligand (↓/↑↑/0). The case of the low spin Co^{II} antiferromagnetically coupled to the both radical ligands (↑/↓/↑) is discarded since it would lead to the organic-radical species which would be in contradiction to the result obtained from ERP spectroscopy. The situation (↑/↑/↓) can be discarded as well, since it would require the strong antiferromagnetic coupling between the two remote ligands that seems to be unlikely in the highly twisted arrangement of **3** (*vide infra*). The two structures remain: Co^{II} in (↓/↑↑↑/↓) and Co^{III} in (↓/↑↑/0), between which we cannot choose.

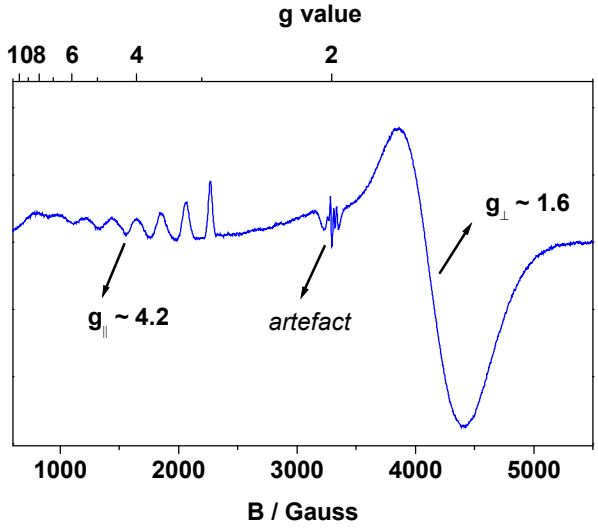

Figure 14. X-band EPR spectrum of **3** in frozen $CHCl_3$ measured at 10 K. (*Dr. Burghaus, Marburg*)

The ground state of **3** can be effectively probed by EPR spectroscopy at cryogenic temperatures. The large anisotropy of the *g* tensor and the well resolved hyperfine structure at $g_{\|}$ (^{59}Co, $I = 7/2$) are indicative of the system with $S = 1/2$ and the spin density located predominantly on the metal d-orbitals (Fig. 14). A very similar EPR spectrum is observed for $[Co^{II}(^{F}DAD)_2]$.[33]

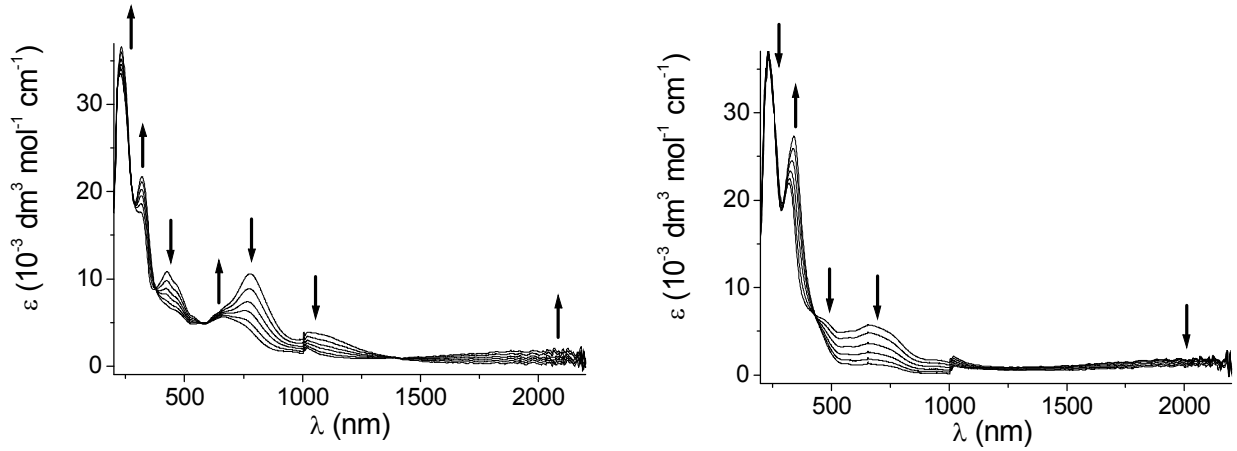

Figure 15. UV-vis-NIR spectroelectrochemical response of the transitions **3** → **3**$^{-}$ (top) and **3**$^{-}$ → **3**$^{2-}$ (bottom) in CH_3CN/0.1 M Bu_4NPF_6.

The reduction of the cobalt complex **3** produces a long-wavelength absorption at 2050 nm in the first step, assigned to the LLIVCT transition. On second reduction this feature disappears completely (Fig. 15).

According to the bond lengths analysis the paramagnetic copper complex **4** is a three electron system. The effective magnetic moment of **4** is virtually temperature-independent in the temperature range 50 – 300 K being 1.7 μ_B (Fig. 16). This value is in excellent agreement with the spin-only value of 1.73 μ_B for one unpaired electron. This indicates a strong antiferromagnetic coupling within the system and totally non-populated quartet state. According to the results of EPR spectroscopy the spin density is predominantly located on the ligand and not on the metal.

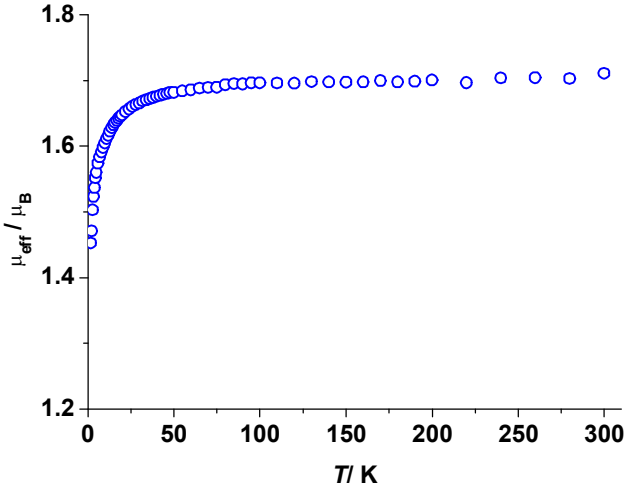

Figure 16. Temperature dependence of the effective magnetic moment of **4** measured at the field of 1 T.

Thus, the strong antiferromagnetic coupling between the magnetic orbital of Cu^{II} and those of radical ligands is expected ($|J_{Cu–R}| >> 200$ cm^{-1}). Because of the twisted geometry, the remote ligands couples very likely antiferromagnetically, but much weaker compared to the antiferromagnetic coupling between the metal and the radical ligand ($|J_{R–R}| << |J_{Cu–R}|$). This results differ from those obtained for Cu^{II} complexes with *N*,*O*-donor *o*-benzosemiquinonemonoiminato(1–) ligands in square-planar[11] or twisted[35] geometries, where dominating antiferromagnetic coupling between the remote ligands[11] or comparable values of $J_{R–R}$ and $J_{Cu–R}$ leading to the population of excited states[35] were reported.

With decreasing temperature below 50 K μ_{eff} decreases gradually and reaches the value of 1.45 μ_B at 1.8 K. Such behavior can be ascribed to antiferromagnetic intermolecular interactions in solid **4**. In fact, the magnetic susceptibility data can be readily simulated with classical Currie-Weiss equation giving a negative Weiss constant.

The alternative arrangements of the three spins as ↑/↓/↑ or ↑/↑/↓ (L–Cu–L sequence) to obtain an $S = 1/2$ ground state can be best probed by means of EPR spectroscopy. The first model

(↑/↓/↑) would give the ligand-based spin, whereas the second spin pattern (↑/↑/↓) would result in metal-based unpaired spin.[33,35]

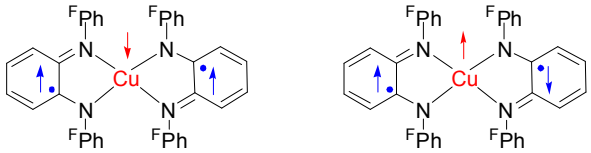

The high-frequency EPR spectrum in Figure 17 clearly shows that the ↑/↓/↑ situation with predominantly ligand-centered spin is realized. This is ascribed to the less efficient antiferromagnetic coupling between two remote radical ligands in highly twisted system compared to the square planar complexes.[35] The $g < 2$ situation signifies low-lying excited states in agreement with previous observations.[35]

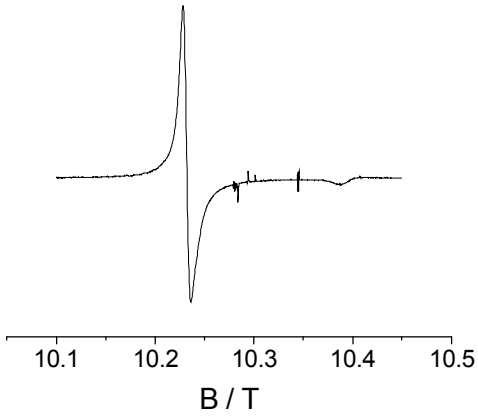

Figure 17. EPR spectrum of **4** at 285 GHz in CH_2Cl_2 : toluene = 4 : 1 at 5 K; $g_\perp = 1.989$, $g_\parallel = 1.959$.

In agreement with recently reported observations on a twisted bis(*o*-benzosemiquinonemonoiminato)copper(II) system[35a] the reduction **4** → **4**$^-$ produces a long-wavelength band at about 2000 nm (Fig. 18). This band was assigned to LLIVCT transition.

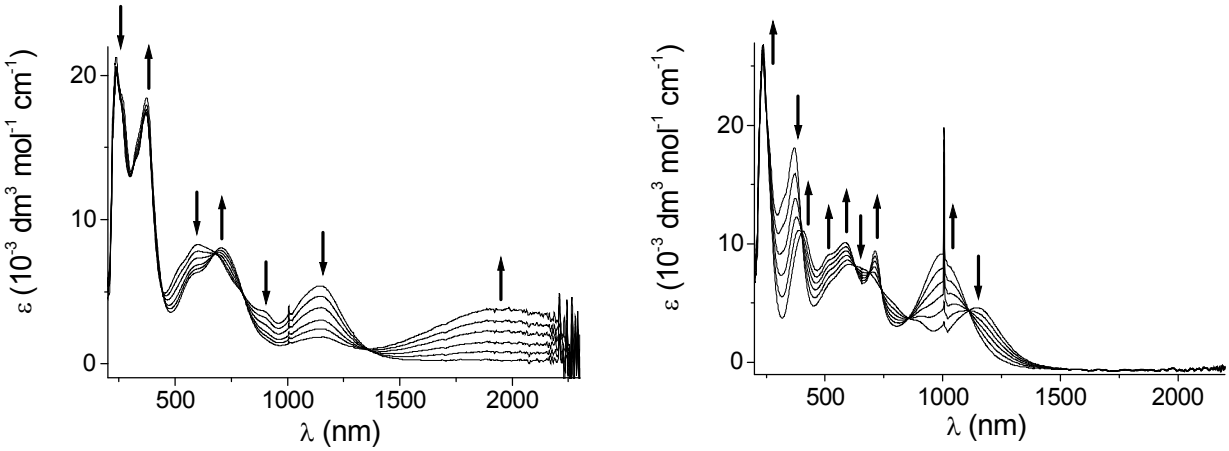

Figure 18. UV-vis-NIR spectroelectrochemical response of the transitions **4** → **4**$^-$ (left) and **4** → **4**$^+$ (right) in CH_3CN/0.1 M Bu_4NPF_6.

On the other hand, one-electron oxidation **4** → **4**$^{+}$ results in appearance of a higher energy NIR band, assigned to the LLIVCT transition between the *o*-benzosemiquinonediiminato(1–) and the *o*-benzoquinonediimine ligands in a less twisted configuration because of possible Cu^{II} contributions; higher intensity and energy are the result from enhanced overlap.

Conclusions.

Employing the bulky *N*,*N*′-bis(pentafluorophenyl)-*o*-phenylenediamine (H_2BPPD) we succeeded in the synthesis of the five homoleptic complexes [M(BPPD)$_2$] (M = Fe, Co, Ni, Pd, Cu) showing strongly (Fe, Co, Ni, Cu) or moderately (Pd) twisted geometry around the metal centers. The twisted geometry of the complexes is defined by repulsion forces between the two pairs of the perfluorinated rings.

Oxidation state of redox active ligands and the metals were derived from single crystal X-ray crystallography at low temperatures by means of bond lengths analysis. The Ni (**1**), Pd (**2**), and Cu (**4**) complexes comprise two radical monoanions [^{F}sbqdi]$^{-}$ and divalent metals, whereas the Fe complex (**5**) consists of the radical [^{F}sbqdi]$^{-}$, the closed-shell [pda]$^{2-}$ and a ferric center. The oxidation state pattern in the Co complex (**3**) may be described by either [Co^{II}(^{F}sbqdi)$_2$] or class III mixed-valence [Co^{III}(^{F}sbqdi)(^{F}pda)] ↔ [Co^{III}(^{F}pda)(^{F}sbqdi)].

Electronic structures of the complexes **1**–**4** and of some of their cationic and/or anionic neighboring redox states were probed using EPR and UV-vis-NIR spectroelectrochemistry. Twisted geometry of the complexes results in considerable changes of their electronic structures compared to the strictly planar *o*-phenylenediamine derived complexes reported previously. Such a distorted ligand arrangement may lead to the high-spin state of Ni^{II}, Fe^{III}, and Co^{II}/Co^{III} in the corresponding complexes. Furthermore, the superexchange interactions between the remote radical ligands are not as effective as in the planar complexes. This leads, for example, to the ligand-centered spin ground state in Cu^{II} complex, and not to the metal-centered spin as in the planar analogue.

The electron withdrawing *N*-C_6F_5 groups considerably stabilize reduced species and destabilize oxidized ones. Much less negative reduction potentials, compared to the known complexes, found for complexes **1**–**4**, afford an opportunity for isolation and crystallographic characterization of the doubly reduced species [M(lig)]$^{2-}$ that has never been realized before.

Experimental Part.

The precursor *N,N´*-bis(pentafluorophenyl)-*o*-phenylenediamine (H_2BPPD = $^{F}H_2$pda) was prepared from *o*-phenylenediamine and hexafluorobenzene according to a known procedure.[42] *n*-Butyllithium (1.6 M solution in *n*-hexane) was purchased from Aldrich. The anhydrous metal salts $NiCl_2$·DME,[43] $FeCl_2$,[44] and $PdCl_2(SMe_2)_2$[45] were prepared according to the literature procedures. Anhydrous $CoCl_2$ and $CuCl_2$ were obtained by refluxing of $CoCl_2$·nH_2O of $CuCl_2$·nH_2O, respectively, with $SOCl_2$ for several hours followed by removing the volatiles under reduced pressure at 90ºC. All syntheses were performed under a dry, oxygen-free argon atmosphere using standard Schlenk techniques and dry solvents.

Physical Measurements.

High-resolution mass spectra were obtained on a Finnigan MAT 95S mass spectrometer (70 eV, EI). IR spectra were obtained using a Nicolet 510 FT-IR. NMR spectra were recorded at room temperature on a Bruker ARX 200 spectrometer at 200.1 MHz for ^{1}H and at 188.3 MHz for ^{19}F. ^{1}H NMR spectra were referenced (in ppm) to the residual proton signal of $CDCl_3$ (7.26 ppm), ^{19}F NMR spectra were referenced to the external standard $CFCl_3$. $CDCl_3$ was used as solvent in all cases. Abbreviations used are: s = singlet, d = doublet, t = triplet, pst = pseudo-triplet. EPR spectra in the X band were recorded with a Bruker System ESP 300 equipped with a Bruker ER035M gaussmeter and a HP 5350B microwave counter. EPR spectra at 285 GHz were recorded using a multifrequency spectrometer. A Gunn diode operating at 95 GHz and equipped with a third harmonic generator has been used as a radiation source. An InSb bolometer (QMC Instruments) was used for detection. The main magnetic field was provided by a superconducting magnet (Cryogenics Consultant) which generates fields up to 12 T. Owing to different field sweep conditions, the absolute values of the *g* components were obtained by calibrating the precisely measured *g* anisotropy data with the isotropic *g* value from X-band measurements. While this procedure does not account for the temperature dependence of *g*, the values extracted are identical with those obtained using an added standard. The accuracy of *g* values is estimated at ±0.0003. UV-vis-NIR absorption spectra were recorded on J&M TIDAS and Bruins Instruments Omega 10 spectrophotometers. Cyclic voltammetry was carried out in 0.1 M Bu_4NPF_6 solutions using a three-electrode configuration (glassy carbon working electrode, Pt counter electrode, Ag/AgCl reference) and a PAR 273 potentiostat and function generator. The ferrocene/ferrocenium (Fc/Fc^{+}) couple served as internal reference. A two-electrode capillary was used in radical complex generation for X band EPR studies. The magnetic susceptibility measurements were performed on

powder samples using a Quantum Design MPMS XL7 SQUID magnetometer. The data were corrected for the diamagnetic contributions to the molar magnetic susceptibility using Pascal´s constants and for temperature independent paramagnetism.

X-ray Crystallographic Data Collection and Refinement of the Structures.

Dark single crystals of **1 – 5** were coated with inert perfluoropolyether oil, picked up with a glass fibre and mounted in the cold nitrogen stream of a STOE IPDS 2 diffractometer. Intensity data were collected at 193 K (**5**: 130 K) using graphite monochromated Mo-K_α radiation (λ = 0.71073 Å). Data collection was performed by hemisphere runs taking frames at every 1.0° in ω. Final cell constants were obtained from a least squares fit of a subset of several thousand strong reflections. Intensity data of **1** and **2** were corrected using the semiempirical correction routine MulScanAbs.[46] For the other compounds an absorption correction did not improve the quality of the data. There was disordered solvent present in the crystal structures of **1**, **3**, and **4** which could not be modeled successfully. In **1** and **4** the difference electron density has been fitted to the formula sum of one *n*-hexane molecule per complex molecule, in **3** the data set has been modified using the Squeeze[46] routine, and it was assumed that two molecules of THF per complex molecule were present. In **2** four molecules of THF are present per one complex molecule, in **5** one molecule of diethyl ether. All structures have been solved by the direct methods in SHELXS-97[47] (**1** – **4**) or SIR2004[48] (**5**) and refined using the full matrix least squares refinement procedure of SHELXL97.[47] All non-hydrogen atoms were treated anisotropically, H atoms were placed at calculated positions and refined using the riding model with $U_{iso}(H)=1.2U_{eq}(C)$ (**1**, **2**, **4**, **5**). In **3** the positions and isotropic displacement parameters of the non solvent H atoms were refined. Crystallographic data of the compounds are listed in Table 1.

Synthesis of [Ni^{II}(^{F}sbqdi)$_2$] (1).

$^{F}H_2$pda (2.64 g, 6.00 mmol) was dissolved in diethyl ether (50 mL) and the resulting solution was cooled to –50°C. A solution of 1.6 M *n*-BuLi in *n*-hexane (7.5 mL, 12.00 mmol) was added slowly, dropwise at the end, with vigorous stirring. After the mixture was stirred for 15 min, a suspension of anhydrous $NiCl_2$·DME (0.66 g, 3.00 mmol) in diethyl ether (15 mL) was added through a cannula. The yellow color of the reaction mixture changed immediately to red. The mixture was allowed to warm to room temperature and stirred overnight under an atmosphere of argon. The oxidation was accomplished by passing a stream of pure oxygen through the solution for 5 min and stirring the resulting dark-purple suspension for 30 min. Solvents were removed *in vacuo*, the crude product was repeatedly extracted with boiling *n*-hexane from a glass frit to give

dark microcrystals in *n*-hexane solution. The Schlenk flask with crystals was cooled to –80°C, the *n*-hexane solution was decanted, the crystals were washed with cold *n*-pentane and dried *in vacuo*. The yield was 1.86 g (66%). The yield can be increased by adding of 5 g of silica gel (Merck 60) to the residue suspended in toluene (50 mL), stirring for about 20 min, filtering, evaporating the toluene, and washing of the dark-purple microcrystals with cold *n*-pentane. An additional amount of 0.51 g analytically pure complex was thus obtained. Single crystals of **1** suitable for X-ray crystallography were obtained from a THF/*n*-hexane mixture (1:6) by cooling.

Overall yield: 2.37 g (85%).

M.p. 241°C (decomp.).

$C_{36}H_8F_{20}N_4Ni$ (935.14): calcd. C 46.24, H 0.86, N 5.99; found C 45.52, H 0.71, N 6.83.

HRMS (EI): m/z = 933.9765 [M^+, calcd. for $C_{36}H_8F_{20}N_4Ni$ 933.9783].

^1H NMR (200.1 MHz, $CDCl_3$, 300 K): δ = 6.52 – 6.57 (4H, m), 8.12 – 8.20 (4H, m) ppm.

^{19}F NMR (188.3 MHz, $CDCl_3$, 300 K): δ = –162.7 (8F, pst, ^3J=20 Hz, F_{meta}), –156.8 (4F, t, ^3J=20 Hz, F_{para}), –146.6 (8F, d, ^3J=20 Hz, F_{ortho}) ppm.

IR (Nujol): $\tilde{\nu}$ = 516 (m), 600 (m), 737 (s), 771 (m), 802 (m), 831 (w), 876 (m), 1000 (s), 1115 (m), 1165 (s), 1307 (m), 1326 (s), 1349 (m), 1447 (s), 1505 (s), 1586 (w), 1631 (w), 1647 (w), 3061 (w) cm^{-1}.

Synthesis of [Pd^{II}(^{F}sbqdi)$_2$] (2).

^{F}H_2pda (500 mg, 1.136 mmol) was dissolved in diethyl ether (20 mL) and the resulting solution was cooled to –50°C. A solution of 1.6 M *n*-BuLi in *n*-hexane (1.4 mL, 2.240 mmol) was added slowly, dropwise at the end, with vigorous stirring. After the mixture was stirred for 15 min, a suspension of $PdCl_2(SMe_2)_2$ (0.172 g, 0.570 mmol) in THF (10 mL) was added through a cannula. The mixture was allowed to warm to room temperature and stirred overnight under an atmosphere of argon. The oxidation was accomplished by passing a stream of pure oxygen through the solution for 5 min and stirring the resulting grey-blue suspension for 1 h. After solvents were removed *in vacuo*, the mixture was extracted with toluene. The toluene extract was filtered through a layer of SiO_2 (Merck 60) and concentrated by a rotary evaporator. The raw product was recrystallized from a toluene/THF mixture (5:4) to give a sky-blue precipitate that was washed with cold *n*-pentane and dried *in vacuo*. Single crystals of **2** suitable for X-ray crystallography were obtained from a THF/*n*-hexane mixture (1:2) by cooling.

Yield: 188 mg (34%). When $PdCl_2(COD)$ or $PdCl_2(PhCN)_2$ were used instead of $PdCl_2(SMe_2)_2$ the yield was lower.

M.p. 303 – 306°C (decomp.).

$C_{36}H_8F_{20}N_4Pd$ (982.87): calcd. C 43.99, H 0.82, N 5.70; found C 44.88, H 0.86, N 5.95.

HRMS (EI): *m/z* = 981.9475 [M^+, calcd. for $C_{36}H_8F_{20}N_4Pd$ 981.9464].

^1H NMR (200.1 MHz, $CDCl_3$, 300 K): δ = 6.18 – 6.23 (4H, m), 6.71 – 6.76 (4H, m) ppm.

^{19}F NMR (188.3 MHz, $CDCl_3$, 300 K): δ = –162.5 (8F, pst, ^3J=20 Hz, F_{meta}), –155.6 (4F, t, ^3J=20 Hz, F_{para}), –144.1 (8F, d, ^3J=20 Hz, F_{ortho}) ppm.

IR (Nujol): $\tilde{\nu}$ = 498 (m), 597 (s), 643 (w), 699 (m), 713 (w), 728 (s), 738 (m), 771 (w), 800 (m), 823 (m), 887 (w), 928 (m), 995 (s), 1010 (s), 1034 (m), 1117 (m), 1148 (m), 1169 (s), 1288 (s), 1318 (m), 1346 (m), 1445 (s), 1505 (s), 1514 (s), 1533 (m), 1584 (w), 1631 (w), 1647 (w), 3058 (w), 3086 (w) cm^{-1}.

Synthesis of [Co(BPPD)$_2$] (3).

^{F}H$_2$pda (4.48 g, 10.18 mmol) was dissolved in diethyl ether (60 mL) and the resulting solution was cooled to –50°C. A solution of 1.6 M *n*-BuLi in *n*-hexane (12.7 mL, 20.32 mmol) was added slowly, dropwise at the end, with vigorous stirring. After the mixture was stirred for 15 min, a solution of anhydrous $CoCl_2$ (0.6 g, 4.62 mmol) in THF (100 mL) was added through a cannula. The mixture was allowed to warm to room temperature and stirred overnight under an atmosphere of argon. A color change from yellow to orange was observed. The oxidation was accomplished by passing a stream of pure oxygen through the solution for 5 min and stirring the resulting dark-green suspension for 30 min. Solvents were removed *in vacuo*, the raw product was repeatedly extracted with boiling *n*-hexane (100 mL) from a glass frit to give dark microcrystals in *n*-hexane solution. The Schlenk flask with crystals was cooled to –80°C, the *n*-hexane solution was decanted, the crystals were washed with cold *n*-hexane and dried *in vacuo*. Single crystals of **3** suitable for X-ray crystallography were obtained from a THF/*n*-hexane mixture (1:1) by cooling.

Yield: 2.91 g (67%).

M.p. 191°C (decomp.).

$C_{36}H_8F_{20}N_4Co$ (935.39): calcd. C 46.23, H 0.86, N 5.99; found C 46.06, H 0.80, N 6.60.

HRMS (EI): *m/z* = 934.9771 [M^+, calcd. for $C_{36}H_8F_{20}N_4Co$ 934.9762].

IR (Nujol): $\tilde{\nu}$ = 516 (m), 575 (w), 597 (m), 638 (w), 693 (m), 725 (s), 739 (s), 772 (m), 802 (m), 834 (w), 875 (m), 995 (s), 1007 (s), 1116 (m), 1141 (m), 1165 (m), 1278 (m), 1341 (m), 1507 (s), 1587 (w), 1629 (w), 1646 (w), 3063 (w) cm^{-1}.

Synthesis of [Cu^{II}(^{F}sbqdi)$_2$] (4).

^{F}H$_2$pda (1.76 g, 4.00 mmol) was dissolved in diethyl ether (40 mL) and the resulting solution was cooled to –50°C. A solution of 1.6 M *n*-BuLi in *n*-hexane (5.0 mL, 8.00 mmol) was added

slowly, dropwise at the end, with vigorous stirring. After the mixture was stirred for 15 min, a suspension of anhydrous well-ground $CuCl_2$ (0.27g, 2.00 mmol) in THF (15 mL) was added through a cannula. The mixture was allowed to warm to room temperature and stirred for 2 d under an atmosphere of argon. The color of the reaction mixture changed gradually from yellow to green. The oxidation was accomplished by passing a stream of pure oxygen through the solution for 5 min and stirring the resulting dark-blue suspension for 30 min. After solvents were removed *in vacuo*, the mixture was extracted with toluene and the extract was concentrated by a rotary evaporator. The raw product was dissolved in wet ethyl acetate and the resulting solution was quickly filtered through a layer of neutral Al_2O_3 (*Fluka*). The filtrate was concentrated under reduced pressure to yield a dark-blue solid. Recrystallization from a THF/*n*-hexane mixture (1:1) gave a microcrystalline precipitate that was washed with cold *n*-pentane and dried *in vacuo*. Single crystals of **4** suitable for X-ray crystallography were obtained from a THF/*n*-hexane mixture (2:1) by cooling.

Yield: 0.80 g (42%).

M.p. 190°C (decomp.).

$C_{36}H_8F_{20}N_4Cu$ (940.00): calcd. C 46.00, H 0.86, N 5.96; found C 45.38, H 0.70, N 8.22.

HRMS (EI): *m/z* = 938.9722 [M^+, calcd. for $C_{36}H_8F_{20}N_4Cu$ 938.9726].

IR (Nujol): $\tilde{\nu}$ = 482 (m), 591 (m), 639 (w), 736 (s), 749 (m), 803 (m), 833 (m), 856 (m), 872 (m), 995 (s), 1008 (s), 1025 (m), 1119 (m), 1141 (m), 1165 (m), 1298 (m), 1315 (m), 1353 (m), 1420 (m), 1499 (s), 1515 (s), 1585 (w), 1621 (w), 1643 (w) cm^{-1}.

Synthesis of [Fe^{III}(^{F}sbqdi)(^{F}pda)] (5).

$^F H_2$pda (1.38 g, 3.13 mmol) was dissolved in diethyl ether (30 mL) and the resulting solution was cooled to –50°C. A solution of 1.6 M *n*-BuLi in *n*-hexane (3.9 mL, 6.24 mmol) was added slowly, dropwise at the end, with vigorous stirring. After the mixture was stirred for 15 min, a suspension of anhydrous $FeCl_2$ (0.20 g, 1.58 mmol) in THF (15 mL) was added through a cannula. The mixture was allowed to warm to room temperature. The color of the reaction mixture changed form yellow to orange. After the mixture was stirred overnight under an atmosphere of argon, it was cooled to 0°C and a solution of anhydrous $FeCl_3$ (0.51 g, 3.14 mmol) in THF (5 mL) was added with a syringe. The resulting mixture was allowed to warm to room temperature and stirred for 1 h. Solvents were removed *in vacuo*, the residue was extracted with toluene (120 mL) and recrystallized from a Et_2O/toluene mixture (2:1). The air- and moisture-sensitive dark-blue-green crystals were washed with cold *n*-pentane and dried *in vacuo*. Single crystals of **5** suitable for X-ray crystallography were obtained from a toluene/Et_2O mixture (1:2) by cooling.

Yield: 1.02 g (70%).

M.p. 176 – 179°C (decomp.).

$C_{36}H_8F_{20}N_4Fe$ (932.30): calcd. C 46.38, H 0.86, N 6.01; found C 46.00, H 0.57, N 6.96.

HRMS (EI): *m/z* = 931.9816 [M^+, calcd. for $C_{36}H_8F_{20}N_4Fe$ 931.9779].

IR (Nujol): $\tilde{\nu}$ = 534 (m), 575 (m), 593 (m), 701 (m), 737 (s), 775 (m), 804 (m), 837 (m), 878 (m), 997 (s), 1008 (s), 1025 (m), 1060 (w), 1123 (s), 1160 (s), 1235 (s), 1315 (m), 1331 (w), 1502 (s), 1515 (s), 1546 (m), 1580 (w), 1631 (w), 1646 (w), 3057 (w) cm^{-1}.

Synthesis of $(AsPh_4)_2[Co^{II}(^{F}pda)_2]$.

Solution of *n*-BuLi in *n*-hexane (0.85 mL, 1.6 M, 1.36 mmol) was added to the solution of $^{F}H_2pda$ (300 mg, 0.68 mmol) in THF at –60ºC. After the reaction mixture was stirred for 10 min, a suspension of $CoCl_2$ (44 mg, 0.34 mmol) in THF was added. The resulting mixture was stirred for 3 h at room temperature, and $[AsPh_4]Cl$ (285 mg, 0.68 mmol) suspended in THF was added. After the mixture was kept for a night at +5ºC, the large bright-orange crystals of the target salt were collected. The salt is extremely sensitive towards both water and oxygen. Unfortunately, the large crystals obtained from the reaction mixture were of bad quality, presumably twinned. This compound was not analyzed further.

References.

[1] (a) Ward, M. D.; McCleverty, J. A. *J. Chem. Soc., Dalton Trans.* **2002**, 275–288. (b) Vlček, Jr. A. *Coord. Chem. Rev.* **2002**, *230*, 225–242. (c) Chaudhuri, P.; Wieghardt, K. *Prog. Inorg. Chem.* **2001**, *50*, 151–216. (d) Lever, A. B. P.; Gorelsky, S. I. *Structure and Bonding (Berlin)* **2004**, *107*, 77–114. (e) Pierpont, C. G. *Coord. Chem. Rev.* **2001**, *216–217*, 99–125. (f) Kaim, W.; Schwederski, B. *Pure Appl. Chem.* **2004**, *76*, 351–364.

[2] Mederos, A.; Domínguez, S.; Hernández-Molina, R.; Sanchiz, J.; Brito, F. *Coord. Chem. Rev.* **1999**, *193–195*, 913–939.

[3] Balch, A. L.; Holm, R. H. *J. Am. Chem. Soc.* **1966**, *88*, 5201–5209.

[4] Stiefel, E. I.; Waters, J. H.; Billig, E.; Gray, H. B. *J. Am. Chem. Soc.* **1965**, *87*, 3016–3017.

[5] Herebian, D.; Bothe, E.; Neese, F.; Weyhermüller, T.; Wieghardt, K. *J. Am. Chem. Soc.* **2003**, *125*, 9116–9128.

[6] Bill, E.; Bothe, E.; Chaudhuri, P.; Chlopek, K.; Herebian, D.; Kokatam, S.; Ray, K.; Weyhermüller, T.; Neese, F.; Wieghardt, K. *Chem. Eur. J.* **2005**, *11*, 204–224.

[7] (a) Reshetnikov, A. V.; Talismanova, M. O.; Sidorov A. A.; Nefedov, S. E.; Eremenko, I. L.; Moiseev, I. I. *Russ. Chem. Bull., Int. Ed.* **2001**, *50*, 142–146. (b) Talismanova, M. O.; Fomina, I. G.; Sidorov, A. A.; Aleksandrov, G. G.; Berberova, N. T.; Okhlobystin, A. O.; Shinkar', E. V.; Golovaneva, I. F.; Eremenko, I. L.; Moiseev, I. I. *Russ. Chem. Bull., Int. Ed.* **2003**, *52*, 2701–2706. (c) Fomina, I. G.; Sidorov, A. A.; Aleksandrov, G. G.; Nefedov, S. E.; Eremenko, I. L.; Moiseev, I. I. *J. Organomet. Chem.* **2001**, *636*, 157–163.

[8] (a) Bachler, V.; Olbrich, G.; Neese, F.; Wieghardt, K. *Inorg. Chem.* **2002**, *41*, 4179–4193. (b) Herebian, D.; Wieghardt, K. E.; Neese, F. *J. Am. Chem. Soc.* **2003**, *125*, 10997–11005.

[9] Peng, S.-M.; Chen, C.-T.; Liaw, D.-S.; Chen, C.-I; Wang, Y. *Inorg. Chim. Acta* **1985**, *101*, L31–L33.

[10] We use the abbreviation "lig" for doubly deprotonated forms of *o*-phenylenediamine when the ligand oxidation state is not assigned or doubtful.

[11] Chaudhuri, P.; Verani, C. N.; Bill, E.; Bothe, E.; Weyhermüller, T.; Wieghardt, K. *J. Am. Chem. Soc.* **2001**, *123*, 2213–2223.

[12] Bandoli, G.; Gerber, T. I. A.; Perils, J.; du Preez, J. G. H. *Inorg. Chim. Acta* **1998**, *278*, 96–100.

[13] Tabernero, V.; Cuenca, T.; Herdtweck, E. *Eur. J. Inorg. Chem.* **2004**, 3154–3162.

[14] Darensbourg, D. J.; Klausmeyer, K. K.; Reibenspies, J. H. *Inorg. Chem.* **1996**, *35*, 1535–1539.

[15] Cheng, H.-Y.; Lin, C.-C.; Tzeng, B.-C.; Peng, S.-M. *J. Chin. Chem. Soc.* **1994**, *41*, 775–778.

[16] Cheng, P.-H.; Cheng, H.-Y.; Lin, C.-C.; Peng, S.-M. *Inorg. Chim. Acta* **1990**, *169*, 19–21.

[17] Nèmeth, S.; Simandi, L. I.; Argay, G.; Kálman, A. *Inorg. Chim. Acta* **1989**, *166*, 31–33.

[18] Christoph, G. G.; Goedken, V. L. *J. Am. Chem. Soc.* **1973**, *95*, 3869–3875.

[19] Rall, J.; Stange, A. F.; Hübler, K.; Kaim, W. *Angew. Chem., Int. Ed.* **1998**, *37*, 2681–2682.

[20] Venegas-Yazigi, D.; Mizra, H.; Lever, A. B. P.; Lough, A. J.; Costamagna, J.; Latorre, R. *Acta Cryst.* **2000**, *C56*, e281–e282.

[21] Venegas-Yazigi, D.; Mizra, H.; Lever, A. B. P.; Lough, A. J.; Costamagna, J.; Vega, A.; Latorre, R. *Acta. Cryst.* **2000**, *C56*, e245–e246.

[22] Jüstel, T.; Bendix, J.; Metzler-Nolte, N.; Weyhermüller T.; Nuber, B.; Wieghardt, K. *Inorg. Chem.* **1998**, *37*, 35–43.

[23] Hall, G. S.; Soderberg, R. H. *Inorg. Chem.* **1968**, *7*, 2300–2303.

[24] (a) Cheng, H.-Y.; Tzeng, B.-C.; Peng, S.-M. *Bull. Inst. Chem. Acad. Sin.* **1994**, *41*, 51–60. (b) Cheng, H.-Y.; Cheng, P.-H.; Lee, C.-F.; Peng, S.-M. *Inorg. Chim. Acta* **1991**, *181*, 145–147.

[25] Within complexes the abbreviation "BPPD" is used for the doubly deprotonated form of H_2BPPD with undetermined oxidation state, while $(^{F}pda)^{2-}$, $(^{F}sbqdi)^{1-}$ and $(^{F}bqdi)^{0}$ are BPPD-based ligands of known oxidation state.

[26] Khusniyarov, M. M.; Harms, K.; Sundermeyer, J. *J. Fluorine Chem.* **2006**, *127,* 200–204; Chapter II in this Dissertation.

[27] Jörgensen, C. K. *Oxidation Numbers and Oxidation States*, Springer: Heidelberg, Germany, **1969**.

[28] The NCCN plane is defined by the six carbon atoms of the *o*-phenylenediamine ring, the two attached nitrogen atoms, and the metal.

[29] tom Dieck, H.; Svoboda, M.; Greiser, T. *Z. Naturforsch.* **1981**, *36b*, 823–832.

[30] The distances between an aryl C_6 centroid and the corresponding aryl C_6 least-squares plane are reported. If the two least-squares planes are not parallel, then the smaller value is given.

[31] Lorenzo, S.; Lewis, G. R.; Dance, I. *New J. Chem.* **2000**, *24*, 295–304.

[32] Thornberry, M. P.; Slebodnick, C.; Deck, P. A.; Fronczek, F. R. *Organometallics* **2000,** *19*, 5352–5369.

[33] Khusniyarov, M. M.; Harms, K.; Burghaus, O.; Sundermeyer, J. *Eur. J. Inorg. Chem.* **2006**, article online; Chapter III in this Dissertation.

[34] Sun, X.; Chun, H.; Hildenbrand, K.; Bothe, E.; Weyhermüller, T.; Neese, F.; Wieghardt, K. *Inorg. Chem.* **2002**, *41*, 4295–4303.

[35] (a) Ye, S.; Sarkar, B.; Lissner, F.; Schleid, Th.; van Slageren, J.; Fiedler, J.; Kaim, W. *Angew. Chem.* **2005**, *117*, 2140–2143; *Angew. Chem. Int. Ed.* **2005**, *44*, 2103–2106. (b) Ye, S.; Kaim, W.; Niemeyer, M.; Lissner, F.; Schleid, Th.; van Slageren, J.; Fiedler, J.; Sarkar, B.; Duboc, C., manuscript in preparation.

[36] Chlopek, K.; Bill, E.; Weyhermüller, T.; Wieghardt K. *Inorg. Chem.* **2005**, *44*, 7087–7098.

[37] Wolfgang Kaim and Biprajit Sarkar (*Institut für Anorganische Chemie der Universität Stuttgart*, Germany), Joris van Slageren (*1. Physikalisches Institut der Universität Stuttgart*, Germany), Carole Duboc (*Grenoble High Magnetic Field Laboratory*, France), and Jan Fiedler (*J. Heyrovsky-Institute of Physical Chemistry*, Czech Republic) were involved.

[38] Bond, A. M. *Electrochemistry: General Introduction*, in McCleverty, J. A.; Meyer, T. J. (Eds.), *Comprehensive Coordination Chemistry II*, vol. 2, p 197; Elsevier Pergamon: Oxford, **2004**.

[39] Kaim, W. *Coord. Chem. Rev.* **1987**, *76*, 187–235.

[40] Weil, J. A.; Bolton, J. R.; Wertz, J. E. *Electron Paramagnetic Resonance*; Wiley: New York, **1994**, p 532, 533.

[41] Kokatam, S.; Weyhermüller, T.; Bothe, E.; Chaudhuri, P.; Wieghardt, K. *Inorg. Chem.* **2005**, *44*, 3709–3717.

[42] D. Sorokin, Ph.D. Thesis, Philipps-Universität Marburg, **2006**.

[43] L. G. L. Ward, D. M. Paul, *Inorg. Synth.* **1971**, *13*, 154–164.

[44] P. Kovacic, N. O. Brace, *Inorg. Synth.* **1960**, *6*, 172–173.

[45] P. K. Byers, A. J. Canty, H. Jin, D. Kruis, B. A. Markies, J. Boersma, G. van Koten, *Inorg. Synth.* **1998**, *32*, 162–172.

[46] PLATON, A Multipurpose Crystallographic Tool, Utrecht University, Utrecht, The Netherlands, A. L. Spek, **2005**.

[47] SHELX97 – Programs for Crystal Structure Analysis (Release 97-2). G. M. Sheldrick, Institüt für Anorganische Chemie der Universität, Tammanstrasse 4, D-3400 Göttingen, Germany, **1998**.

[48] M. C. Burla, R. Caliandro, M. Camalli, B. Carrozzini, G. L. Cascarano, L. De Caro, C. Giacovazzo, G. Polidori, R. Spagna, *J. Appl. Cryst.* **2005,** *38*, 381–388.

Chapter II

Reactivity of the homoleptic complexes of Fe, Co, Ni, Pd, and Cu with *N*,*N*'-bis(pentafluorophenyl)-*o*-phenylenediamine (H_2BPPD) derived ligands.

Introduction.

In spite of the fact that *o*-phenylenediamine derived complexes of the type $[M(lig)_2]$ were for the first time synthesized by Balch and Holm as early as 1966,[1] information about their reactivity is scarce. The ligand *o*-phenylenediamide is a non-innocent ligand existing in three redox forms displayed in the following scheme:

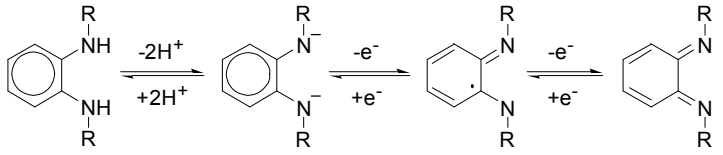

(H_2pda) $(pda)^{2-}$ $(sbqdi)^{1-}$ (bqdi)

(R = H, Alkyl, Aryl)

For the different redox forms of the *o*-phenylenediamide we will use the following abbreviations: $(pda)^{2-}$ for the closed-shell dianion, $(sbqdi)^{1-}$ for the open-shell radical anion, $(bqdi)^0$ for the closed shell neutral ligand. These abbreviations are referred to the parent unsubstituted *o*-phenylenediamine. For substituted *o*-phenylenediamines the upper index will be added (for example, $(^1pda)^{2-}$) with corresponding comments. In addition, abbreviation "lig" will be used within some complexes where several oxidation states of the ligand were reported by different authors, or oxidation state of the ligand is unambiguous or unknown. For more information concerning synthesis and determination of the oxidation states of $[M(lig)_2]$ complexes, one is referred to the Chapter I.

In their pioneering work[1] Balch and Holm showed that the neutral complexes $[M^{II}(sbqdi)_2]$ (M=Ni, Pd, Pt) and $[Co(lig)_2]$ can be electrochemically reduced and oxidized twice. Both reduction and oxidation processes were reported to occur at the ligand preserving the oxidation state of the metal. Moreover these authors were able to oxidize the neutral complexes chemically with one equivalent of iodine and to isolate cationic complexes $[M^{II}(sbqdi)(bqdi)]I$.

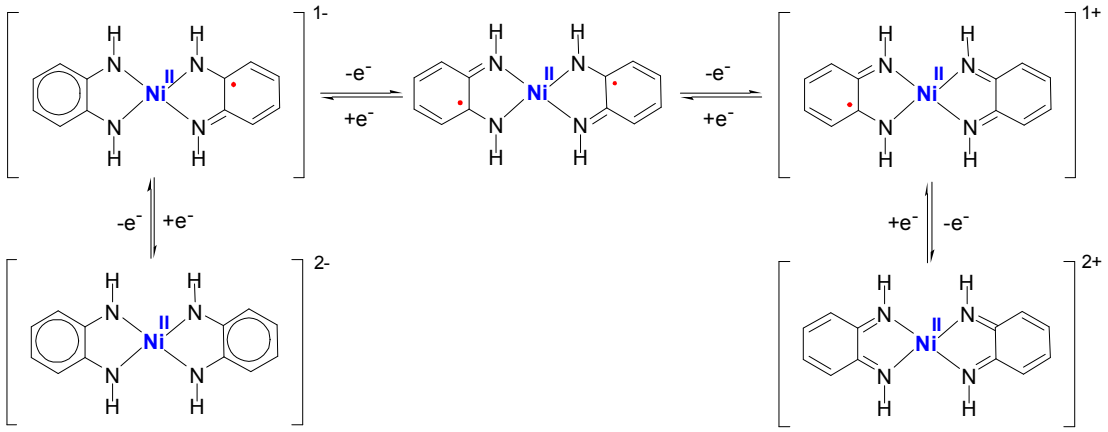

In 1977 Warren reported synthesis and properties of some new complexes of cobalt, iron and ruthenium with *o*-phenylenediamine derived ligand.[2] It was shown that ligand exchange can occur. For example $[Co(lig)_3](PF_6)$ reacts with triphenylphosphine in dichloromethane giving $[Co(lig)_2(PPh_3)](PF_6)$. Later it was established that the third ligand in $[Co(lig)_3]^+$ is only weakly coordinated monodentate ligand.[3] The correct structure of the cation $[Co(lig)_3]^+$ was then reported by Peng et al.[4] On the basis of the bond distances reported before,[3] IR and ^1H NMR spectroscopies they concluded that the cation consists of the two chelated radical anions $(sbqdi)^{1-}$, monodentate H_2pda and cobalt(III) center.

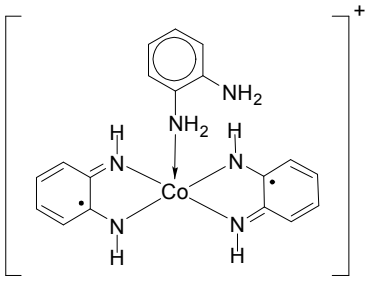

Similar to the cobalt complex the ligand exchange occurs in a corresponding iron complex.[2] Black $[Fe(lig)_3](PF_6)_2$ reacts with sodium iodide in acetone giving $[Fe(lig)_2I]$. In contrast to the cation $[Co(lig)_3]^+$ dication $[Fe(lig)_3]^{2+}$ was shown to consist of the three fully oxidized $(bqdi)^0$ ligands and an iron(II) center.[4]

Miles and Wilson reported the synthesis and investigation of properties of semiconducting metal-organic salts,[5] obtained via oxidation of $[M^{II}(sbqdi)_2]$ (M = Ni, Pd) with silver hexafluoroantimonate in acetonitrile. The cationic products $[M^{II}(sbqdi)(bqdi)](SbF_6)$ were then allowed to react with $(NEt_4)[^2ML_2]$ (L is ethylenedithiolato, 1,2-benzenedithiolato, toluenedithiolato, maleonitriledithiolato, 2-iminobenzenethiolato; ^2M = Pd, Ni, Co, Fe). Semiconducting metal-organic salts comprising electron donor and electron acceptor of the general formula $[M^{II}(sbqdi)(bqdi)]_x[^2ML_2]_y$ (x, y = 1, 2) were obtained.

Previous studies on *o*-phenylenediamine derived complexes of transition metals are complex and often conflicting since the oxidation states of the ligands and the metals and coordination

modes (monodentate versus bidentate) were not determined. By employing single crystal X-ray diffractometry more reliable information about the complexes can be obtained.

In 1985 Peng et al.[4] have showed that $[Co^{II}(sbqdi)_2]$ (but its valence-tautomeric form $[Co^{III}(sbqdi)(pda)]$ cannot be excluded[6]) may be oxidized not only by iodine but with CCl_4 as well. After $[Co^{II}(sbqdi)_2]$ was stirred with CCl_4 in DMF for two days the square pyramidal $[Co^{III}(sbqdi)_2Cl]$ with a chlorine atom in the axial position was isolated. Németh et al.[7] and van Eldik et al.[8] investigated in detail the axial substitution reactions of $[Co^{III}(sbqdi)_2Y]^+$. Kinetic studies as well as the mechanism of the substitution are reported[7, 8] with axial ligands Y as Ph_3P, Ph_3As, Ph_3Sb, $P(OEt)_3$, pyridine, pyrrolidine, *N*-methyl-imidazole, benzimidazole, imidazole, SCN^-, I^-, etc.

In 1990 Wilkinson et al.[9] reported synthesis of the series of rhenium complexes containing three *o*-phenylenediamine derived ligands. The parent cation formulated as $[Re^{VII}(pda)_3]^+$ can be reduced with sodium giving the neutral $[Re^{VI}(pda)_3]$. The latter can be reoxidized with $AgPF_6$ to the parent cation. Several deprotonated complexes could be obtained as well. Thus reaction of $[Re^{VII}(pda)_3][Re^{VII}O_4]$ with a small excess of methanolic KOH resulted in the neutral, singly deprotonated product, formulated as $[Re^{V}(pda)_2(pda\text{-}H)]$. Further reaction of Re^V species with a large excess of KOH gave a doubly deprotonated product formulated as $K[Re^{III}(pda\text{-}H)_2(pda)]$. All redox processes described are believed to be metal related.

Recently Eremenko et al.[10] reported interesting reactions of $[M^{II}(^1sbqdi)_2]$ with metal carbonyls (M = Ni, Pt; $(^1sbqdi)^{1-}$ – radical form of the *N*-phenyl-*o*-phenylenediamine). They showed that refluxing of the complexes in the presence of $[Fe(CO)_5]$ resulted in the transfer of $(^1sbqdi)^{1-}$ to the iron atoms and its reduction giving the diamagnetic binuclear complex $Fe_2(CO)_6[\mu\text{-}(NH)(NPh)C_6H_4]$.

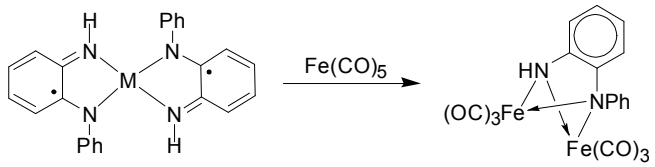

$[M^{II}(^1sbqdi)_2]$

The heterometallic binuclear $(OC)Pt(\mu\text{-}N,N\text{-}o\text{-}(N)(NPh)C_6H_4]_2ReCl[(NH)(NPh)C_6H_4]$ complex was formed in the reaction of $[Pt^{II}(^1sbqdi)_2]$ with the mononuclear rhenium(I) complex $[Re(CO)_5Cl]$, which has been preliminarily treated with silver triflate upon UV irradiation in *m*-xylene.

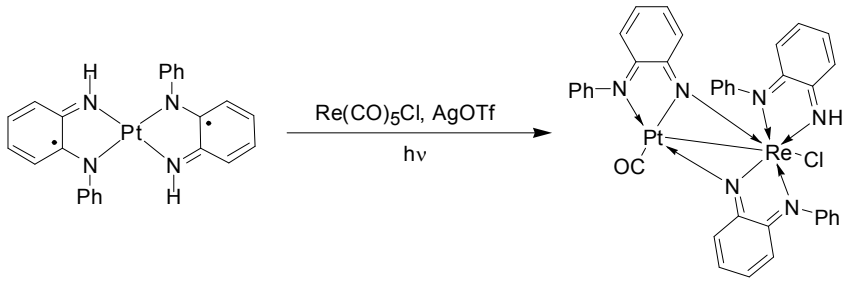

Very recently Wieghardt et al. have prepared and investigated in detail Ni, Pd, Pt, Co and Fe complexes with substituted $^{1}H_2$pda and $^{2}H_2$pda *o*-phenylenediamine derived ligands ($^{1}H_2$pda – *N*-phenyl-*o*-phenylenediamine, $^{2}H_2$pda – 3,5-di-*tert*-butyl-*o*-phenylenediamine). They showed that oxidation of the homoleptic *trans*-[Pt^{II}(^{1}sbqdi)$_2$] with one equiv of AgOTf yielded diamagnetic dimer {*trans*-[Pt^{II}(^{1}sbqdi)(^{1}bqdi)]$_2$}(OTf)$_2$.[11] The oxidation process is ligand based as confirmed by an X-ray structure analysis of the dimer. Diamagnetic dimers [Pt^{II}(sbqdi)(bqdi)]$_2$(OTf)$_2$,[12] {*cis*-[Pt^{II}(^{1}sbqdi)(^{1}bqdi)]$_2$}(OTf)$_2$,[13] {*cis*-[Pd(^{1}sbqdi)(^{1}bqdi)]$_2$}(OTf)$_2$[14] as the products of the oxidation of the parent complexes with AgOTf were reported by Eremenko et al. The coordination of *t*Bu-py to cobalt in the square-planar complex *trans*-[Co(^{1}lig)$_2$] was reported by Wieghardt et al.[6] The *physical* oxidation states of the metals and the ligands in *trans*-[Co(^{1}lig)$_2$] and *trans*-[Co(^{1}lig)$_2$(*t*Bu-py)] could not be assigned unambiguously.

In 2005 Wieghardt et al.[15] reported synthesis of diamagnetic dimer *trans*-[Fe^{III}(^{1}sbqdi)(^{1}pda)]$_2$. This complex was a useful starting material for the synthesis of the five-coordinated mononuclear complexes. Thus it reacts with such bases (B) as tri-*n*-butylphosphane, *tert*-butyl isocyanide, cyclohexyl isocyanide, and 4,5-diphenylimidazole to form complexes [Fe^{II}(^{1}sbqdi)$_2$(B)]. The coordination of the ligand in axial position is accompanied by intramolecular redox process: iron(III) is reduced to iron(II), thereby (^{1}pda)$^{2-}$ is oxidized to (^{1}sbqdi)$^{1-}$. [Fe^{II}(^{1}sbqdi)$_2$(PBu_3)] was oxidized by ferrocenium hexafluorophosphate giving [Fe^{III}(^{1}sbqdi)$_2$(PBu_3)](PF_6), the oxidation is metal based as confirmed by X-ray analysis. The parent dimer *trans*-[Fe^{III}(^{1}sbqdi)(^{1}pda)] can be oxidized with iodine as well. This oxidation is ligand based, the isolated product was [Fe^{III}(^{1}sbqdi)$_2$I].

Summarizing, the chemistry of [M(lig)$_2$] complexes is limited mainly to redox reactions, where both the ligand and the metal can be affected, and to additions of the third ligand in square-planar complexes of iron and cobalt. Having synthesized new distorted tetrahedral complexes [M(BPPD)$_2$] (M = Fe, Co, Ni, Pd, Cu; H_2BPPD – *N*,*N*′-bis(pentafluorophenyl)-*o*-phenylenediamine, see Chapter I) we have examined their reactivity in "classical" redox and addition reactions as well as in reactions of ligand metathesis and oxidative alkylation/arylation.

Results and Discussion.

First of all we have investigated the reactivity of the $[M(BPPD)_2]$ complexes towards several oxidizing agents. Oxidants of different strength were under consideration starting with the weakest chloroform and tetrachloromethane and including strong oxidants with iodosobenzene PhIO and iodosyldichloride $PhICl_2$. Most reactions were tested on cobalt complex **3**, since the possibility of the metal oxidation $Co^{II} \rightarrow Co^{III}$ without the oxidation of the ligands was anticipated.

We are noting that valence tautomerism can not be excluded in case of cobalt complex **3**: $[Co^{II}(^{F}sbqdi)_2] \leftrightarrow [Co^{III}(^{F}sbqdi)(^{F}pda)]$ as well as in all $[Co(lig)_2]$ reported previously. In the following, we will use $[Co^{II}(^{F}sbqdi)_2]$ description for **3**. The following abbreviations are used through this Chapter: $(^{F}pda)^{2-}$ – doubly deprotonated ligand, $(^{F}sbqdi)^{1-}$ – doubly deprotonated one electron oxidized radical ligand, $(^{F}bqdi)^{0}$ – doubly deprotonated two electron oxidized neutral ligand, BPPD – any redox form of the doubly deprotonated ligand. For more details concerning the determination of the oxidation states of the ligands and the metals one is referred two Chapter I.

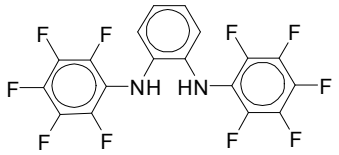

H_2BPPD

BPPD derived complexes of this work

$[Ni^{II}(^{F}sbqdi)_2]$ (**1**) $[Co(BPPD)_2]$ (**3**)

$[Pd^{II}(^{F}sbqdi)_2]$ (**2**) $[Cu^{II}(^{F}sbqdi)_2]$ (**4**)

$[Fe(^{F}sbqdi)(^{F}pda)]$ (**5**)

Reactions with weak oxidizing agents.

It was shown, that **3** does not react with solvents like $CHCl_3$, CH_2Cl_2, and CCl_4, which may act as donors of chlorine radicals particularly to paramagnetic metal ions. Oxidation of **3** with iodine in toluene failed as well. In all cases no color change of solutions under investigation were observed even by prolonged reaction time. Only unreacted complex **3** was observed by TLC in all cases.

In contrast to **3** oxidation $Co^{II} \rightarrow Co^{III}$ in complexes containing less bulky $(sbqdi)^{1-}$ or similar *o*-iminobenzosemiquinonato(1–) and *o*-iminothiobenzosemiquinonato(1–) moieties is known and proceeds employing I_2, CH_2Cl_2, $CHCl_3$, or CCl_4 as oxidants.[4,16] Two reasons can be referred to the low ability of **3** to react with these oxidants: higher oxidation potential of cobalt in **3** and the blocking of an extra coordination site for a chloro ligand by C_6F_5-rings. The latter is more likely since employment of strong oxidizing agents results in oxidation of the complex at the ligand but not at the metal.

Reaction with $PhICl_2$.

Using strong oxidizing agents we proved that **3** can be oxidized not only electrochemically (see Chapter I) but chemically as well. After 2 equiv of dark-green **3** was treated with 1 equiv of $PhICl_2$ in acetonitrile at room temperature the dark-yellow substance **6** was isolated. **6** is diamagnetic as may be expected for five coordinated Co^{III} species. ^1H and ^{19}F NMR spectra showed unexpected and very intriguing patterns. Instead of three multiplets in ^{19}F NMR and two multiplets in ^1H NMR spectra, which are expected for two equivalent BPPD ligands attached to the cobalt center, seven and three multiplets with incomprehensible intensities were observed in ^{19}F and ^1H NMR spectra, respectively. Since we were not able to determine the structure of **6** by NMR spectroscopy and being facilitated by the properties of the substance in question, the structure of **6** was clarified by a single crystal X-ray analysis. Compound **6** was shown to be a "pure" organic substance: 1,2,2,3,4-pentafluoro-10-(2,3,4,5,6-pentafluorophenyl)-2,10-dihydrophenazine.

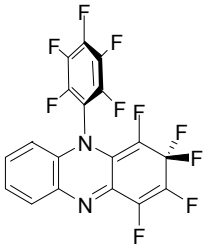

Thus our attempt to oxidize Co^{II} with the chlorine radical source $PhICl_2$ results in ligand oxidation, decomplexation and isolation of substituted phenazine **6,** an isomer of the unknown fully oxidized *N*,*N*'-bis(pentafluorophenyl)-*o*-benzoquinonediimine $(^{F}bqdi)^0$. The oxidation is believed to occur not at the metal center, but at the redox active ligand. In fact, a single crystal structure determination of **3** reveals, that the four sterically demanding C_6F_5 moieties block the introduction of the chlorine atom at the metal. A proposed mechanism of the ligand oxidation and its transformation is shown in the following scheme:

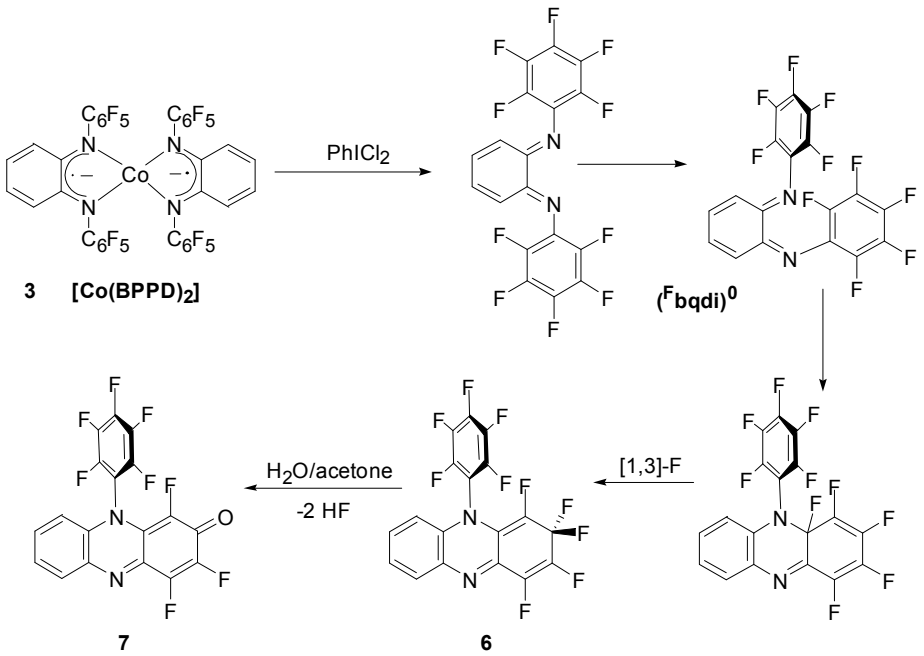

One of the $(^{F}sbqdi)^{1-}$ ligands is oxidized to $(^{F}bqdi)^{0}$ followed by cleavage of the complex on two moieties: $(^{F}bqdi)^{0}$ and $[Co(BPPD)]^{+}$. Formation of nonfluorinated $(bqdi)^{0}$ is also proposed by Simándi et al.,[17] who obtained 2,3-diaminophenazine in the reaction of unsubstituted *o*-phenylenediamine with dioxygen in the presence of Co^{II} salts.

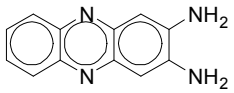

It is known,[18] that $(bqdi)^{0}$ may be stabilized with electron-withdrawing groups such as SO_2Ar and COAr at both N atoms. However, $(^{F}bqdi)^{0}$ carrying two electron-withdrawing C_6F_5-groups seems to be unstable unless attached to a metal. $(^{F}bqdi)^{0}$ decomplexation leads to rearrangement into its isomer; intramolecular nucleophilic attack of nitrogen at the carbon atom of the adjacent C_6F_5-ring leads to formation of a new six-membered ring. Reaction is completed by 1,3-migration of a fluorine atom arising from the preference, according to Bent's rule,[19] to be attached to sp^3-hybridized carbon rather than to sp^2-hybridized. Though the 1,3-fluorine migration was reported previously,[20] up to now it is uncertain whether the mechanism of this process involves an intramolecular 1,3-fluorine shift, successive 1,2-fluorine migrations, or a dissociative pathway. No intermediates species were detected during our studies.

The parent *o*-phenylenediamine is well known to undergo oxidative dimerization in the presence of the transition metals ions and air giving 2,3-diaminophenazine.[21] The ring substituted phenazines result in formation of the substituted phenazines.[5] Recently Chlopec et al.[15] and Eremenko et al.[13] reported the molecular structures of phenazine derivatives obtained by oxidation of the *o*-phenylenediamine derived complexes.

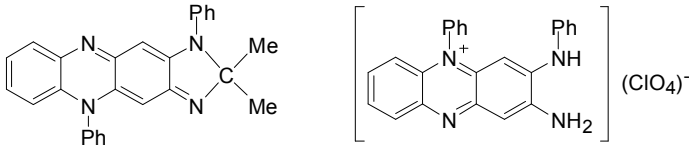

Eremenko et al. Chlopec et al.

In all cases dimerization of the *o*-phenylenediamine unit was observed. For complex **3** the intramolecular nucleophilic attack of the nitrogen at the electrophilic carbon of C_6F_5-ring leads to the phenazine formation without dimerization.

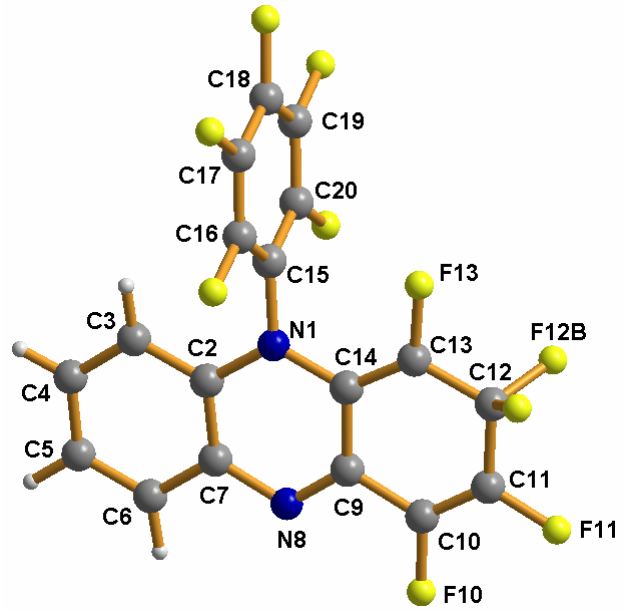

Figure. 1. Molecular structure of **6**.

Characterization of the phenazine derivative (6).

Compound **6** crystallizes in the triclinic space group $P\bar{1}$ with two molecules in the unit cell. Selected distances and angles are given in Table 1. Its structure consists of two essentially flat fragments: the phenazine ring and the fluorinated benzene ring attached to the N atom of the former (Fig. 1). Carbon–carbon bonds C13–C14, C10–C11 reveal double character with C=C distances 1.347(2) and 1.317(3) Å, respectively, whereas C9–C14, C9–C10, C11–C12, C12–C13 are single bonds (1.454(3) – 1.477(3) Å). C9–N8 is a double bond with a distance 1.292(2) Å, whereas the other three C–N bonds in C4N2 central ring of the phenazine are single bonds (1.389(2) – 1.412(2) Å). The bond angles around N1 atom are 120.5(2), 120.2(1) and 118.8(2)° giving the sum of 359.5°, that is in accord with sp^2-type hybridization of N1 atom. Hence N1 atom is involved in formation of a common π-system of the heterocycle. Two rings C_6F_5 and C_6H_4 are slightly deformed delocalized rings with C–C distances 1.372(3) – 1.381(3) and 1.375(3) – 1.401(3) Å respectively.

Table 1. Selected bond lengths (Å) and angles (°) for compound **6**.

C2–C7	1.395(3)	C7–C2–N1	118.59(2)
C2–N1	1.412(2)	N8–C7–C2	122.30(2)
C7–N8	1.389(2)	N8–C9–C14	125.07(2)
C9–N8	1.292(2)	C10–C9–C14	117.11(2)
C9–C10	1.454(3)	C11–C10–C9	122.85(2)
C9–C14	1.465(3)	C10–C11–C12	122.77(2)
C10–C11	1.317(3)	C13–C12–C11	113.17(2)
C11–C12	1.477(3)	C14–C13–C12	125.09(2)
C12–C13	1.475(3)	C13–C14–C9	118.92(2)
C13–C14	1.347(2)	N1–C14–C9	115.48(2)
C14–N1	1.395(2)	C14–N1–C2	120.49(2)
C15–N1	1.426(2)	C14–N1–C15	120.18(1)
		C2–N1–C15	118.76(2)
		C9–N8–C7	118.05(2)

Figure 2 shows a packing diagram for the cell of **6**. Phenazine rings form layers parallel to plane [100] leading to π-π stacking with an interplanar spacing of 3.500 Å between two molecules in one cell and 3.802 Å between two molecules in adjacent cells (symmetry codes: 1–x, 1–y, 1–z and –x, 1–y, 1–z, respectively).

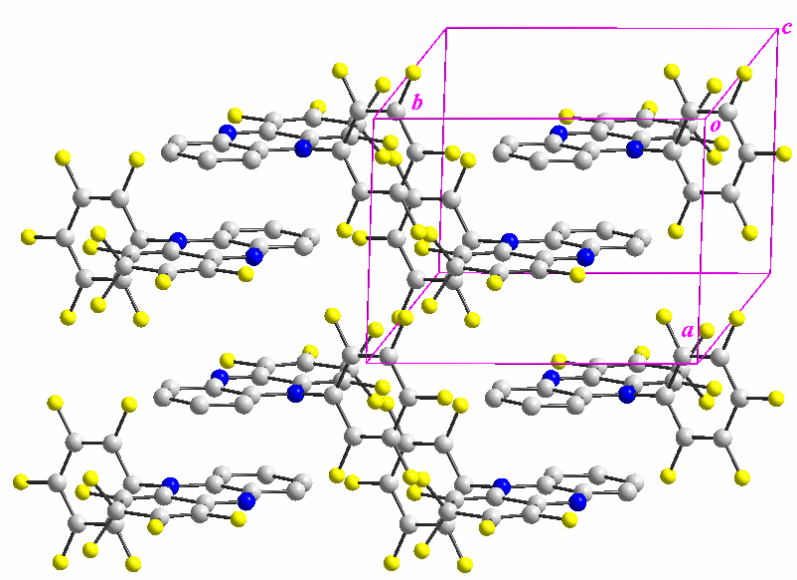

Figure 2. Packing diagram of (I) showing presence of π-π stacking along *a* axis. For clarity, all hydrogens have been omitted.

The ^{19}F NMR spectrum of **6** shows six multiplets in the region from –145 to –175 ppm and one separated signal at –88.9 ppm referring to fluorine atoms of a CF_2-group. The latter signal is close to that of the CF_2-group in octafluorocyclohepta-1,3,5-triene, being –90.3 ppm.[22] The ^{1}H NMR spectrum contains three multiplets in the aromatic region. Signals from H3 and F13 in the ^{1}H and ^{19}F NMR spectra, respectively, are shifted into the high field region, since they could be affected by an anisotropic effect of the benzene ring; its plane forms a dihedral angle with the phenazine plane of 86.19(7)° in the solid state.

By comparing distances C15–H3, C15–F13 (2.522 Å and 2.672 Å, respectively) with C15–F20, C15–F16 (2.342 Å and 2.346 Å, respectively) it is evident, that rotation of benzene ring around C15–N1 bond is not possible without great deformation of the whole molecule. Hindered rotation even in solution gives rise to the previously mentioned anisotropic shift of signals in the NMR spectra, which belong to the atoms lying above and under the benzene ring, namely H3 and F13.

It was noted that the dark-yellow phenazine **6** slowly develops into an intensive red color on staying in contact with air. Decomposition of **6** is much faster in solutions, even very diluted solutions of decomposed **6** were highly colored. Since formation of the red dye was observed in different reactions of $[M(BPPD)_2]$ described below, the nature of the red substance was of great interest.

Synthesis and characterization of the phenazinone derivative (7).

Thus it was shown that with wet acetone the yellow compound **6** is slowly hydrolyzed at the CF_2-group leading to the red phenazinone **7** (Fig 3.). Hydrolysis of **6** is facilitated in this case by activation of the CF_2-group towards hydrolysis by two adjacent vinyl-groups.[22] The low field signal at –88.9 ppm is absent in the ^{19}F NMR spectrum of **7** confirming complete hydrolysis of **6**.

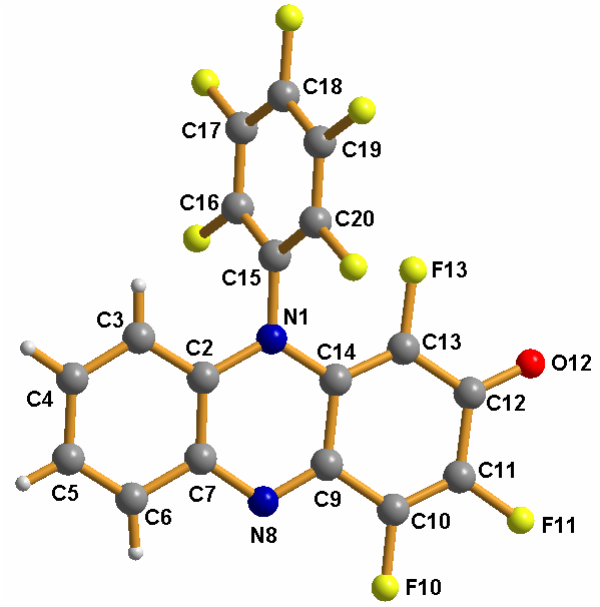

Figure 3. Molecular structure of **7**, disordered molecules of solvent (toluene) are not shown.

Phenazinone **7** crystallizes in the monoclinic space group *C* 2/c with 8 phenazinone and 4 toluene solvent molecules in the unit cell. Solvent molecules are disordered in the crystal. Selected distances and angles are given in Table 2. The molecular structure of **7** reveals a considerable deviation from planarity of the phenazinone moiety compared to derivative **6**. The phenazinone ring adopts a twisted geometry with a dihedral angle of 5.5(1)° between two six-membered carbon rings. The only other known structure of 2-phenazinones, namely that of the 10-(3-phenylpropyl)-2-

(10H)phenazinone is twisted also with a corresponding dihedral angle of 2.9°.[23] The bond pattern in **7** is similar to the bond pattern of **6** showing C13–C14, C10–C11 and C9–N8 to be double bonds. The bond distance of C–O is 1.232(3) Å (1.240(3) Å in 10-(3-phenylpropyl)-2-(10H)phenazinone) [23]). The ring incorporating C=O bond resembles a quinoid structure similar to that of *p*-benzoquinone.[24]

Table 2. Selected bond lengths (Å) and angles (°) for compound **7**.

C2–C7	1.399(3)	C7–C2–N1	118.5(2)
C2–N1	1.405(3)	N8–C7–C2	122.4(2)
C7–N8	1.377(3)	N8–C9–C14	124.9(2)
C9–N8	1.300(3)	C10–C9–C14	117.2(2)
C9–C10	1.442(3)	C11–C10–C9	121.9(3)
C9–C14	1.462(3)	C10–C11–C12	123.1(2)
C10–C11	1.324(4)	O12–C12–C13	123.4(3)
C11–C12	1.454(4)	O12–C12–C11	122.0(2)
C12–C13	1.437(3)	C13–C12–C11	114.6(2)
C13–C14	1.362(3)	C14–C13–C12	124.3(2)
C14–N1	1.392(3)	C13–C14–C9	118.8(2)
C15–N1	1.433(3)	N1–C14–C9	115.3(2)
C12–O12	1.232(3)	C14–N1–C2	120.7(2)
		C14–N1–C15	120.7(2)
		C2–N1–C15	118.6(2)
		C9–N8–C7	118.1(2)

Hydrolysis of the CF_2-group leads to simplification of the ^{19}F NMR spectrum. Nevertheless, on the basis of chemical shifts and coupling constants the signals from F10 and F11 could not be assigned unambiguously. Signals from H3 and F13 in ^{1}H and ^{19}F NMR spectra, respectively, are shifted into the high field region, while in the solid state the angle between planes of the phenazinone moiety and the benzene ring is decreased to 74.89(1)°.

Interactions between benzene hydrogens H4, H5 and $O12^{i}$ (symmetry code: (i) –1/2+x, 1/2+y, z) can be attributed to weak hydrogen bonding of C–H...O type.[25] Parameters of hydrogen-bonding geometry are given in Table 3, while the packing diagram is shown in Figure 4.

Table 3. Hydrogen-bond parameters (Å, °) for **7.**

	D–H	H...*A*	D...A	*D*–H...*A*
C4–H4...O12^{i}	0.99 (3)	2.54 (3)	3.232 (3)	127 (2)
C5–H5...O12^{i}	0.91 (3)	2.81 (3)	3.363 (4)	120 (2)

Symmetry code: (i) –½+x, ½ +y, z

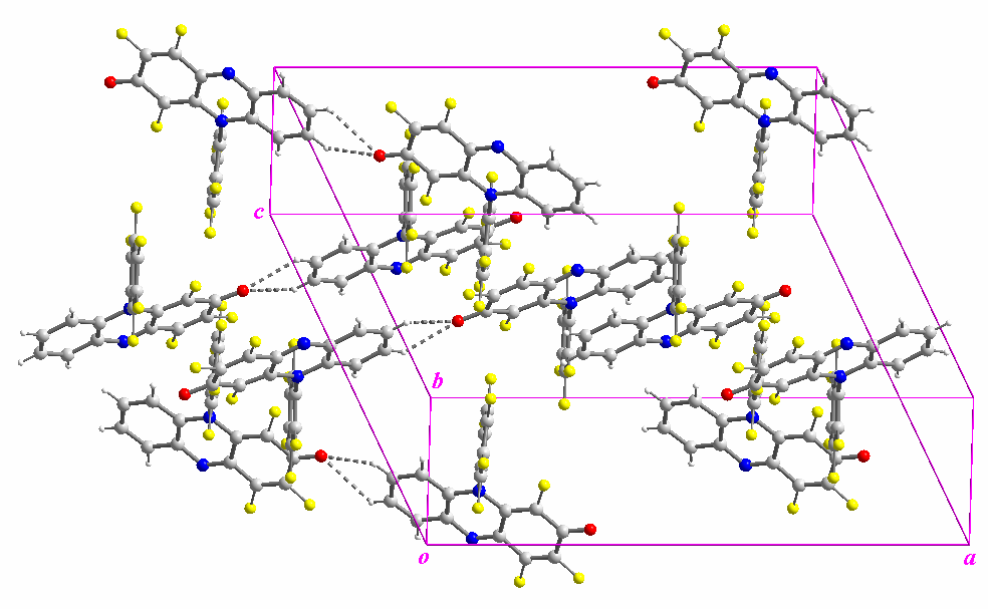

Figure 4. Packing diagram of **7** showing C–H...O hydrogen bonding between molecules lying in adjacent cells. Disordered molecules of solvent are not shown.

Although our attempts to prepare [$Co^{III}(^{F}bqdi)_2Cl$] failed, new highly fluorinated phenazine derivatives **6** and **7** were isolated in pure form and characterized. Taking into account numerous applications known for phenazines, for instance, they can be used as dyes,[26, 27] organic conductors,[28] components of the solar cells,[29] their biological activity is well known too,[30] our "failed" experiments could be of significance. Only several examples of fluorinated phenazine derivatives are known so far.[31] Very often they are isolated in low yield reactions or as by-products and their properties are not studied. Further investigation of the properties of the interesting compounds **6** and **7** is therefore needed.

Reactions with PhIO and $PhI(OAc)_2$.

Cobalt complex **3** was tested in reactions with iodosobenzene PhIO and iodosyldiacetate $PhI(OAc)_2$. Reactions were performed at different temperatures with varying equivalents of the oxidants. In all cases two quite similar fractions were obtained. The fraction soluble in hexane was shown to consist mostly of the mixture of **6** + **7**, whereas highly colored fraction insoluble in hexane was paramagnetic.

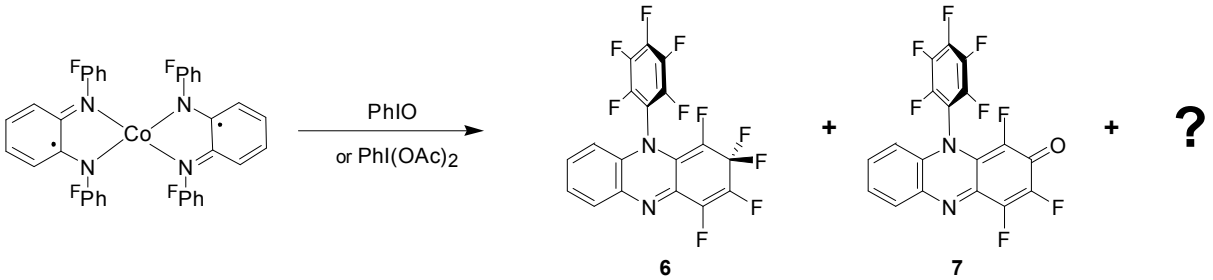

6 **7**

Numerous attempts to obtain crystalline material of paramagnetic solid failed. The purple solid was good soluble in the most polar solvents but did not reveal the properties of the individual substance. The absence of any signals in EI-MS suggests a polymeric nature[32] of the solid in question. It was concluded that the purple solid represents a polymeric mixture containing chromophoric groups (unsaturated system) and paramagnetic Co^{II} centers.

Reaction with AgOTf.

Nickel complex **1** was allowed to react with 1 equiv of silver triflate in acetone. After the reaction mixture was stirred overnight, a "silver mirror" was observed confirming the complex oxidation. Since the raw product was very good soluble in dichloromethane, formation of the salt $[Ni(BPPD)_2](OTf)$ can be reliably excluded. The intensively colored red product was separated from the unreacted **1** by column chromatography. The red dye was shown to be identical to the phenazinone **7** obtained by hydrolysis of phenazine **6**.

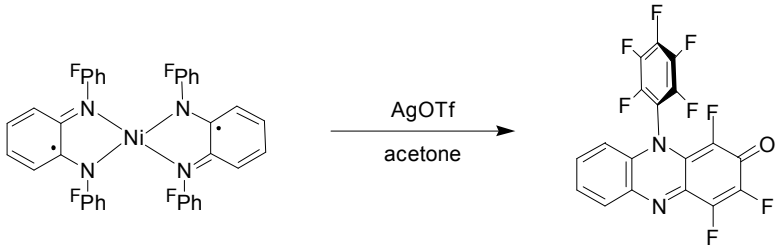

Reactions with PhI=NTs and TsN_3.

Reaction of **3** with nitrene precursors PhI=NTs and TsN_3 resulted in complex decomposition. Phenazine **6** and phenazinone **7** were detected by ^1H and ^{19}F NMR. As well as in reactions with PhIO and $PhI(OAc)_2$ the purple paramagnetic solid not soluble in hexane but good soluble in polar solvents was obtained. The properties of the solid closely resemble that obtained in reactions with PhIO and $PhI(OAc)_2$. Recrystallization attempts failed as well. It was concluded that the purple solid represents a polymeric mixture and paramagnetic Co^{II} closely related to the mixture obtained in reaction with PhIO.

Reactions with CO and pyridine.

Several test reactions were performed to study possibility of introduction of the neutral ligand like carbon monoxide and pyridine to the metal center. However the attempt to synthesize five-coordinated cobalt complex $[Co(BPPD)_2(py)]$ failed. Complex **3** did not react with pyridine, addition of the pyridine during the synthesis of **3** resulted in formation of the latter only. Complex **3** did not show any activity towards CO as well. In contrast five-coordinated cobalt complex $[Co^{III}(^1sbqdi)(^1pda)(t\text{Bu-py})]$ was reported by Bill et al.[6]

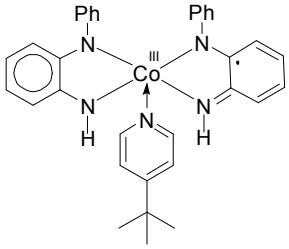

The parent $[Co^{III}(^{1}sbqdi)(^{1}pda)]\leftrightarrow[Co^{II}(^{1}sbqdi)_2]$ is strictly planar[6] and the metal ion is available for coordination of additional ligand (Fig. 5). We ascribe the inability of **3** to form five-coordinated complexes to the presence of bulky C_6F_5-substituents, which prevent the insertion of even such a small ligand as CO.

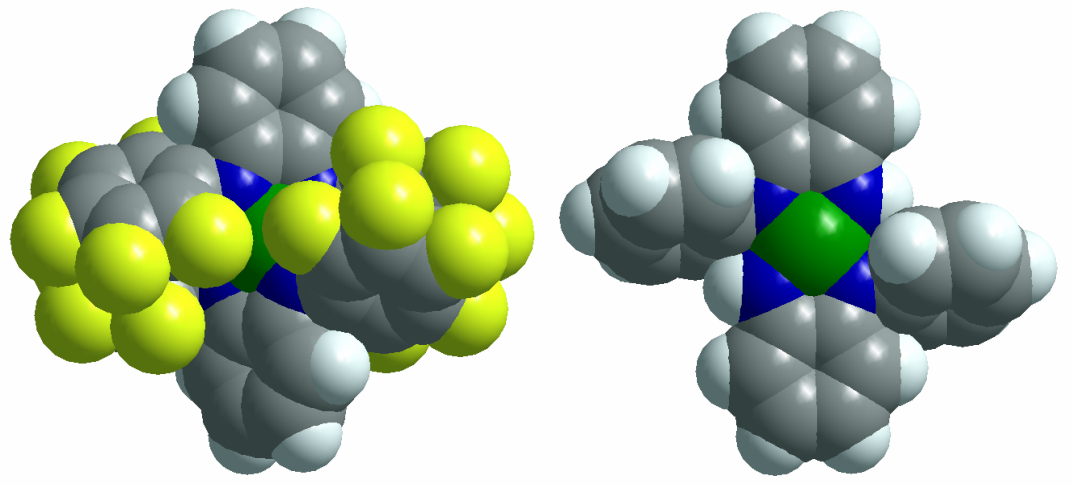

Figure 5. Space-filling models for $[Co(BPPD)_2]$ of current work (left) and $[Co^{II}(^{1}sbqdi)_2]$ from Wieghardt[6] (right).

Assuming that $(sbqdi)^{1-}$ donates 5 electrons and planar $(pda)^{2-}$ donates 6, iron compound **5** may be described as formally electron deficient $16e^-$ complex. From electronic point of view **5** is therefore expected to react with CO, but it does not as confirmed by IR spectroscopy. This was ascribed to overcrowded coordination sphere of **5**.

In order to demonstrate the ability of $16e^-$ iron complexes carrying *o*-phenylenediamine derived ligands to react with carbon monoxide, we tried two synthesize unknown unsubstituted $[Fe^{III}(sbqdi)(pda)]$ following the same procedure employed for the synthesis of $[Fe(BPPD)_2]$. Unfortunately, our attempts to synthesize $[Fe^{III}(sbqdi)(pda)]$ failed. The purple paramagnetic solid obtained is most likely of polymeric nature. It was not sublimable, EI-MS revealed the presence of 2,3-diaminophenazine only.

Synthesis of the cobalamin model compounds.

Cobalamins including coenzyme and vitamin B_{12} are classical study objects in bioinorganic chemistry of cobalt (Fig. 6).

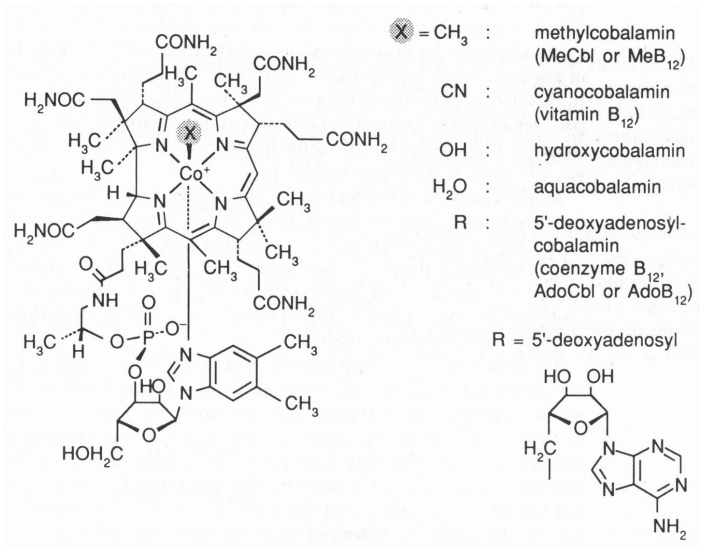

Figure 6. Cobalamin derivatives.

Suitable model systems of the cobalamins are of considerable interest as functional biomimetica for coenzyme B_{12}-catalyzed reactions. Some well known model systems are bis(diacetyldioxime) complexes ("cobaloximes"), "Costa complexes", complexes of bis(salicylaldehyde)ethylenediimine ("salen").[33] The synthesis of the new model for B_{12} system based on **3** was of our interest.

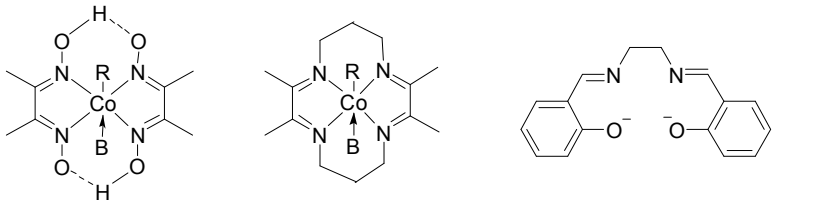

Our attempts to perform oxidative alkylation/arylation of **3** with methylhydrazine/phenylhydrazine and pure oxygen or *tert*-butyl hydroperoxide failed. The decomposition of **3** was observed in all cases. Reduction of the radical ligand (^{F}sbqdi)$^{1-}$ to the parent H_2BPPD was confirmed by ^{1}H and ^{19}F NMR. Very promising X-ray quality crystals obtained in the reaction of **3** with phenylhydrazine and oxygen were shown to be the salt $[Hpy]^{+}[Co^{II}(py)Cl_3]^{-}$. Its structure was already reported.[34]

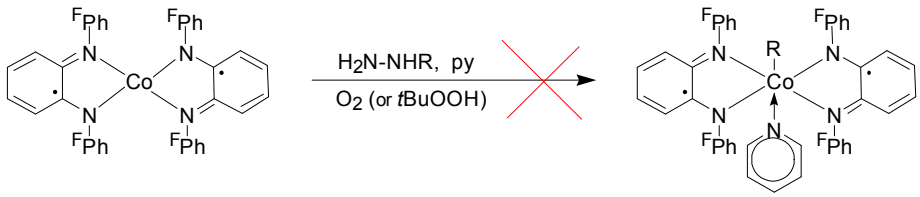

Oxidative alkylation of Co^{II} complexes containing salen or N_4-macrocyclic ligands is well known.[35] Such a reaction with the parent $[Co^{II}(sbqdi)_2]$ was proposed to take place by Peng et

al.,[4] but no data was published. However, oxidative alkylation was successively performed on the related diaminomaleonitrile derived complex $[Co(sdisn)_2]_2$ giving cobalt(III) organometallic species.[36]

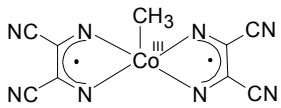

We ascribe unsuccessful oxidative alkylation to inability of **3** to take the fifth ligand in its crowded coordination sphere.

Ligand metathesis.

Ligand metathesis reactions of $[M(BPPD)_2]$ towards NaCp and 1,2-dimercaptobenzene $C_6H_4(SH)_2$ were investigated. Cobalt complex **3** stirred overnight with NaCp in THF was reisolated. No change of color along with results of TLC analysis confirm that reaction did not occur.

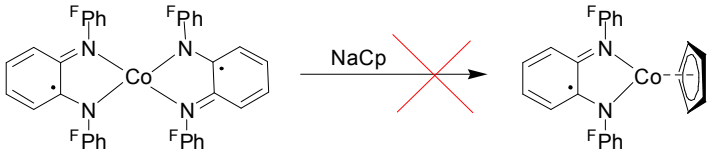

When nickel complex **1** was stirred in toluene with equimolar amount of 1,2-dimercaptobenzene for 30 hours at 60ºC formation of the black solid was observed. Still colored solution was confirmed by ^1H and ^{19}F NMR to contain parent H_2BPPD and some unreacted complex **1**. It was concluded that reaction did take place. The subsequent analysis of the black powder is inconsistent with its formulation as $[Ni(BPPD)(C_6H_4S_2)]$. It was not soluble in common organic solvents, nevertheless its low solubility in DMSO allowed to carry out NMR analysis. Unexpectedly, the black solid was paramagnetic showing broad signals of the solvents in ^1H NMR, no signals were observed in ^{19}F NMR. The elemental analysis confirms absence of any sufficient amounts of nitrogen in the solid. On the other hand, the results of the elemental analysis are inconsistent with the formulation of the black substance as $[Ni(C_6H_4S_2)_2]$. Attempts to sublime the substance in question failed as well as EI-MS analysis pointing on likely polymeric nature of the solid. The possible metal-organic salt formation[5] $[Ni(BPPD)_2]^+[Ni(C_6H_4S_2)_2]^-$ was rejected since nitrogen was not detected by the elemental analysis.

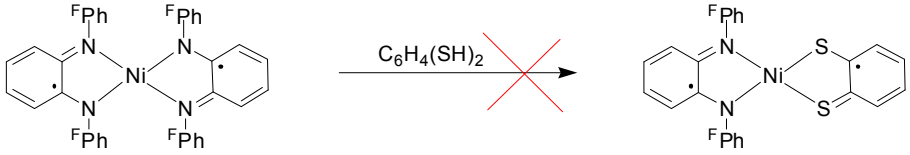

We suppose that likely preformed $[Ni(BPPD)(C_6H_4S_2)]$ undergoes subsequent substitution of BPPD in favor of $[Ni(C_6H_4S_2)_2]$ formation. When a large access of dimercaptobenzene was used the same undefined black solid was obtained. The hypothetical complex $[Ni(C_6H_4S_2)_2]$ seems to be unstable and has never been isolated. Recently, Sellmann et al.[37] reported that their attempts to

oxidize anionic $[Ni(C_6H_4S_2)_2]^-$ with various oxidizing reagents yielded grey-black products being insoluble and intractable. The products obtained by us and that obtained by Sellmann are believed to be very similar.

Conclusions.

The reactivity of $[M(BPPD)_2]$ complexes was investigated. It was shown that $[M(BPPD)_2]$ complexes are not feasible to coordinate a third ligand in addition, oxidative addition, and oxidative alkylation/arylation reactions. The observed inability is described to the steric factor, since the bulky perfluorinated phenyl rings are efficiently blocking the metal center from the subsequent coordination. The oxidation of the ligand within the complexes can be performed by using silver triflate or iodosyldichloride $PhICl_2$. One electron oxidized complexes are not stable and undergo further reactions resulting in formation of phenazine derivatives as the products of intramolecular nucleophilic reaction. Two fluorinated phenazine derivatives were isolated in pure form and thoroughly characterized by means of NMR, IR, MS, UV-vis, elemental, and X-ray analysis.

Experimental Part.

Complexes **1**–**5** were synthesized as described in Chapter I. Reagents PhIO,[38] PhI=NTs,[39] were prepared by known procedures. For detailed Physical Measurements one is referred to the Chapter I.

X-ray Crystallographic Data Collection and Refinement of the Structures.

Crystal structure determinations[40]: crystals have been mounted in a drop of oil and frozen in the cold nitrogen stream of the cooling device on a STOE IPDS-2 diffractometer at T = 193 K. Data have been collected using graphite monochromated MoKα radiation, θmax = 26°. The structures have been solved using direct methods and refined using the full matrix least squares method with all independent data (SHELX-97).

Compound **6**: the hydrogen atoms have been located and refined isotropically with C–H bond lengths in the range 0.95 to 1.01 Å. Compound **7**: H3, H4, H5, and H6 have been located and refined isotropically with C–H bond lengths in the range 0.91 to 0.99 Å. The toluene molecule is disordered. A rigid model including hydrogen atoms has been fitted into the electron density with the methyl group disordered over two positions and a site occupation factor 0.5 for all atoms (respective 0.25 for the atoms of the disordered CH_3-group). Due to the crystallographic C_2 symmetry there is an additional disorder. This leads to four toluene molecules in the unit cell.

Reaction of [Co(BPPD)$_2$] (3) with CCl_4.

Complex **3** (187 mg, 0.200 mmol) was stirred in dried CCl_4 (10 mL) for 3 days at room temperature. Absence of color change along with TLC confirmed that no reaction occurred.

Reaction of [Co(BPPD)$_2$] (3) with I_2.

Solution of I_2 (27 mg, 0.107 mmol) in toluene (5 mL) was added to the complex **3** (200 mg, 0.214 mmol) suspended in toluene (10 mL). After stirring for 20 hours at room temperature no reaction was detected (color, TLC). The 4-fold excess of I_2 (108 mg, 0.426 mmol) was then added as a crystalline material. After stirring overnight toluene and unreacted iodine were removed in vacuo. The remaining dark solid was confirmed to be **3** by TLC.

Reaction of [Co(BPPD)$_2$] (3) with $PhICl_2$: synthesis of phenazine (6).

Complex **3** (561 mg, 0.600 mmol) was treated with $PhICl_2$ (82 mg, 0.300 mmol) in dry acetonitrile (35 mL) at room temperature. The mixture was stirred for 50 min under argon and

volatiles were removed under reduced pressure. Extraction with hexane followed by reducing of its volume and cooling down to –20°C afforded a dark-yellow solid, which was washed with cold pentane and dried in vacuo. Crystals, suitable for single-crystal X-ray diffraction, were obtained from THF / hexane mixture by cooling.

Yield: 201 mg (76 % based on $PhICl_2$).

M.p. 172ºC (decomp.).

$C_{18}H_4F_{10}N_2$ (438.23): calcd. C 49.3, H 0.9, N 6.4; found C 49.3, H 1.0, N 6.6.

MS (EI): m/z = 438 [M^+], 419 [$M - F^+$], 388 [$M - CF_2^+$].

^{1}*H NMR* (200.1 MHz, C_6D_6, 300 K): δ = 5.91 – 5.96 (m, 1H, H3), 6.68 – 6.84 (m, 2H, H4, H5), 7.58 (dd, ^3J=8 Hz, ^4J=2 Hz, 1H ,H6) ppm.

^{19}*F NMR* (376.4 MHz, C_6D_6, 300 K): δ = –88.9 (td, ^3J=23 Hz, ^4J=9 Hz, 2F, F12A, F12B), –145.6 (m, 2F, F16, F20), –148.8 (tt, ^3J=22 Hz, ^4J=3 Hz, 1F, F18), –151.3 (psq, ^3J=^4J=10 Hz, 1F, F10), –152.8 (tdd, ^3J=22 Hz, ^3J=10 Hz, ^4J=4 Hz, 1F, F11), –159.6 (m, 2F, F17, F19), –172.1 (td, ^3J=24 Hz, ^4J=4 Hz, 1F, F13) ppm.

IR (Nujol): wavenumber = 743 (w), 758 (m), 995 (s), 1033 (s), 1249 (m), 1262 (m), 1274 (m), 1306 (m), 1317 (m), 1519 (s), 1604 (w), 1666 (m) cm^{-1}.

UV-vis ($CHCl_3$): λ_{max} = 442 nm.

Hydrolysis of phenazine (6) to phenazinone (7).

Hydrolysis of **6** at room temperature with wet acetone for several days afforded red dye **7** in almost quantitative yield. Crystals, suitable for single-crystal X-ray diffraction, were obtained from toluene / hexane mixture by cooling.

Yield: ~ 100%.

M.p. 221ºC.

$C_{18}H_4F_8N_2O$ (416.23): calcd. C 51.9, H 1.0, N 6.7; found C 51.5, H 1.1, N 6.5.

MS (EI): m/z = 416 [M^+], 388 [$M - CO^+$].

^{1}*H NMR* (400.1 MHz, C_6D_6, 300 K): δ = 6.12 (bd, ^3J=8 Hz, 1H, H3), 6.79 – 6.83 (m, 1H), 6.87 – 6.91 (m, 1H), 7.72 (dd, ^3J=8 Hz, ^4J=1.5 Hz, 1H, H6) ppm.

^{19}*F NMR* (376.4 MHz, C_6D_6, 300 K): δ = –141.2 (dd, ^3J=13 Hz, J=7 Hz, 1F), –144.5 (m, 2F, F16, F20), –145.3 (dd, ^3J=13 Hz, J=3 Hz, 1F), –146.5 (tt, ^3J=22 Hz, ^4J=3 Hz, 1F, F18), –157.9 (m, 2F, F17, F19), –160.3 (dd, J=7 Hz, J=3 Hz, 1F, F13) ppm.

IR (Nujol): wavenumber = 738 (w), 756 (m), 995 (s), 1033 (s), 1067 (m), 1121 (m), 1161 (m), 1261 (m), 1308 (m), 1321 (m), 1352 (m), 1520 (s), 1592 (s), 1612 (s), 1639 (s), 1683 (w) cm^{-1}.

UV-vis ($CHCl_3$): λ_{max} = 365, 522 nm.

Reaction of [Co(BPPD)$_2$] (3) with PhIO.

Complex **3** (200 mg, 0.214 mmol) suspended in MeCN (10 mL) was cooled to –40ºC and PhIO (43 mg, 0.214 mmol) was added as a powder. The reaction mixture was allowed to warm slowly to room temperature and stirred for 2 hours. The reaction was accompanied by the change of color from dark-green to dark-red. After MeCN was removed in vacuo, resulting purple solid was extracted with hexane to give orange solution. Analysis of the extract by ^{1}H and ^{19}F NMR reveals the presence of phenazine **6** as a main fraction, small amount of phenazinone **7** and impurities. Purple solid not soluble in hexane was paramagnetic and showed no any signal in EI-MS. Several attempts to recrystallize the paramagnetic solid failed.

Reaction of [Co(BPPD)$_2$] (3) with PhI(OAc)$_2$.

To the complex **3** (220 mg, 0.235 mmol) suspended in MeCN (20 mL) PhI(OAc)$_2$ (38 mg, 0.118 mmol) was added as a powder. After about 1 hour the color of the reaction mixture became reddish. The mixture was then stirred overnight, MeCN was removed in vacuo to get a purple solid. It was extracted with hexane and the extract was analyzed by ^{1}H and ^{19}F NMR. The extract consists mostly of the decomposition products of **3**: phenazine **6** and phenazinone **7**. The purple rest not soluble in hexane was paramagnetic. Attempts to recrystallize the paramagnetic solid failed.

Reaction of [Ni^{II}(^{F}sbqdi)$_2$] (1) with Ag(OTf).

To the complex **1** (187 mg, 0.200 mmol) dissolved in acetone (10 mL) solid Ag(OTf) (51 mg, 0.200 mmol) was added. After stirring overnight formation of the metallic silver („silver mirror“) was observed. Solution was filtered, acetone was removed in vacuo and the resulting solid was dissolved in a small amount of CH_2Cl_2. Layering of the dichloromethane solution with hexane and keeping the Schlenk flask at –30ºC for a night resulted in additional formation of the metallic silver. The solution was filtered through the Celite layer and evaporated to dryness. By means of TLC it was established that the final red powder consisted of two main components: unreacted **1** and an unknown red dye. The substance in question was preliminary purified by means of column chromatography (neutral Al_2O_3, benzene:hexane = 1:1 $\rightarrow$ benzene $\rightarrow$ Et_2O) and recrystallized from toluene/hexane mixture (~1:1) by cooling. The crystals obtained were of X-ray crystallographic quality. The ^{1}H, ^{19}F NMR and EI-MS measured for the red dye were identical to that obtained for phenazinone 7 (see “Hydrolysis of phenazine (**6**)”).

Reaction of [Co(BPPD)$_2$] (3) with PhI=NTs.

Complex **3** (200 mg, 0.214 mmol) was suspended in MeCN (10 mL) and the resulting dark-green suspension was cooled to –40ºC. After PhI=NTs (74 mg, 0.213 mmol) was added as a powder, the mixture was allowed to warm to room temperature and stirred for 4 hours. Acetonitrile was removed in vacuo to get a purple solid. The orange hexane extract reveals decomposition products of **3** in ^{1}H and ^{19}F NMR spectra: phenazine **6** and phenazinone **7** along with $TsNH_2$. Not soluble in hexane part of the purple solid is paramagnetic and shows no any signal in EI-MS, recrystallization attempts failed.

Reaction of [Co(BPPD)$_2$] (3) with TsN_3.

To the complex **3** (306 mg, 0.327 mmol) dissolved in THF (10 mL) TsN_3 (0.05 mL, 65 mg, 0.327 mL) was added at 0ºC. After the reaction mixture was stirred overnight at room temperature, no reaction occurred (TLC, color). The dark-green solution was then refluxed for 3 hours thereby the color changed to green-yellow. After THF was removed in vacuo, the resulting solid was extracted with hexane. ^{1}H and ^{19}F spectra from extract show impure phenazine **6** and TsN-rest. Not soluble in hexane solid is paramagnetic and shows no any signal in EI-MS.

Reaction of [Co(BPPD)$_2$] (3) with CO.

Complex **3** (100 mg, 0.107 mmol) was suspended in Et_2O (10 mL) and a stream of CO-gas was passed through the suspension for 1 min. The dark-green color of the reaction mixture did not change. According to TLC and IR no reaction occurred.

Reaction of [Fe^{III}(^{F}sbqdi)(^{F}pda)] (5) with CO.

Complex **5** (160 mg, 0.172 mmol) was dissolved in toluene followed by passing the CO-gas through the solution during 3 min. No color change was observed. After the solution was stirred for ½ hour, toluene was removed in vacuo and the solid was dried at room temperature. The IR spectra measured for the complex **5** before and after the passing of CO are identical. Hence, no reaction took place.

Attempt to synthesize [Fe^{III}(sbqdi)(pda)].

n-BuLi (5.8 mL, 1.6 M, 9.247 mmol) was added to the *o*-phenylenediamine (500 mg, 4.624 mmol) suspended in Et_2O (30 mL) at 0ºC. The resulting yellow suspension was stirred for one hour at room temperature, then cooled down to –30ºC. After $FeCl_2$ (293 mg, 2.312 mmol) suspended in Et_2O (15 mL) was added, the reaction mixture was stirred overnight at room temperature. The

dirty-brown solution was cooled to 0ºC and $FeCl_3$ (750 mg, 4.624 mmol) in THF (15 mL) was slowly added with a syringe. After the mixture was stirred for 1.5 hours, solvents were removed in vacuo giving the black powder. It was not soluble in hexane, toluene and Et_2O. The sublimation performed at 60ºC and $p=5\cdot10^{-4}$ mbar failed. EI-MS revealed the presence of the free ligand (M^+=108) and 3,4-diaminophenazine (M^+=210).

Reaction of [Co(BPPD)$_2$] (3) with NaCp.

NaCp (19 mg, 0.214 mmol) suspended in THF (6 mL) was added to the THF solution (6 mL) of **3** (200 mg, 0.214 mmol) maintained by –15ºC. The reaction mixture was stirred overnight at room temperature however no any color change was observed. TLC confirms the reaction not to occur.

Attempt to synthesize [Co^{III}(CH$_3$)(py)(^{F}sbqdi)$_2$] using O$_2$ as oxidant.

To the complex **3** (200 mg, 0.214 mmol) dissolved in CH_2Cl_2 (15 mL) methylhydrazine (0.1 mL, 86 mg, 1.867 mmol) was added under the atmosphere of pure oxygen. After stirring for 10 min pyridine (0.5 mL, 508 mg, 6.343 mmol) was added. The resulting mixture was stirred 10 min and all volatiles were then removed in vacuo. ^{1}H and ^{19}F NMR reveal presence of the free diamine H_2BPPD along with undefined paramagnetic species.

Attempt to synthesize [Co^{III}(CH$_3$)(py)(^{F}sbqdi)$_2$] using *t*-BuOOH as oxidant.

To the complex **3** (200 mg, 0.214 mmol) dissolved in CH_2Cl_2 (10 mL) methylhydrazine (0.1 mL, 86 mg, 1.867 mmol) was added with a syringe under the argon atmosphere. Formation of the orange suspension was accompanied with gas evolution. After the reaction mixture was stirred for 15 min, *t*-BuOOH (0.07 mL, 63 mg, ω~80%, 0.555 mmol) was added, the gas evolution was observed again. Stirring of the reaction mixture for 15 min was followed by adding of pyridine (0.5 mL, 508 mg, 6.343 mmol). The resulting black precipitate suspended in dark-orange solution was stirred for the next 15 min, all volatiles were then removed in vacuo. ^{1}H and ^{19}F NMR show the presence of the free diamine H_2BPPD and undefined paramagnetic species.

Attempt to synthesize [Co^{III}(Ph)(py)(^{F}sbqdi)$_2$] using O$_2$ as oxidant.

Phenylhydrazine (0.1 mL, 116 mg, 1.069 mmol) was added to the CH_2Cl_2 solution (10 mL) of complex **3** (200 mg, 0.214 mmol) under the atmosphere of pure oxygen. The resulting solution was stirred for 30 min and pyridine (0.5 mL, 508 mg, 6.343 mmol) was then added leading to the formation of the bright-green solution. All volatiles were removed in vacuo, the resulting viscous

oil was dissolved in CH_2Cl_2 and hexane was added. After the solution was stored at –30ºC for a night, blue paramagnetic powder was obtained. Single crystals suitable for X-ray crystallography were obtained from a d_3-MeCN/toluene mixture directly in NMR-tube. The substance under investigation is shown to be $[Hpy]^+[Co^{II}(py)Cl_3]^-$.

Attempt to synthesize $[Ni^{II}(^{F}sbqdi)(C_6H_4S_2)]$.

To the complex **1** (467 mg, 0.500 mmol) suspended in toluene (15 mL) 1,2-dimercaptobenzene (58 μL, 71 mg, 0.500 mmol) was added with a microsyringe. The resulting mixture was stirred for 30 hours at 60ºC under the argon atmosphere resulting in purple solution and black precipitate. By ^{19}F NMR the solution was shown to contain the parent *o*-phenylenediamine H_2BPPD and unreacted **1**. The solution was then decanted, the black solid was washed with toluene twice, THF and finally with hexane. The black solid is not soluble in the most common organic solvents. EI-MS shows no any signal except for toluene (91). No signals were observed in ^{19}F NMR spectrum (d_6-DMSO, green solution), whereas ^1H NMR shows the broadened signals of non-coordinated THF and toluene. The elemental analysis gives C: 38.51, H: 2.61 %, the nitrogen was not detected.

References.

[1] A. L. Balch, R. H. Holm, *J. Am. Chem. Soc.* **1966**, 5201–5209.

[2] L. F. Warren, *Inorg. Chem.* **1977**, *16*, 2814–2819.

[3] M. Zehnder, H. Löliger, *Helv. Chim. Acta* **1980**, *63*, 754–760.

[4] S.-M. Peng, C.-T. Chen, D.-S. Liaw, C.-I Chen, Y. Wang, *Inorg. Chim. Acta* **1985**, *101*, L31–L33.

[5] M. G. Miles, J. D. Wilson, *Inorg. Chem.* **1975**, *14*, 2357–2360.

[6] E. Bill, E. Bothe, P. Chaudhuri, K. Chlopek, D. Herebian, S. Kokatam, K. Ray, T. Weyhermüller, F. Neese, K. Wieghardt, *Chem. Eur. J.* **2005**, *11*, 204–224.

[7] a) L. I. Simándi, S. Neméth, *Inorg. Chim. Acta* **1998**, 326–329. b) S. Neméth, L. I. Simándi, *Inorg. Chem.* **1994**, *33*, 5964–5966.

[8] B. M. Alzoubi, M. S. A. Hamza, C. Dücker-Benfer, R. van Eldik, *Eur. J. Inorg. Chem*. **2003**, 2972–2978.

[9] A. A. Danopoulos, A. C. C. Wong, G. Wilkinson, M. B. Hursthouse, B. Hussain, *J. Chem. Soc. Dalton Trans.* **1990**, 315–331.

[10] a) I. G. Fomina, A. A. Sidorov, G. G. Aleksandrov, S. E. Nefedov, I. L. Eremenko, I. I. Moiseev, *J. Organomet. Chem.* **2001**, *636*, 157–163. b) A. V. Reshetnikov, M. O. Talismanova, A. A. Sidorov, S. E. Nefedov, I. L. Eremenko, I. I. Moiseev, *Russ. Chem. Bull., Int. Ed.* **2001**, *50*, 142–146.

[11] D. Herebian, E. Bothe, F. Neese, T. Weyhermüller, K. Wieghardt, *J. Am. Chem. Soc.* **2003**, *125*, 9116–9128.

[12] A. A. Sidorov, M. O. Pomina, S. E. Nefedov, I. L. Eremenko, Y. A. Ustynyuk, Y. M. Luzikov, *Zh. Neorg. Khim.* **1997**, *42*, 952–956; translated to English: *Russ. J. Inorg. Chem.* **1997**, *42*, 853–857.

[13] I. L. Eremenko, S. E. Nefedov, A. A. Sidorov, M. O. Ponina, P. V. Danilov, T. A. Stromnova, I. P. Stolarov, S. B. Katser, S. T. Orlova, M. N. Vargaftik, I. I. Moiseev, Y. A. Ustynyuk, *J. Organomet. Chem.* **1998**, *551*, 171–194.

[14] M. O. Talismanova, I. G. Fomina, A. A. Sidorov, G. G. Aleksandrov, N. T. Berberova, A. O. Okhlobystin, E. V. Shinkar, I. F. Golovaneva, I. L. Eremenko, I. I. Moiseev, *Russ. Chem. Bull., Int. Ed.* **2003**, *52*, 2701–2706.

[15] K. Chlopek, E. Bill, T. Weyhermüller, K. Wieghardt, *Inorg. Chem.* **2005**, *44*, 7087–7098.

[16] a) D. Herebian, P. Ghosh, H. Chun, E. Bothe, T. Weyhermüller, K. Wieghardt, *Eur. J. Inorg. Chem.* **2002,** 1957–1967. b) A. I. Poddel'sky, V. K. Cherkasov, G. K. Fukin, M. P. Bubnov, L. G. Abakumova, G. A. Abakumov, *Inorg. Chim. Acta* **2004**, *357*, 3632–3640.

[17] L. I. Simándi, T. Barna, Z. Szeverényi, S. Németh, *Pure Appl. Chem.* **1992,** *64*, 1511–1518.

[18] R. Adams, W. Reifschneider, *Bull. Soc. Chim. Fr.* **1958**, 23–65; and references therein.

[19] H. A. Bent, *Chem. Rev.* **1961**, *61*, 275–311.

[20] a) M. J. Burk, J. C. Calabrese, F. Davidson, R. L. Harlow, D. C. Roe, *J. Am. Chem. Soc.* **1991**, *113*, 2209–2222. b) A. G. Avent, R. Taylor, *Chem. Commun.* **2002**, *22*, 2726–2727.

[21] a) S. Németh, L. I. Simándi, *J. Mol. Catal.* **1984**, *22*, 341–348. b) S. Németh, L. I. Simándi, *J. Mol. Catal.* **1982**, *14*, 241–246. c) S. Németh, L. I. Simándi, G. Argay, A. Kálmán, *Inorg. Chim. Acta* **1989**, *166*, 31–33. d) S.-M. Peng, D.-S. Liaw, *Inorg. Chim. Acta* **1986**, *113*, L11–L12.

[22] D. J. Dodsworth, C. M. Jenkins, R. Stephens, J. C. Tatlow, *J. Fluorine Chem.* **1984**, *24*, 41–60.

[23] A. Sugimoto, Y. Yoshino, R. Watanabe, K. Mizuno, *J. Heterocycl. Chem.* **1999**, *36*, 1057–1064.

[24] J. Trotter, *Acta Cryst.* **1960**, *13*, 86–95.

[25] T. Steiner, *Chem. Commun.* **1997**, 727–734.

[26] N. Hughes, *Six-membered heterocyclic compounds with two hetero-atoms from Group V of the Periodic Table*, in: M. Ansell (Ed.), Rodd's Chemistry of Carbon Compounds, Vol. IV, Part I–J, 2nd ed., Elsevier, Amsterdam, **1989**.

[27] G. A. Swan, D. G. I. Felton, *Phenazines*, in: A. Weissberger (Ed.), The Chemistry of Heterocyclic Compounds, Vol. XI, Interscience, London, **1957**.

[28] D. J. Sandman, *J. Am. Chem. Soc.* **1978**, *100*, 5230–5232.

[29] T. Mikayama, H. Matsuoka, M. Ara, K. Uehara, A. Sugimoto, K. Mizuno, *Sol. Energy Mater. Sol. Cells* **2001**, *65*, 133–139.

[30] a) W. Wang, P. Preville, N. Morin, S. Mounir, W. Cai, M. A. Siddiqui, *Bioorg. Med. Chem. Lett.* **2000**, *10*, 1151–1154 b) G. W. Rewcastle, W. A. Denny, B. C. Baguley, *J. Med. Chem.* **1987**, *30*, 843–851. c) J. Shoji, R. Sakazaki, H. Nakai, Y. Terui, T. Hattori, O. Shiratori, E. Kondo, T. Konishi, *J. Antibiot.* **1988**, *41*, 589–594. d) J. F. O'Sullivan, M. L. Conalty, N. E. Morrison, *J. Med. Chem.* **1988**, *31*, 567–572.

[31] a) V. D. Shteingarts, A. G. Budnik, *Izvestiya Sibirskogo Otdeleniya Akademii Nauk SSSR, Seriya Khimicheskikh Nauk* **1967**, *3*, 124–127. b) A. G. Hudson, A. E. Pedler, J. C. Tatlow, *Tetrahedron* **1970**, *26*, 3791–3797. c) A. G. Hudson, M. L. Jenkins, A. E. Pedler, J. C. Tatlow, *Tetrahedron* **1970**, *26*, 5781–5787. d) E. Leyva, C. Medina, E. Moctezuma, S. Leyva, *Can. J. Chem.* **2004**, *82*, 12, 1712–1715. e) R. E. Banks, A. Prakash, *J. Chem. Soc. Perkin Trans. I* **1974,** 1365–1371. f) R. E. Banks, I. M. Madany, R. G. Pritchard, *Acta Crystallogr., Sect. C: Cryst. Struct. Commun.* **1993**, *C49*, 1988–1990.

[32] a) T. Nogami, T. Hishida, M. Yamada, H. Mikawa, Y. Shirota, *Bull. Chem. Soc. Jpn.* **1975**, *48*, 3709–3714. b) "Chemistry of Carbon Compounds", ed. by E. H. Rodd, Elsevier, Amsterdam, Houston, London, New York, **1954**, Vol. III, p. 451; Vol. IV, p. 1500, 1541, 1549.

[33] W. Kaim, B. Schwederski, *Bioinorganic Chemistry: Inorganic Elements in the Chemistry of Life, An Introduction and Guide*, **1994**, John Wiley & Sons, Chichester, p. 39; and references therein.

[34] F. E. Hahn, D. Scharn, T. Lugger*, Z. Kristallogr.-New Cryst. Struct.* **1997**, *212*, 472.

[35] a) V. L. Goedken, S.-M. Peng, Y. Park, *J. Am. Chem. Soc.* **1974**, *96*, 284–285. b) E. G. Samsel, J. K. Kochi, *Inorg. Chem.* **1986**, *25*, 2450–2457; and references therein.

[36] a) S.-M. Peng, Yu. Wang, S.-L. Wang, M.-C. Chuang, *J. Chem. Soc., Chem. Commun.* **1981**, 329–330. b) S.-M. Peng, D.-S. Liaw, Ya. Wang, A. Simon, *Angew. Chem.* **1985**, *97*, 223–224.

[37] D. Sellmann, H. Binder, D. Häußinger, F. W. Heinemann, J. Sutter, *Inorg. Chim. Acta* **2000**, *300–302*, 829–836.

[38] H. Saltzman, J. G. Sharefkin, *Organic Synthesis* **1963**, *43*, 60–61.

[39] a) Y. Yamada, T. Yamamoto, O. Makoto, *Chem. Lett.* **1975**, *4*, 361–362. b) M. J. Sodergren, D. A. Alonso, A. V. Bedekar, P. G. Andersson, *Tetrahedron Lett.* **1997**, *38*, 6897–6900.

[40] CCDC 278836 (**6**) and CCDC 278837 (**7**) contain the supplementary crystallographic data for this paper. These data can be obtained free of charge via www.ccdc.cam.ac.uk/conts/retrieving.html (or from the CCDC, 12 Union Road, Cambridge CB2 1EZ, UK; fax +44 1223 336033; e-mail: deposit@ccdc.cam.ac.uk).

☙ Chapter III ❧

Molecular and electronic structures of homoleptic nickel and cobalt complexes with non-innocent bulky diimine ligands derived from fluorinated 1,4-diaza-1,3-butadien (DAD) and bis(arylimino)acenaphthene (BIAN).

Abstract.

The diimine complexes with bulky fluorinated *N*-substituents $[Ni^{II}(^{F}DAD)_2]$ **8** and $[Co^{II}(^{F}DAD)_2]$ **9** (^{F}DAD – *N,N'*-bis(pentafluorophenyl)-2,3-dimethyl-1,4-diaza-1,3-butadiene) as well as diimine complexes with an extended π-system $[Ni^{II}(^{F}BIAN)_2]$ **10** and $[Co^{I}(^{F}BIAN)_3]$ **11** (^{F}BIAN – bis[*N*-{3,5-bis(trifluoromethyl)phenyl}imino]acenaphthene) were synthesized. Compound **11** represents the first complex with three bis(imino)acenaphthene ligands synthesized so far. The molecular structures of the complexes **8** – **11** were determined by X-ray crystallography at 193 K. Complexes **8**, **9** and **10** comprise the divalent metal ions with pairs of radical monoanionic ligands, whereas **11** is best described as a cobalt(I) complex with two neutral $(^{F}BIAN)^{0}$ and one $(^{F}BIAN)^{1-}$ ligand in the radical monoanionic form. The electronic structures of the paramagnetic cobalt complexes **9** and **11** were investigated by SQUID measurements and X-band EPR spectroscopy. Both complexes possess a doublet ground state, with electron density located predominantly in the metal d-orbitals. The doublet–quartet energy gap for **11** was established to be 159 cm^{-1}.

Introduction.

Homoleptic complexes of substituted 1,4-diaza-1,3-butadien with late transition metals $[M(DAD)_2]$ are well know since the first publication of Balch and Holm in early 1966.[1] They synthesized extremely oxygen sensitive complex $[Ni(Ph\text{-}DAD(Me))_2]$ and proposed the electronic structure of it as Ni^{II} center with two radical monoanionic $(DAD)^{1-}$ ligands.

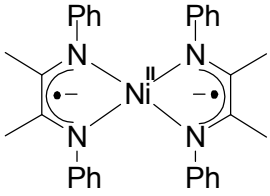

Nowadays, it is clearly established that the $(DAD)^0$ ligand possessing a low lying antibonding π^* orbital is able to accept one or two electrons giving open-shell monoanion $(DAD)^{1-}$ or closed-shell dianion $(DAD)^{2-}$, respectively. Thus DAD along with related *o*-phenylenediamido ligand belong to the classical *N,N′*-coordinating non-innocent ligands.[2]

R'-DAD(R) :

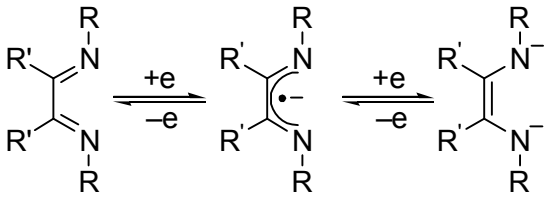

DAD^0 **DAD^{1-}** **DAD^{2-}**

The class of $[M(DAD)_2]$ complexes was expanded by the groups of tom Dieck (M = Fe[3], Ni[4]) and von Walther (M = Fe[5], Co[5,6], Ni[7]). Later, several $[Ni(DAD)_2]$ complexes were characterized by single crystal X-ray analysis.[8,9] In contradiction to the electronic model given by Balch and Holm all these complexes were formulated as zero-valent metal species with pairs of closed-shell $(DAD)^0$ ligands. At the same time closely related complexes derived from *o*-phenylenediamine $[Ni^{II}(sbqdi)_2]$[10] (sbqdi – semibenzoquinonediiminato(1–)) and diaminomaleonitrile $[Ni^{II}(sdisn)_2]$[11] (sdisn – semidiiminosuccinonitrilo(1–)) are well known to consist of a divalent metal and a pair of monoanionic radical ligands.

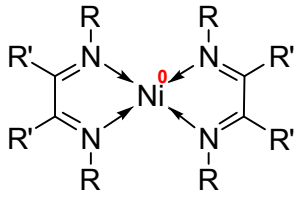

$[Ni^0(DAD)_2]$

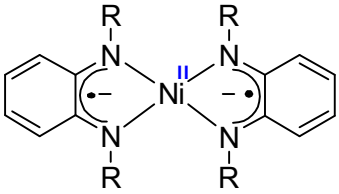

$[Ni^{II}(sbqdi)_2]$

R, R' = H, Alk, Ar

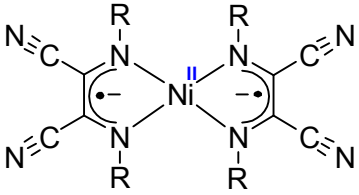

$[Ni^{II}(sdisn)_2]$

Throughout this paper we carefully distinguish between formal[12] and spectroscopic (or physical)[13] oxidation states. The formal oxidation state of a metal ion in a given coordination compound is a non-measurable, physically meaningless, usually integral number that is derived by heterolytic removal of all ligands in their closed-shell electron configuration, whereas the spectroscopic oxidation state is derived from the actual electron configuration of the metal ion in a given ligand regime.

Complexes of late transition metals with redox active non-innocent ligands[2] are of particular interest with regard to their electronic structures. Since late transition metals commonly have several oxidation states available, ambiguity of oxidation state determination may arise with

transition metal coordinated to the non-innocent ligand. Often spectroscopic (or physical) oxidation state of the non-innocent ligand can be elegantly determined using a high-quality single crystal X-ray analysis, as different oxidation states of the ligand reveal different characteristic bond distances.[14]

Following our studies on complexes of late transition metals containing non-innocent ligands[15] we report here the first structurally characterized $[Co(DAD)_2]$ complex along with its Ni analogue. Both molecular and electronic structures of them are being investigated by X-ray analysis, EPR spectroscopy, and variable-temperature magnetic susceptibility measurements.

Similar to DAD bis(arylimino)acenaphthene (BIAN)[16] owing to its non-innocent nature is known to form complexes in different ligand oxidation states.

Ar-BIAN:

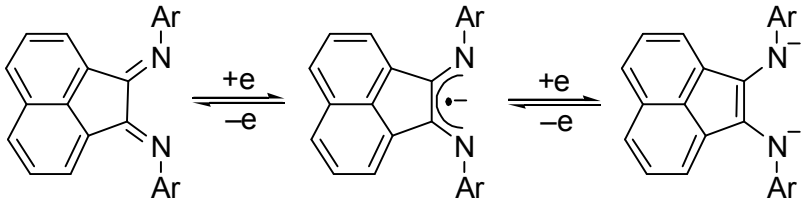

BIAN^0 **BIAN^{1-}** **BIAN^{2-}**

Very recently, Fedushkin et al.[17] reported the first homoleptic complexes of the type $[M^{II}(BIAN)_2]$ (M = Mg, Ca). The molecular structure of $[Ca^{II}(Dip\text{-}BIAN)_2]$ (dip – 2,6-diisopropylphenyl) was established and monoanionic nature of both ligands along with conventional oxidation state for calcium were established. To the best of our knowledge homoleptic complexes of the type $[M(BIAN)_2]$ with transition metals have been not isolated and structurally characterized so far. Therefore, the class of homoleptic DAD complexes has been further expanded by us to corresponding BIAN complexes. Molecular structures of BIAN complexes of nickel and cobalt are reported. The electronic structure of the paramagnetic cobalt complex is investigated in detail by means of EPR spectroscopy and variable-temperature magnetic susceptibility measurements.

Results and Discussion.

Synthesis and Characterization of DAD Complexes.

In order to synthesize complexes **8** and **9** we employed a variation of the well know *in situ* reduction method.[7,8] Complexes **8** and **9** were obtained in moderate to high yields by complexation of anhydrous metal salts with two equivalents of the ligand in the presence of two equivalents of C_8K as a reducing agent. The target complexes are oxygen and moisture sensitive and should be handled and stored under strictly anaerobic conditions.

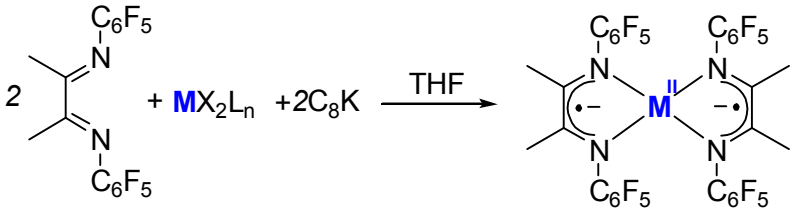

M = **Ni**, X = Br, L = DME, n = 1 **[Ni^{II}(^{F}DAD)$_2$]** **8**

M = **Co**, X = Cl, n = 0 **[Co^{II}(^{F}DAD)$_2$]** **9**

At room temperature complex **8** is diamagnetic in solution and shows three sharp multiplets in the ^{19}F NMR spectrum in the expected region –150…–164 ppm versus $CFCl_3$. It is interesting to note significant changes in the ^{1}H NMR spectrum accompanying the complexation. While in the free ligand the methyl group is observed at 2.24 ppm, it is slightly broadened ($W_{1/2}$ = 6 Hz) and strongly high-field shifted in the complex and observed at –1.98 ppm. The same observation was made by tom Dieck et al. for a series of [Ni(DAD)$_2$] complexes.[8] We ascribe this unusual shift to residual paramagnetism of **8** derived from low lying triplet state populated at room temperature. The signal at –1.98 ppm in the ^{1}H NMR spectrum of **8** was virtually temperature-independent, it was only slightly low-field shifted to –1.79 ppm by cooling the sample from 300 to 243 K.

Although a distorted tetrahedral environment of Ni^{II} (*vide infra*) results in high-spin complex (S_{Ni} = 1), the two radical ligands seem to couple antiferromagnetically with the metal giving ultimately a diamagnetic complex. Quenching of inherent paramagnetism of Ni^{II} in a distorted tetrahedral arrangement of two chelating radical ligands has recently been reported by Wieghardt et al.[18] EPR spectroscopy applied to **8** gave evidence for its diamagnetism. Complex **8** was X-band EPR silent in solution/frozen solution at temperatures 4–300 K.

Complex **9** is paramagnetic both in solid state and in solution, with effective magnetic moment μ_{eff} = 3.26 (in μ_B) measured for the solid at room temperature. This value is close to the spin state S = 3/2, further investigation of the electronic structure of **9** is given below. Several attempts to synthesize copper and iron analogues of **8** and **9** were unsuccessful (see Exper. Part).

Crystal Structures of DAD Complexes.

The molecular structure of **8** consists of two *N,N'*-chelating ^{F}DAD ligands coordinated to the metal center (Figure 1). Two ^{F}DAD ligands form a dihedral angle 55.28(9)° reflecting a twisted tetrahedral geometry at the metal center. The complex shows C_2 symmetry having 2-fold symmetry axis defined by Ni atom and the centroids of the diimine C–C bonds. Two metallacycles NiNCCN do not show any bend along NN'-axis, which would be the characteristic feature for doubly reduced DAD ligands.[19] In contrast they are essentially planar with maximum deviation of 0.031(2) Å from the best-fit planes defined by E_1 (Ni1N1C1C1'N1') and E_2 (Ni1N2C3C3'N2'). The sum of angles at each nitrogen atom is close to 360° typical for planar sp^2-hybridized *N*-centers. Since the bond distances in two diimines are the same within ± 0.012 Å (3σ) two ligands have an identical oxidation state.

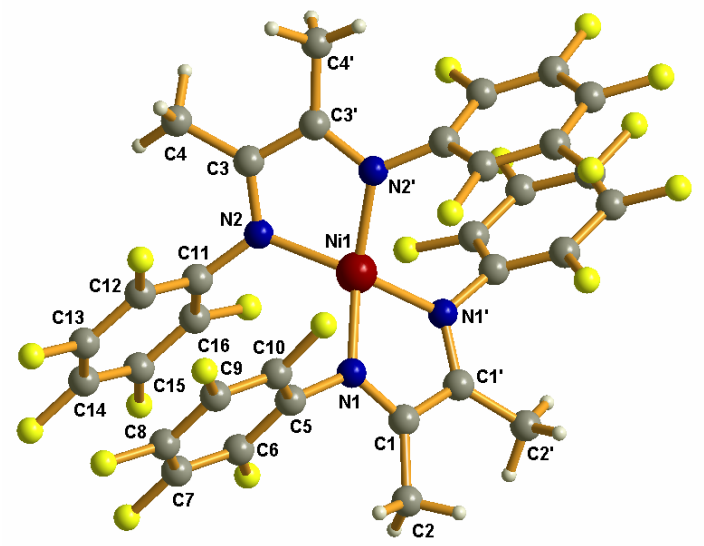

Figure 1. Molecular structure of **8**, thermal ellipsoids are drawn at 30% probability level.

The oxidation state of the ligands and consequently of the metal can be unambiguously assigned on the basis of the bond lengths analysis. In comparison of C–C and C–N bond distances of diimine moieties in **8** (Table 1) with corresponding bond distances in complexes, whose structures were determined accurately (Scheme 1), it is evident that both ligands in **8** are radical monoanions $(^{F}DAD)^{1-}$. The C–N bond length at average (av.) 1.344(3) Å along with C–C bond of NCCN-backbone at av. 1.413(5) Å are in good agreement with the presence of an open-shell $(^{F}DAD)^{1-}$.[20] Since the complex possesses no extra charge, the physical (or spectroscopic)[13] oxidation state of Ni is +II (d^8 electronic configuration).

Table 1. Selected bond lengths [Å] of complexes **8**, **9**.

$[Ni^{II}(^{F}DAD)_2]$ (**8**)		$[Co^{II}(^{F}DAD)_2]$ (**9**)	
Ni1–N1	1.9173(18)	Co1–N1	1.932(3)
Ni1–N2	1.9165(17)	Co1–N2	1.931(3)
C1–N1	1.340(3)	C7–N1	1.352(5)
C3–N2	1.348(3)	C15–N2	1.357(5)
C1–C1#	1.414(5)	C7–C7#	1.408(8)
C3–C3#	1.411(4)	C15–C15#	1.412(8)

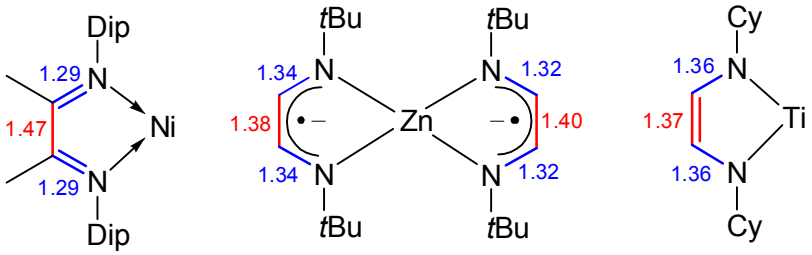

Scheme 1. Characteristic bond lengths for DAD ligand in different oxidation states: $(DAD)^0$ in $[Ni^{II}$(Dip-DAD(Me))$(CH_2SiMe_3)_2]$[21] (left), $(DAD)^{1-}$ in $[Zn^{II}$(*t*Bu-DAD(H))$_2]$[20] (middle), and $(DAD)^{2-}$ in $[Ti^{IV}$(Cy-DAD(H))$Cl_2(THF)_2]$[22] (right).

The molecular structures of several homoleptic complexes $[Ni(DAD)_2]$ were reported previously.[8,9] All of them were formulated as Ni^0 complexes containing a pair of closed-shell $(DAD)^0$ ligands. Taking into account the bond distances of diimine moieties found in these complexes we suggest reformulation of their electronic structures. For example, the structure of $[Ni(dmp\text{-}DAD(H))_2]$[8b] (dmp – 2,6-dimethylphenyl) reveals the C–N bonds at av. 1.341(2) Å and C–C bonds of NCCN-backbone at av. 1.374(2) Å. The bond distance pattern observed in the former is in better agreement with the presence of the open-shell $(DAD)^{1-}$ rather than the closed-shell $(DAD)^0$. Having analyzed molecular structures of a series of reported $[Ni(DAD)_2]$ complexes we suggest new electronic structures for the following complexes: $[Ni^{II}(Cy\text{-}DAD(H))^{1-}{}_2]$,[8a] $[Ni^{II}(dmp\text{-}DAD(H))^{1-}{}_2]$,[8b] $[Ni^{II}(t\text{Bu-}DAD(H))^{1-}{}_2]$,[9a] $[Ni^{II}(Dip\text{-}DAD(H))^{1-}{}_2]$.[9b]

Almost all related homoleptic *o*-phenylenediamine derived complexes $[Ni^{II}(sbqdi)_2]$[10a,23] and diaminomaleonitrile derived $[Ni^{II}(sdisn)_2]$[11a] show strictly square-planar geometry, whereas **8** as well as $[Ni(DAD)_2]$ structurally characterized previously reveal twisted tetrahedral geometry. The dihedral angle formed by two diimine moieties varies from 44.5° in $[Ni(dmp\text{-}DAD(H))_2]$[8b] to 88.95° in $[Ni(t\text{Bu-}DAD(H))_2]$.[9a] The large deviation from a square-planar geometry observed in $[Ni(DAD)_2]$ complexes can be rationalized by steric repulsion of bulky *N*-substituents. In contrast, a series of $[Ni^{II}(sbqdi)_2]$ and $[Ni^{II}(sdisn)_2]$ complexes with small N–H substituents do not show any deviation from square-planar geometry, whereas $[Ni^{II}(sbqdi)_2]$ having bulky C_6F_5-groups attached

to four nitrogen atoms does show tetrahedral distortion: the two planar ligands form dihedral angle of 53.7(1)º.[24]

The heavy distortion from planarity in **8** is caused by interaction between the bulky C_6F_5-groups engaged in intramolecular C_6F_5–C_6F_5 stacking. The phenyl rings form dihedral angles in the range of 65.7(1)–67.3(1)° with corresponding diimine NCCN-planes and are pairwise close to coplanar with an interplanar angle of 2.9(1)°. The smaller distance between C_6F_5 centroid and the least-squares plane of adjacent C_6F_5 ring is 3.23 Å. If we assume that complex **8** adopts a square-planar geometry without significant changes in bond distances and angles, a simple geometrical consideration predicts that the coplanar C_6F_5-rings would be forced to a face-to-face distance of approximately 2.9 Å. Recently, by DFT calculations Lorenzo et al.[25] have shown that energy minimum for the gas-phase dimer $(C_6F_6)_2$ in face-to-face configuration is reached when the interplanar distance C_6F_6–C_6F_6 is 3.31–3.37 Å. Assuming that the energy minima for the pair C_6F_5–C_6F_5 in **8** and the calculated pair C_6F_6–C_6F_6 are reached at the close distances we expect strong repulsion between two pairs of C_6F_5-rings of the hypothetical square-planar complex **8**.

A tetrahedral distortion of the complex and synchronous rotation of the phenyl rings provide a relaxation of repulsive interaction and sufficient increase of the C_6F_5–C_6F_5 distances. The molecular structure of **8** reveals a slipped arrangement of two pairs of C_6F_5-rings. The interplanar C_6F_5–C_6F_5 distance found at 3.23 Å is in good agreement with distances 3.23 and 3.32 Å between C_6F_5-rings engaged in intramolecular stacking in the sandwich complex bis[η^5-1,2,4-tris(pentafluorophenyl)cyclopentadienyl]-iron(II)[26] and with distances 3.20–3.28 Å in the series of complexes [M(^{F}sbqdi)$_2$] (M = Co, Ni, Pd, Cu, ^{F}sbqdi – radical anion derived from doubly deprotonated *N,N′*-bis(pentafluorophenyl)-*o*-phenylenediamine).[24]

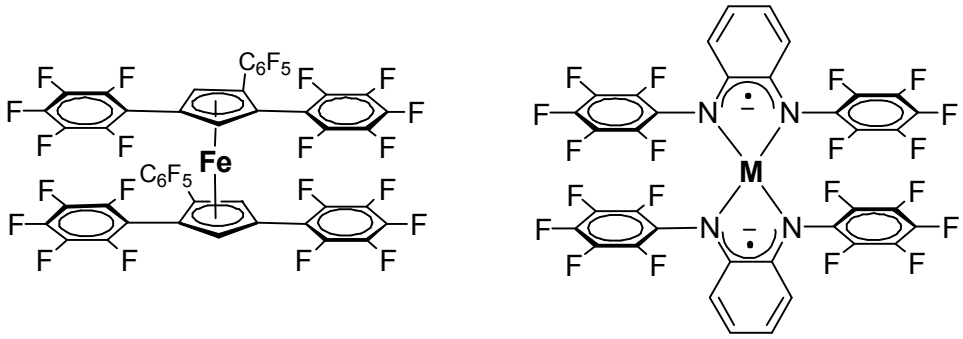

In conclusion, the twisted tetrahedral geometry of **8** is determined by repulsion forces between the two pairs of perfluorinated rings, which is a typical feature of four-coordinated Ni^{II} complexes with bulky ligands.

Although the synthesis of one homoleptic cobalt complex [Co(Ph-DAD(Ph))$_2$] was reported earlier[5,6] up to now no structural information about [Co(DAD)$_2$] complexes is available. The molecular structure of [Co^{II}(^{F}DAD)$_2$] (**9**), which is isomorphous with **8**, is shown in Figure 2. The

cobalt atom is located in a twisted tetrahedral environment of two chelating ^{F}DAD ligands, nearly planar diimine moieties form a dihedral angle of 58.0(2)°. The molecule is symmetrical having a C_2-axis defined by the cobalt atom and the centroids of the diimine C–C bonds. The five-membered metallacycles formed are essentially planar: the maximum deviation from the best-fit plane is 0.027(4) Å for both rings. The bond distances and angles within the two ^{F}DAD moieties are the same within 3σ.

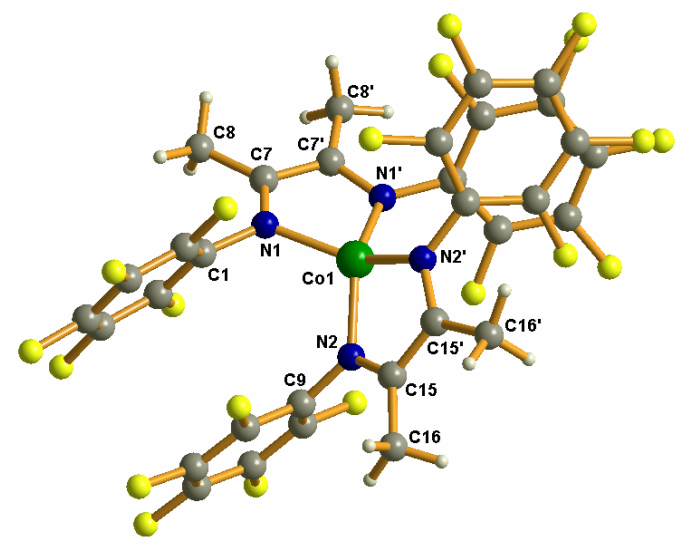

Figure 2. Molecular structure of **9** showing distorted tetrahedral geometry around the metal center; thermal ellipsoids are drawn at 30% probability level.

By comparison of the bond distance pattern of the NCCN-moieties in **9** with that of **8** it is found that ^{F}DAD ligands in both complexes are nearly similar (Table 1). In complex **9** C–N bond distances at av. 1.355(5) Å along with C–C bonds of the NCCN-backbone at av. 1.410(8) Å are in good agreement with the presence of two radical monoanions $(^{F}DAD)^{1-}$. Taking into account that the complex is not charged we assign the cobalt oxidation state to be +II (d^7 electronic configuration).

Slight C–N bond lengthening of 0.011 Å along with negligibly small C–C bond shortening of 0.003 Å in NCCN-backbone of **9** compared to **8** are ascribed to slightly higher population of π* orbitals of the ligands in **9**. Nearly coplanar C_6F_5-rings with a dihedral angle of 3.9(2)° display an interplanar distance close to that observed in **8**: the smaller distance between C_6F_5-centroid and the least-squares plane of adjacent C_6F_5 ring is 3.27 Å. Close interplanar distances C_6F_5–C_6F_5 observed for **8** and **9** confirm that the geometry of both complexes is governed by intramolecular C_6F_5–C_6F_5 interactions.

Synthesis and Characterization of BIAN Complexes.

Complexes **10** and **11** were prepared by ligand reduction with C_8K in the presence of the metal salts as described before for ^{F}DAD complexes. Surprisingly, reaction of 2 equiv of the ligand with 1 equiv of $CoCl_2$ gave neutral [Co(^{F}BIAN)$_3$] but not expected [Co(^{F}BIAN)$_2$]. Subsequent reaction of $CoCl_2$ with 3 equiv of ^{F}BIAN led to formation of the same [Co(^{F}BIAN)$_3$] with improved yield. Both complexes are sensitive towards oxygen and water. Strict anaerobic conditions should be applied by working with extremely sensitive [Co(^{F}BIAN)$_3$].

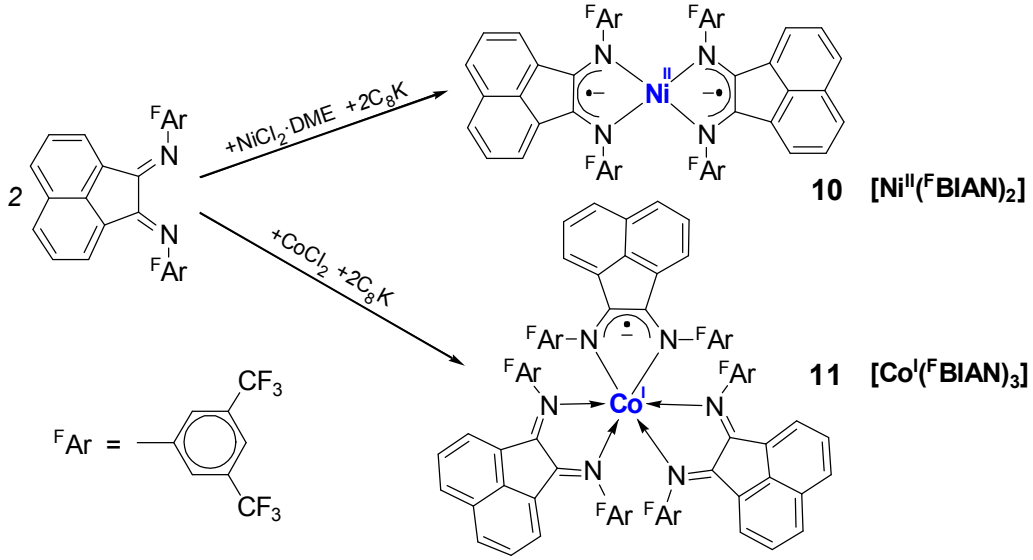

[Ni^{II}(^{F}BIAN)$_2$] shows sharp signals in ^{1}H and ^{19}F NMR spectra demonstrating its diamagnetism, whereas **11** is clearly paramagnetic. The μ_{eff} measured for solid **11** at room temperature is found to be 3.80 μ_B, which is consistent with three unpaired electrons per molecular unit and spin state S = 3/2. By means of NMR and X-band EPR spectroscopies we did not detect any equilibrium between **10** and free ^{F}BIAN with a hypothetical octahedral nickel analogue of **11**. Complex **10** was EPR silent in solution/frozen solution in temperature range 4–300 K.

Several attempts to synthesize homoleptic ^{F}BIAN complexes with iron, copper and palladium were unsuccessful (see Exper. Part).

Crystal Structures of BIAN Complexes.

The molecular structure of **10** consists of two planar chelating ^{F}BIAN ligands attached to the nickel atom (Figure 3). Similar to **8** and **9** the two ^{F}BIAN ligands in **10** form a distorted tetrahedral NiN_4 ligand environment. The dihedral angle formed by two diimine chelates is found to be 83.66(8)º.

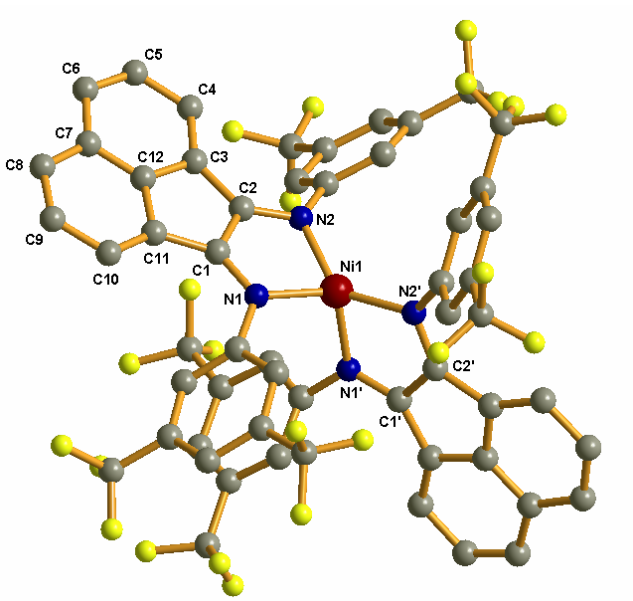

Figure 3. Molecular structure of **10**: disordered fluorine atoms are shown as semitransparent ellipsoids, hydrogen atoms are omitted for clarity, thermal ellipsoids are drawn at 30% probability level.

It is interesting to note that the two almost orthogonal diimine ligands do not form a regular tetrahedron. Instead, one ligand seems to be turned around the axis through Ni, perpendicular to the plane of the other diimine. For visualization of this unusual geometry the first coordination sphere of **10** is depicted in Figure 4.

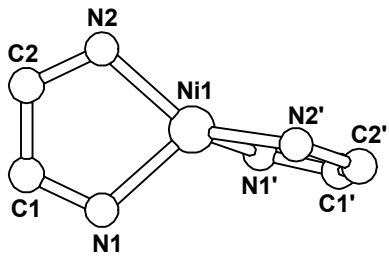

Figure 4. Ligands arrangement in **10**: a view exactly perpendicular to the plane defined by Ni1N1C1C2N2 (paper plane).

Consequently, local symmetry is missing completely in **10**. In contrast, complexes **8**, **9**, and all structurally characterized [Ni(DAD)$_2$] complexes with diverse sterically demanding *N*-substituents,[8,9] as well as [Ca(Dip-BIAN)$_2$] with bulky *N*-Dip groups[17] all form distorted tetrahedra with pseudo C_2/D_2 symmetry. The distorted tetrahedral geometry of **10** can be ascribed to intermolecular arene–arene interactions observed in the crystal structure. The acenaphthene rings involved in π-stacking are parallel with respect to each other and show an interplanar distance of 3.533 Å (Figure 5).

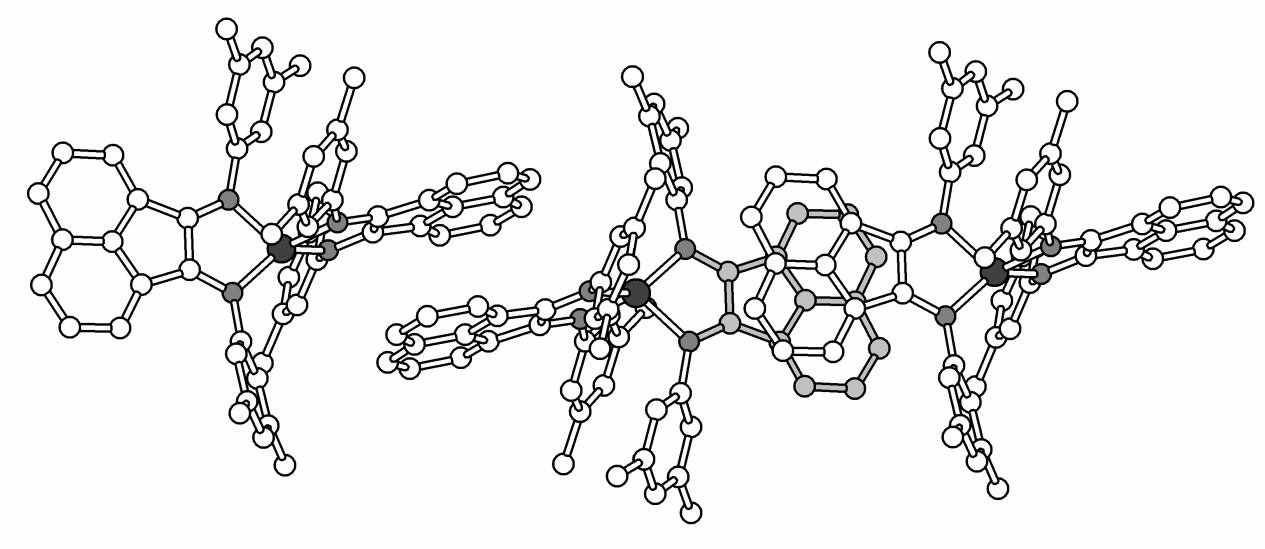

Figure 5. Crystal structure of $[Ni^{II}(^{F}BIAN)_2]$ (**10**) showing intermolecular π-stacking between ^{F}BIAN ligands; hydrogen and distorted fluorine atoms are omitted for clarity.

Oxidation state of the ligands can be unambiguously assigned by a bond lengths analysis. Typical bond lengths of bis(arylimino)acenaphthene ligand in different oxidation states are represented in Scheme 2. As the naphthalene system does not show distinct changes in bond lengths only C–N and C–C bond lengths of diimine moieties are given for the ligand in different oxidation states. In complex **10** diimine C–N bond is found at av. 1.339(2) Å and diimine bridging C–C bond at 1.427(3) Å (Table 2). Having compared bond distance pattern observed in **10** with those of known structures we assign both diimines in **10** to be in monoanionic radical form (Scheme 2). It implies that the oxidation state of Ni is +II and the electronic configuration of the metal is d^8.

Table 2. Selected bond lengths [Å] of complexes **10**, **11**.

$[Ni^{II}(^{F}BIAN)_2]$ (**10**)		$[Co^{I}(^{F}BIAN)_3]$ (**11**)			
		I		**II**	
Ni1–N1	1.9399(15)	Co1–N1	2.144(2)	Co1–N3	2.125(2)
Ni1–N2	1.9370(15)	Co1–N2	2.119(2)		
C1–N1	1.333(2)	C1–N1	1.302(4)	C29–N3	1.331(3)
C2–N2	1.344(2)	C2–N2	1.304(3)		
C1–C2	1.427(3)	C1–C2	1.474(4)	C29–C29#	1.442(5)

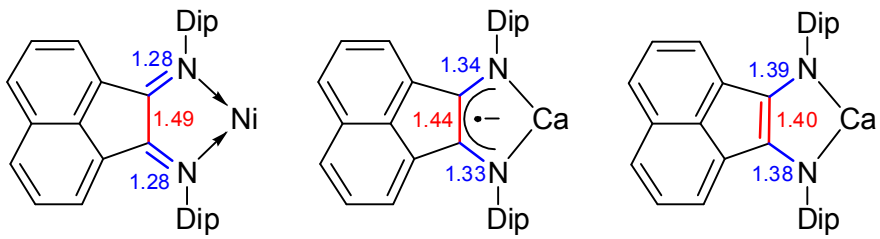

Scheme 2. Characteristic bond lengths for BIAN ligand in different oxidation states: $(BIAN)^0$ in $[Ni^{II}(Dip\text{-}BIAN)Br_2]_2$[27] (left), $(BIAN)^{1-}$ in $[Ca^{II}(Dip\text{-}BIAN)_2]$[17] (middle), and $(BIAN)^{2-}$ in $[Ca^{II}(Dip\text{-}BIAN)(THF)_3]$[28] (right).

The *N*-phenyl rings in **10** form dihedral angles 57.9(1) and 49.9(1)º with corresponding diimine moieties, hence the influence of these rings on the π-system of ^{F}BIAN is negligible. The observed dihedral angles along with deviation of N–C(phenyl) bonds from the diimine planes can be readily ascribed to intramolecular interactions between sterically demanding substituted phenyl rings. The only structurally characterized complex of the type [M(BIAN)$_2$] was reported very recently by Fedushkin et al.[17] The crystal structure of paramagnetic [Ca^{II}(Dip-BIAN)$_2$] reveals the dihedral angle 28º between diimine moieties and shows no any π-stacking between diimine moieties in the crystal lattice.

The molecular structure of cobalt complex **11** is represented in Figure 6. It consists of three(!) sterically demanding ^{F}BIAN ligands attached to the metal center. While complexes containing three less demanding DAD ligands are known,[29] to the best of our knowledge, complexes containing three BIAN ligands are unknown so far.

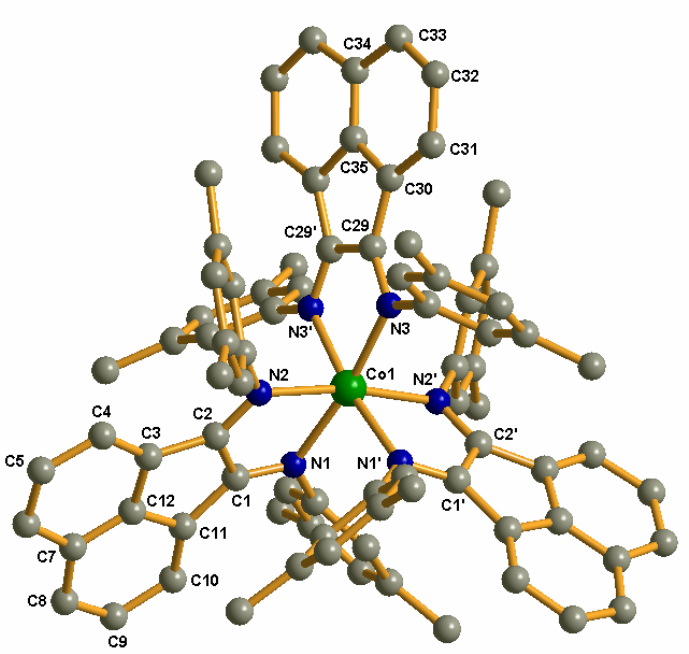

Figure 6. Molecular structure of **11**: hydrogen and disordered fluorine atoms are omitted for clarity, thermal ellipsoids are drawn at 30% probability level.

The cobalt ion in **11** has a slightly distorted octahedral environment. Three diimine ligands show considerable planarity and planes of them are almost perpendicular to each other, as expected for a perfect octahedron. Taking into account that synthesis of complex **11** is performed under strong reducing conditions we reject its description as Co^{III} with three (^{F}BIAN)$^{1-}$ ligands. The oxidation state of the metal is assumed to be +II or lower. Analysis of bond distances of diimines shows non-equivalence of the three ligands. Two ^{F}BIAN ligands are crystallographically identical (Table 2, form **I**), whereas the third one (form **II**) reveals a distinctly differing bond pattern. The bond distance pattern observed in **II** closely resembles that in complex **10**. The diimine C–N bond

at av. 1.331(3) Å in **II** (av. 1.339(2) Å in complex **10**) and diimine C–C bond at 1.442(5) Å in **II** (1.427(3) Å in complex **10**) are in agreement with formulation of **II** as a radical monoanion. On the other hand C–N bonds in **I** are significantly shorter (av. 1.303(4) Å) and diimine C–C bond is significantly longer (1.474(4) Å) compared to **II** indicating neutral diimine character. Comparison of bond distances in **I** with those of previously characterized complexes (Scheme 2) confirms that **I** is best described as neutral ligand. Hence, complex **11** contains one diimine in form of the radical monoanion and two neutral diimine ligands. This implies that the oxidation state of the cobalt atom in **11** is best described as +I with d^8 electronic configuration and correct description of **11** is $[Co^{I}(^{F}BIAN)^{0}_{2}(^{F}BIAN)^{1-}]$.

As expected the Co–N distances were found to be much longer in **11** compared to **9**. This is due to the increase of effective ionic radius $Co^{II} \rightarrow Co^{I}$ and to a change of coordination number from four in complex **9** to six in complex **11**. It can be noted that in complex **11** the distances Co–N in monoanionic $(^{F}BIAN)^{1-}$ at 2.125(2) Å are slightly shorter then those in closed-shell $(^{F}BIAN)^{0}$ at av. 2.132(2) Å. We refer this difference to the additional attraction between monoanionic $(^{F}BIAN)^{1-}$ and positive charged metal, which is lacking in the case of the neutral $(^{F}BIAN)^{0}$. The observed Co–N bond distances are close to that reported for $[Co(bpy)_3]Cl$ at av. 2.11(2) Å.[30]

Magnetochemistry and EPR Spectroscopy.

The electronic structures of the paramagnetic complexes **9** and **11** were further investigated by variable-temperature magnetic susceptibility measurements and X-band EPR spectroscopy.

The temperature dependence of the effective magnetic moment (μ_{eff}) of **9** is shown in Figure 7. The magnetic moment decreases gradually from 3.26 μ_B at 300 K to 2.36 μ_B at 5 K. From the crystal structure we have established that **9** contains Co^{II} ion (d^7) and two radical anionic ligands. Therefore **9** represents a three center odd electron system. The value of μ_{eff} at low temperatures is in accord with a doublet ground state (S = 1/2). The first excited quartet state (S = 3/2) becomes populated with increasing temperature.

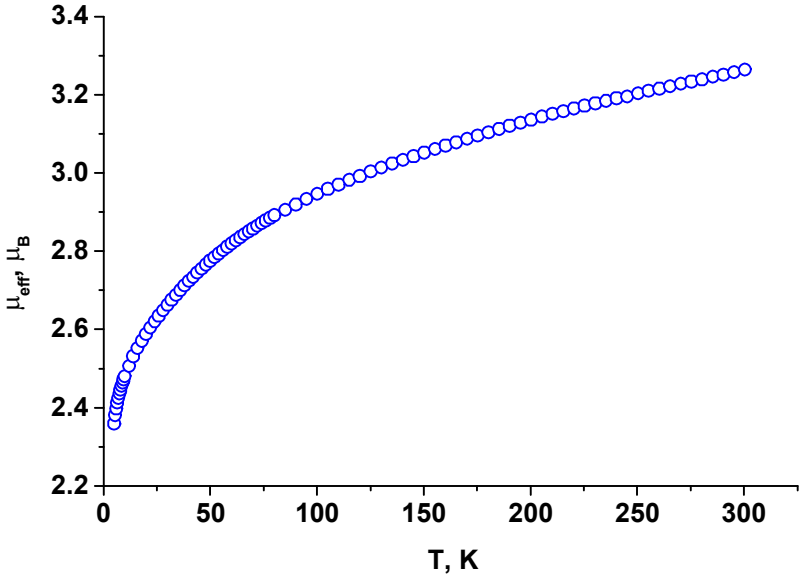

Figure 7. Temperature dependence of the effective magnetic moment of **9**.

The spin state of cobalt is not inherently clear because of the twisted coordination geometry around the metal center of **9**. Most cobalt(II) complexes are high-spin compounds (S_{Co} = 3/2) in tetrahedral, but low-spin (S_{Co} = 1/2) in planar environment. The molecular structure of **9** showing the dihedral angle of 58.0(2)° between the two diimines moieties takes an intermediate position between the tetrahedral and the planar geometries. The doublet ground state can be achieved by combination of the high-spin cobalt ion with the two radical ligands both coupled antiferromagnetically with the metal (Scheme 3, **A**). Another possibility to achieve the ground state doublet is to let the low-spin cobalt ion couple with two organic radicals, where two more types of electronic structures are to be considered. Two organic radicals couple in ferromagnetic fashion with each other but in antiferromagnetic fashion with the metal (**B**) yielding required S = 1/2. Or the two ligand spins couple antiferromagnetically with each other so that the metal spin is aligned ferromagnetically to one of the ligand spin but antiferromagnetically to the other one resulting in the doublet ground state (**C**).

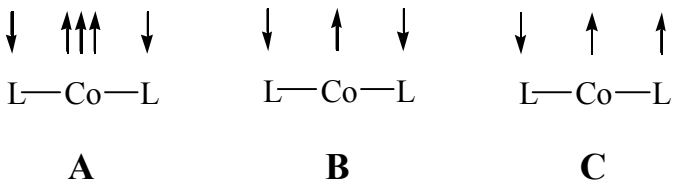

Scheme 3. Ground state spin models for **9**.

In recent papers of Wieghardt et al.[10] it was shown that related planar complexes [M^{II}(sbqdi)$_2$] (M = Ni, Pd, Pt) containing radical ligands reveal strong antiferromagnetic coupling between two remote ligands. The ligands interact strongly with each other via an efficient superexchange mechanism that is mediated by a back-bonding interaction to the central metal. Such

a superexchange interaction between two remote radicals is efficient only for certain geometries of the complexes. Very recently Ye et al.[31] showed, that if the geometry of such complexes deviates significantly from planarity, the interaction between two remote radical ligands becomes significantly weaker. Therefore, the spin state of **9** is likely to be of type **A** or **B,** with dominating antiferromagnetic interactions between the cobalt and radical ligand, but unlikely **C**, with dominating antiferromagnetic coupling between two radical ligands.

For fitting the experimental data we used tentatively the following Hamiltonian:

$$\mathbf{H} = -J_{ab}(\mathbf{S_{Co}}\cdot\mathbf{S_1} + \mathbf{S_{Co}}\cdot\mathbf{S_2}) - J_{aa}(\mathbf{S_1}\cdot\mathbf{S_2}) + \beta[(\mathbf{S_1} + \mathbf{S_2})\cdot\mathbf{g_R} + \mathbf{S_{Co}}\cdot\mathbf{g_{Co}})]\cdot H \qquad (1)$$

Here the first term is the Heisenberg term accounting for the isotropic exchange interaction between the metal and the radical ligands with J_{ab}, the second term relates to the isotropic exchange between two radical ligands with J_{aa}, and the third one is the Zeeman perturbation term. For the spin model **A** $S_{Co} = 3/2$ and for the model **B** $S_{Co} = 1/2$. The $\mathbf{g_{Co}}$ and $\mathbf{g_R}$ were assumed to be isotropic with g_{Co} and g_R principal values, for radical ligands $S_1 = S_2 = 1/2$.

Since equation for magnetic susceptibility derived from Hamiltonian (1) in the case $S_{Co} = 3/2$, $S_1 = S_2 = 1/2$ was not found in the literature, we deduce the target equation from the general formula reported by Kahn[32]. For symmetrical trinuclear ABA system the general expression for χ was reported to be

$$\chi = \frac{N\beta^2}{3kT}\frac{\sum_{S'=0}^{2S_A}\sum_{S=|S'-S_B|}^{S'+S_B} g_{S,S'}^2 S(S+1)(2S+1)\exp(-E(S,S')/kT)}{\sum_{S'=0}^{2S_A}\sum_{S=|S'-S_B|}^{S'+S_B}(2S+1)\exp(-E(S,S')/kT)} \qquad (2)$$

$$\text{relative energies } E(S,S') = -\frac{J}{2}S(S+1) - \frac{J'-J}{2}S'(S'+1) \qquad (3)$$

here J – isotropic interaction parameter for pair A–B, J' – isotropic interaction parameter for pair A–A; S' varies by an integer value from 0 to $2S_A$, and for each S' value, S varies by an integer value from $|S'-S_B|$ to $S'+S_B$. A $g_{S,S'}$ factor correspond to each of the spins states with the energy $E(S,S')$, which is related to the local tensors g_A and g_B through[33]

$$g_{S,S'} = \frac{g_A[S(S+1) + S'(S'+1) - S_B(S_B+1)] + g_B[S(S+1) - S'(S'+1) + S_B(S_B+1)]}{2S(S+1)}. \qquad (4)$$

In our case, that is high-spin cobalt(II) and two radical ligands, $S_A = S_1 = S_2 = 1/2$, $S_B = S_{Co} = 3/2$, $J = J_{ab}$, $J' = J_{aa}$. The relative energies $E(S, S')$ deduced from Eq. 3 are

$$\begin{aligned} E(\tfrac{1}{2},1) &= \tfrac{3}{2}J & E(\tfrac{3}{2},1) &= 0 \\ E(\tfrac{5}{2},1) &= -\tfrac{5}{2}J & E(\tfrac{3}{2},0) &= (J'-J) \end{aligned} \qquad (5)$$

The level $E(3/2,1)$ was taken as the energy origin. According to Eq. 4 $g_{S,S'}$ factors are

$$g_{3/2,0} = g_B \qquad g_{5/2,1} = \frac{14g_A + 21g_B}{35}$$
$$g_{3/2,1} = \frac{4g_A + 11g_B}{15} \qquad g_{1/2,1} = \frac{-2g_A + 5g_B}{3} \qquad (6)$$

After substitution of calculated values $E(S,S')$ and $g_{S,S'}$ into Eq. (2) the final expression for magnetic susceptibility is

$$\chi = \frac{N\beta^2}{4kT}\left[\frac{10g_{3/2,0}^2 \exp\left(\frac{J-J'}{kT}\right) + 10g_{3/2,1}^2 + 35g_{5/2,1}^2 \exp\left(\frac{5J}{2kT}\right) + g_{1/2,1}^2 \exp\left(-\frac{3J}{2kT}\right)}{2\exp\left(\frac{J-J'}{kT}\right) + 2 + 3\exp\left(\frac{5J}{2kT}\right) + \exp\left(-\frac{3J}{2kT}\right)}\right] \qquad (7)$$

Analogously, the expression for magnetic susceptibility can be derived for the case of low-spin cobalt, i.e. $S_{Co} = S_1 = S_2 = 1/2$.

$$\chi = \frac{N\beta^2}{4kT}\left[\frac{g_{1/2,1}^2 + g_{1/2,0}^2 \exp\left(\frac{J-J'}{kT}\right) + 10g_{3/2,1}^2 \exp\left(\frac{3J}{2kT}\right)}{1 + \exp\left(\frac{J-J'}{kT}\right) + 2\exp\left(\frac{3J}{2kT}\right)}\right] \qquad (8)$$

where

$$g_{1/2,0} = g_B$$
$$g_{1/2,1} = \frac{4g_A - g_B}{3} \qquad (9)$$
$$g_{3/2,1} = \frac{2g_A + g_B}{3}$$

For details concerning deduction of Eq. 8 one is referred to the book of Kahn.[32]

Unfortunately, we were not able to obtain a reasonable fit to the experimental data for both low- and high-spin cobalt complex models using Eq. 8 and Eq. 7, respectively. The introduction of the intermolecular interactions and paramagnetic impurities did not improve the fit significantly. A more accurate model considering the local anisotropy and/or anisotropic interactions is therefore needed.

In spite of the unsuccessful simulations of magnetic susceptibility data, the ground state of **9** can be determined by EPR spectroscopy at cryogenic temperatures. Indeed, if we reject **C** because of geometrical reasons, then **A** and **B** would give apparently different EPR spectra at low temperatures. Model **A** would give the EPR signal typical for cobalt(II) complexes, whereas **B** would give a spectrum of an organic radical.

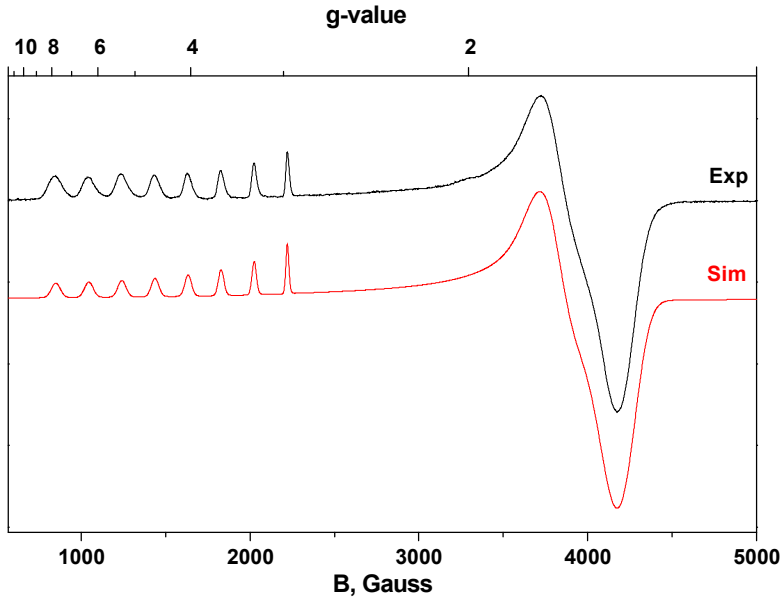

Figure 8. X-band EPR spectrum of **9**. Conditions: THF/toluene ~ 1:1 at 20 K; frequency 9.2265 GHz; power 5.0 μW; modulation amplitude 10 G. The fit parameters are given in the text.

The X-band EPR spectrum of **9** measured in a frozen solution at 20 K is shown in Figure 8. The large anisotropy of the *g* tensor and the hyperfine splitting of ^{59}Co (I = 7/2) indicate that the unpaired electron is located mostly on the metal d-orbitals and not on the ligands. Therefore the model **A** with high-spin Co^{II} is the most plausible description of this system. The EPR spectrum of **9** has been successfully simulated by using the rhombic *g* tensor: g_1 = 4.296, g_2 = 1.676, g_3 = 1.625, with ^{59}Co hyperfine coupling constants: A_1 = 197, A_2 = 52, A_3 = 56 G. Furthermore, the line width dependence was introduced as follows:

$$\Delta B(m_I) = \sum_{i=1}^{3} \alpha_i + \beta_i m_I + \gamma_i m_I^2 \qquad (10)$$

here m_I is the nuclear spin (m_I = –7/2, …, +7/2 for ^{59}Co nucleus); α_i, β_i, γ_i – orientation dependent (i = *x, y, z*) line width parameters.

The temperature dependence of μ_{eff} of **11** is shown in Figure 9. The magnetic moment measured at 300 K is 3.80 μ_B indicates the presence of three unpaired electrons (S = 3/2). With decreasing temperature μ_{eff} gradually decreases to the value of 2.07 μ_B at 10 K followed by a steep descent to 1.79 μ_B at 1.8 K. This behavior is explainable by the presence of the high-spin Co^{I} (d^8, S_{Co} = 1, pseudo-octahedral environment) and a radical ligand (S_R = 1/2) coupled in antiferromagnetic fashion. Thus, the ground state of **11** is a doublet with an excited quartet populated at higher temperatures. The abrupt decreasing of the magnetic moment at temperatures below 10 K can be ascribed to the intermolecular antiferromagnetic interactions in the solid.

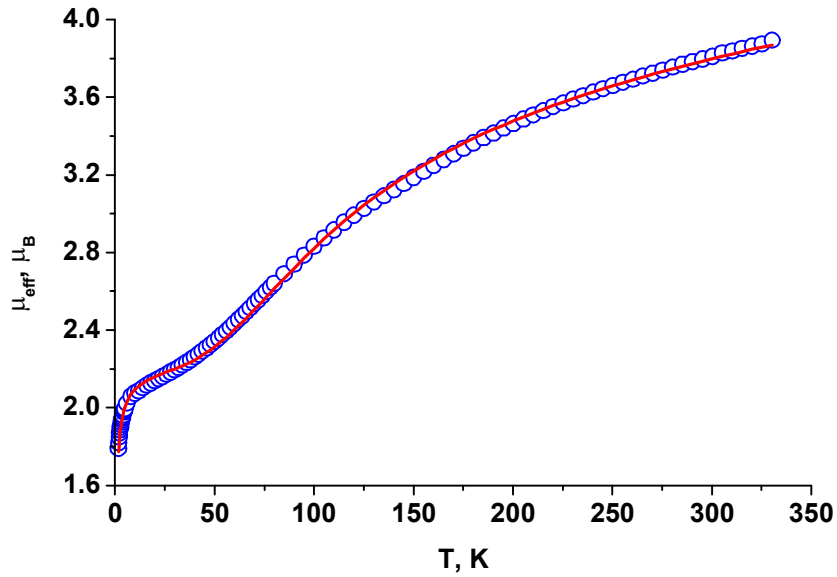

Figure 9. Temperature dependence of the effective magnetic moment of **11**, the fit parameters are given in the text.

To fit the experimental data we used the following Hamiltonian:

$$\mathbf{H} = -J\mathbf{S_{Co}}\cdot\mathbf{S_R} + \beta(\mathbf{S_{Co}}\cdot\mathbf{g_{Co}} + \mathbf{S_R}\cdot\mathbf{g_R})\cdot H \qquad (11)$$

where the first term is the Heisenberg term related to the isotropic exchange interaction (J) between two magnetic centers and the second term is the Zeeman perturbation, nonequivalence of **g** tensors is supposed. Assuming tensors $\mathbf{g_{Co}}$ and $\mathbf{g_R}$ to be isotropic with g_{Co} and g_R principal values and taking $S_{Co} = 1$, $S_R = 1/2$ the equation for magnetic susceptibility can be then derived:[32]

$$\chi = \frac{N\beta^2}{4kT}\frac{g_{1/2}^2 + 10g_{3/2}^2\exp(3J/2kT)}{1+2\exp(3J/2kT)} \qquad (12)$$

Here $g_{1/2}$ and $g_{3/2}$ factors correspond to each of the spin states, they are related to the local g factors through:

$$g_{1/2} = (4g_{Co} - g_R)/3 \qquad (13)$$
$$g_{3/2} = (2g_{Co} + g_R)/3$$

By adding temperature-independent paramagnetism (*TIP*) into Eq. 12 it was possible to obtain a good fit for magnetic susceptibility for the temperature range 10–330 K. To fit the data on the whole temperature range we modified Eq. 12 according to the molecular field approximation for weak intermolecular interactions: [34]

$$\chi' = \frac{\chi}{1-(2zJ'/Ng^2\beta^2)\chi} + TIP \qquad (14)$$

Here z is the number of the nearest neighbors around a given magnetic molecule in the crystal lattice and J' is the interaction parameter, the g factor in Eq. 14 was taken as equal to 2.

The best fit using Eq. 14 was obtained with the following parameters: $g_R = 2.00$ (fixed), $g_{Co} = 2.37$, $J = -106.0$ cm^{-1}, $zJ' = -0.78$ cm^{-1}, $TIP = 1.23\times10^{-3}$ cm^{3}mol^{-1}. The accuracy of the fit used is

very good showing $R^2 = 0.99924$. Hence, the ground state doublet is separated from the excited quartet by $-3J/2 = 159$ cm^{-1}. Week intermolecular antiferromagnetic interactions are present in the polycrystalline sample of **11**, as indicated by negative value of $zJ' = -0.78$ cm^{-1}. Abrupt decreasing of μ_{eff} of **11** at low temperatures may be governed by zero-field splitting effect as well, this supposition was not examined.

The X-band EPR spectrum of **11** measured in frozen solution at 4 K is shown in Figure 10. It is evident that more than one paramagnetic species is present. We propose two compounds to exist in the frozen solution. The first one is a cobalt complex with a large anisotropy of the *g* tensor (**Tet**): a well resolved octet centered at $g \sim 3.8$ and a less resolved signal at $g \sim 1.9$. The second species is a cobalt complex as well, but with a higher symmetric arrangement at the metal (**Oct**), its signal is partly hidden by those of **Tet** and centered at $g \sim 2.3$. Because **11** is extremely sensitive towards both oxygen and moisture, the EPR experiment was repeated several times with freshly prepared solutions. All samples measured gave nearly identical spectra. It was concluded that the two cobalt species observed originate not from decomposition of **11**, but from partially dissociation.

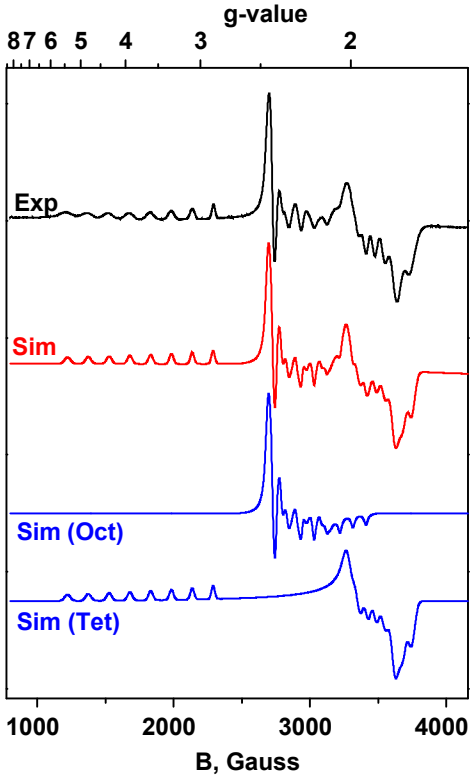

Figure 10. X-band EPR spectrum of **11**. Conditions: THF/toluene ~ 1:1 at 4 K; frequency 9.2278 GHz; power 1.3 μW; modulation amplitude 10 G. The fit parameters are given in the text.

Thus the distorted octahedral complex **11** partially dissociates in solution (toluene/THF ~ 1:1) into the neutral species [Co(^{F}BIAN)$_2$], which has very likely distorted tetrahedral geometry, and the free ligand ^{F}BIAN. Assuming that this dissociation takes place we can readily assign the signals in the EPR spectrum. Species **Tet** is expected to be [Co(^{F}BIAN)$_2$], whereas **Oct** is

apparently **11**. The EPR spectrum is therefore best explained by the superposition of two rhombic signals. The spectrum has been successfully simulated by using the following parameters: for **Oct** $g_1 = 2.363$, $g_2 = 2.243$, $g_3 = 2.143$, hyperfine coupling constants (^{59}Co) $A_1 = 17$, $A_2 = 58$, $A_3 = 96$ G; for **Tet** $g_1 = 3.756$, $g_2 = 1.874$, $g_3 = 1.895$, hyperfine structure (^{59}Co) $A_1 = 153$, $A_2 = 65$, $A_3 = 38$ G. For **Tet** showing the large anisotropy the line width dependence was included in the simulation. On warming, the signal of **Oct** disappears much faster than that of **Tet**. At 100 K only the poorly resolved signal of **Tet** is observed (Figure 11). This indicates that the relaxation time for **Oct** compared to **Tet** is small.

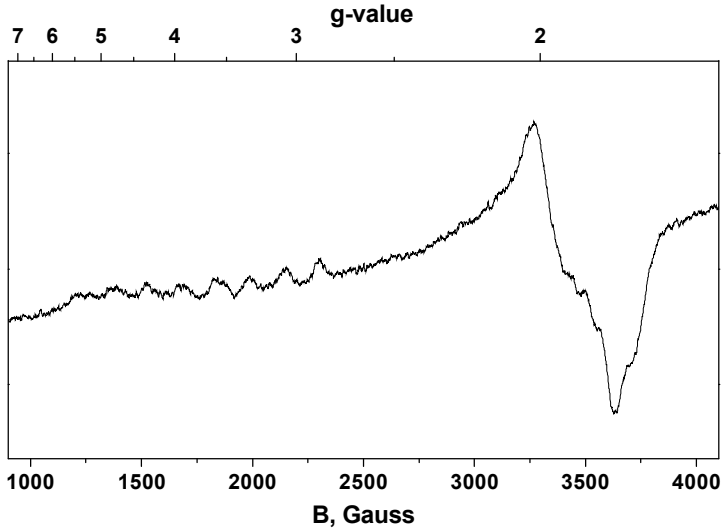

Figure 11. X-band EPR spectrum of **11**. Conditions: THF/toluene ~ 1:1 at 100 K; frequency 9.2265 GHz; power 0.3 mW; modulation amplitude 10 G.

Electronic Spectra.

Electronic spectra of the complexes **8**–**11** in chloroform and in *n*-hexane solutions were recorded at room temperature in the range 200–1100 nm. Spectra of DAD complexes **8** and **9** consist of a strong ($\varepsilon > 10^4$ dm^3·mol^{-1}·cm^{-1}) band in ultra-violet and weaker two (**8**) or four bands (**9**) in visible region. The absorption in ultra-violet can be assigned to intra-ligand (IL) transition, since the free ligand absorbs in the similar region. The long-wavelength bands in visible, determining the intensive color of the complexes presumably are charge-transfer (CT) transitions. Solvent dependence and high intensity renders them easy distinguishable from solvent independent and low intensive d–d transitions. The two bands in visible are characteristic for [Ni(DAD)$_2$] complexes, as was observed by tom Dieck for series of such complexes.[8]

UV-vis spectra of BIAN complexes **10**, **11** are dominated by intense IL electronic transitions (329–332 nm, $\varepsilon > 10^4$ dm^3·mol^{-1}·cm^{-1}), and three transitions in visible/NIR (Figure 12). The latter are supposed to be CT transitions relying on their relative high intensities ($\varepsilon = 8–10\times10^3$ and $5–12\times10^3$ dm^3·mol^{-1}·cm^{-1} for **10** and **11**, respectively) and solvatochromism. High-energy absorption

maxima in visible at 512 and 519 nm for **10** and **11**, respectively, are indicative for the presence of radical anion $(BIAN)^{1-}$. Several complexes reported recently by Fedushkin[35] containing radical $(BIAN)^{1-}$ all show absorption maximum/maxima in the region 420–530 nm.

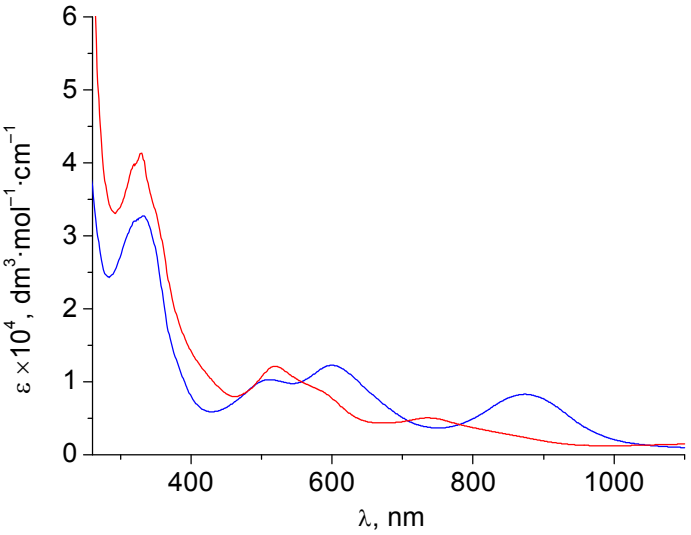

Figure 12. Electronic spectra of **10** (blue) and **11** (red) recorded in $CHCl_3$.

We refrain from discussing the more specific assignment of electronic absorptions of **8**–**11** in visible/NIR as sufficient confidence may only be achieved in combination with high-quality excited-state TD-DFT calculations.

Conclusions.

We have synthesized new complexes of nickel and cobalt containing the non-innocent highly π-acidic diimine ligands ^{F}DAD and ^{F}BIAN with bulky fluorinated *N*-substituents. The oxidation states of the ligands and subsequently of the metals were determined by single crystal X-ray analysis at low temperatures. The electronic structure of $[Ni^{II}(^{F}DAD)_2]$ as well as electronic structures of $[Ni(DAD)_2]$ complexes previously characterized by X-ray analysis were shown to be consistent with a divalent nickel d^8 ion and a pair of radical monoanionic ligands. The unique $[Co^{I}(^{F}BIAN)_3]$ comprises a cobalt(I) ion, two neutral $(^{F}BIAN)^0$ ligands and one radical monoanion $(^{F}BIAN)^{1-}$. Both $[Co^{II}(^{F}DAD)_2]$ and $[Co^{I}(^{F}BIAN)_3]$ possess a doublet ground state with electron density located mostly in the metal d-orbitals as was concluded from magnetic susceptibility measurements and X-band EPR spectroscopy.

Experimental Part.

The ligand C_6F_5-DAD(Me) (= ^{F}DAD) can be prepared by a known procedure with low yield.[36] Here we describe an alternative method of its preparation with much higher yield (*vide infra*). Anhydrous metal salts $NiCl_2$·DME,[37] $NiBr_2$·DME[37], $FeCl_2$[38], $PdCl_2(PhCN)_2$[39] as well as (3,5-$(CF_3)_2C_6H_3$)-BIAN[40] (= ^{F}BIAN) and C_8K[41] were prepared according to the known procedures. Anhydrous $CoCl_2$ and $CuCl_2$ were obtained by refluxing of $CoCl_2$·$n$$H_2O$ of $CuCl_2$·$n$$H_2O$, respectively, with $SOCl_2$ for several hours followed by removing the volatiles under reduced pressure at 90ºC. Syntheses of all complexes were performed under a dry argon atmosphere using standard Schlenk techniques and dried solvents.

Physical Measurements.

Mass spectra were obtained on a Finnigan MAT 95S mass spectrometer (70 eV, EI). IR spectra were obtained in Nujol mull using a Nicolet 510 FT-IR. UV-vis spectra were measured on a Shimadzu UV-1601PC instrument in absolute $CHCl_3$ and *n*-hexane at concentrations 10^{-4} – 10^{-5} mol·L^{-1}. NMR spectra were recorded at room temperature on a Bruker ARX 200 spectrometer at 200.13 MHz for ^{1}H and 188.29 MHz for ^{19}F. ^{1}H NMR spectra are referenced (in ppm) to residual proton signals of $CDCl_3$ (7.26 ppm) and C_6D_6 (7.15 ppm); ^{19}F NMR spectra were referenced to external standard $CFCl_3$. Abbreviations used are the following: s = singlet, d = doublet, t = triplet, pst = pseudo-triplet, m = multiplet. EPR spectra were recorded in the X-band on a Bruker System ESP 300. The magnetic susceptibility measurements were performed on a powder samples using a Quantum Design MPMS2 SQUID magnetometer with an applied field of 1 T. Experimental susceptibility data were corrected for the underlying diamagnetism using Pascal's constants.

X-ray Crystallographic Data Collection and Refinement of the Structures.

Single crystals of **8 – 11** were coated with inert oil, picked up with a glass fiber and mounted in the nitrogen cold stream of the STOE IPDS2 (**8**, **10**, **11**) or STOE IPDS diffractometer (**9**). Intensity data were collected at 193 K using graphite monochromated Mo-K_α radiation (λ = 0.17073 Å). Data collection was performed by hemisphere runs taking frames at 1.0° in ω. Final cell constants were obtained from a least squares fit of a subset of several thousand strong reflections. Intensity data of **8** and **10** were corrected using indexed crystal faces, the data of **11** using the semiempirical correction routine MulScanAbs.[42] For **9** an absorption correction did not improve the quality of the data and was not applied. There was disordered solvent (toluene) present in the crystal structures of **8**, **9**, and **11**. In the crystal structures of **10** and **11** the CF_3-groups are

disordered: two positions for each fluorine atom with different occupancies were found. All structures have been solved by the direct methods in SHELXS-97[43] (**8**, **10**, **11**) or SIR92[44] (**9**) and refined using the full matrix least squares refinement procedure of SHELXL97,[43] all non-hydrogen atoms anisotropically; H atoms have been located and isotropically refined (**8**, **10**) or have been placed at calculated positions and have been refined using a riding model with $U_{iso}(H) = 1.2U_{eq}(C)$ (**9**, **11**). Crystallographic data of the compounds are listed in Table 3. CCDC 290299–290302 contain the supplementary crystallographic data for complexes **8**–**11**. These data can be obtained free of charge from The Cambridge Crystallographic Data Centre via www.ccdc.cam.ac.uk/data_request/cif.

Table 3. Crystallographic Data for **8**·(C_7H_8), **9**·(C_7H_8), **10**, and **11**·2(C_7H_8).

	8·(C_7H_8)	**9**·(C_7H_8)	**10**	**11**·2(C_7H_8)
Empirical formula	C_{39} H_{20} F_{20} N_4 Ni	C_{39} H_{20} Co F_{20} N_4	C_{56} H_{24} F_{24} N_4 Ni	C_{98} H_{52} Co F_{36} N_6
Formula mass [g/mol]	983.30	983.52	1267.50	2056.39
Crystal size [mm]	0.45 x 0.12 x 0.06	0.28 x 0.06 x 0.04	0.28 x 0.27 x 0.05	0.40 x 0.14 x 0.04
Crystal shape	plate	needle	plate	prism
Crystal system	orthorhombic	orthorhombic	monoclinic	monoclinic
Space group	P b c n	P b c n	C 2/c	C 2/c
a [Å]	a = 20.0534(10)	20.077(2)	18.3645(19)	28.843(2)
b [Å]	b = 12.9233(7)	12.9232(14)	18.1763(14)	13.3691(9)
c [Å]	c = 14.2875(10)	14.3559(12)	16.7383(18)	23.2949(19)
β [°]			113.662(12)	101.695(6)
V [Å^3]	3702.7(4)	3724.8(6)	5119.1(9)	8796.3(11)
Z	4	4	4	4
$D_{calcd.}$ [g/cm^3]	1.764	1.754	1.645	1.553
μ [mm^{-1}]	0.663	0.599	0.511	0.325
$\theta_{min}/\theta_{max}$ [°]	1.87/26.24	1.87/26.26	1.65/26.01	1.44/26.20
T_{max}/T_{min}	0.95/0.80		0.97/0.87	0.95/0.91
Reflections collected	33387	28558	25039	62074
Reflections unique	3719	3744	4890	8806
Reflections observed	2536	1825	3355	4840
No. of parameters	328	312	544	790
R(F)	0.0315	0.0527	0.0330	0.0507
Rw (F^2)	0.0810	0.0916	0.0714	0.1139
S (GOF) on F^2	0.896	0.910	0.876	0.908
$\Delta\rho_{max}$ [e/Å^3]/$\Delta\rho_{min}$ [e/Å^3]	0.30/–0.19	0.27/–0.35	0.26/–0.25	0.52/–0.38

Synthesis of C_6F_5-DAD(Me) (8a).

To 2,3,4,5,6-pentafluoroaniline (9.15 g, 0.050 mol) dissolved in dry MeOH (15 mL) 2,3-butanedione (3.2 mL, 0.038 mol), *p*-toluenesulfonic acid (about 0.2 g), and trimethyl orthoformate (10.0 mL, 0.097 mol) were added. After stirring for 1 day at room temperature the pale yellow precipitate was filtered, washed with cold MeOH and dried *in vacuo*.

Yield: 5.19 g (50%).

^{1}*H NMR* (200.13 MHz, $CDCl_3$, 300 K): δ = 2.24 (t, *J* = 1.2 Hz, 6H, CH_3) ppm.

^{19}F NMR (188.29 MHz, $CDCl_3$, 300 K): δ = –151.3 (d, $^3J_{F,F}$ = 20 Hz, 4F, Ar_{ortho}), –161.3 (t, $^3J_{F,F}$ = 21 Hz, 2F, Ar_{para}), –162.9 (pst, $^3J_{F,F}$ = 20 Hz, 4F, Ar_{meta}) ppm.

Synthesis of [$Ni^{II}(C_6F_5$-DAD(Me))$_2$] (8).

$NiBr_2$·DME (371 mg, 1.20 mmol), C_8K (341 mg, 2.52 mmol) and **8a** (1000 mg, 2.40 mmol) were placed in a Schlenk flask and THF (50 mL) was added. The reaction mixture was stirred overnight at room temperature. The mixture was filtered via Celite and THF was removed *in vacuo* giving a purple powder. The raw product was repeatedly extracted with boiling toluene (50 mL) from a glass frit until almost colorless solution. After the toluene extract was stored for a night at –30°C, dark-purple crystals were collected by decantation of the solvent. The crystals were washed with cold *n*-hexane (2 × 5 mL) and dried *in vacuo*. Single crystals of **8** suitable for X-ray crystallography were obtained from a THF/toluene mixture (1:2) by cooling.

Yield: 660 mg (62%).

M.p. 200 – 203 °C.

$C_{32}H_{12}F_{20}N_4Ni$ (891.13): calcd. C 43.13, H 1.36, N 6.29; found C 43.66, H 1.85, N 5.96.

MS (EI): *m/z* = 889 [M – H^+], 474 [M – $(DAD)^+$], 416 [$(DAD)^+$].

^1H NMR (200.13 MHz, $CDCl_3$, 300 K): δ = –1.98 (s, 12H, CH_3) ppm.

^{19}F NMR (188.29 MHz, $CDCl_3$, 300 K): δ = –150.2 (m, 8F, Ar_{ortho}), –160.1 (t, $^3J_{F,F}$ = 21 Hz, 4F, Ar_{para}), –164.0 (m, 8F, Ar_{meta}) ppm.

IR (Nujol): $\tilde{\nu}$ = 1630 (w), 1508 (s), 1408 (s), 1308 (w), 1260 (w), 1196 (m), 1146 (w), 1117 (m), 1033 (s), 987 (s), 928 (m), 798 (w), 732 (m), 696 (w), 644 (w), 598 (w), 558 (w), 466 (w) cm^{-1}.

UV-vis ($CHCl_3$): λ_{max} (ε_{max}/dm^3·mol^{-1}·cm^{-1}) = 756 sh (3200), 524 (8000), ~292 (15200) nm.

UV-vis (*n*-hexane): λ_{max} = 753, 520, ~310 nm.

Synthesis of [$Co^{II}(C_6F_5$-DAD(Me))$_2$] (9).

$CoCl_2$ (156 mg, 1.20 mmol), C_8K (341 mg, 2.52 mmol) and **8a** (1000 mg, 2.40 mmol) were placed in a Schlenk flask and THF (40 mL) was added. The reaction mixture was stirred overnight at room temperature. The mixture was filtered and THF was removed *in vacuo* giving a brown powder. The raw product was extracted with *n*-hexane (65 mL), concentrated *in vacuo* and washed with cold benzene (5 mL). Brown single crystals of **9** suitable for X-ray crystallography were obtained from a THF/toluene mixture (3:1) by cooling.

Yield: 431 mg (40%).

M.p. 194 – 196 °C.

$C_{32}H_{12}CoF_{20}N_4$ (891.38): calcd. C 43.12, H 1.36, N 6.29; found C 42.92, H 1.69, N 5.91.

MS (EI): *m/z* = 890 [M – H^+], 475 [M – $(DAD)^+$], 416 [$(DAD)^+$].

IR (Nujol): $\tilde{\nu}$ = 1632 (w), 1514 (s), 1504 (s), 1402 (m), 1308 (w), 1197 (m), 1142 (w), 1119 (m), 1030 (s), 987 (s), 929 (m), 797 (w), 683 (m), 640 (w), 597 (w) cm^{-1}.

UV-vis ($CHCl_3$): λ_{max} (ε_{max}/$dm^3 \cdot mol^{-1} \cdot cm^{-1}$) = 697 (1200), 529 (3100), 470 (5400), 429 (5200), 335 (11600) nm.

Synthesis of [Ni^{II}((3,5-$(CF_3)_2C_6H_3$)-BIAN)$_2$] (10).

$NiCl_2$·DME (610 mg, 1.00 mmol), C_8K (143 mg, 1.06 mmol) and ^{F}BIAN (111 mg, 0.51 mmol) were placed in a Schlenk flask and THF (30 mL) was added. The reaction mixture was stirred overnight at room temperature. The resulting dark-blue suspension was concentrated under reduced pressure. The raw product was extracted with toluene (40 mL). After toluene was removed, a dark-blue fine crystalline material was obtained, which was washed with MeCN and dried *in vacuo*. Single crystals of **10** suitable for X-ray crystallography were obtained from a saturated *n*-hexane solution by cooling.

Yield: 518 mg (81%).

M.p. 321 – 323 °C.

$C_{56}H_{24}F_{24}N_4Ni$ (1267.47): calcd. C 53.07, H 1.91, N 4.42; found C 52.53, H 2.01, N 4.41.

MS (EI): *m/z* = 1266 [M^+], 1247 [M – F^+], 662 [M – $(BIAN)^+$].

^1H NMR (200.13 MHz, C_6D_6, 300 K): δ = 8.98 (s, 4H, H_{Ph}), 7.97 (m, 4H, H_{Ph}, H_{naph}), 7.10 (d, $^3J_{H,H}$ = 7.2 Hz, 2H, H_{naph}), 6.41 (pst, $^3J_{H,H}$ = 7.7 Hz, 2H, H_{naph}) ppm.

^{19}F NMR (188.29 MHz, C_6D_6, 300 K): δ = –63.0 (s, 12F, CF_3) ppm.

IR (Nujol): $\tilde{\nu}$ = 1776 (w), 1600 (m), 1510 (w), 1418 (w), 1275 (s), 1243 (w), 1127 (s), 1091 (s), 1014 (s), 974 (m), 884 (m), 850 (m), 812 (m), 761 (m), 700 (m), 678 (m), 544 (w), 496 (w) cm^{-1}.

UV-vis ($CHCl_3$): λ_{max} (ε_{max}/$dm^3 \cdot mol^{-1} \cdot cm^{-1}$) = 874 (8300), 600 (12200), 512 (10300), ~332 (32700) nm.

UV-vis (*n*-hexane): λ_{max} = 870, 594, 506, ~326 sh, ~228 nm.

Synthesis [Co^{I}((3,5-$(CF_3)_2C_6H_3$)-BIAN)$_3$] (11).

$CoCl_2$ (43 mg, 0.33 mmol), C_8K (95 mg, 0.70 mmol) and ^{F}BIAN (604 mg, 1.00 mmol) were placed in a Schlenk flask and THF (15 mL) was added. The reaction mixture was stirred overnight at room temperature. THF was removed *in vacuo* and the raw product was extracted with toluene (50 mL). Toluene solution was concentrated to 25 mL, *n*-hexane (25 mL) was added and the resulting solution was stored for a night at –30°C. Solution was decanted, dark-purple crystals were

washed with *n*-hexane and dried *in vacuo*. Yield: 283 mg (46%). Single crystals of **11** suitable for X-ray crystallography were obtained from a toluene/*n*-hexane mixture by cooling.

Yield: 518 mg (81%).

M.p. 275 – 278 °C.

$C_{84}H_{36}CoF_{36}N_6$ (1872.13): calcd. C 53.89, H 1.94, N 4.49; found C 53.44, H 1.96, N 4.47.

MS (EI): *m/z* = 1267 [M – (BIAN)$^+$], 1248 [M – (BIAN) – F$^+$], 663 [M – 2(BIAN)$^+$].

IR (Nujol): $\tilde{\nu}$ = 1600 (w), 1278 (s), 1261 (m), 1242 (m), 1175 (s), 1140 (s), 1102 (m), 1035 (m), 1019 (m), 972 (m), 892 (m), 856 (m), 846 (m), 822 (w), 795 (w), 770 (m), 723 (m), 705 (w), 683 (m), 668 (m), 616 (w), 576 (w), 533 (m), 513 (m), 481 (m) cm^{-1}.

UV-vis ($CHCl_3$): λ_{max} (ε_{max}/dm^3·mol^{-1}·cm^{-1}) = 735 (5000), 519 sh (12100), ~329 (41300) nm.

Attempt to synthesize [Fe(^{F}BIAN)$_2$].

The ligand ^{F}BIAN (302 mg, 0.500 mmol) and $FeCl_2$ (31 mg, 0.250 mmol) were placed in a Schlenk flask then THF (15 mL) was added. The resulting brown-orange solution was stirred for an hour at room temperature and transferred to a Schlenk flask with weighted C_8K (74 mg, 0.550 mmol). After the mixture was stirred for a day, solution was filtered, THF was removed *in vacuo*. The heaviest ion detected in EI-MS was *m/z* = 603 assigned to the ligand [^{F}BIAN – H$^+$] ion.

Attempt to synthesize [Pd(^{F}BIAN)$_2$].

The ligand ^{F}BIAN (500 mg, 0.827 mmol), C_8K (140 mg, 1.034 mmol), $PdCl_2(PhCN)_2$ (159 mg, 0.414 mmol) were placed in a Schlenk flask and THF (25 mL) was added. After the mixture was stirred for 24 hours, THF was removed *in vacuo* and the resulting solid was extracted with benzene (~30 mL). By ^{1}H, ^{19}F NMR the extract was shown to contain the free ligand mostly.

Attempt to synthesize [Cu(^{F}DAD)$_2$].

The ligand ^{F}DAD (300 mg, 0.721 mmol), C_8K (102 mg, 0.757 mmol), and $CuCl_2$ (48 mg, 0.360 mmol) were placed in a Schlenk flask and THF (25 mL) was added. After the mixture was stirred for 2 days it was filtered giving a light-brown solution, THF was then removed *in vacuo*. ^{1}H and ^{19}F NMR spectra showed the free ligand only, no molecular peak referred to the target complex was observed in EI-MS spectrum.

Attempt to synthesize [Cu(^{F}BIAN)$_2$].

The ligand ^{F}BIAN (500 mg, 0.827 mmol), C_8K (117 mg, 0.869 mmol), and $CuCl_2$ (56 mg, 0.414 mmol) were placed in a Schlenk flask and THF (30 mL) was added. After stirring for 2 days a

green solution was obtained. It was filtered, THF was removed *in vacuo* giving a dark-green powder. ^{1}H and ^{19}F NMR spectra reveal the presence of the free ligand only. The heaviest ion detected by EI-MS spectrometry was *m/z* = 603 that is referred to the free ligand [^{F}BIAN – H^{+}] ion.

Attempt to synthesize [Fe(^{F}DAD)$_2$] in two steps using C_8K as reductant.

The ligand ^{F}DAD (333 mg, 0.800 mmol) and $FeCl_2$ (51 mg, 0.400 mmol) were combined in a Schlenk flask and Et_2O (15 mL) was added. A dark precipitate, most likely [Fe(DAD)Cl_2], was formed within one hour. The resulting suspension was transferred in a Schlenk with weighted C_8K (114 mg, 0.840 mmol). The red-brown solution formed after stirring overnight was filtered, Et_2O was removed *in vacuo*. The heaviest ion detected by EI-MS spectrometry was *m/z* = 416 that is referred to the free ligand ion.

Attempt to synthesize [Fe(^{F}DAD)$_2$] in two steps using Na as reductant.

The ligand ^{F}DAD (308 mg, 0.740 mmol) and $FeCl_2$ (47 mg, 0.370 mmol) were combined in a Schlenk flask and Et_2O (15 mL) was added. A dark precipitate, most likely [Fe(^{F}DAD)Cl_2], was formed within one hour. The resulting suspension was transferred in a Schlenk with weighted sodium (17 mg, 0.740 mmol). The mixture was stirred at room temperature for 2 days until the sodium was completely consumed. The brown-yellow solution was then filtered, Et_2O was removed *in vacuo*. The heaviest ion detected by EI-MS spectrometry was *m/z* = 416 that is referred to the free ligand ion.

Attempt to synthesize [Fe(^{F}DAD)$_2$] in one step using Na as reductant.

The ligand ^{F}DAD (344 mg, 0.826 mmol), $FeCl_2$ (53 mg, 0.418 mmol), and sodium (19 mg, 0.826 mmol) were combined in a Schlenk flask and THF (10 mL) was added. The mixture was stirred at room temperature for 2 days until the sodium was completely consumed. The resulting solution was filtered, THF was removed *in vacuo* giving a brown-green powder. The heaviest ion detected by EI-MS spectrometry was *m/z* = 416 that is referred to the free ligand ion.

References.

[1] A. L. Balch, R. H. Holm, *J. Am. Chem. Soc.* **1966**, 5201–5209.

[2] a) M. D. Ward, J. A. McCleverty, *J. Chem. Soc., Dalton Trans.* **2002**, 275–288; b) A. Vlček, Jr., *Coord. Chem. Rev.* **2002**, *230*, 225–242; c) P. Chaudhuri, K. Wieghardt, *Prog. Inorg. Chem.* **2001**, *50*, 151–216.

[3] H. tom Dieck, H. Bruder, *J. Chem. Soc., Chem. Commun.* **1977**, 24–25.

[4] H. tom Dieck, M. Svoboda, J. Kopf, *Z. Naturforsch., B: Chem. Sci.* **1978**, *33*, 1381–1385.

[5] D. von Walther, G. Kreisel, R. Kirmse, *Z. Anorg. Allg. Chem.* **1982**, *487*, 149–160.

[6] R. Kirmse, J. Stach, D. von Walther, R. Boettcher, *Z. Chem.* **1980**, *29*, 224–225.

[7] D. von Walther, *Z. Anorg. Allg. Chem.* **1974**, *405*, 8–18.

[8] a) M. Svoboda, H. tom Dieck, *Z. Naturforsch., B: Chem. Sci.* **1981**, *36*, 814–822; b) H. tom Dieck, M. Svoboda, T. Greiser, *Z. Naturforsch., B: Chem. Sci.* **1981**, *36*, 823–832.

[9] a) H. Görls, D. Walther, J. Sieler, *Cryst. Res. and Technol.* **1987**, *22*, 1145–1151; b) W. Bonrath, K. R. Pörschke, R. Mynott, C. Krüger, *Z. Naturforsch., B: Chem. Sci.* **1990**, *45*, 1647–1650.

[10] a) D. Herebian, E. Bothe, F. Neese, T. Weyhermüller, K. Wieghardt, *J. Am. Chem. Soc.* **2003**, *125*, 9116–9128; b) D. Herebian, K. E. Wieghardt, F. Neese, *J. Am. Chem. Soc.* **2003**, *125*, 10997–11005; c) V. Bachler, G. Olbrich, F. Neese, K. Wieghardt, *Inorg. Chem.* **2002**, *41*, 4179–4193.

[11] a) S.-M. Peng, Y. Wang, C.-K. Chiang, *Acta Crystallogr., Sect. C: Cryst. Struct. Commun.* **1984**, *40*, 1541–1542; b) C.-S. Lee, T.-S. Hwang, Y. Wang, S.-M. Peng, C.-S. Hwang, *J. Phys. Chem.* **1996**, *100*, 2934–2941.

[12] L. S. Hegedus, *Transition Metals in the Synthesis of Complex Organic Molecules*; University Science Books: Mill Valley, CA, **1994**, p. 3.

[13] C. K. Jörgensen, *Oxidation Numbers and Oxidation States*, Springer: Heidelberg, Germany, **1969**.

[14] P. Chaudhuri, C. N. Verani, E. Bill, E. Bothe, T. Weyhermüller, K. Wieghardt, *J. Am. Chem. Soc.* **2001**, *123*, 2213–2223.

[15] M. M. Khusniyarov, K. Harms, J. Sundermeyer, *J. Fluorine Chem.* **2006**, *127*, 200–204; Chapter II in this Dissertation.

[16] a) R. van Asselt, C. J. Elsevier, W. J. J. Smeets, A. L. Spek, R. Benedix, *Recl. Trav. Chim. Pays-Bas* **1994**, *113*, 88–98; b) R. van Asselt, C. J. Elsevier, C. Amatore, A. Jutand, *Organometallics* **1997**, *16*, 317–328; c) L. K. Johnson, C. M. Killian, M. Brookhart, *J. Am. Chem. Soc.* **1995**, *117*, 6414–6415; d) C. M. Killian, D. J. Tempel, L. K. Johnson, M. Brookhart, *J. Am. Chem. Soc.* **1996**, *118*, 11664–11665.

[17] I. L. Fedushkin, A. A. Skatova, V. A. Chudakova, V. K. Cherkasov, S. Dechert, H. Schumann, *Russ. Chem. Bull., Int. Ed.* **2004**, *53*, 2142–2147.

[18] S. Blanchard, F. Neese, E. Bothe, E. Bill, T. Weyhermüller, K. Wieghardt, *Inorg. Chem.* **2005**, *44*, 3636–3656.

[19] a) L. R. Chamberlain, L. D. Durfee, P. E. Fanwick, L. M. Kobriger, S. L. Latesky, A. K. McMullen, B. D. Steffey, I. P. Rothwell, K. Folting, J. C. Huffman, *J. Am. Chem. Soc.* **1987**, *109*, 6068–6076; b) S. L. Latesky, A. K. McMullen, G. P. Niccolai, I. P. Rothwell, J. C. Huffman, *Organometallics* **1985**, *4*, 1896–1898; c) W. A. Herrmann, M. Denk, W. Scherer, F.-R. Klingan, *J. Organomet. Chem.* **1993**, *444*, C21–C24; d) K. Mashima, Y. Matsuo, K. Tani, *Organometallics* **1999**, *18*, 1471–1481; e) R. L. Huff, S.-Y. S. Wang, K. A. Abboud, J. M. Boncella, *Organometallics* **1997**, *16*, 1779–1785; f) K. Mashima, Y. Matsuo, K. Tani, *Chem. Lett.* **1997**, 767–768; g) T.-G. Ong, D. Wood, G. P. A. Yap, D. S. Richeson, *Organometallics* **2002**, *21*, 1–3; h) Y. Matsuo, K. Mashima, K. Tani, *Angew. Chem., Int. Ed.* **2001**, *40*, 960–962; i) J. Scholz, M. Dlikan, D. Strohl, A. Dietrich, H. Schumann, K.-H. Thiele, *Chem. Ber.* **1990**, *123*, 2279–2285; j) J. Wunderle, J. Scholz, U. Baumeister, H. Hartung, *Z. Kristallogr.* **1996**, *211*, 423–424; k) G. A. Hadi, J. Wunderle, K.-H. Thiele, R. Froehlich, *Z. Kristallogr.* **1994**, *209*, 372; l) B. Richter, J. Scholz, J. Sieler, K.-H. Thiele, *Angew. Chem., Int. Ed.* **1995**, *34*, 2649–2651; m) A. Merkoulov, K. Harms, J. Sundermeyer, *Z. Anorg. Allg. Chem.* **2005**, *631*, 2877–2880.

[20] M. G. Gardiner, G. R. Hanson, M. J. Henderson, F. C. Lee, C. L. Raston, *Inorg. Chem.* **1994**, *33*, 2456–2461.

[21] T. Schleis, T. P. Spaniol, J. Okuda, J. Heinemann, R. Mülhaupt, *J. Organomet. Chem.* **1998**, *569,* 159–167.

[22] T. Spaniel, H. Görls, J. Scholz, *Angew. Chem., Int. Ed.* **1998**, *32*, 1862–1865.

[23] a) G. S. Hall, R. H. Soderberg, *Inorg. Chem.* **1968**, *7*, 2300–2303; b) A. V. Reshetnikov, A. A. Sidorov, S. S. Talismanov, G. G. Aleksandrov, Y. A. Ustynyuk, S. E. Nefedov, I. L. Eremenko, I. I. Moiseev, *Russ. Chem. Bull. (Translation of Izv. Akad. Nauk SSSR, Ser. Khim.)* **2000**, *49*,

1771–1774; c) H.-Y. Cheng, C.-C. Lin, B.-C. Tzeng, S.-M. Peng, *J. Chin. Chem. Soc. (Taipei)* **1994**, *41*, 775–781.

[24] M. M. Khusniyarov, K. Harms, J. Sundermeyer, B. Sarkar, W. Kaim, J. van Slageren, C. Duboc, J. Fiedler, manuscript in preparation; Chapter I in this Dissertation.

[25] S. Lorenzo, G. R. Lewis, I. Dance, *New J. Chem.* **2000**, *24*, 295–304.

[26] M. P. Thornberry, C. Slebodnick, P. A. Deck, F. R. Fronczek, *Organometallics* **2000**, *19*, 5352–5369.

[27] J. O. Liimatta, B. Lofgren, M. Miettinen, M. Ahlgren, M. Haukka, T. T. Pakkanen, *J. Polym. Sci., Part A: Polym. Chem.* **2001**, *39*, 1426–1434.

[28] I. L. Fedushkin, A. A. Skatova, V. A. Chudakova, G. K. Fukin, S. Dechert, H. Schumann, *Eur. J. Inorg. Chem.* **2003**, 3336–3346.

[29] a) M. J. Blandamer, J. Burgess, J. Fawcett, P. Guardado, C. D. Hubbard, S. Nuttall, L. J. S. Prouse, S. Radulovic, D. R. Russell, *Inorg. Chem.* **1992**, *31*, 1383–1389; b) P. J. Daff, M. Etienne, B. Donnadieu, S. Z. Knottenbelt, J. E. McGrady, *J. Am. Chem. Soc.* **2002**, *124*, 3818–3819; c) K.-H. Thiele, B. Richter, B. Neumüller, *Z. Anorg. Allg. Chem.* **1994**, *620*, 1627–1630; d) M. N. Bochkarev, A. A. Trifonov, F. G. N. Cloke, C. I. Dalby, P. T. Matsunaga, R. A. Anderson, H. Schumann, J. Loebel, H. Hemling, *J. Organomet. Chem.* **1995**, *486*, 177–182; e) B. Chaudret, H. Koster, R. Poilblanc, *Chem. Commun.* **1981**, 266–268; f) B. Chaudret, C. Cayret, H. Koster, R. Poilblanc, *J. Chem. Soc., Dalton Trans.* **1983**, 941–945; g) B. Richter, J. Scholz, B. Neumüller, R. Weimann, H. Schumann, *Z. Anorg. Allg. Chem.* **1995**, *621*, 365–372.

[30] D. J. Szalda, C. Creutz, D. Mahajan, N. Sutin, *Inorg. Chem.* **1983**, *22*, 2372–2379.

[31] S. Ye, B. Sarkar, F. Lissner, T. Schleid, J. van Slageren, J. Fiedler, W. Kaim, *Angew. Chem. Int. Ed.* **2005**, *44*, 2103–2106.

[32] O. Kahn, *Molecular Magnetism*, VCH, New York, **1993**.

[33] D. Gatteschi, A. Bencini, in "*Magneto-Structural correlations in Exchange Coupled Systems*", R. D. Willett, D. Gatteschi, O. Kahn, eds., p. 241, NATO ASI Series. Reidel, Dordrecht, **1985**.

[34] C. J. O'Connor, *Prog. Inorg. Chem.* **1982**, *29*, 203–283.

[35] a) I. L. Fedushkin, A. A. Skatova, V. K. Cherkasov, V. A. Chudakova, S. Dechert, M. Hummert, H. Schumann, *Chem. Eur. J.* **2003**, *9*, 5778–5783; b) I. L. Fedushkin, A. A. Skatova, V. A. Chudakova, V. K. Cherkasov, G. K. Fukin, M. A. Lopatin, *Eur. J. Inorg. Chem.* **2004**, 388–393; c) I. L. Fedushkin, N. M. Khvoinova, A. Y. Baurin, G. K. Fukin, V. K. Cherkasov, M. P. Bubnov, *Inorg. Chem.* **2004**, *43*, 7807–7815; d) I. L. Fedushkin, A. A. Skatova, M. Hummert, H. Schumann, *Eur. J. Inorg. Chem.* **2005**, 1601–1608.

[36] J. C. Gordon, P. Shukla, A. H. Cowley, J. N. Jones, D. W. Keogh, B. L. Scott, *Chem. Comm.* **2002**, 2710–2711.

[37] L. G. L. Ward, D. M. Paul, *Inorg. Synth.* **1971**, *13*, 154–164.

[38] P. Kovacic, N. O. Brace, *Inorg. Synth.* **1960**, *6*, 172–173.

[39] a) M. S. Kharasch, R. C. Seyler, F. R. Mayo, *J. Am. Chem. Soc.* **1938**, *60*, 882–884; b) J. R. Doyle, P. E. Slade, H. B. Jonassen, *Inorg. Synth.* **1960**, *6*, 216–219.

[40] M. Gasperini, F. Ragaini, S. Cenini, *Organometallics* **2002**, *21*, 2950–2957.

[41] F. A. Cotton, E. A. Hillard, C. A. Murillo, X. Wang, *Inorg. Chem.* **2003**, *42*, 6063–6070.

[42] PLATON, A Multipurpose Crystallographic Tool, Utrecht University, Utrecht, The Netherlands, A. L. Spek, **2005**.

[43] SHELX97 – Programs for Crystal Structure Analysis (Release 97-2). G. M. Sheldrick, Institüt für Anorganische Chemie der Universität, Tammanstrasse 4, D-3400 Göttingen, Germany, **1998**.

[44] A. Altomare, G. Cascarano, C. Giacovazzo, A. Guagliardi, *J. Appl. Crystallogr.* **1993**, *26*, 343–350.

☙ Chapter IV ❧

Ethylene polymerization with new bis(arylimino)acenaphthene (BIAN) complexes of iron and copper activated with MAO.

Introduction.

During the last decade several new catalytic systems for olefin polymerization, so called non-metallocene or post-metallocene catalysts, have been developed and are currently under detailed investigation.[1] Olefin polymerization catalysts based on late transition metals are very tempting in comparison with "classical" early transition metal catalysts due to attractive features of the formers being less sensitive towards common contaminants, being more tolerant towards polar groups if present in monomer, and being cheaper is some cases. Furthermore, the most active post-metallocene catalysts show activities close to that of metallocene systems.

Two families of catalysts based on late transition metals are of great attention. The first family originates from bis(imino)pyridine complexes of iron and cobalt.[2,3] The activities of cobalt catalysts are in general an order of magnitude lower than those for their iron analogues. The catalysts show exceptionally high activities for ethylene polymerization, producing strictly linear, high-molecular-weight polymer.[4]

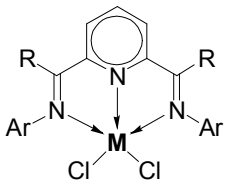

M = Fe, Co

The second family is α-diimine nickel and palladium catalysts introduced by Brookhart and coworkers.[5] These catalysts can be used for polymerization of ethylene, α-olefins, and cyclic olefins and copolymerization of non-polar olefins with a variety of functionalized olefins.[1b] Polydispersities of polymers are generally low, and at low temperatures (–10 °C) and low monomer concentrations, it is possible to achieve living polymerization of α-olefins with α-diimine nickel catalysts.[6]

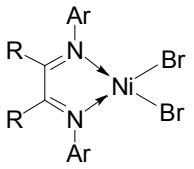

Although copper ethylene chemistry is well developed,[7] information about copper based catalysts for polymerization of α-olefins is scarce both in academic and patent literature. The amidinate ligand, *N*,*N*'-ditrimethylsilylbenzamidinato, has been reported to support copper catalyzed ethylene polymerization.[8,9]

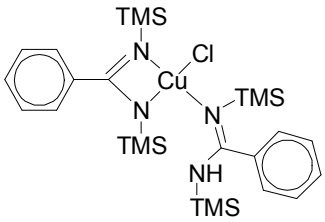

The copper complex shown above, when activated with methylaluminoxane (MAO), produced polyethylene (PE) with M_w = 820000 and T_m = 138°C.[10] In another patent, ethylene was polymerized with 2,2'-bis[2-(1-ethylbenzimidazol-2-yl)biphenyl]copper(II) chloride and cocatalyst MAO to give PE melting at 139°C and having a M_n = 4900.[8]

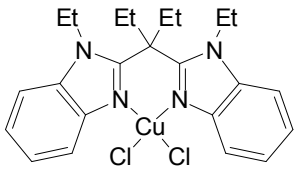

Other derivatives of the parent catalyst were prepared and tested in ethylene polymerization.[11,12] Both catalytic systems show low ethylene polymerization activities.

Very recently Gibson et al. have shown that the simplest α-diimine copper(II) complex is able to produce very high-molecular-weight PE with moderate activity.[13]

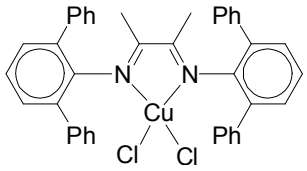

When activated with MAO (500 equiv) this diimine complex could polymerize ethylene at 30 bar with activity of 300 kg PE/(mol·h). Gibson's report has stimulated us to synthesize new copper complexes based on rigid **b**is(aryl**i**mino)**a**ce**n**aphthene (BIAN) ligand and to test them in ethylene polymerization. The related iron complexes were synthesized and tested in ethylene polymerization as well.

Results and Discussion.

Synthesis and Characterization.

Two BIAN ligands with bulky *N*-substituents were used in this work: (3,5-$(CF_3)_2C_6H_3$)-BIAN = ^{F}BIAN and (2,6-(iPr)$_2C_6H_3$)-BIAN = Dip-BIAN.

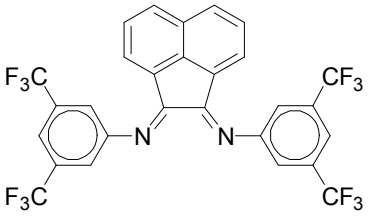

^{F}**BIAN**

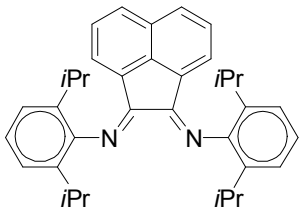

Dip-BIAN

The copper complexes **12** and **13** could be obtained in reaction of $CuCl_2$ with appropriate BIAN ligand in dried ethanol. After stirring overnight, the target complexes were collected by filtration with high yields. Similar reaction in ethanol with $FeCl_2$ failed. After adding ethanol solution of $FeCl_2$ to suspended in ethanol Dip-BIAN and stirring for two days at room temperature only unreacted ligand was collected. It was concluded that Fe^{II} ion has higher affinity to oxygen, to ethanol in this particular case, than Cu^{II} ion. Thus, probably formation of more stable ethanol solvates of Fe^{II} prevents coordination of *N*-donor ligand. Indeed, when Et_2O instead of EtOH was used as reaction medium, iron complexes **14** and **15** were successfully isolated.

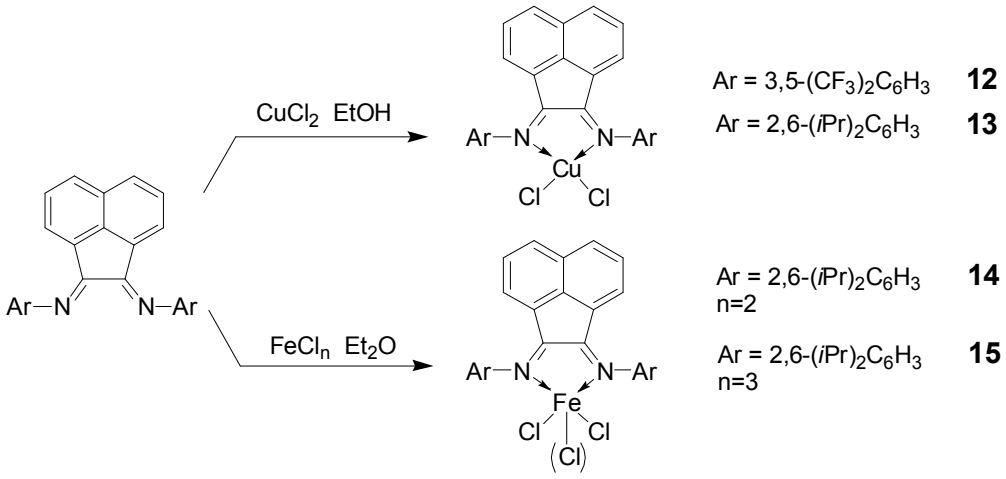

Formation of the complexes can be easily observed by change of color of reaction mixtures in case of **13–15,** whereas the color of **12** (brown-yellow) does not differ significantly from those of the metal salt $CuCl_2$ (brown-yellow) and the free ligand (yellow). While complexes of the type [Fe(DAD)X_n] (DAD – derived 1,4-diaza-1,3-butadiene; X – halogen; n = 2, 3) are well known and thoroughly investigated by tom Dieck[14] and others,[15] complexes of the type [Fe(BIAN)X_n] are unknown so far. The only example of a BIAN complex with iron reported to date is

$[Fe^{II}(Dip\text{-}BIAN)(bpy)_2](ClO_4)_2$ (bpy is 2,2'-bipyridine).[16] As the ferrous iron is located in the strong octahedral field, this complex was reported to be diamagnetic.[16]

The purity of all synthesized complexes was checked by elemental analysis. Signals corresponding to the molecular ions were not detected by EI-MS. Typically the heaviest ion for **13**–**15** was [Dip-BIAN – *i*Pr$^+$] cation with *m/z* = 457, whereas the signal at *m/z* = 603 was detected in case of **12**, which corresponds to [^{F}BIAN – H$^+$] cation. Several attempts to detect molecular ion signals by ESI-MS and MALDI-TOF failed.

As expected complexes **12**–**15** are paramagnetic that was confirmed by NMR spectroscopy. Magnetic properties of the complexes were investigated by magnetic susceptibility measurements in solution for **13**–**15** and in the solid for **12**. Magnetic measurements of **12** in solution are problematic because of the relatively low solubility of the complex.

According to Evans method[17] magnetic susceptibility can be determined utilizing the difference in chemical shift of a NMR signal from an inert reference material in the presence and absence of a paramagnetic solute. The value of magnetic susceptibility correlates with experimental data as follows:

$$\chi_g = \frac{3\Delta f}{2\pi f m} + \chi_0 + \frac{\chi_0 (d_0 - d_S)}{m} \qquad (1)$$

where:

χ_g – mass susceptibility of the solute (cm^3/g),

Δf – observed frequency shift of reference resonance (Hz),

f – spectrometer frequency (Hz),

χ_0 – mass susceptibility of solvent (cm^3/g),

m – mass of substance per cm^3 of solution,

d_0 – density of solvent (g/cm^3),

d_S – density of solution (g/cm^3).

Grant[18] has showed that the third term in eq 1 partially or completely compensates the second. Thus, less error will be introduced by neglecting both the second and the third terms rather than the current practice of neglecting the third term only.

$$\chi_g = \frac{3\Delta f}{2\pi f m} \qquad (2)$$

It is important to note that aforementioned equations are still valid as long as we perform measurements on the old low-field NMR spectrometers based on permanent magnets or electromagnets that create a field perpendicular to the axis of the sample. When a high-field superconducting NMR spectrometer, which creates a field parallel to the axis of the sample, is used, eq 2 should be corrected as follows:[19]

$$\chi_g = -\frac{3\Delta f}{4\pi f m} \qquad (3)$$

In our experiments, we used the following solvent mixture: $CHCl_3$: $CDCl_3$: TMS = 10 : 0.5 : 1. TMS served as a second reference substance. Deuterated chloroform was added to have an opportunity to homogenize the field via a lock-system of the spectrometer. The inner standard being the same solvent mixture sealed in the glass capillary was used. The results of the measurements are listed in Table 1, while a representative ^{1}H NMR spectrum obtained for **14** is shown in Figure 1.

Table 1. Magnetic susceptibilities of **13–15** measured in solution (Evans method).

complex	M_r	m, mg	Δf_{TMS}, Hz	Δf_{CHCl_3}, Hz	χ_m(TMS), cm^3mol^{-1}	χ_m($CHCl_3$), cm^3mol^{-1}	χ_{diamag}, cm^3mol^{-1}	μ_{eff}(TMS), μ_B	μ_{eff}($CHCl_3$), μ_B
13	636.2	8.210	41.3	31.5	0.001222	0.000932	–0.000402	1.97	1.79
14	627.5	7.106	328	329	0.011063	0.011097	–0.000404	5.25	5.25
15	662.9	8.191	456	438	0.014096	0.013539	–0.000425	5.90	5.79

Conditions: f = 500 MHz, T = 300 K, V = 0.8 mL. Values of χ and μ were calculated according to eq 3 and eq 4.

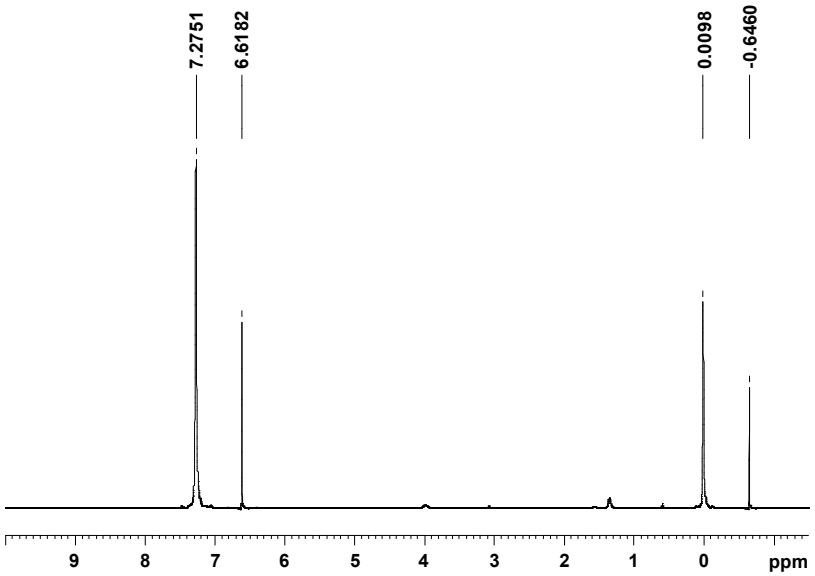

Figure 1. ^{1}H NMR spectrum measured for **14** with inner standard. See Table 1 and text for details.

The molar susceptibility χ_m is related to the mass susceptibility χ_g through $\chi_m = M_r\chi_g$. The calculated molar susceptibilities were then corrected to diamagnetic components using Pascal's constants. Effective magnetic moment μ_{eff} is related to magnetic susceptibility according to

$$\mu_{eff} = 2.828\sqrt{\chi_m T} \text{ (CGS units)} \qquad (4)$$

The effective magnetic moment (μ_{eff}) of copper complex **13** measured at 300 K is 1.97 μ_B determined on the shift of TMS signal and 1.79 μ_B ($CHCl_3$ signal). The spin-only value 1.73 μ_B is expected for one unpaired electron per molecule that is in good agreement with that of **13**. Magnetic

moment of solid **12** measured on a SQUID magnetometer at the field of 1 T is 2.13 μ_B. The magnetic moments of **12** and **13** are in good agreement with those of square-planar (*vide infra*) complexes of Cu(II).[20]

The effective magnetic moment of ferrous complex **14** is 5.25 μ_B. This value is close to the spin-only value of 4.90 μ_B expected for $S = 2$. Therefore **14** is a high-spin complex with 4 unpaired electrons. The observed μ_{eff} is comparable with that of four-coordinated ferrous complexes with *N*-donors.[14d, 21] The values of μ_{eff} measured for ferric complex **15** are 5.90 μ_B (determined on the shift of TMS signal) and 5.79 μ_B ($CHCl_3$ signal). Observed values are consistent with a high-spin Fe(III) ion and the spin-only value of 5.92 μ_B expected for 5 unpaired electrons.

Crystal Structure of [Cu^{II}(Dip-BIAN)Cl_2] (13).

Single crystals of **13** suitable for X-ray crystallography were obtained directly in a NMR tube ($CHCl_3$: $CDCl_3$ = 10 : 1) by cooling. Complex **13** crystallizes in the orthorhombic crystal system with the space group $P_{2_12_12_1}$. Four molecules of **13** together with 16 molecules of the solvent – chloroform were found in the cell with a = 11.5571(5), b = 20.1850(13), c = 21.8028(10) Å. The molecular structure of **13** is shown in Figure 2, while selected bond distances and angles are listed in Table 2. Copper has slightly distorted planar environment formed by two nitrogen atoms and two chlorine atoms. The two Cu–N bonds with distances at 2.052(3) and 2.037(2) Å are typical donor-acceptor Cu^{II}←N(diimine) bonds.[22]

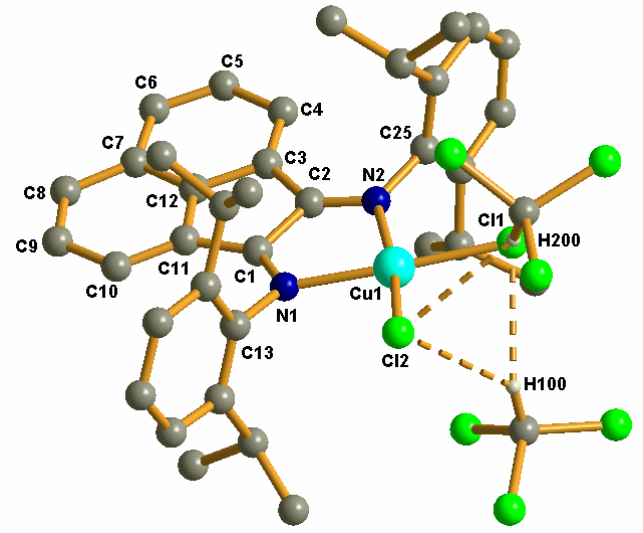

Figure 2. Molecular structure of **13** with two chloroform molecules. All hydrogen atoms except those of chloroform molecules are not shown.

Table 2. Selected bond distances [Å] and angle [º] of **13**.

C1–N1	1.283(4)	C7–C12	1.410(5)	N2–Cu1	2.037(2)
C1–C11	1.455(4)	C7–C8	1.421(5)	Cl1–Cu1	2.2135(9)
C1–C2	1.512(4)	C8–C9	1.376(5)	Cl2–Cu1	2.1976(8)
C2–N2	1.274(4)	C9–C10	1.394(5)	C1–N1–C13	118.6(3)
C2–C3	1.465(4)	C10–C11	1.374(5)	C1–N1–Cu1	112.6(2)
C3–C4	1.379(4)	C11–C12	1.411(4)	C13–N1–Cu1	128.1(2)
C3–C12	1.422(5)	C13–N1	1.448(4)	C2–N2–C25	117.9(2)
C4–C5	1.415(5)	C25–N2	1.452(4)	C2–N2–Cu1	112.8(2)
C5–C6	1.354(5)	N1–Cu1	2.052(3)	C25–N2–Cu1	129.1(2)
C6–C7	1.411(5)				

The chelating diimine is essentially planar, the maximum deviation from the best-fit plane, defined by 12 carbon atoms of acenaphthene backbone and two nitrogen atoms, is 0.051(3) Å (N2). The two chlorine atoms are substantially out of plane, deviations from the best-fit diimine plane of 0.448(1) Å for Cl2 and 0.108(1) Å for Cl1 are observed. The two *N*-phenyl rings are almost orthogonal to the diimine moiety forming dihedral angles of 87.2(1)º and 87.8(1)º. It is interesting to note that short contacts between chlorine atoms Cl1, Cl2 and hydrogens of two chloroform molecules were found in the crystal structure. The short contacts are listed in Table 3. Hydrogen atoms were placed at calculated positions. Two chlorine atoms Cl1, Cl2 and two hydrogen atoms H100, H200 form a distorted tetrahedron as shown in Figure 2.

Table 3. The short contacts [Å] in crystal structure of **13**.

Cl1–H100	2.68	Cl2–H100	2.70
Cl1–H200	2.57	Cl2–H200	2.80

Polymerization of ethylene.

Complexes **12**–**15** activated with methylaluminoxane (MAO) were tested in polymerization reactions of ethylene. Polymerization conditions were as follows: T = 35ºC, $p(C_2H_4)$ = 4 atm, m(complex) = 50 μmol, complex : MAO ~ 1 : 500 (mol), medium – toluene (250 mL), c(complex) = 0.2 mM, t(time of polymerization) = 1 hour. The results of polymerization runs with the catalyst precursors **12–15** are listed in Table 4. Since activity of catalyst can be significantly affected by polymerization conditions such as temperature, monomer pressure, catalyst concentration, purity of monomer, etc., for adequate comparison a polymerization run on well known highly active Eurocen 5031 [Zr^{IV}(*n*BuCp)$_2$Cl$_2$] was performed under the same conditions. Activity of Eurocen 5031 is included in Table 4 for comparison.

Table 4. Ethylene polymerization with **12–15** activated with MAO.

catalyst precursor	yield, mg of PE	Activity, kg PE/mol_{cat}·h·atm
12 $Cu^{II}(^{F}BIAN)Cl_2$	traces	–
13 Cu^{II}(Dip-BIAN)Cl_2	traces	–
14 Fe^{II}(Dip-BIAN)Cl_2	551	2.8
15 Fe^{III}(Dip-BIAN)Cl_3	547	2.7
Zr^{IV}(*n*BuCp)$_2Cl_2$	42360*	1077

Conditions: T = 35ºC, $p(C_2H_4)$ = 4 atm, m(complex) = 50 μmol, complex : MAO ~ 1 : 500 (mol), medium – toluene (250 mL), c(complex) = 0.2 mM, t = 1 hour.
*Average temperature during the run was about 65ºC

The copper complexes **12** and **13** activated with MAO were inactive in ethylene polymerization. Only trace amounts of solid polymer were collected after one hour of polymerization run. The iron catalysts **14**/MAO, **15**/MAO do polymerize ethylene, though they show low activity. After 1 hour of polymerization run about 0.5 g of PE was collected for both catalytic systems. These yields correspond to catalyst activities of 2.8 for **14**/MAO and 2.7 kg PE/mol_{cat}·h·atm for **15**/MAO. Similar low catalytic activities observed for iron(II) and iron(III) catalyst precursors are indicating that identical active centers are formed after catalyst activation. Similarly, formation of the same active species from iron(II) and iron(III) bis(imino)pyridine precursors was suggested by Gibson et al.[4]

Except for highly active bis(imino)pyridine complexes, other iron complexes show low if any activity in ethylene polymerization.[1c] Very recently Spencer et al.[23] have reported synthesis of related complexes of pyridine- and imidazole-phosphinimine complexes of iron.

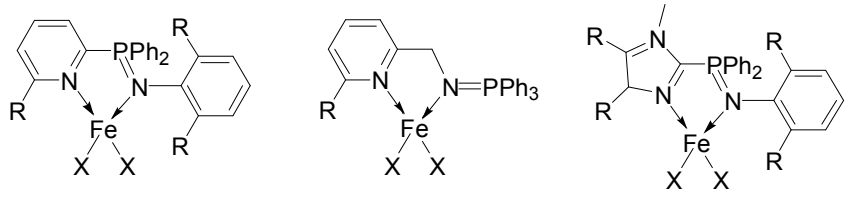

Upon activation with MAO, these complexes are active in ethylene dimerization only.

Low activity of iron complexes **14**, **15** and inactivity of copper complexes **12**, **13** in ethylene polymerization are likely of electronic than steric reasons. The exact mechanism of activation of iron complexes with bis(imino)pyridine ligand and the active species are not known so far.[4,24] But if we assume that activation of the complexes **12–15** proceeds rather similar to activation of diimine complexes of nickel,[25] namely, with formation of cation-anion pairs, we are allowed to apply an electron-counting formalism for the metal centers in the hypothetical active species.

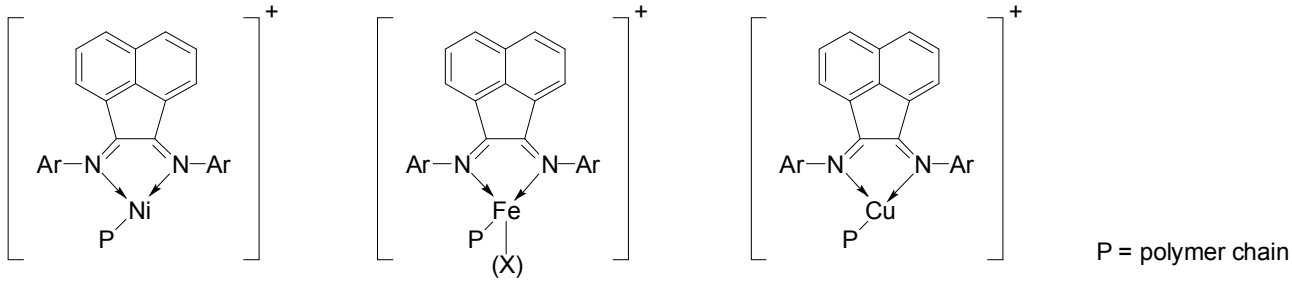

Figure X. Active species in ethylene polymerization proposed by Brookhart for Ni diimine complexes(left) and hypothetical active species of Fe (center) and Cu (right) complexes of current study.

According to Gibson,[1c] complexes could be a high active catalyst for olefin polymerization if the active site formed after the catalyst activation contains a) a vacant coordination site adjacent to the growing polymer chain, b) a positively charged metal center, which enhances the electrophilicity of the active site, c) an electron deficient metal, mostly with 14 v.e. (valence electrons). Iron catalysts based on **14** and **15** have only 12 v.e. (probably 13 v.e. for complex **15**) that is less than required. Copper catalysts based on **12** and **13** have 15 v.e. that is more than required. At the same time the most active catalysts discovered so far, such as nickel(II) diimine system, iron(II) bis(imino)pyridine system, as well as classical metallocene catalysts of zirconium(IV) and titanium(IV) all are supposed to form 14 v.e. active species.

Conclusions.

We have synthesized four new complexes of iron and copper with bulky BIAN ligands. These complexes were thoroughly characterized by MS, UV-vis, and IR spectroscopies. The high-spin states of the iron complexes [Fe^{II}(Dip-BIAN)Cl_2] and [Fe^{III}(Dip-BIAN)Cl_3] were established by means of magnetic susceptibility measurements in solution. The crystal structure of [Cu^{II}(Dip-BIAN)Cl_2] was determined. The complexes activated with MAO were tested in ethylene polymerization. The iron complexes are able to polymerize ethylene with low activity, while copper complexes are no catalysts for ethylene polymerization.

Experimental Part.

Ligands ^{F}BIAN[26] and Dip-BIAN[27] were prepared by known procedures. Iron dichloride was prepared from iron trichloride by reaction with chlorobenzene.[28] For detailed physical measurements one is referred to the Chapter III.

Synthesis of [Cu^{II}(^{F}BIAN)Cl_2] (12).

To the solution of $CuCl_2$ (0.22 g, 1.655 mmol) in EtOH (20 mL) the ligand ^{F}BIAN (1.00 g, 1.655 mmol) was added as a solid. After the reaction mixture was stirred overnight, the brown-yellow precipitate was collected by filtration. It was washed with EtOH (5 mL), Et_2O (5 mL) and dried *in vacuo*.

Yield: 1.05 g (86 %).

M.p. 322ºC.

$C_{28}H_{12}Cl_2CuF_{12}N_2$ (738.85): calcd. C 45.52, H 1.64, N 3.79; found C 45.74, H 1.84, N 3.54.

MS (EI): *m/z* = 603 [M – $CuCl_2$ – H^+], 535 [M – $CuCl_2$ – CF_3^+].

IR (Nujol): wavenumber = 3107 (w), 3043 (w), 1659 (w), 1635 (m), 1596 (m), 1585 (m), 1278 (s), 1188 (s), 1141 (s), 1053 (w), 977 (m), 897 (m), 863 (w), 847 (m), 831 (m), 775 (m), 704 (m), 680 (m) cm^{-1}.

UV-vis ($CHCl_3$): λ_{max} (ε_{max}/$dm^3 \cdot mol^{-1} \cdot cm^{-1}$) = 273 (24300) nm.

Synthesis of [Cu^{II}(Dip-BIAN)Cl_2] (13).

Solution of $CuCl_2$ (123 mg, 0.909 mmol) in EtOH (5 mL) was added to the ligand Dip-BIAN (501 mg, 1.000 mmol) suspended in EtOH (15 mL). After stirring overnight the red precipitate was collected by filtration. It was washed with EtOH (4 mL), Et_2O (3×5 mL), pentane (5 mL) and dried *in vacuo*. Single crystals of **13** suitable for X-ray crystallography were obtained directly in NMR tube ($CHCl_3$/$CDCl_3$) by cooling.

Yield: 493 mg (85 %).

M.p. 225–227ºC.

$C_{36}H_{40}Cl_2CuN_2$ (635.18): calcd. C 68.07, H 6.35, N 4.41; found C 66.58, H 6.23, N 4.49.

MS (EI): *m/z* = 457 [M – $CuCl_2$ – iPr$^+$].

IR (Nujol): wavenumber = 3063 (w), 1651 (w), 1630 (s), 1594 (m), 1580 (s), 1435 (s), 1418 (m), 1363 (m), 1322 (w), 1289 (s), 1254 (w), 1221 (w), 1179 (m), 1149 (w), 1127 (w), 1086 (w), 1042 (m), 938 (m), 847 (w), 834 (m), 798 (s), 781 (s), 759 (s), 611 (w), 543 (m) cm^{-1}.

UV-vis ($CHCl_3$): λ_{max} (ε_{max}/$dm^3 \cdot mol^{-1} \cdot cm^{-1}$) = 406 (4760), 311 (18100), 266 (21600) nm.

Synthesis of [Fe^{II}(Dip-BIAN)Cl_2] (14).

The diimine Dip-BIAN (450 mg, 0.899 mmol) and $FeCl_2$ (76 mg, 0.560 mmol) were placed in a Schlenk flask and Et_2O (20 mL) was added. After the reaction mixture was stirred overnight at room temperature the green precipitate was collected by filtration. The raw product was repeatedly washed with Et_2O on a glass frit and dried *in vacuo*.

Yield: 123 mg (23 %).

M.p. 260–262ºC.

$C_{36}H_{40}Cl_2FeN_2$ (627.48): calcd. C 68.91, H 6.43, N 4.46; found C 65.11, H 5.98, N 4.28.

MS (EI): *m/z* = 457 [M – $FeCl_2$ – *i*Pr^+].

IR (Nujol): wavenumber = 1645 (m), 1615 (w), 1593 (m), 1577 (s), 1438 (s), 1365 (m), 1324 (w), 1283 (s), 1183 (m), 1123 (m), 1047 (m), 949 (m), 938 (m), 835 (m), 799 (s), 783 (s), 759 (s), 541 (m) cm^{-1}.

UV-vis ($CHCl_3$): λ_{max} (ε_{max}/$dm^3 \cdot mol^{-1} \cdot cm^{-1}$) = 701 (840), 633 (480), 321 (10900), 261 (21500) nm.

Synthesis of [Fe^{III}(Dip-BIAN)Cl_3] (15).

Solution of $FeCl_3$ (97 mg, 0.599 mmol) in Et_2O (10 mL) was added to the ligand Dip-BIAN (324 mg, 0.647 mmol) suspended in Et_2O (10 mL). After stirring overnight the orange precipitate was collected by filtration. It was washed with Et_2O (10 mL), toluene (10 mL), and finally with pentane (10 mL) and dried *in vacuo*.

Yield: 395 mg (100 %).

M.p. 213ºC.

$C_{36}H_{40}Cl_3FeN_2$ (662.93): calcd. C 65.22, H 6.08, N 4.23; found C 63.69, H 5.85, N 4.02.

MS (EI): *m/z* = 457 [M – $FeCl_3$ – *i*Pr^+].

IR (Nujol): wavenumber = 1653 (w), 1624 (s), 1581 (s), 1290 (m), 1181 (m), 1053 (m), 936 (m), 835 (m), 800 (s), 779 (s), 757 (s), 720 (s), 541 (w) cm^{-1}.

UV-vis ($CHCl_3$): λ_{max} (ε_{max}/$dm^3 \cdot mol^{-1} \cdot cm^{-1}$) = 313 (14300), 277 (16600) nm.

Ethylene Polymerization.

Polymerization of ethylene was performed in a 250 mL glass autoclave equipped with an inert mechanical stirrer, a cooling jacket, and a pressure passage. The ethylene used was purified by passing through the two columns charged with Na/K supported on Al_2O_3 (*SOLVONA*). The activator MAO was purchased from Crompton as 30% solution in toluene. Toluene and free $AlMe_3$ were removed *in vacuo*, the obtained polycrystalline MAO was stored in the glove-box. Solutions of catalyst precursors and activator were prepared directly before use.

The typical polymerization run was carried out as follows. The autoclave with the connected pressure funnel were evacuated for at least 30 min, thereby the autoclave was warmed (+80ºC) by means of the warming jacket. Unfortunately, it was not possible to hold the pressure passage warmed. The whole system was then filled with the monomer. At 30ºC the autoclave was charged with a freshly prepared solution of the catalyst precursor (190 mL of toluene, 50 μmol of the complex, $c = 2.63 \cdot 10^{-4}$ M). The disconnected from the autoclave pressure funnel was charged with a freshly prepared solution of activator MAO (60 mL of toluene, 25 mmol of MAO, c = 0.417 M). Both solutions in the autoclave and pressure funnel were saturated with the ethylene at required pressure (4 atm) for at least 20 min, thereby the required temperature (+35ºC) was adjusted for the autoclave.

The polymerization was started after content of the pressure funnel was released to the autoclave: MAO solution was added during several seconds to the solution of the complex under investigation. As soon as the activator was added, the change of color in the autoclave was observed. The temperature in the autoclave and the pressure of the monomer were held constant during the run. After one hour, polymerization was stopped by injection of acidified ethanol solution (20–30 mL, ~5% of HCl). The polymer was collected on a glass filter, washed thoroughly with acidified ethanol. The low-boiling oligomers were not investigated. The raw polyethylene was dried on air for several hours and then overnight in the drying oven (120ºC). The activity of the catalysts was calculated in [$kg_{PE}/mol_{cat} \cdot h \cdot atm_{monomer}$] units.

References.

[1] a) V. C. Gibson, G. J. P. Britovsek, D. F. Wass, *Angew. Chem., Int. Ed.* **1999**, *38*, 428–447. b) S. D. Ittel, L. K. Johnson, M. Brookhart, *Chem. Rev.* **2000,** *100*, 1169–1203. c) V. C. Gibson, S. K. Spitzmesser, *Chem. Rev.* **2003,** *103*, 283–315. d) S. Park, Y. Han, S. K. Kim, J. Lee, H. K. Kim, Y. Do, *J. Organomet. Chem.* **2004**, *689*, 4263–4276.

[2] B. L. Small, M. Brookhart, A. M. A. Bennett, *J. Am. Chem. Soc.* **1998**, *120*, 4049–4050.

[3] G. J. P. Britovsek, V. C. Gibson, B. S. Kimberley, P. J. Maddox, S. J. McTavish, G. A. Solan, A. J. P. White, D. J. Williams, *Chem. Commun.* **1998**, 849–850.

[4] G. J. P. Britovsek, M. Bruce, V. C. Gibson, B. S. Kimberley, P. J. Maddox, S. Mastroianni, S. J. McTavish, C. Redshaw, G. A. Solan, S. Stromberg, A. J. P. White, D. J. Williams, *J. Am. Chem. Soc.* **1999**, *121*, 8728–8740.

[5] L. K. Johnson, C. M. Killian, M. Brookhart, *J. Am. Chem. Soc.* **1995**, *117*, 6414–6415.

[6] C. M. Killian, D. J. Tempel, L. K. Johnson, M. Brookhart, *J. Am. Chem. Soc.* **1996**, *118*, 11664–11665.

[7] a) B. R. Straub, F. Eisentrager, P. Hofmann, *Chem. Commun.* **1999**, 2507–2508. b) J. S. Thompson, R. L. Harlow, J. F. Whitney, *J. Am. Chem. Soc.* **1983**, *105*, 3522–3527. c) J. S. Thompson, J. F. Whitney, *Inorg. Chem.* **1984**, *21*, 2813–2819. d) J. S. Thompson, R. M. Swiatek, *Inorg. Chem.* **1985**, *24*, 110–113.

[8] Y. Suzuki, T. Hayashi, JP Patent 10298231 to Mitsui Chemicals Inc., Japan, priority date April 23, **1997**.

[9] K. Shibayama, M. Ogasa, M. (Sekisui Chemical Co., Ltd., Japan). PCT Int. Appl. O9835996, **1998**; *Chem. Abstr.* **1998**, *129*, 203390.

[10] R. T. Stibrany, D. N. Schulz, S. Kacker, A. O. Patil, WO Patent Application 9930822 to Exxon Research and Engineering Company, priority date Dec 16, **1997**.

[11] a) R. T. Stibrany, A. O. Patil, S. Zushma, *PMSE-Preprints*, 223rd ACS National Meeting, Orlando, FL, April 7–11, **2002**; American Chemical Society: Washington, DC, **2002**; Vol. 86, 323–324. b) R. T. Stibrany, D. N. Schulz, S. Kacker, A. O. Patil, (Exxon Research and Engineering Co., USA). PCT Int. Appl. WO9930822, **1999**; *Chem. Abstr.* **1999**, *131*, 45236.

[12] R. T. Stibrany, D. N. Schultz, S. Kacker, A. O. Patil, L. S. Baugh, S. P. Rucker, S. Zushma, E. Berluche, J. A. Sissano, *Macromolecules* **2003**, *36*, 8584–8586.

[13] V. C. Gibson, A. Tomov, D. F. Wass, A. J. P. White, D. J. Williams, *Chem. Soc., Dalton Trans.* **2002**, 2261–2262.

[14] a) H. tom Dieck, R. Diercks, *Angew. Chem.* **1983**, *95*, 801–802. b) H. tom Dieck, J. Dietrich, *Chem. Ber.* **1984**, *117*, 694–701. c) H. tom Dieck, J. Dietrich, G. Wilke, *Angew. Chem.* **1985**, *97*, 795–796. d) H. tom Dieck, R. Diercks, L. Stamp, H. Bruder, T. Schuld, *Chem. Ber.* **1987**, *120*, 1943–1950. e) K.-U. Baldenius, H. tom Dieck, W. A. Koenig, D. Icheln, T. Runge, *Angew. Chem., Int. Ed.* **1992**, *31*, 305–307.

[15] a) J. Breuer, H.-W. Frühauf, W. J. J. Smeets, A. L. Spek, *Inorg. Chim. Acta* **1999**, *291*, 438–447. b) V. C. Gibson, R. K. O'Reilly, W. Reed, D. F. Wass, A. J. P. White, D. J. Williams, *Chem. Comm.* **2002**, 1850–1851. c) V. C. Gibson, R. K. O'Reilly, D. F. Wass, A. J. P. White, D. J. Williams, *Macromolecules* **2003**, *36*, 2591–2593.

[16] A. Paulovicova, U. El-Ayaan, K. Umezawa, C. Vithana, Y. Ohashi, Y. Fukuda, *Inorg. Chim. Acta* **2002**, *339*, 209–214.

[17] a) D. F. Evans, *J. Chem. Soc.* **1959**, 2003–2005. b) H. P. Frizt, K.-E. Schwarzhans, *J. Organomet. Chem.* **1964**, 208–211. c) T. H. Crawford, J. Swanson, *J. Chem. Ed.* **1971**, *48*, 382–386. d) J. Löliger, R. Scheffold, *J. Chem. Ed.* **1972**, *49*, 646–647.

[18] D. H. Grant, *J. Chem. Ed.* **1995**, *72*, 39–40.

[19] E. M. Schubert, *J. Chem. Ed.* **1992**, *69*, 62.

[20] E. A. Boudreaux, L. N. Mulay, *Theory and Applications of Molecular Paramagnetism*, John Wiley & Sons, New Your-London-Sydney-Toronto, **1976**, p. 241.

[21] a) S. C. Bart, E. J. Hawrelak, A. K. Schmisseur, E. Lobkovsky, P. J. Chirik, *Organometallics* **2004**, *23*, 237–246. b) B. C. K. Chan, M. C. Baird, *Inorg. Chim. Acta* **2004**, *357*, 2776–2782.

[22] a) U. El-Ayaan, F. Murata, S. El-Derby, Y. Fukuda, *J. Mol. Struct.* **2004**, *692*, 209–216. b) A. Paulovicova, U. El-Ayaan, K. Shibayama, T. Morita, Y. Fukuda, *Eur. J. Inorg. Chem.* **2001**, 2641–2646.

[23] L. P. Spencer, R. Altwer, P. Wei, L. Gelmini, J. Gauld, D. W. Stephan, *Organometallics* **2003**, *22*, 3841–3854.

[24] a) H.-K. Luo, Z.-H. Yang, B.-Q. Mao, D.-S. Yu, R.-G. Tang, *J. Mol. Catal. A: Chem.* **2002**, *177*, 195–207. b) E. A. H. Griffiths, G. J. P. Britovsek, V. C. Gibson, I. R. Gould, *Chem. Commun.* **1999**, 1333–1334. c) L. Q. Deng, P. Margl, T. Ziegler, *J. Am. Chem. Soc.* **1999**, *121*, 6479–6487. d) D. V. Khoroshun, D. G. Musaev, T. Vreven, K. Morokuma, *Organometallics* **2001**, *20*, 2007–2026. e) J. Ramos, V. Cruz, A. Munoz-Escalona, J. Martinez-Salazar, *Polymer* **2002**, *43*, 3635–3645. f) E. P. Talsi, D. E. Babushkin, N. V. Semikolenova, V. N. Zudin, V. N. Panchenko, V. A. Zakharov, *Macromol. Chem. Phys.* **2001**, *202*, 2046–2051. g) G. J. P. Britovsek, G. K. B. Clentsmith, V. C. Gibson, D. M. L. Goodgame, S. J. McTavish, Q. Pankhurst, *Catal. Commun.* **2002**, *3*, 207–211.

[25] a) S. A. Svejda, L. K. Johnson, M. Brookhart, *J. Am. Chem. Soc.* **1999**, *121*, 10634–10635. b) D. J. Tempel, L. K. Johnson, R. L. Huff, P. S. White, M. Brookhart, *J. Am. Chem. Soc.* **2000**, *122*, 6686–6700.

[26] M. Gasperini, F. Ragaini, S. Cenini, *Organometallics* **2002**, *21*, 2950–2957.

[27] R. van Asselt, C. J. Elsevier, W. J. J. Smeets, A. L. Spek, R. Benedix, *Recl. Trav. Chim. Pays-Bas* **1994**, *113*, 88–98.

[28] P. Kovacic, N. O. Brace, *Inorg. Synth.* **1960**, *6*, 172–173.

☙ Chapter V ❧

Synthesis and characterization of phthalocyanines of alkaline earth metals.

Introduction.

Phthalocyanine (PcH_2) and its metal complexes comprise one of the most studied class of functional organic materials.[1,2] The diverse and useful functionality of the phthalocyanine macrocycle originates from its 18π-electronic aromatic system, which is closely related to that of the naturally occurring porphyrin ring.

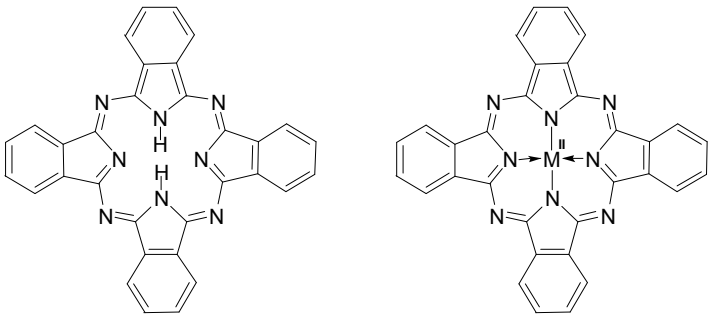

Figure 1. Phthalocyanine PcH_2 (left) and a simplest metallophthalocyanine PcM (right).

Their intensive color coupled with well-known chemical and thermal stability, explains the extensive use of phthalocyanines as highly stable blue or green pigments and dyes.[3] In addition to their long established use as colorants, phthalocyanines are exploited commercially for optical data storage,[4] catalysis,[5] and as photoconductors in xerography.[6] They are also of interest as materials for nonlinear optics,[7] liquid crystals,[8] ordered thin films,[2a, 9] photodynamic cancer therapy,[10] molecular semiconductors,[11] components of highly conducting charge-transfer salts[12] and polymers,[13] photovoltaic devices,[14] electrochromic devices,[15] fuel cells,[16] and sensors.[17]

Phthalocyanine and its metal compounds possess electronic and morphologic characteristics, which are vary favorable or necessary for semiconductive or conductive properties. Recently a review concerning conducting properties of metallophthalocyanines and related compounds was presented by Hanack.[18] The electrical properties of phthalocyanines and related compounds depend very much on the morphology of the macrocyclic system. In order to achieve good semiconducting of even conducting properties a certain spatial arrangement of the macrocycles, namely either planar or stacked, is necessary.

The planar arrangement of the macrocycles is achieved in polymeric phthalocyanines. A planar polymerized phthalocyaninato copper $[PcCu]_n$ prepared from 1,2,4,5-tetracyanobenzene is shown in Figure 2.[19]

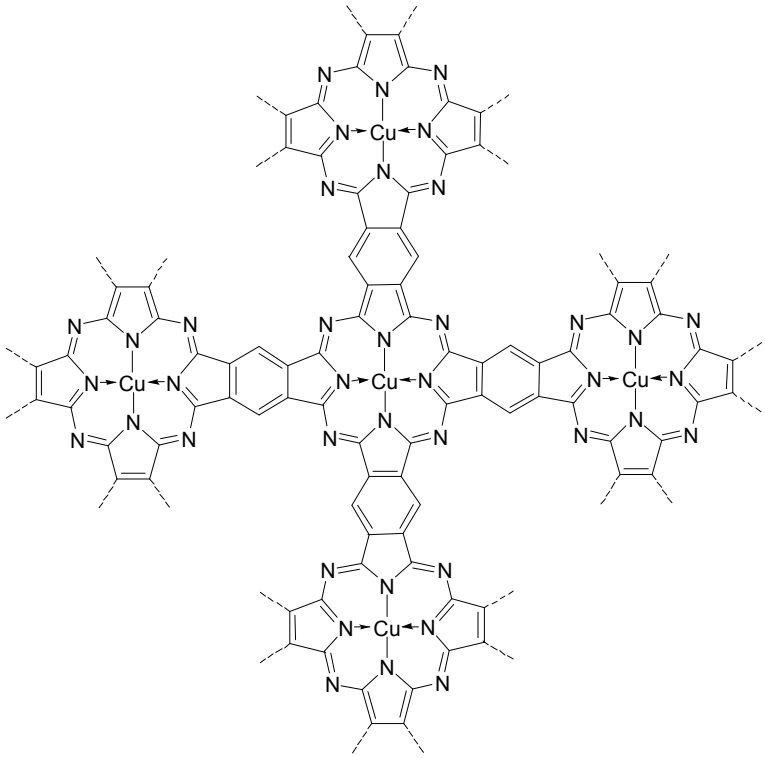

Figure 2. Schematic drawing of a planar two-dimensional arrangement of $[PcCu]_n$.

The purification and identification of planar polymerized phthalocyanines is, however, quite difficult. They are practically insoluble in organic solvents, but soluble, for example, in concentrated sulphuric acid. Theoretical calculations indicate that planar phthalocyanine polymers should exhibit good electrical in plane conductivities.[20] It was shown that phthalocyaninato copper polymers, for example, exhibit conductivities between 10^{-11} and 10^{-1} S/cm[21] rendering these polymers semiconductors.

Another condition for achieving good electrical conductivities of phthalocyanines is a stacked arrangement of the macrocycles (Figure 3). Assuming a suitable small distance between cofacially stacked planar macrocycles possessing an extended π-electron system, electron delocalization by π–π overlap of the perpendicular p_z orbitals in the stacked arrangement is possible. Partial oxidation (or less frequently reductive doping) of the macrocycles generates electron holes as charge carriers leading to semiconducting or conducting pseudo-one-dimensional materials. Phthalocyanines, however, do not tend to crystallize in this stacked arrangement, except in one case: phthalocyaninato lead(II) [PcPb] in its monoclinic modification.[22] Metallophthalocyanines in general crystallize in inclined stacked modifications, which are not favorable for π-orbital overlap and thus for the formation of a conduction band (Figure 3).

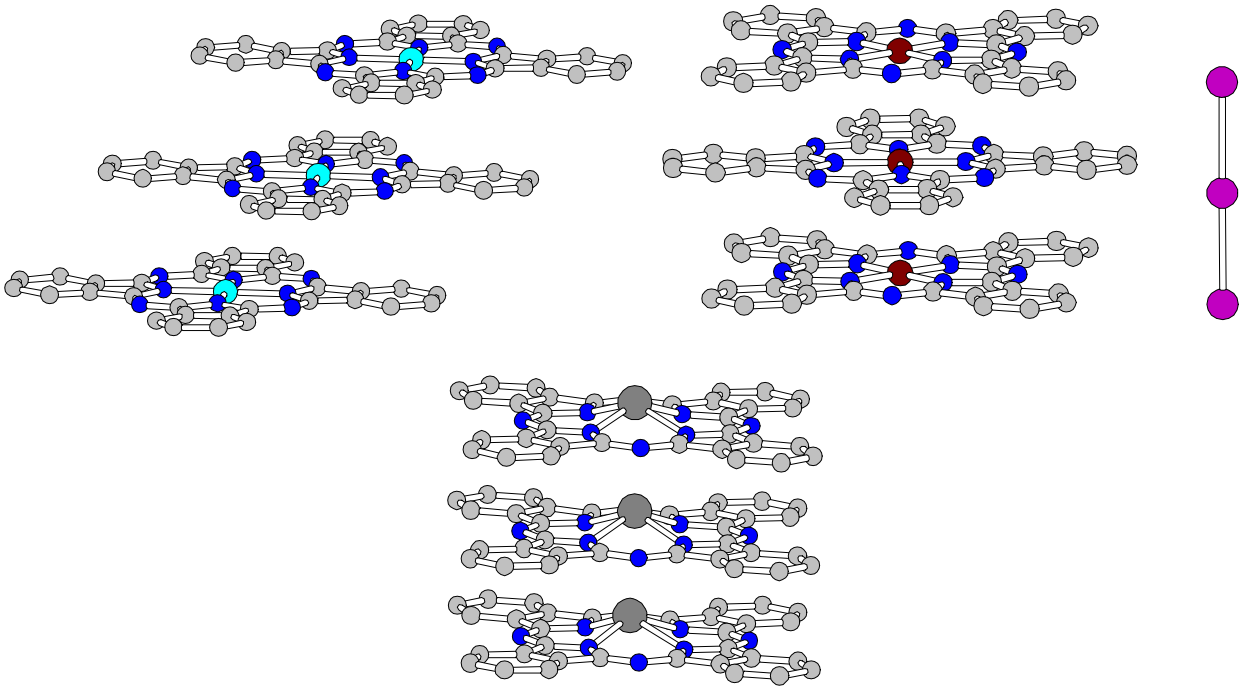

Figure 3. Crystal structures of inclined stacked β-[PcCu][23] (left), columnar stacked [PcNiI][25a] (right), and columnar stacked [PcPb][22] (bottom).

Doping of weakly conducting phthalocyanines leads to a dramatic change in the conductive behavior. Oxidative doping of PcM, for example with iodine, often results in greatly increased conductivities of the polycrystalline samples. Undoped β-[PcNi] has a powder conductivity of 10^{-11} S/cm, whereas [PcNiI][24] formed by iodine doping exhibits a powder conductivity of 0.7 S/cm.[25] The crystal structure is known for many doped, especially iodinated, metal complexes.[25a, 26] Depending on the stoichiometry, they form stacked structures as shown in Figure 3. In the stacking direction of the single crystals, e.g. of [PcNiX] (X = I^-, Br^-, ClO_4^-), room-temperature conductivities between 40 and 750 S/cm have been measured.[25] The charge transport, e.g. in [PcNiI] and [PcCuI], occurs via hole-hoping through the π-system of the oxidized stacked macrocycles. If the central metal atom is oxidized, e.g. in [PcCoI], the charge transport can occur through the metal backbone.[27]

Another possibility to achieve the columnar stacking in a crystal structure of a metallophthalocyanine is to connect metal centers with a bridging ligand. Polycondensation of $[PcM(OH)_2]$ (M = Si, Ge, Sn) yields covalently bridged stacked polyphthalocyanines $[PcMO]_n$.[18,28]

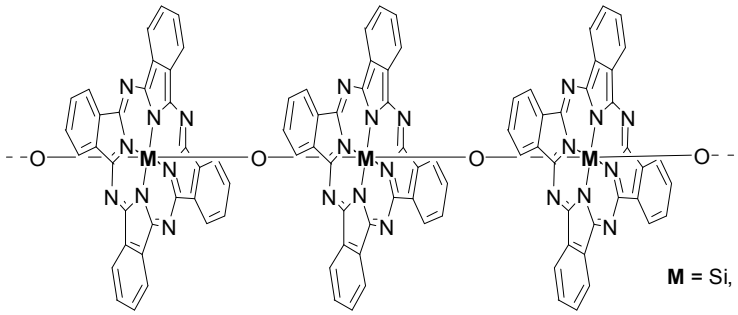

These polymers show conductivities in the range 10^{-11} – 10^{-6} S/cm when used in pure forms and in the range 10^{-6} – 10^{-1} S/cm when doped with iodine.[29] Other examples of stacked phthalocyanines are the bridged fluorophthalocyaninato complexes $[PcMF]_n$ (M = Al, Ga, Cr).[30] The highest conductivity of 5 S/cm was observed for iodine doped $[(PcAlF)I_{3.3}]_n$. A more detailed description of the electrical properties of the polymetalloxanes $[PcMO]_n$ (M = Si, Ge, Sn), the bridged fluorophthalocyaninato complexes $[PcMF]_n$ (M = Al, Ga, Cr) and related compounds is given in the literature.[31]

Phthalocyaninato complexes of transition metals can be linked with bridged ligands as well. As bridging neutral ligands pyrazine, triazine, tetrazines, *p*-diisocyanobenzenes, *p*-phenylenediamine, dabco (**di**a**bic**yclo[2.2.2.]**o**ctane), tetrafluoroterephthalic acid dinitrile $C_6F_4(CN)_2$, fumarodinitrile NC–CH=CH–CN, dicyanoacetylene, and dicyan were reported.[18] Most such complexes reveal powder conductivity in the range 10^{-6} – 10^{-7} S/cm. However, many of them can be doped either chemically or electrochemically leading to semiconductor materials with σ_{RT} = 10^{-5} – 10^{-1} S/cm. The tetrazine bridged phthalocyanines in contrast to other bridged compounds $[PcM(\mu\text{-}L)]_n$ (M = Fe, Ru, Os; L = pyrazine, *p*-diisocyanobenzene) exhibit good semiconducting properties even without external oxidative doping (σ_{RT} = 0.05 – 0.3 S/cm).

Summarizing, columnar stacked arrangement, required for phthalocyanines to exhibit semi-/conducting properties, can be achieved by oxidative/reductive doping of phthalocyaninato metal complexes and/or by linking the metal centers of macrocycles with bridging ligands.

Tri- and especially tetravalent metals having large ionic radius, such as lanthanides and actinides, are well known to form double-decker (sandwich) structures $[Pc_2M]$.[32] Because of the large ionic radius, the lanthanides and actinides do not fit into the cavity of the rigid macrocycle. The metal is displaced from the phthalocyanine plane being able to coordinate the second macrocycle. Complexes with tetravalent metal center possess two "normal" macrocycles charged -2, whereas in case of trivalent metal, one phthalocyanine ring is in a doubly reduced form $(Pc)^{2-}$ and the second is in an oxidized monoanionic radical form $(Pc)^{1-}$.

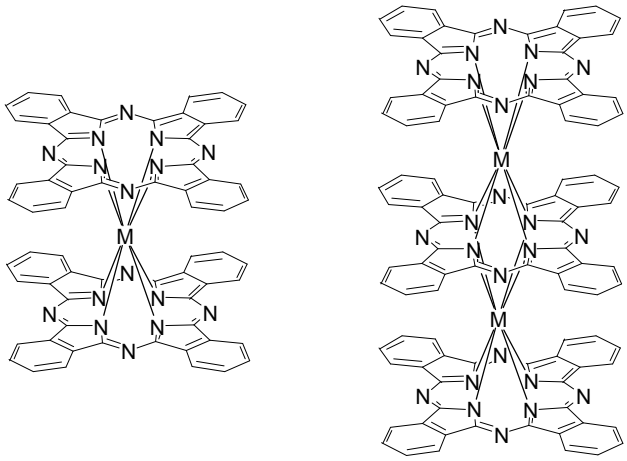

Figure 4. Double-decker [Pc_2M] (left) and triple-decker [Pc_3M_2] (right) phthalocyanines.

Moreover, trivalent lanthanides and actinides are able to form triple-decker complexes [Pc_3M_2], where the negative charge of three phthalocyaninato macrocycles (–6) is compensated by the two positive charged ions M^{3+}. Recently crystal structures of several triple-decker complexes were reported.[33]

With respect to the tendency for the large metals to form double- and triple-decker complexes we anticipate that the use of divalent metals possessing large ionic radius may facilitate formation of columnar stacked structures. Such complexes would be promising pseudo one-dimensional conducting materials.

Despite phthalocyanines were discovered about one century ago,[34] and about 70 different elements introduced into the macrocycle,[32] surprisingly only little is known about phthalocyanines of group 2 metals. The chemistry of alkaline earth metals is restricted to magnesium,[35] whereas phthalocyanines of heavier elements calcium, strontium, and barium are still unexplored.

Herein, we report on the synthesis and characterization of calcium, strontium, and barium phthalocyanines along with phthalocyanine complexes with crown ethers. Thereby phthalocyaninato barium and likely phthalocyaninato strontium are potential pseudo-one-dimensional semi-/conducting materials.

Results and Discussion.

As already mentioned in the introduction, phthalocyanine chemistry of heavy alkaline earth metals calcium, strontium, and barium compared to light elements beryllium and magnesium is still uninvestigated. Nevertheless little information concerning heavy metals phthalocyanines can be found in the literature. In classical works of Linstead in 1930's formation of [PcCa] and [PcBa] is proposed.[36] No information about these phthalocyanines except elemental analysis is reported. Linstead mentioned difficulties regarding purification of these phthalocyanines. Since the common method of purification of phthalocyanines at that time was recrystallization from concentrated sulphuric acid(!), Linstead's attempts to purify [PcCa] and [PcBa] failed leading to hydrolysis and formation of the metal-free PcH_2. In the following part we describe synthesis and characterization of [PcCa], [PcSr], and [PcBa].

Synthesis and properties of unsubstituted phthalocyanines of Ca, Sr, and Ba.

Our first attempt to synthesize phthalocyaninato calcium [PcCa] **16** was performed according to the method reported by Tomoda et al.[37] They described the synthesis of several transition metal phthalocyanines under mild condition in alcoholic medium with good yields. Since the mechanism of formation of phthalocyanines in alcoholic medium is well recognized,[2b] and relatively mild conditions (~140°C) employed lead likely to less byproducts, we have chosen the method of Tomoda.

After water-free(!) $CaCl_2$ was refluxed for 3 h in 1-pentanol in the presence of phthalonitrile and DBU (1,8-diazabicyclo[5.4.0]undec-7-ene) as catalysts, [PcCa] was collected. The yield of the purified (washing method) complex was very good and constituted 84%. The complex is stable in contact with air, but slowly hydrolyzes when in solution or in suspension. The product is insoluble in most organic solvents, negligible solubility is observed in hot pyridine and in hot quinoline. The solubility of **16** in *O*-donor solvents, e.g. DMF and DMSO, was little better. Care must be taken when the crude product is washed with organic solvents. Fine particles of **16** obtained in the reaction make extraction of more soluble impurities from the product on a glass frit difficult. Therefore, this method is not recommended, instead employing of "addition of solvent – centrifugation – decantation" cycles is advised.

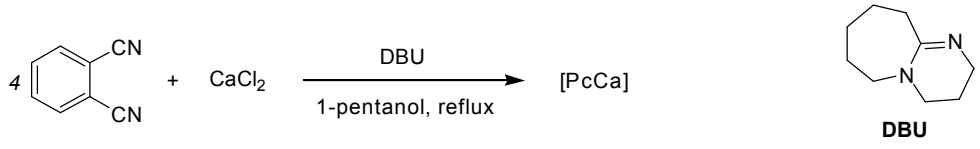

A common byproduct in the phthalocyanine chemistry is the metal-free phthalocyanine PcH_2. Formation of PcH_2 in our reaction did not occur as was judged from MALDI-TOF spectrometry. The signal centered at *m/z* = 514 corresponding to the molecular peak of PcH_2 was absent in the spectrum of the product obtained. The product was not sublimable at 200ºC and $p = 3 \cdot 10^{-5}$ mbar. During the attempted sublimation only small amount of brown material was volatile, which was not analyzed. No decomposition of **16** was observed during the attempt of sublimation as was judged from IR spectroscopy. The two IR spectra of **16** before and after sublimation were identical. Thus, the purity of **16** can be increased by sublimation of badly soluble impurities.

Formation of nucleophilic alkoxide anions is believed to initiate cyclotetramerization in alcoholic medium. The role of DBU in this reaction is to generate pentanolate anions, which attack a nitrile carbon of the phthalonitrile. Generation of alkoxide anions may be performed without catalyst if the bulk zero-valent metal is able to displace proton in alcohol, that is widely used in preparation of [$PcLi_2$], [$PcNa_2$], and [PcK_2].[36] Therefore, we performed a reaction without catalyst DBU but with bulk calcium metal. As expected, this reaction resulted in formation of **16**, but with lower yield being 43%. The purified product was identical to that obtained in reaction employing $CaCl_2$ and DBU.

Since the reaction employing $CaCl_2$ as a metal source led to higher yield compared to the reaction employing metallic calcium, the former procedure was firstly applied for the synthesis of [PcSr] **17** and [PcBa] **18**, that is $SrCl_2$ and $BaCl_2$ were used as metal sources. In both cases, the product consisted mostly of metal-free PcH_2, as was judged from IR spectroscopy. The three IR spectra obtained from purchased PcH_2 and from the products collected in reactions of phthalonitrile with metal halides were almost identical. The great attention was made to the region of N–H valence modes, since no signal is expected in this region when complexes **17** and **18** are formed without contamination with PcH_2. The MALDI-TOF does confirm formation of the target complexes showing molecular peaks at 600 and 650 for **17** and **18**, respectively. The signal corresponding to PcH_2 with *m/z* = 514 was present in mass spectra of both samples. The ratio PcH_2/[PcM] cannot be obtained by analyzing intensities in mass spectrum.

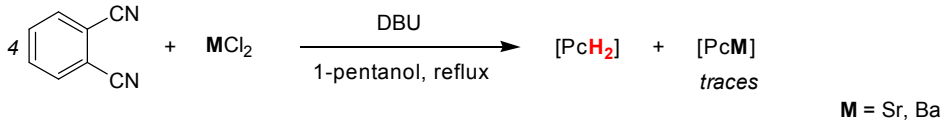

Thus, we have detected **17** and **18** but as byproducts with the main fraction being PcH_2. No attempts were made to separate the metal-free and the metal-containing phthalocyanines. We ascribed failure in preparation of [PcSr] and [PcBa] compared to the high yield synthesis of [PcCa] under identical conditions to very low solubility of $BaCl_2$ and $SrCl_2$ in 1-pentanol even at high temperatures. The deficiency of Ba^{2+} and Sr^{2+} dications in alcoholic solution leads predominantly to

formation of PcH_2. For the high yield reaction to occur, good solubility of the parent metal salt was underlined in original work of Tomoda.[37b]

A much effective way to dissolve strontium and barium in 1-pentanol is to heat the bulk metals in the solvent. Thus, Sr and Ba were successively dissolved in refluxing 1-pentanol with evolution of hydrogen gas. To get the target complexes **17** and **18**, metallic Sr and Ba, respectively, were heated in 1-pentanol in the presence of the phthalonitrile. After refluxing for 1 h, the crude products were collected by decantation of the liquid phase. Thorough washings with different solvents (see Exper. Part) gave [PcSr] and [PcBa] with 37% and 68% yields, respectively.

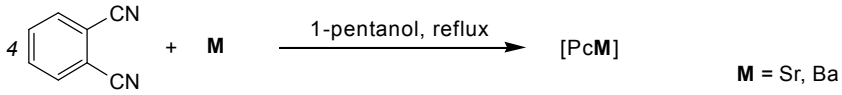

Both complexes **17** and **18** are stable in the solid state, but hydrolyzed in solutions. The speed of hydrolysis increases in the line: [PcCa] < [PcSr] < [PcBa]. This tendency is ascribed to the increasing of displacement of the metal atom from the macrocyclic ligand plane and as a consequence the rising opportunity for the metal to be attacked by nucleophiles/donors, e.g. water. Special care must be taken by working with solution/suspension of [PcBa], it seems to be exposed to solvolysis even by prolonged staying in protic solvents such as ethanol.

Since getting a single crystal of **18** was one of the main goals of this work, solubility of **18** in different solvents was thoroughly investigated. The phthalocyaninato barium complex **18** was not soluble in hexane, toluene, Et_2O, CH_2Cl_2, CCl_4, $MeNO_2$, DME, diglyme. Negligible solubility was detected in solvents such as THF, EtOH, MeCN, triglyme (on heating). Sometimes it was difficult to determine between a real solution and a fine suspension even by passing the "solution" under investigation through a micro-filter (0.45 μm). The solubility of **18** in such solvents as THF, EtOH, MeCN, and triglyme was so little (if any) as to allow purification of **18** by washing with these solvents. Better solubility of **18** was observed in pyridine, quinoline, DMF, and DMSO on heating. The solubility in *O*-donor solvents DMF and DMSO was much better as in *N*-donor solvents pyridine and quinoline that is expected from higher affinity of Ba^{2+} to *O*-donors than *N*-donors.

Relatively good solubility of **18** in DMSO on heating allowed us to perform NMR investigation in deuterated solvent. Phthalocyaninato barium was not pure as judged from the ^1H NMR spectrum. Two small, relative to the main signals of **18,** signals detected in aromatic region were observed. We refrain on comments regarding to the ratio between **18** and the "aromatic" impurity since solubility of the two substances is expected not to be the same. Several attempts to purify **18** further by means of washing with hot pyridine or DMF, or extraction with hot pyridine or DMF failed, leading occasionally to partially hydrolysis of [PcBa], but not to increasing of its

purity. The complex **18** was not sublimable at 200ºC and $p = 2 \cdot 10^{-5}$ mbar. It was stable at these conditions and no decomposition occurred as was confirmed by IR spectroscopy.

In general, solubility of [PcSr] **17** was higher than solubility of [PcBa], therefore care must be taken during purification of **17** by means of washing. Despite of the low yield reaction, **17** was pure as was judged from the ^{1}H NMR spectrum.

Nevertheless, traces of metal-free PcH_2 are present in samples of **17** and **18**, since corresponding peak *m/z* = 514 were detected in the MALDI-TOF spectra. IR spectroscopy show no any detectable signals corresponding to N–H stretches of PcH_2 confirming that only small amount of PcH_2 is present in the target complexes. One of the best method to elucidate the ratio PcH_2/[PcM] would be NMR spectroscopy. Unfortunately, it seems to be impossible in this particular case to apply NMR spectroscopy, since PcH_2 is soluble in sulphuric acid only, which leads to immediate hydrolysis of **17** and **18**.

Spectroscopic characterization of 16 – 18.

Solid-state IR spectroscopy as well as mass spectrometry were used as the first tools for characterization. Most attention was devoted to N–H stretches region in IR spectra. Since the metal-free phthalocyanine PcH_2 have two hydrogen atoms delocalized within the set of four isoindole nitrogen atoms, its IR spectrum exhibits an absorption band at 3268 cm^{-1}. This band is not as intensive as for typical N–H containing compounds. We ascribe low intensity of N–H band in PcH_2 to delocalization of the hydrogen atoms in the molecule, and consequently decreasing of the dipole moment of N–H fragment. No absorption at 3268 cm^{-1} was observed for complexes **16 – 18** suggesting that PcH_2 was not formed (Fig. 5). Weak absorption at 3295 cm^{-1} in the IR spectrum of **18** was not referred to N–H stretches of PcH_2. When **18** was hydrolyzed to PcH_2, the band corresponding to N–H stretches was observed at 3268 cm^{-1}, but not at 3295 cm^{-1}. Therefore, we assign the weak absorption at 3295 cm^{-1} to an overtone absorption band.[38]

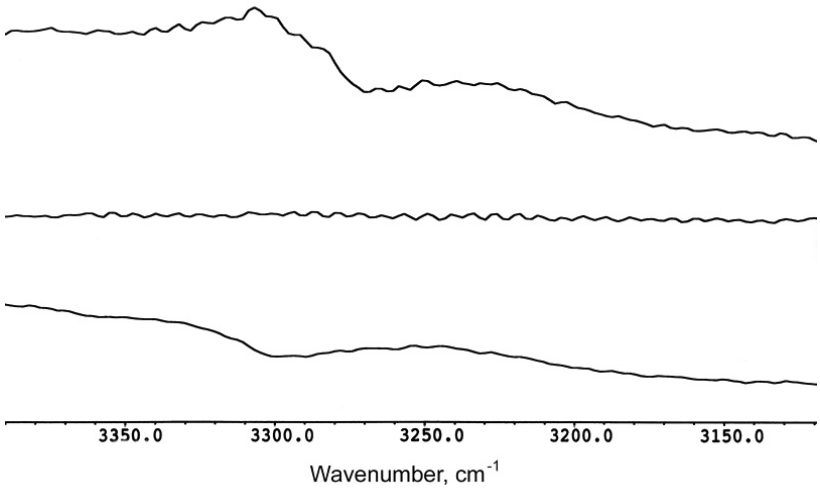

Figure 5. IR spectra of PcH_2 (top), [PcCa] (middle), and [PcBa] (bottom), N–H stretches region is shown only.

Although IR spectroscopy reveals that complexes **16–18** were not contaminated with metal-free phthalocyanine, by means of mass spectrometry (MALDI-TOF) molecular ion with *m/z* = 514 referred to PcH_2 was detected in case of complexes **17**, **18** but not in the case of [PcCa]. The isotopic pattern of the signal at 514 is in agreement with isotopic pattern expected for PcH_2. Thus, it was concluded that strontium and barium phthalocyanines were contaminated with PcH_2 but at minor degree, since no N–H stretches were observed in IR spectra of their samples. Calcium phthalocyanine **16** was free from PcH_2, that is in accord with less ability of **16** to undergo hydrolysis. For all complexes **16–18** molecular ions with corresponding isotopic pattern were detected. As an example, theoretical and experimentally obtained isotopic patterns for molecular peak of **18** at *m/z* = 650 are shown in Figure 6.

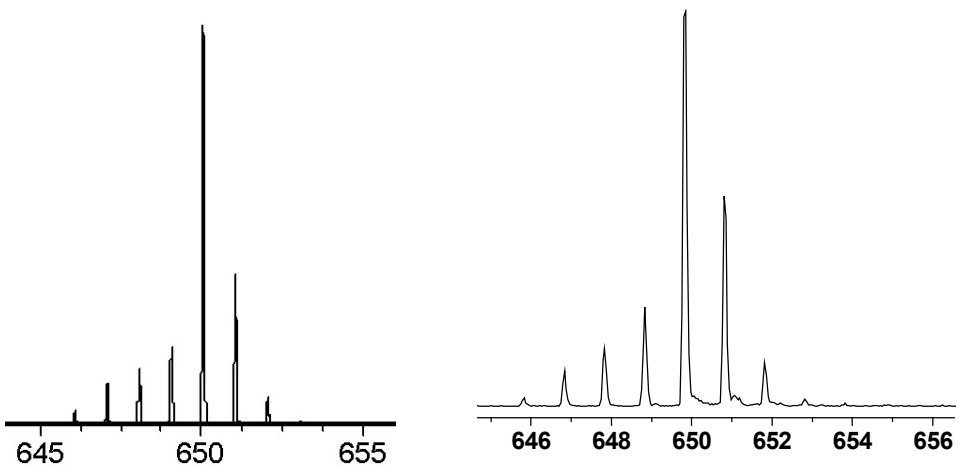

Figure 6. Theoretical[39] (left) and experimental (right) isotopic patterns for $[PcBa]^+$.

It is interesting to note that in addition to molecular peaks in samples of **16–18**, heavier ions $[PcM_2]^+$ were detected (M = Ca, Sr, Ba). The isotopic patterns of the signals observed are in

excellent agreement with theoretical patterns. Both, theoretical and experimental patterns for $[PcSr_2]^+$ ion are shown in Figure 7.

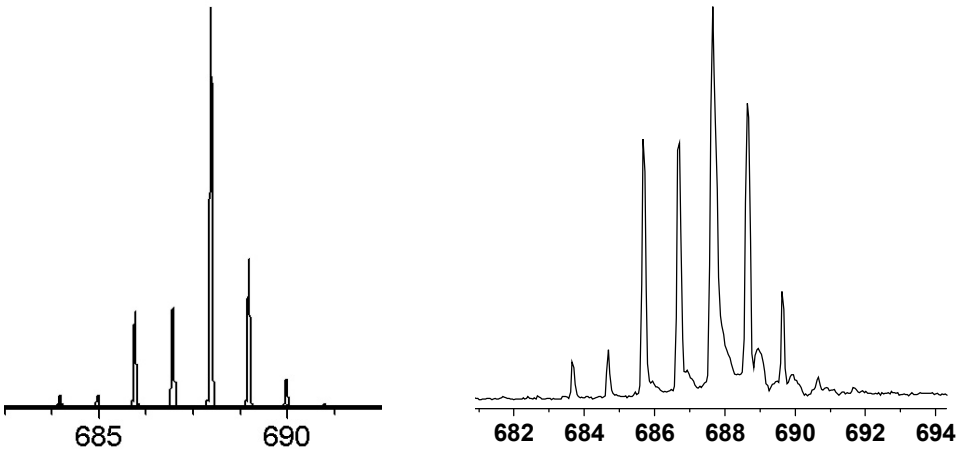

Figure 7. Theoretical (left) and experimental (right) isotopic patterns for $[PcSr_2]^+$.

Observation of $[PcM_2]^+$ ions in mass spectra of **17** and **18** may be indicative for the formation of chain structures in case of strontium and barium phthalocyanines. The origin of $[PcCa_2]^+$ ion in mass spectrum of **16** is unknown. The heavier ions, e.g. $[Pc_2M_2]^+$ (M = Ca, Sr, Ba), were not detected in MALDI-TOF spectra of **16–18**. Other types of ionizations such as EI and ESI seem to be inappropriate for studies of phthalocyanines **16–18**.

Phthalocyanines **17**, **18** were moderately soluble in DMF and DMSO. This allowed us to measure NMR spectra in d_6-DMSO. The ^{1}H NMR spectra of both complexes consist of two multiplets in the aromatic region with nearly the same intensities. The ^{1}H NMR spectrum of **16** could be measured at 500 MHz spectrometer in spite of low solubility of the complex. Two weak multiplets in ^{1}H NMR spectrum of **16** in similar position as in the case of **17** and **18** could be distinguished from the noisy baseline. It is interesting to note how chemical shifts of protons in ^{1}H NMR spectra vary along [PcCa], [PcSr], [PcBa]. While the low field multiplet in **16** is centered at 9.29 ppm, it is high-field shifted in **18** and found at 9.22 ppm. The same multiplet take intermediate position in strontium complex **17** found at 9.23 ppm. The same trend was observed for the high-field multiplet centered at 8.07 ppm in **16**. This observation is in accord with more ionic character of [PcBa] compared to [PcCa] and consequently larger negative charge delocalized over the phthalocyaninato ligand in [PcBa].

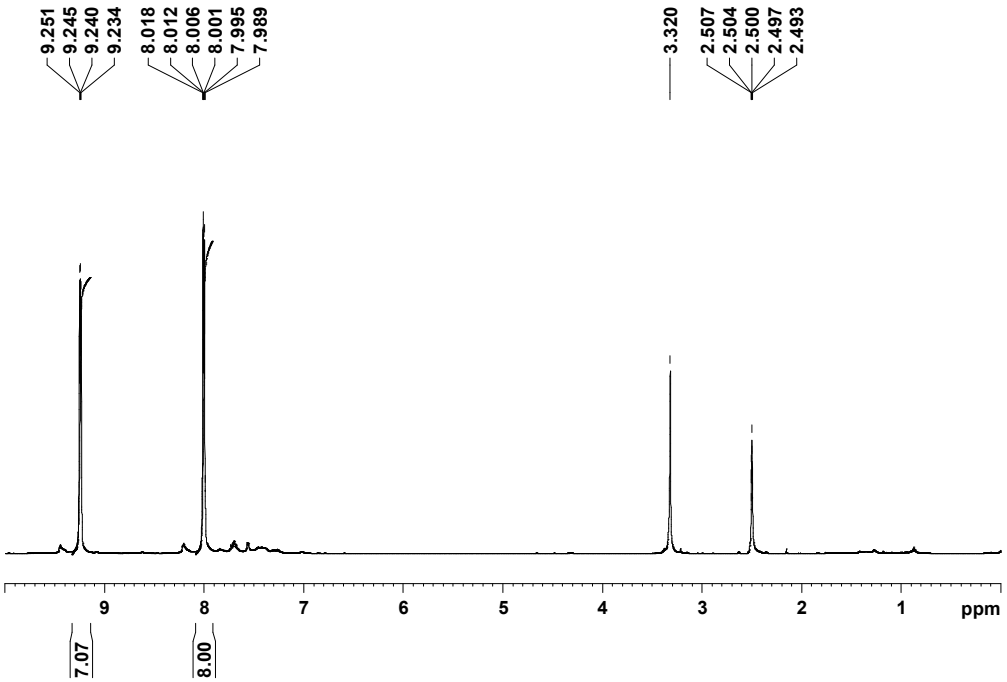

Figure 8. ^{1}H NMR spectrum of [PcSr] **17** recorded in d_6-DMSO.

^{13}C NMR spectra of **17** and **18** were recorded as well. Low solubility prevents **16** from recording of its ^{13}C NMR spectrum. ^{13}C NMR spectra of **17** and **18** are almost identical and comprise four signals as expected for D_{4h} symmetry of the complexes.

UV-vis spectra of **16–18** were measured in freshly distilled DMF at concentrations about 10^{-5} mol·L^{-1}. The absorption spectra of **16–18** are very similar; a representative UV-vis spectrum of **17** is shown in Figure 9.

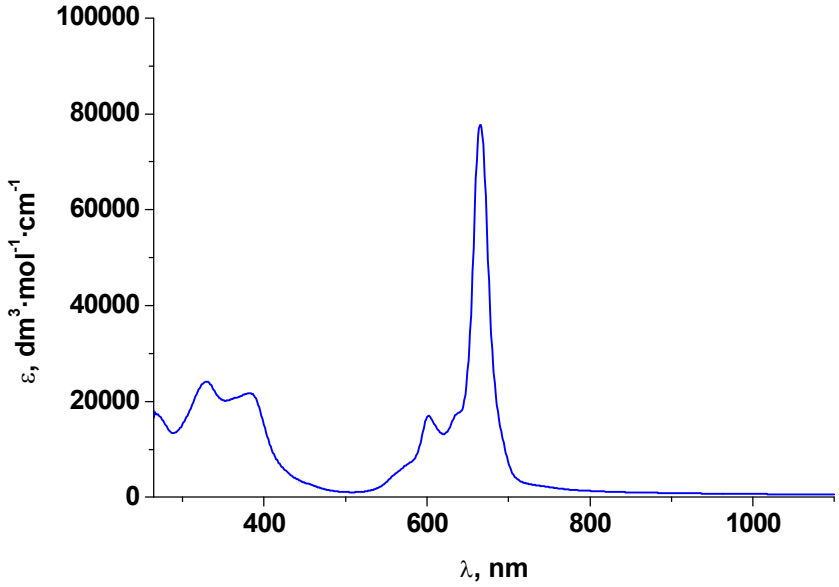

Figure 9. The electronic absorption spectrum of [PcSr] (**17**) recorded in DMF.

Typically for phthalocyanines the UV-vis spectrum of **17** consists of very strong absorption in the visible region, so called Q-band, and a less intensive absorption band in the near-UV region, so

called B- or Soret band. Both bands arise from $\pi \rightarrow \pi^*$ transitions. The low energy Q-band is responsible for HOMO→LUMO transition ($a_{1u} \rightarrow e_g$ for a D_{4h} symmetrical phthalocyanine), while the high energy B-band corresponds to electron transition from low lying π-orbital: $a_{2u} \rightarrow e_g$ for D_{4h} symmetry.[33c, 40] In the electronic spectrum of **17** the Q-band is observed at 665 nm with a weak satellite at 601 nm, while the Soret band is located in near-UV region and represented by the two bands at 384 and 329 nm. Electronic spectra of **16** and **18** are very similar to that of **17**.

Phthalocyaninato barium complexes with crown ethers.

Low solubility of unsubstituted phthalocyanines is ascribed to strong intermolecular π–π interactions in the solid state making efficient solvation difficult. Solubility of phthalocyanines in common organic solvents can be increased by introducing bulky or long-chain substituents either in the periphery of the macrocycle or by attachment of axial ligands to the metal. Substituents are responsible for a larger distance between the stacked macrocycles and enable their solvation.[32]

Since no crystallographic information about [PcM] (M = Ca, Sr, Ba) is available, and our attempts to obtain the single-crystals of unsubstituted phthalocyanines suitable for X-ray diffractometry were only in part successful (*vide infra*), we introduced axial ligands to the metal center of [PcBa] and have tried to obtain crystals of these complexes. In contrast to phthalocyanines, the first two crystal structures of soluble porphyrinato calcium complexes were reported recently by Floriani et al.[41]

One of the best class of coordinating ligands for alkaline earth metals are crown ethers[42] introduced by Pedersen.[43] Among the huge amount of crown ethers available commercially nowadays, two were chosen: 18-CR-6 and DB18-CR-6. Both of them possess the cavity large enough[42a] for the barium cation to be partly introduced.

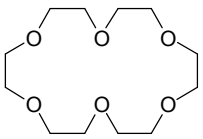

18-CR-6

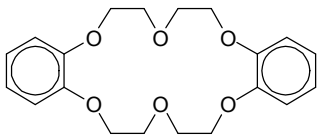

DB18-CR-6

After barium phthalocyanine **18** was stirred in DMF with two fold excess of appropriate crown ether, sandwich complexes [PcBa(18-CR-6)] **19** and [PcBa(DB18-CR-6)] **20** were formed. The target complexes were separated from the liquid phase by decantation and washed out from the excess of the crown ethers with acetonitrile. Although nearly quantitative yield is expected for these reactions, the yield was only 63% for both **19** and **20**. It might be explained as the products were likely lost by decantation of the solution from reaction mixture and by subsequent washings.

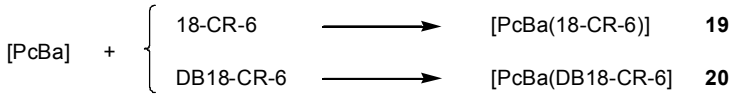

In general, both complexes **19** and **20** were better soluble than the parent [PcBa], the highest solubility was observed in *O*-donor solvents DMF and DMSO.

In addition to two multiplets of phthalocyanine macrocycle protons centered at 9.22 and 7.99 ppm, ^{1}H NMR spectrum of **19** comprise a singlet at 3.51 ppm referred to –CH_2–O– protons of the crown ether. ^{1}H NMR spectrum of **20** comprises additional multiplets originating from DB18-CR-6 centered at 6.90, 4.05 and 3.82 ppm. ^{1}H NMR spectra of **19** and **20** confirm that phthalocyaninato ligand Pc^{2-} and the crown ethers are present in ratio 1:1 in both complexes. ^{13}C NMR spectra of **19** and **20** were recorded as well. Chemical shifts of phthalocyaninato carbon atoms in [PcBa] and in complexes with crown ethers **19**, **20** are almost identical. This allows direct assignment of signals in ^{13}C NMR spectra of **19** and **20** (see Exper. Part).

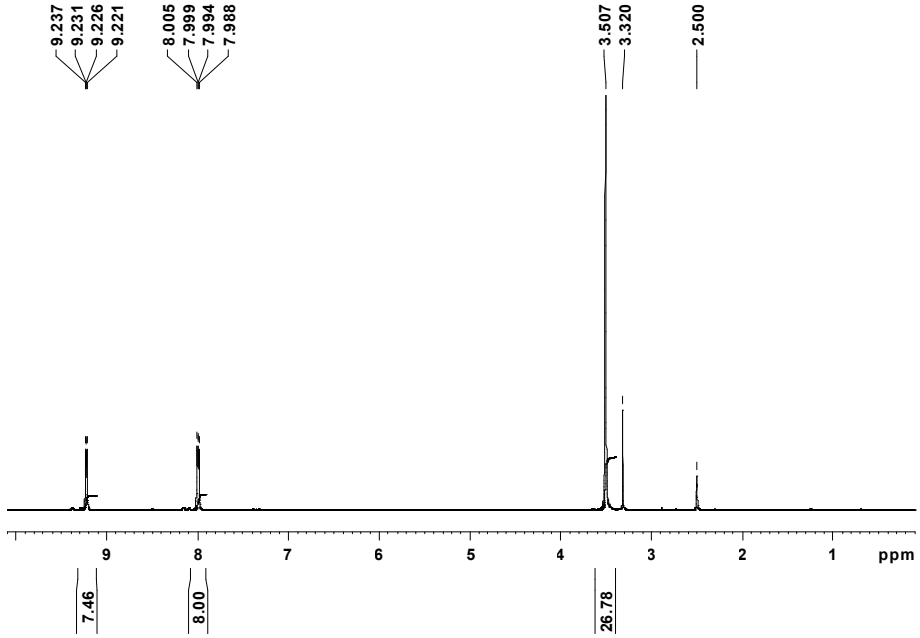

Figure 10. ^{1}H NMR spectrum of [PcBa(18-CR-6)] **19** measured in d_6-DMSO.

In MALDI-TOF spectra of **19** and **20** the high intensity signal corresponding to the ion $[PcBa]^{+}$ was observed. It is in agreement with high lability of crown ethers in the complexes. By applying higher energies in MALDI-TOF, we were able to detect molecular ions of very low intensities for both **19** and **20**. Isotopic patterns of the signals obtained are in excellent agreement with theoretical patterns. Experimentally observed and theoretical isotopic patterns for molecular cation of **20** are shown in Figure 11.

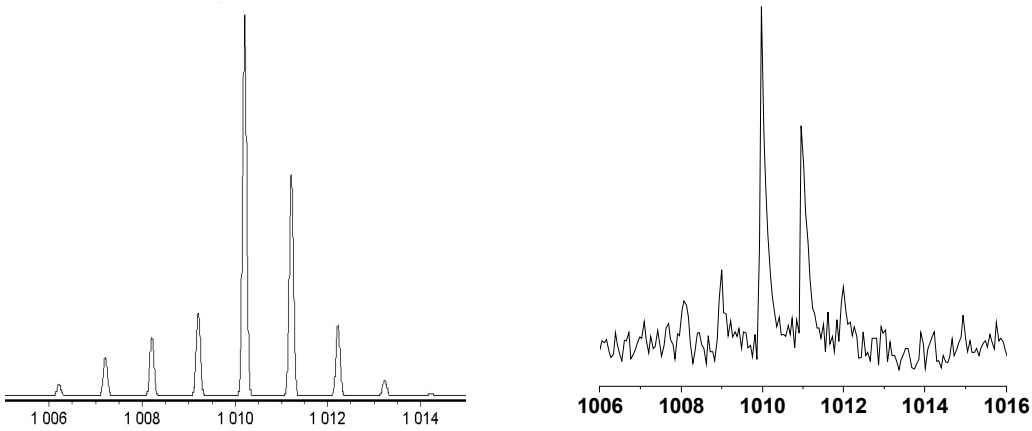

Figure 11. Theoretical (left) and experimental (right) isotopic patterns for $[PcBa(DB18\text{-}CR\text{-}6)]^+$.

Coordination of crown ethers to barium in [PcBa] is accompanied by changes in IR spectra. The IR spectra of [PcBa] and ether adducts **19**, **20** are similar but not identical. The bands in **19** and **20** are slightly shifted compared to corresponding bands of [PcBa]. Furthermore, additional bands related to crown ethers are present in the spectra of **19** and **20**. Two new bands at 1091 and 958 cm^{-1} were found in IR spectrum of **19**. The band at 1091 cm^{-1} was referred to C–O stretching of 18-CR-6. The obtained value can be compared with those reported in the literature.[38, 43a, 44] The new bands at 1247, 1203 cm^{-1} and several strong bands overlapped with the bands of phthalocyaninato ligand in the region 1053 – 1124 cm^{-1} can be found in IR spectrum of **20**. Both spectra of **18** and **20** are shown in Figure 12.

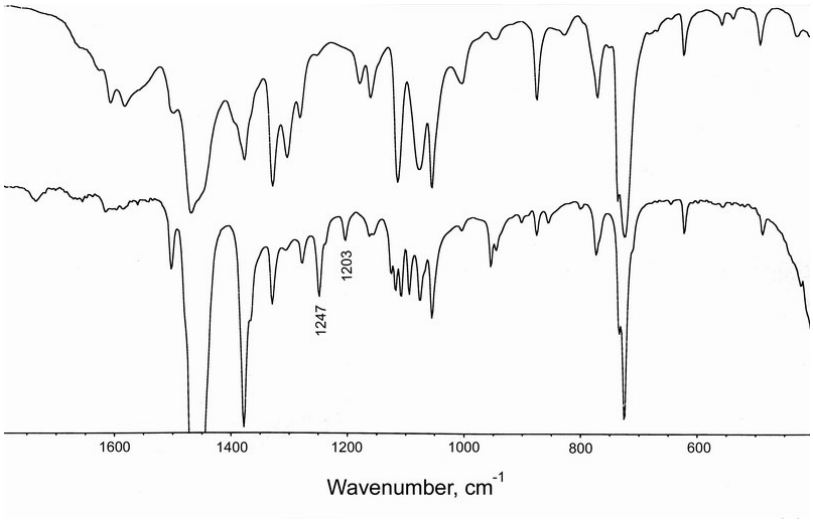

Figure 12. IR spectra of [PcBa] (top) and [PcBa(DB18-CR-6)] (bottom).

The high energy bands at 1247 and 1203 cm^{-1} are assigned to C_{Ar}–O valence vibrations of DB18-CR-6, while the low energy bands in the region 1053 – 1124 cm^{-1} are referred to H_2C–*O* stretchings of the crown ether.[38, 43a,44]

The electronic absorption spectra of crown ether complexes **19**, **20** closely resemble that of "unsubstituted" [PcM] (M = Ca, Sr, Ba). The UV-vis spectrum of **20** is shown in Figure 13. The Q-band centered in complex **20** at 664 nm (663 nm in **18**) has two shoulders and a side band at 602 nm (603 nm in **18**). The B-band in **20** is slightly bathochromic shifted to 334 nm compared to 329 nm in **18**.

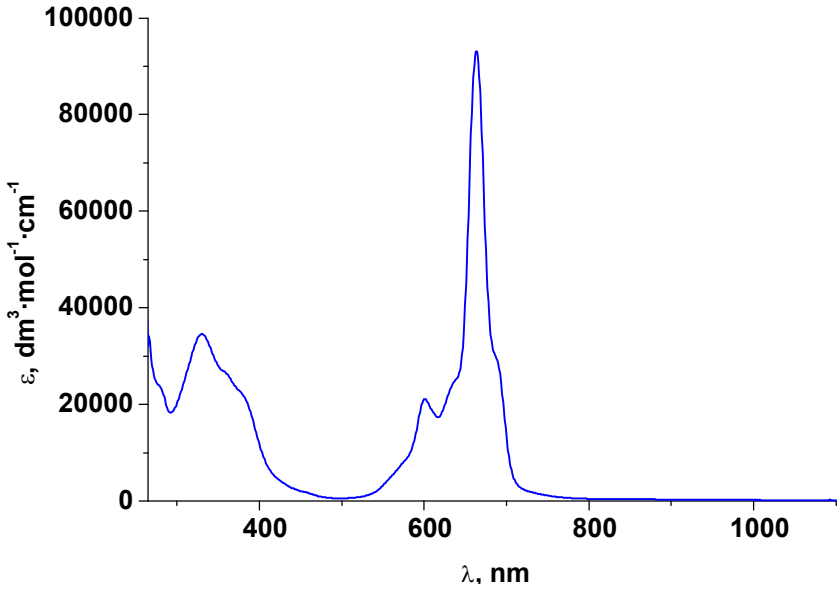

Figure 13. The electronic absorption spectrum of **20** recorded in DMF.

Crystallization of 16 – 20.

In order to establish likely columnar stacked structures of synthesized [PcM] complexes numerous attempts were undertaken to grow single crystals suitable for single crystal X-ray diffractometry. The methods tried included: a) slow cooling of saturated solutions in pyridine, quinoline, DMF, triglyme; b) layering of DMF solutions with MeCN, THF, toluene, Et_2O; c) sublimation in vacuum. The most attention was given to recrystallization from DMF or DMF + solvent, since the highest solubility of **16–18** was observed in DMF. Different DMF solutions were used for layering: concentrated, diluted, prepared at various temperatures. Very large (~ 2 × 2 mm) crystals of [PcBa] were obtained in concentrated DMF solution layered with MeCN and then cooled down to +5°C. Unfortunately, these crystals comprise extremely thin plates and they could not even be taken out the Schlenk flask without their damage. Several attempts to repeat this experiment failed.

On the final stage of writing this dissertation, we obtained crystals of [PcBa] grown from a DMF/MeCN mixture by cooling to –20ºC. Unfortunately, the quality of the crystal measured was not good enough to refine the molecular structure. Nevertheless, a qualitative picture of molecular packing can be obtained from the data.

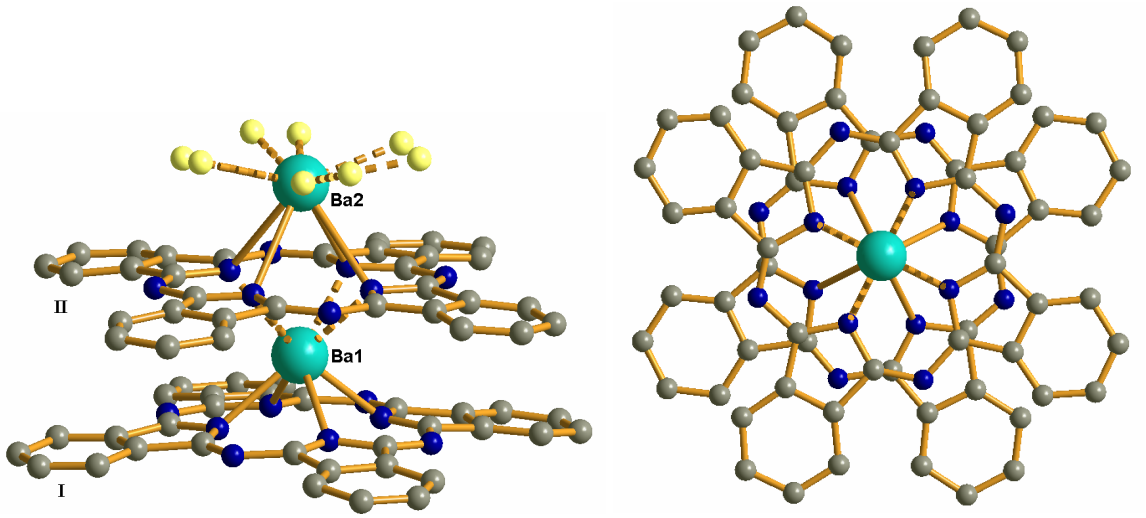

Figure 14. The columnar stacked arrangement of [PcBa]; yellow spheres are disordered solvent donor atoms.

The structure of **18** is shown in Figure 14. In accordance with our expectation, two [PcBa] molecules form a columnar stacked arrangement giving the first two links of the target one-dimensional chain-structure. However, further growth of the stack of coplanar phthalocyanine dianions is terminated by solvent molecules serving as ligands to the terminal barium atom. Unfortunately, the solvent molecules are highly disordered, so that their localization could not be determined in a reliable manner. The subunit $[PcBa]_2$ possesses C_4 symmetry with corresponding axis defined by two Ba atoms. Since two phthalocyanine ligands are in a staggered conformation with respect to each other (related by rotation of 37.1(4)° around Ba–Ba axis) there is no any mirror-plane within the subunit. Both macrocycles are nearly planar with only slight bending in the same direction. The distances Ba–N are different for Ba1 and Ba2. The distance between the sandwich atom Ba1 and isoindole nitrogens of macroring **I** at 2.541(9)Å are slightly shorter than distances between Ba1 and isoindole nitrogens of macroring **II** at 2.622(9)Å serving as bridging ligand between Ba1 and Ba2. The distance Ba2–N(isoindole in **II**) at 3.002(9)Å is considerably longer.

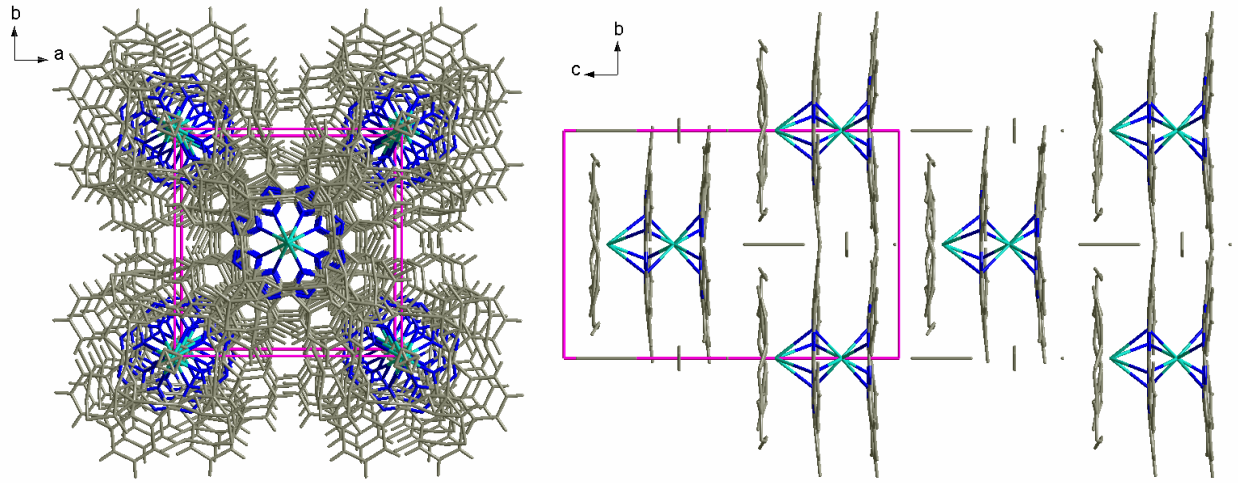

Figure 15. Crystal packing of **18** showing a "broken chain" arrangement of $[BaPc]_2$ subunits.

All subunits of the double-deckers $[PcBa]_2$ are aligned strictly coplanar along *c* axis in the crystal. Thus, as shown in Figure 15, a "broken chain" structure is formed. Disordered atoms (presumably of solvents) form a pseudo-decker at each subunit. Ongoing efforts are aimed at getting a longer one-dimensional chain structure.

The crystal structures of crown ethers complexes **19** and **20** were of considerable interest as well. Crystallization attempts include crystal growing from DMF solutions and two-component mixtures DMF + solvent (*vide supra*). Numerous attempts on getting X-ray quality single crystals were unsuccessful.

Although we did not have success in growing crystals of **19** and **20,** we assign their molecular structures to be double-decker sandwiches. A related triple-decker complex $[PcK_2(18\text{-CR-}6)_2]$ was reported by Ziolo et al.[45] Its molecular structure comprises three columnar stacked ligands connected through the two potassium ion thus forming a heteroleptic triple-decker complex.

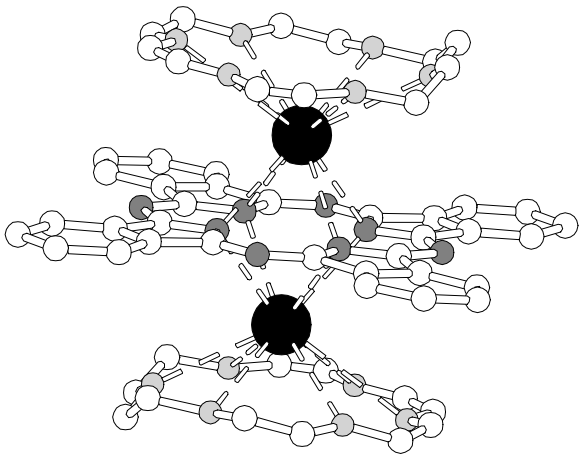

Figure 16. Molecular structure of $[PcK_2(18\text{-CR-}6)_2]$ reported by Ziolo.[45]

Conclusions.

We have synthesized three alkaline earth metallophthalocyanines [PcM] (M = Ca, Sr, Ba) and two sandwich complexes with crown ethers [PcBa(18-CR-6)] and [PcBa(DB18-CR-6)]. Though some claims regarding [PcCa] and [PcBa] were found in literature, these complexes have never been prepared in pure form or characterized before. All prepared complexes were thoroughly characterized by means of NMR, MALDI-TOF, IR, UV-vis spectroscopies and elemental analysis. Single crystal X-ray crystallography reveals a "broken chain" geometry of [PcBa]. Two molecules of [PcBa] do indeed form a columnar stacked arrangement of a solvent-terminated double-decker system. These subunits align in the crystal but do not condense (so far) to an infinite one-dimensional chain structure.

Experimental Part.

Hydrates of $CaCl_2$, $SrCl_2$ and $BaCl_2$ were refluxed in freshly distilled thionyl chloride $SOCl_2$ for several hours. All volatiles were removed under reduced pressure. The salts were then heated at +140°C *in vacuo* for several hours. Hydroscopic 18-CR-6 was dissolved in freshly distilled Et_2O and stirred over sodium as described elsewhere.[46] The crown ether 18-CR-6 as well as the water-free salts should be kept in the glove box. The metals Ca, Sr and Ba were cut in pieces directly before addition into the reactions. Oxide (nitride) layer on the metals were not removed, instead of it small excess of the metals was used. Phthalonitrile used was purified with activated charcoal (CH_2Cl_2 solution) and recrystallized from boiling ethanol.

Physical Measurements.

MALDI-TOF mass spectra were recorded on a Bruker Biflex mass spectrometer. UV-vis spectra were measured on a Shimadzu UV-1601PC instrument in freshly distilled DMF at concentrations about 10^{-5} mol·L^{-1}. NMR spectra were recorded at room temperature on Avance-300 and Bruker DRX-500 spectrometers at 300.13 MHz and 500.13 MHz for ^{1}H, respectively, and at 125.76 MHz for ^{13}C. ^{1}H NMR spectra are referenced (in ppm) to residual proton signal of d_6-DMSO (2.50 ppm); ^{13}C NMR spectra are referenced to ^{13}C signal of d_6-DMSO (39.52 ppm). For more details concerning physical measurements one is referred to the Chapter III.

Synthesis of [PcCa] (16) from $CaCl_2$.

Phthalonitrile (1.02 g, 8.00 mmol), $CaCl_2$ (0.22 g, 2.00 mmol), and DBU (1.2 mL, 1.22 g, 8.00 mmol) were placed in a Schlenk flask and absolute 1-pentalnol (20 mL) was added. After the reaction mixture was refluxed for 3 hours, it was cooled down to room temperature, toluene (~30 mL) was added followed by stirring for one hour. Solvents were decanted carefully, the purple precipitate was washed several times with MeOH, toluene, hexane, and Et_2O until colorless solutions were obtained. The product dried *in vacuo* was of blue color and it was not soluble in common organic solvents. A sublimation performed at 200ºC and $p = 3\cdot10^{-5}$ mbar failed.

Yield: 0.92 g (84 %).

$C_{32}H_{16}CaN_8$ (552.60): calcd. C 69.55, H 2.92, N 20.28; found C 67.41, H 3.34, N 18.94.

MS (MALDI-TOF): *m/z* = 592 [M + Ca^+], 552 [M^+].

^{1}*H NMR* (500.13 MHz, d_6-DMSO, 300 K): δ = 9.29 (m, 8H, H_{Pc}), 8.07 (m, 8H, H_{Pc}) ppm.

IR (Nujol): wavenumber = 3041 (w), 1642 (w), 1609 (m), 1588 (w), 1408 (w), 1320 (s), 1278 (m), 1159 (m), 1112 (s), 1078 (m), 1057 (m), 1000 (w), 938 (w), 881 (m), 771 (m), 738 (s), 725 (s) cm^{-1}.

UV-vis (DMF): λ_{max} = 663 sh, 611, 328 sh nm.

Synthesis of [PcCa] (16) from metallic Ca.

Phthalonitrile (2.16 g, 16.88 mmol) and calcium (0.186 g, 4.64 mmol) were placed in a Schlenk flask and 1-pentanol (40 mL) was added. After the reaction mixture was refluxed for 30 min, it was cooled down to room temperature. The dark-brown solution was decanted carefully and the purple precipitate was washed thoroughly with MeOH, MeCN, THF, toluene, and finally with hexane. The dried product was of blue color and spectroscopic identical to that obtained in reaction of $CaCl_2$ with phthalonitrile (*vide supra*).

Yield: 1.10 g (43 %).

Synthesis of [PcSr] (17) from metallic Sr.

Phthalonitrile (287 mg, 2.241 mmol) and strontium (54 mg, 0.616 mmol) were refluxed in 1-pentanol (10 mL) for 1 hour. The cooled solution was carefully decanted, the raw product was washed thoroughly with MeCN, toluene, and Et_2O. The dried product was of green-blue color and only slightly soluble in common organic solvents.

Yield: 126 mg (37 %).

$C_{32}H_{16}SrN_8$ (600.14): calcd. C 64.04, H 2.69, N 18.67; found C 59.28, H 3.11, N 16.84.

MS (MALDI-TOF): *m/z* = 688 [M + Sr^+], 600 [M^+].

^{1}*H NMR* (300.13 MHz, d_6-DMSO, 300 K): δ = 9.23 (m, 8H, H_{Pc}), 8.00 (m, 8H, H_{Pc}) ppm.

^{13}*C NMR* (125.76 MHz, d_6-DMSO, 300 K): δ = 121.2, 127.3, 140.0, 155.7 ppm.

IR (Nujol): wavenumber = 3042 (w), 1607 (w), 1400 (m), 1328 (s), 1307 (m), 1280 (m), 1180 (w), 1157 (m), 1111 (s), 1074 (s), 1056 (s), 1001 (w), 943 (w), 876 (m), 772 (m), 738 (m), 724 (s) cm^{-1}.

UV-vis (DMF): λ_{max} = 665 sh, 601 sh, 384 sh, 329 nm.

Attempt to synthesize [PcSr] (17) from $SrCl_2$.

Phthalonitrile (500 mg, 3.905 mmol), $SrCl_2$ (154 mg, 0.972 mmol), and DBU (0.6 mL, 594 mg, 3.905 mmol) were refluxed in 1-pentanol (15 mL) for about 3 hours. After cooling to room temperature the brown solution was decanted, the purple precipitate was washed with EtOH and

Et_2O. Though formation of the target complex was confirmed by MALDI-TOF (M^+ = 600), IR spectrum clearly showed the presence of the metal-free phthalocyanine PcH_2 as the main product.

Attempt to synthesize [PcBa] (18) from $BaCl_2$.

Phthalonitrile (300 mg, 2.343 mmol), $BaCl_2$ (122 mg, 0.586 mmol), and DBU (0.35 mL, 357 mg, 2.343 mmol) were refluxed in 1-pentanol (5 mL) for 1 hour. After the reaction mixture was cooled down to room temperature MeCN (~20 mL) was added. The suspension was stirred for one hour, the brown solution was then decanted. The purple solid was washed thoroughly with MeCN, THF, toluene, and hexane followed by drying *in vacuo*. Though formation of the target complex was confirmed by MALDI-TOF (M^+ = 650), IR spectrum clearly showed the presence of the metal-free phthalocyanine PcH_2 as the main product.

Synthesis of [PcBa] (18) from metallic Ba.

Phthalonitrile (1.024 g, 8.00 mmol) and barium (310 mg, 2.26 mmol) were refluxed in 1-pentanol (20 mL) for 1 hour. Cooled solution was decanted carefully, the purple precipitate was thoroughly washed with MeCN, THF, toluene, and Et_2O. The dried product had green-blue color, it was insoluble in common organic solvents except pyridine, DMF, and quinoline, where it shows bad solubility. A sublimation performed at 200ºC and $p = 2 \cdot 10^{-5}$ mbar failed.

Yield: 889 mg (68 %).

$C_{32}H_{16}BaN_8$ (649.86): calcd. C 59.14, H 2.48, N 17.24; found C 55.14, H 3.13, N 15.21.

MS (MALDI-TOF): *m/z* = 788 [M + Ba^+], 650 [M^+].

^1H *NMR* (300.13 MHz, d_6-DMSO, 300 K): δ = 9.22 (m, 8H, H_{Pc}), 7.99 (m, 8H, H_{Pc}) ppm.

^{13}C *NMR* (100.60 MHz, d_6-DMSO, 300 K): δ = 121.2, 127.2, 140.1, 155.7 ppm.

IR (Nujol): wavenumber = 3296 (w), 3036 (w), 1604 (m), 1580 (m), 1498 (w), 1328 (s), 1303 (m), 1281 (m), 1180 (w), 1160 (m), 1113 (s), 1076 (s), 1054 (s), 1005 (w), 948 (w), 874 (m), 770 (m), 723 (s) cm^{-1}.

UV-vis (DMF): λ_{max} = 663 sh, 631, 603 sh, 329 sh nm.

Synthesis of [PcBa(18-CR-6)] (19).

[PcBa] (291 mg, 0.448 mmol) and 18-CR-6 (237 mg, 0.897 mmol) were stirred in DMF (20 mL) for 1 hour at room temperature. Toluene (20 mL) was added and the resulting suspension was stirred for 30 min. The dark-green solution was decanted carefully, the solid was washed with MeCN twice and dried *in vacuo*. The dried product was of green color.

Yield: 257 mg (63 %).

$C_{44}H_{40}BaN_8O_6$ (914.18): calcd. C 57.81, H 4.41, N 12.26; found C 53.93, H 4.17, N 11.38.

MS (MALDI-TOF): *m/z* = 914 [M^+], 788 [M – (18-CR-6) + Ba^+], 650 [M – (18-CR-6)$^+$].

^{1}*H NMR* (300.13 MHz, d_6-DMSO, 300 K): δ = 9.22 (m, 8H, H_{Pc}), 7.99 (m, 8H, H_{Pc}), 3.51 (s, 24H, H_{crown}) ppm.

^{13}*C NMR* (125.76 MHz, d_6-DMSO, 300 K): δ = 69.7 (*C*H_2), 121.2, 127.2, 140.1, 155.7 (C_{Pc}) ppm.

IR (Nujol): wavenumber = 3465 (w), 3067 (w), 3049 (w), 1605 (m), 1582 (w), 1479 (s), 1352 (w), 1325 (s), 1305 (w), 1276 (m), 1251 (w), 1158 (m), 1106 (s), 1091 (s), 1054 (s), 1061 (w), 958 (m), 873 (m), 834 (w), 770 (m), 762 (m), 730 (s), 723 (s) cm^{-1}.

UV-vis (DMF): λ_{max} = 667, 603, 387, 329 nm.

Synthesis of [PcBa(DB18-CR-6)] (20).

[PcBa] (300 mg, 0.462 mmol) and DB18-CR-6 (333 mg, 0.924 mmol) were stirred overnight in DMF (10 mL) at room temperature. Toluene (25 mL) was added and the resulting suspension was stirred for 30 min. The dark-green solution was decanted carefully, the solid was washed with MeCN twice and dried *in vacuo*. The dried product was of green color.

Yield: 291 mg (63 %).

$C_{52}H_{40}BaN_8O_6$ (1010.27): calcd. C 61.82, H 3.99, N 11.09; found C 58.89, H 3.97, N 11.16.

MS (MALDI-TOF): *m/z* = 1010 [M^+], 788 [M – (DB18-CR-6) + Ba^+], 650 [M – (DB18-CR-6)$^+$].

^{1}*H NMR* (300.13 MHz, d_6-DMSO, 300K): δ = 9.22 (m, 8H, H_{Pc}), 7.99 (m, 8H, H_{Pc}), 6.90 (m, 8H, $H_{crown(Ar)}$), 4.05 (m, 8H, H_{crown}), 3.82 (m, 8H, H_{crown}) ppm.

^{13}*C NMR* (125.76 MHz, d_6-DMSO, 300 K): δ = 67.7 (*C*H_2), 68.9 (*C*H_2), 112.6 (C_{Ph}), 120.7 (C_{Ph}), 121.2 (C_{Pc}), 127.2 (C_{Pc}), 140.1 (C_{Pc}), 148.0 (C_{Ph}), 155.7 (C_{Pc}) ppm.

IR (Nujol): wavenumber = 3484 (w), 3043 (w), 1674 (m), 1613 (m), 1596 (m), 1501 (m), 1477 (m), 1362 (w), 1328 (s), 1275 (m), 1248 (s), 1204 (m), 1160 (w), 1124 (s), 1116 (s), 1107 (s), 1092 (s), 1075 (s), 1053 (s), 1004 (w), 953 (m), 902 (w), 875 (m), 853 (m), 800 (w), 770 (m), 731 (s), 724 (s), 709 (m) cm^{-1}.

UV-vis (DMF): λ_{max} = 664, 637, 602, 334 nm.

References.

[1] C. C. Leznoff, A. B. P. Lever, *Phthalocyanines: Properties and Applications*, VCH: New York, **1989–1996**, volumes 1–4.

[2] a) N. B. McKeown, *Phthalocyanine, Materials: Synthesis, Structure and Function*, Cambridge University Press: Cambridge, UK, **1998**. b) N. B. McKeown, Product class 9: phthalocyanines and related compounds, in *Science of Synthesis* **2004**, *17*, 1237–1368.

[3] a) F. H. Moser, A. L. Thomas, *Phthalocyanine Compounds*, Reinhold: New York, **1963**. b) F. H. Moser, A. L. Thomas, *The Phthalocyanines*, CRC: Boca Raton, Florida, **1983**, volumes 1–2.

[4] M. Emmelius, G. Pawlowski, H. W. Vollmann, *Angew. Chem., Int. Ed.* **1989**, *28*, 1445–1471; *Angew. Chem.* **1989**, *101*, 1475–1502.

[5] S. A. Borisenkova, *Pet. Chem.* **1991**, *31*, 391–408.

[6] K.-Y. Law, *Chem. Rev.* **1993**, *93*, 449–486.

[7] G. de la Torre, P. Vazquez, F. Agulló-López, T. Torres, *J. Mater. Chem.* **1998**, *8*, 1671–1683.

[8] C. Piechocki, J. Simon, A. Skoulios, D. Guillon, P. Weber, *J. Am. Chem. Soc.* **1982**, *104*, 5245–5247.

[9] a) Z. Ali-Abid, G. J. Clarkson, N. B. McKeown, K. E. Treacher, H. F. Gleeson, A. S. Stennett, *J. Mater. Chem.* **1998**, *8*, 2371–2378. b) M. J. Cook, M. F. Daniel, K. J. Harrison, N. B. McKeown, A. J. Thomson, *J. Chem. Soc., Chem. Commun.* **1987**, 1148–1150.

[10] a) D. Phillips, *Prog. React. Kinet.* **1997**, *22*, 175–300. b) R. Bonnett, *Chem. Soc. Rev.* **1995**, *24*, 19–33. c) I. Rosenthal, *Photochem. Photobiol.* **1991**, *53*, 859–870.

[11] J.-J. André, J. Simon, *Molecular Semiconductors*, Springer: Berlin, **1985**.

[12] T. J. Marks, *Angew. Chem., Int. Ed.* **1990**, *29*, 857–879; *Angew. Chem.* **1990**, *102*, 886–908.

[13] N. B. McKeown, *J. Mater. Chem.* **2000**, *10*, 1979–1995.

[14] a) C. W. Tang, *Appl. Phys. Lett.* **1986**, *48*, 183–185. b) M. K. Nazeeruddin, R. Humphry-Baker, M. Gratzel, B. A. Murrer, *Chem. Commun.* **1998**, 719–720.

[15] R. J. Mortimer, *Electochim. Acta* **1999**, *44*, 2971–2981.

[16] A. B. P. Lever, M. R. Hempstead, C. C. Leznoff, W. Liu, M. Melnik, W. A. Nevin, P. Seymour, *Pure Appl. Chem.* **1986**, *58*, 1467–1476.

[17] J. D. Wright, *Prog. Surf. Sci.* **1989**, *31*, 1–60.

[18] M. Hanack, M. Lang, *Adv. Mater.* **1994**, *6*, 819–833.

[19] a) A. J. Epstein, B. S. Wildi, *J. Chem. Phys.* **1960**, *32*, 324–329. b) D. Wöhrle, U. Marose, R. Knoop, *Makromol. Chem.* **1985**, *186*, 2209–2228. c) D. Wöhrle, B. Schulte, *Makromol. Chem.* **1988**, *189*, 1229–1238.

[20] P. Gomez-Romero, Y.-S. Lee, M. Kertesz, *Inorg. Chem.* **1988**, *121*, 3672–3675.

[21] a) C. S. Marvel, J. H. Rassweiler, *J. Am. Chem. Soc.* **1958**, *80*, 1197–1199. b) G. Manecke, D. Wöhrle, *Makromol. Chem.* **1967**, *102*, 1–23. c) H. Shirai, I. Takemae, K. Kobayashi, Y. Kondo, O. Hirabaru, N. Hoyo, *Makromol. Chem.* **1984**, *185*, 1395–1401.

[22] K. Ukei, *Acta Crystallogr.* **1973**, *B 29*, 2290–2292.

[23] C. J. Brown, *J. Chem. Soc. (A)* **1968**, 2488–2493.

[24] The charge distribution is better described as $[\{(PcNi)_3\}^+(I_3)^-]$.

[25] a) C. J. Schramm, R. P. Scaringe, D. R. Stojakovic, B. M. Hoffman, J. A. Ibers, T. J. Marks, *J. Am. Chem. Soc.* **1980**, *102*, 6702–6713. b) S. M. Palmer, J. M. Stanton, B. M. Hoffman, J. A. Ibers, *Inorg. Chem.* **1986**, *25*, 2296–2300. c) M. Almeida, M. G. Kanatzidis, L. M. Tonge, T. J. Marks, H. O. Marcy, W. J. McCarthy, C. R. Kannewurf, *Solid State Commun.* **1987**, *63*, 457–461. d) L. J. Pace, J. Martinsen, A. Ulman, B. M. Hoffman, J. A. Ibers, *J. Am. Chem. Soc.* **1983**, *105*, 2612–2620.

[26] a) S. M. Palmer, J. L. Stanton, N. K. Jaggi, B. M. Hoffman, J. A. Ibers, L. H. Schwartz, *Inorg. Chem.* **1985**, *24*, 2040–2046. b) J. Martinsen, J. L. Stanton, R. L. Greene, J. Tanaka, B. M. Hoffman, J. A. Ibers, *J. Am. Chem. Soc.* **1985**, *107*, 6915–6920. c) B. Latte, A. Kienast, C. Bruhn, A. Loidl, H. Homborg, *J. Porphyrins Phthalocyanines* **1997**, *1*, 267–273. d) M. Y. Ogawa, J. Martinsen, S. M. Palmer, J. L. Stanton, J. Tanaka, R. L. Greene, B. M. Hoffman, J. A. Ibers, *J. Am. Chem. Soc.* **1987**, *109*, 1115–1121.

[27] J. Martinsen, J. L. Stanton, R. L. Green, J. Tanaka, B. M. Hoffman, J. A. Ibers, *J. Am. Chem. Soc.* **1985**, *107*, 6915–6920.

[28] a) D. W. DeWulf, J. K. Leland, B. L. Wheeler, A. J. Bard, D. A. Batzel, D. R. Dininny, M. Kenney, *Inorg. Chem.* **1987**, *26*, 266–270. b) E. Ciliberto, K. A. Doris, W. J. Pietro, G. M. Reisner, D. E. Ellis, I. Frigala, F. H. Herbstein, M. A. Ratner, T. J. Marks, *J. Am. Chem. Soc.* **1984**, *106*, 7748–7761. c) B. N. Diel, T. Inabe, J. W. Lyding, K. F. Schoch, C. R. Kannewurf, T. J. Marks, *J. Am. Chem. Soc.* **1983**, *105*, 1551–1567. d) W. J. Pietro, T. J. Marks, M. A. Ratner, *J. Am. Chem. Soc.* **1985**, *107*, 5387–5391. e) X. Zhou, T. J. Marks, S. H. Carr, *Polym. Mater. Sci. Eng.* **1984**, *51*, 651–654.

[29] a) C. W. Dirk, E. A. Mintz, K. F. Schoch, T. J. Marks, *J. Macromol. Sci. Chem.* **1981**, *A 16*, 275–298. b) T. Inabe, M. K. Moguel, C. R. Kannewurf, T. J. Marks, *Mol. Cryst. Liq. Cryst.* **1983**, *93*, 355–367. c) T. Inabe, M. K. Moguel, T. J. Marks, R. Burton, J. W. Lyding, C. R. Kannewurf, *Mol. Cryst. Liq. Cryst.* **1985**, *118*, 349–352. d) J. Metz, G. Pawlowski, M. Hanack, *Z. Naturforsch.* **1983**, *38b*, 378–382.

[30] a) J. P. Linsky, T. R. Paul, R. S. Nohr, M. E. Kenney, *Inorg. Chem.* **1980**, *19*, 3131–3135. b) P. M. Kuznesof, R. S. Nohr, K. J. Wynne, M. E. Kenney, *J. Macromol. Sci. Chem.* **1981**, *A 16*, 299–312. c) R. S. Nohr, K. J. Wynne, *J. Chem. Soc., Chem. Commun.* **1981**, 1210–1211. d) K. J. Wynne, *Inorg. Chem.* **1985**, *24*, 1339–1342. e) K. J. Wynne, R. S. Nohr, *Mol. Cryst. Liq. Cryst.* **1982**, *81*, 243–254. f) P. Brant, R. S. Nohr, K. J. Wynne, D. C. Weber, *Mol. Cryst. Liq. Cryst.* **1982**, *81*, 255–263.

[31] H. Schultz, H. Lehmann, M. Rein, M. Hanack, *Struct. Bonding (Berlin)* **1991**, *74*, 41–146.

[32] M. Hanack, H. Heckmann, R. Polley, *Houben-Weyl*, vol. E 9d, Phthalocyanines and Related Compounds, Thieme Stuttgart, **1997**, 717–842.

[33] a) J. Janczak, R. Kubiak, J. Richter, H. Fuess, *Polyhedron* **1999**, *18*, 2775–2780. b) K. Benihya, M. Mossoyan-Deneux, F. Hahn, N. Boucharat, G. Terzian, *Eur. J. Inorg. Chem.* **2000**, 1771–1779. c) P. Zhu, Na Pan, R. Li, J. Dou, Y. Zhang, D. Y. Y. Cheng, D. Wang, D. K. P. Ng, J. Jiang, *Chem.-Eur. J.* **2005**, *11*, 1425–1432. d) S. I. Troyanov, L. A. Lapkina, V. E. Larchenko, A. Yu. Tsivadze, *Dokl. Akad. Nauk SSSR (Russ.) (Proc. Nat. Acad. Sci. USSR)* **1999**, *367*, 644–648. e) Y. Bian, L. Li, D. Wang, C.-F. Choi, D. Y. Y. Cheng, P. Zhu, R. Li, J. Dou, R. Wang, Na Pan, D. K. P. Ng, N. Kobayashi, J. Jiang, *Eur. J. Inorg. Chem.* **2005**, 2612–2618.

[34] A. Braun, J. Tcherniak, *Ber. Dtsch. Chem. Ges.* **1907**, *40*, 2709–2714.

[35] a) R. Kubiak, A. Waskowska, A. Pietraszko, E. Bukowska, *Inorg. Chim. Acta* **2005**, *358*, 453–458. b) J. Janczak, Y. M. Idemori, *Polyhedron* **2003**, *22*, 1167–1181. c) J. Janczak, Y. M. Idemori, *Acta Crystallogr., Sect. C: Cryst. Struct. Commun.* **2002**, *58*, m549–m550. d) J. Janczak, R. Kubiak, *Polyhedron* **2002**, *21*, 265–274. e) J. Janczak, R. Kubiak, *Polyhedron* **2001**, *20*, 2901–2909. f) J. Mizuguchi, *Z. Kristallogr.-New Cryst. Struct.* **2002**, *217*, 251–252. g) J. Mizuguchi, M. Mochizuki, *Z. Kristallogr.-New Cryst. Struct.* **2002**, *217*, 244–246. h) J. Mizuguchi, *Z. Kristallogr.-New Cryst. Struct.* **2001**, *216*, 377–378. i) J. Mizuguchi, *J. Phys. Chem. A* **2001**, *105*, 1121–1124. j) S. Matsumoto, A. Endo, J. Mizuguchi, *Z. Kristallogr.* **2000**, *215*, 182–186. k) H. Huckstadt, C. Jaouen, M. Goldner, U. Cornelissen, A. Tutass, H. Homborg, *Z. Anorg. Allg. Chem.* **2002**, *626*, 671–678. l) B. Assmann, G. Ostendorp, G. Lehmann, H. Homborg, *Z. Anorg. Allg. Chem.* **1996**, *622*, 1085–1090. m) M. S. Fischer, D. H. Templeton, A. Zalkin, M. Calvin, *J. Am. Chem. Soc.* **1971**, *93*, 2622–2628. n) I. A. Guzei, R. W. McGaff, H. M. Kieler, *Acta Crystallogr., Sect. C: Cryst. Struct. Commun.* **2005**, *61*, m472–m475.

[36] a) R. P. Linstead, A. R. Lowe, *J. Chem. Soc.* **1934**, 1022–1027. b) P. A. Barrett, C. E. Dent, R. P. Linstead, *J. Chem. Soc.* **1936**, 1719–1736. c) P. A. Barrett, D. A. Frye, R. P. Linstead, *J. Chem. Soc.* **1938**, 1157–1163.

[37] a) H. Tomoda, S. Saito, S. Ogawa, S. Shiraishi, *Chem. Lett.* **1980**, 1277–1280. b) H. Tomoda, S. Saito, S. Shiraishi, *Chem. Lett.* **1983**, 313–316.

[38] M. Hesse, H. Meier, B. Zeeh, *Spektroskopische Methoden in der organischen Chemie*, Georg Thieme Verlag Stuttgart, **1979**.

[39] Theoretical isotopic patterns of ions were calculated with *IsoPro 3.0* program.

[40] J. Janczak, R. Kubiak, *Inorg. Chim. Acta* **2003**, *342*, 64–76.

[41] L. Bonomo, M.-L. Lehaire, E. Solari, R. Scopelliti, C. Floriani, *Angew. Chem., Int. Ed.* **2001**, *40*, 771–774; *Angew. Chem.* **2001**, *113*, 793–796.

[42] a) P. N. Kapoor, R. C. Mehrotra, *Coord. Chem. Rev.* **1974**, 14, 1–27. b) N. S. Poonia, A. V. Bajaj, *Chem. Rev.* **1979**, *79*, 389–445.

[43] a) C. J. Pedersen, *J. Am. Chem. Soc.* **1967**, *89*, 7017–7036. b) C. J. Pedersen, *J. Am. Chem. Soc.* **1970**, *92*, 386–391. c) C. J. Pedersen, *Proc. Fed. Amer. Soc. Exp. Biol.* **1968**, *27*, 1305–1309. d) C. J. Pedersen, *J. Org. Chem.* **1971**, *36*, 254–257.

[44] Ot E. Sielcken, M. M. van Tilborg, M. F. M. Roks, R. Hendriks, W. Drenth, R. J. M. Nolte, J. Am. Chem. Soc. **1987**, *109*, 4261–4265.

[45] R. F. Ziolo, W. H. H. Günther, J. M. Troup, *J. Am. Chem. Soc.* **1981**, *103*, 4629–4630.

[46] D. M. Jenkins, W. Teng, U. Englich, D. Stone, K. Ruhlandt-Senge, *Organometallics* **2001**, *20*, 4600–4606.

Summary

The present work is dedicated to complexes comprising non-innocent *N*-donor ligands and late transition metals of groups VIII–XI or alkaline earth metals. The types of redox active ligands used in this work include *o*-phenylenediamine derived ligands (Chapter I and II), 1,4-diaza-1,3-butadiene derived ligands (DAD, Chapter III), derivatives of bis(*N*-arylimino)acenaphthene (BIAN, Chapter III and IV), and unsubstituted phthalocyanine (Chapter V). While Chapters I–III are aimed on fundamental studies of late transition metal complexes with non-innocent ligands, Chapters IV and V are directed towards applications of such complexes. The results obtained in this work are summarized according the Chapters as follows.

Chapter I.

A series of homoleptic complexes $[M(BPPD)_2]$ (M =Ni (**1**), Pd (**2**), Co (**3**), Cu (**4**), Fe (**5**)) of the new non-innocent ligand *N*,*N*'-bis(pentafluorophenyl)-*o*-phenylenediamine (H_2BPPD) was synthesized. The *physical* (*spectroscopic*) oxidation states of ligands and metals in complexes **1**, **2**, **4**, and **5** were successfully determined by single crystal X-ray crystallography performed at low temperatures by means of bond lengths analysis. Complexes **1**, **2** and **4** consist of divalent metals and two π-radical anions $(BPPD)^{1-}$.

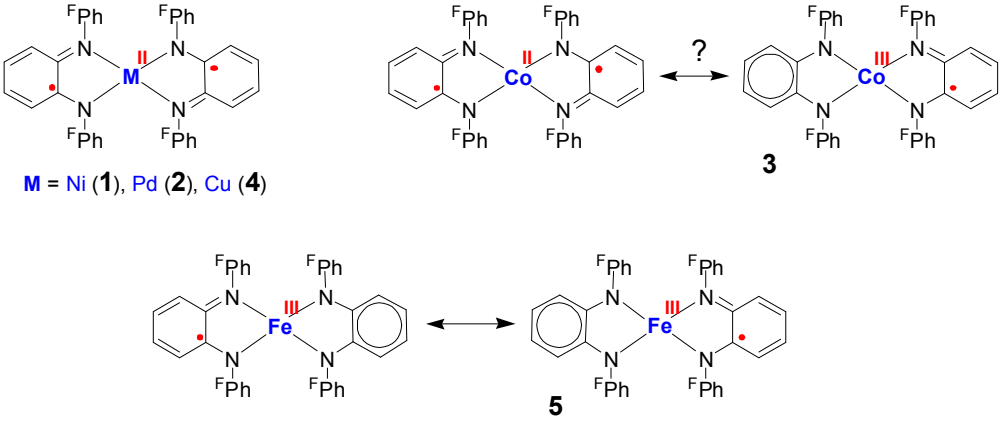

The unique four-coordinated iron complex **5** comprises a ferric center, one π-radical anion $(BPPD)^{1-}$ and one closed-shell dianion $(BPPD)^{2-}$. The complex **5** behaves as a Class III mixed-valence system with electron delocalization over both ligands. Since the ligand bond pattern of **3** takes an intermediate position of that of **1** (**2**, **4**) and **5**, the *physical* oxidation state of the cobalt atom in **3** is still unclear.

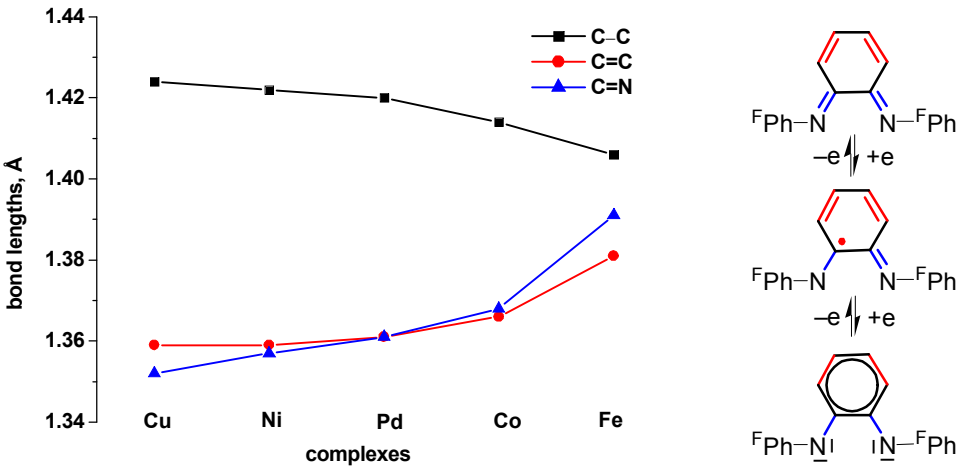

Figure 1. Characteristic averaged bond lengths in the complexes $[M(BPPD)_2]$.

The bulky *N*-C_6F_5 substituents force the complexes **1** and **3 – 5** to adopt heavily distorted tetrahedral (twisted) geometry, which is a striking contrast to the strictly planar *o*-phenylenediamine derived complexes reported previously. Because of the large ionic radius of Pd compared to the first row transition metals, complex **2** adopts a close to square-planer less twisted geometry.

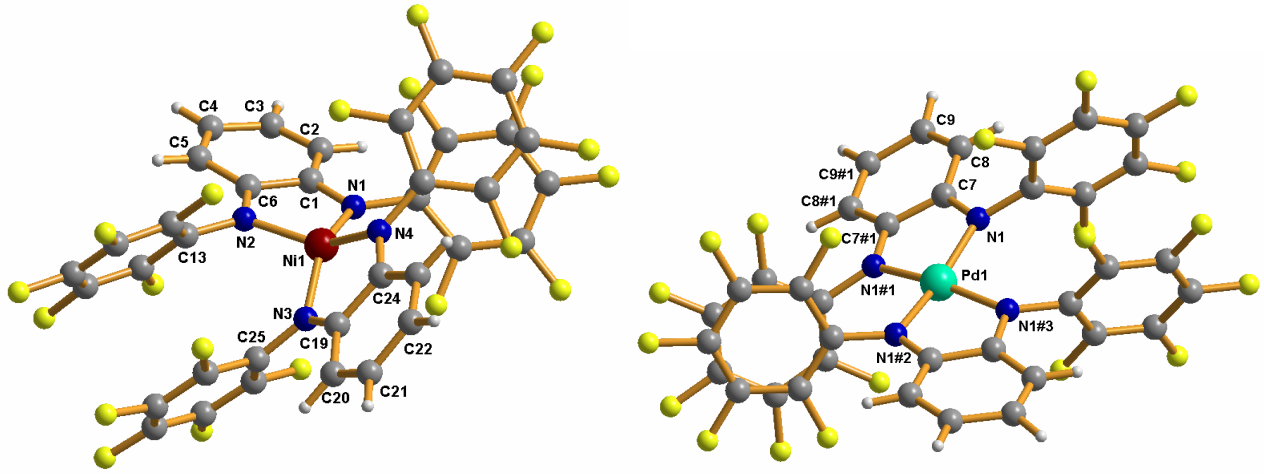

Figure 2. Molecular structures of highly twisted **1** (53.7(1)º between NCCN planes), and less twisted **2** (22.4(2)º).

Electronic structures of the complexes **1 – 4** and of some of their cationic and/or anionic neighboring redox states were probed using EPR and UV-vis-NIR spectroelectrochemistry (in collaboration with Prof. Kaim, Stuttgart). Twisted geometry of the complexes tends to result in considerable changes in their electronic structures compared to the strictly planar complexes reported previously, whereas the strong electron withdrawing *N*-C_6F_5 groups have a great influence on redox properties. Distorted tetrahedral ligands arrangement may lead to the high-spin state of Ni^{II}, Fe^{III}, and Co^{II}(?) in the corresponding complexes. The superexchange interactions between the remote radical ligands are not as effective as in the planar complexes. This leads to the ligand-centered spin ground state in distorted tetrahedral Cu^{II} complex, and not to the metal-centered spin as in the planar analogue.

Chapter II.

The reactivity of [M(BPPD)$_2$] (M = Fe, Co, Ni, Pd, Cu; H_2BPPD = *N*,*N*′-bis(pentafluorophenyl)-*o*-phenylenediamine) complexes **1** – **5** has been investigated in detail. The homoleptic complexes **1** – **5** were shown to be unable to coordinate any further ligand in addition, oxidative addition, and oxidative alkylation/arylation reactions. This inertness is ascribed to the steric factor, since the bulky perfluorinated phenyl rings efficiently shield the metal center and inhibit any increase of the coordination number. Oxidation of the redox active ligand within the complexes can be performed by using silver triflate or iodosyldichloride $PhICl_2$. One-electron-oxidized complexes are not stable and undergo decomplexation and further reactions resulting in formation of phenazine derivatives as the products of an intramolecular nucleophilic reaction. The mechanism of this conversion has been suggested.

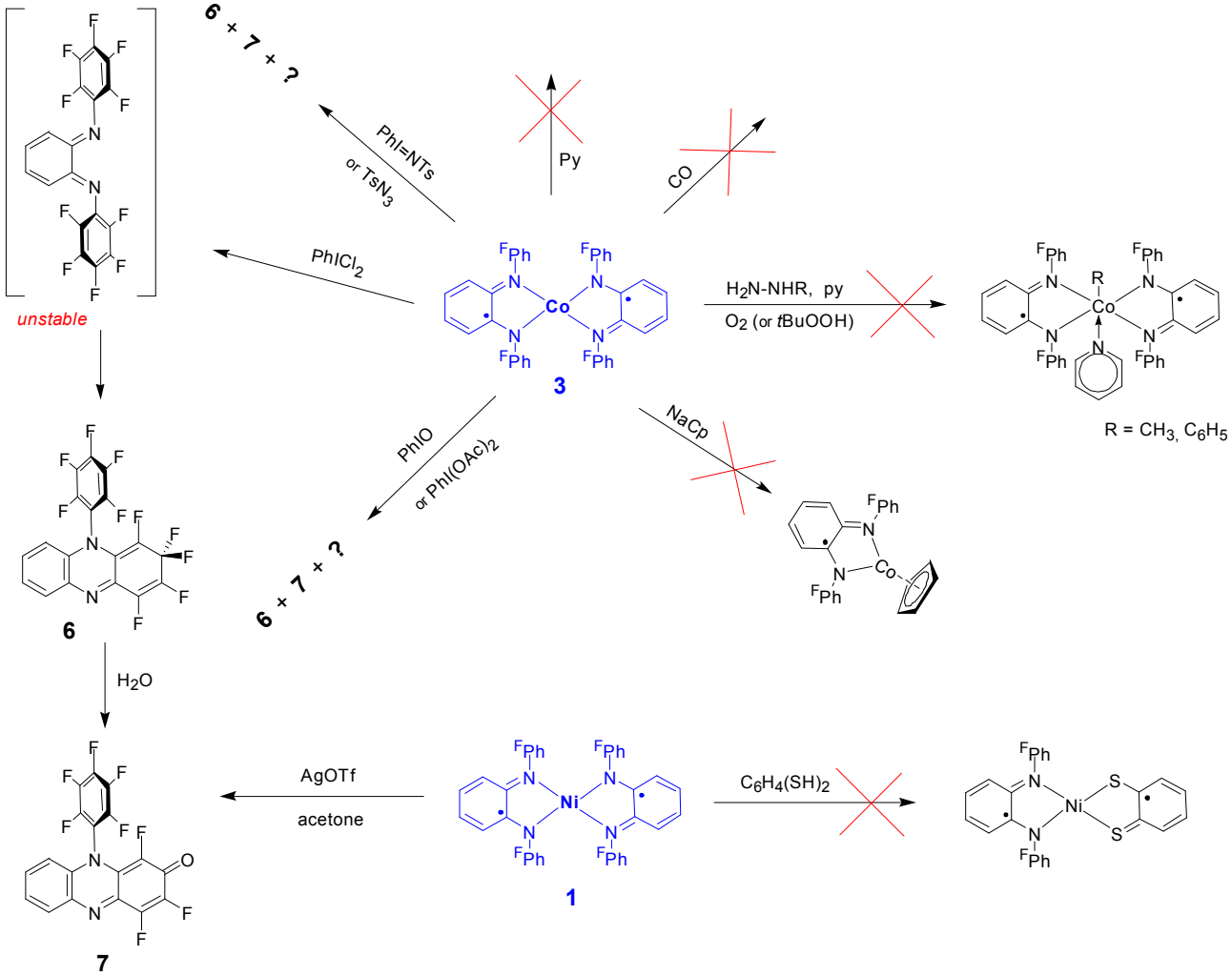

Figure 3. Reactivity of [M(BPPD)$_2$] complexes.

Oxidation of [Co(BPPD)$_2$] with $PhICl_2$ resulted in formation of phenazine derivative **6** that undergoes subsequent hydrolysis giving substituted phenazinone **7**. The same phenazinone **7** was obtained by reaction of [Ni(BPPD)$_2$] with silver triflate in acetone. Organic compounds phenazine **6**

and phenazinone **7** were isolated in pure form and thoroughly characterized by means of mass spectrometry, NMR, IR, UV-vis spectroscopies, elemental and X-ray analysis. ^{1}H, ^{19}F NMR spectroscopy together with X-ray analysis confirm that F13, H3 atoms in **6** and **7** are infected by the anisotropic effect of close lying C_6F_5-ring. Since phenazine/phenazinone derivatives possess numerous applications, further investigation of their physicochemical and physiological properties is promising.

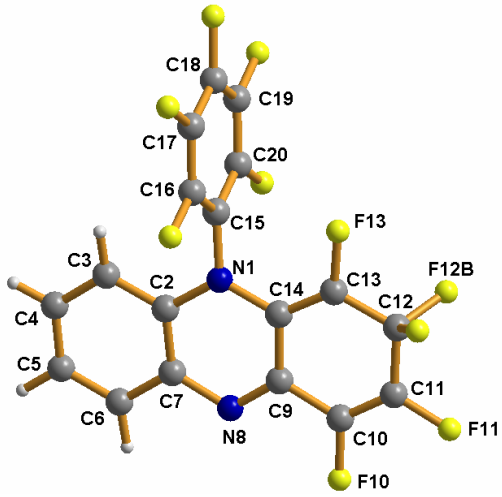

Figure 4. Molecular structure of phenazine derivative **6.**

Chapter III.

Diimine complexes with bulky fluorinated *N*-substituents $[Ni^{II}(^{F}DAD)_2]$ **8** and $[Co^{II}(^{F}DAD)_2]$ **9** (^{F}DAD – *N,N′*-bis(pentafluorophenyl)-2,3-dimethyl-1,4-diaza-1,3-butadiene) as well as diimine complexes with extended π-system $[Ni^{II}(^{F}BIAN)_2]$ **10** and $[Co^{I}(^{F}BIAN)_3]$ **11** (^{F}BIAN – bis[*N*-{3,5-bis(trifluoromethyl)phenyl}imino]acenaphthene) were synthesized. Compound **11** represents the first complex with three bis(imino)acenaphthene ligands synthesized so far, while **10** is the first late transition metal complex with two BIAN ligands.

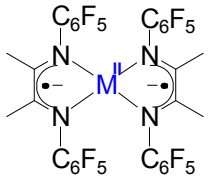

$[Ni^{II}(^{F}DAD)_2]$ **8**
$[Co^{II}(^{F}DAD)_2]$ **9**

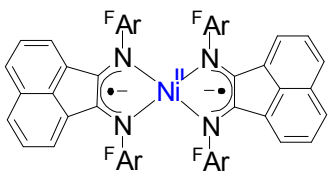

$[Ni^{II}(^{F}BIAN)_2]$ **10**

^{F}Ar = 3,5-$(CF_3)_2C_6H_3$

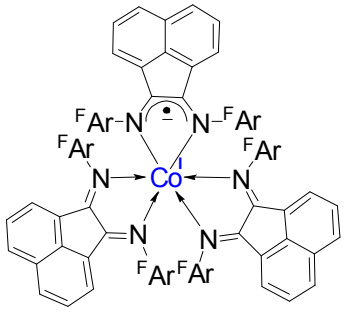

$[Co^{I}(^{F}BIAN)_3]$ **11**

Both diimines BIAN and DAD are non-innocent ligands and may exist in three redox states: neutral diimine L^0, π-radical anion L^{1-} and closed-shell dianion L^{2-}. The *physical (spectroscopic)* oxidation states of the ligands and the metals in complexes **8** – **11** were determined by single-crystal

X-ray diffraction studies at low temperatures (193 K). On the basis of bond length analysis complexes **8 – 10** comprise divalent metal ions Ni^{II} d^8 and Co^{II} d^7 with pairs of monoanionic π-radical ligands, whereas the unique complex **11** is best described as a cobalt(I) complex with two neutral $(^{F}BIAN)^0$ and one radical $(^{F}BIAN)^{1-}$ ligands.

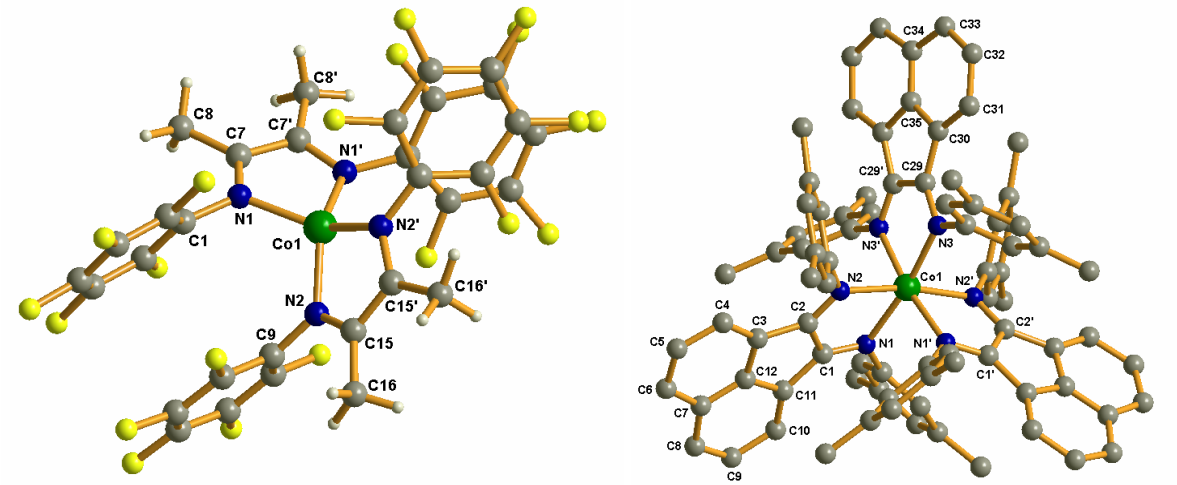

Figure 5. Molecular structures of $[Co^{II}(^{F}DAD)_2]$ **9** (left) and $[Co^{I}(^{F}BIAN)_3]$ **11** (right). Fluorine and hydrogen atoms in structure of **11** are omitted for clarity.

Electronic structures of the paramagnetic cobalt complexes **9** and **11** were investigated by SQUID measurements and X-band EPR spectroscopy. Both complexes possess a doublet ground state with electron density located mostly at the metal d-orbitals. The doublet–quartet energy gap of 159 cm^{-1} was established for **11** by fitting magnetic susceptibility data to a two magnetic center model with isotropic exchange interaction. The corresponding spin Hamiltonian is shown in Fig. 6.

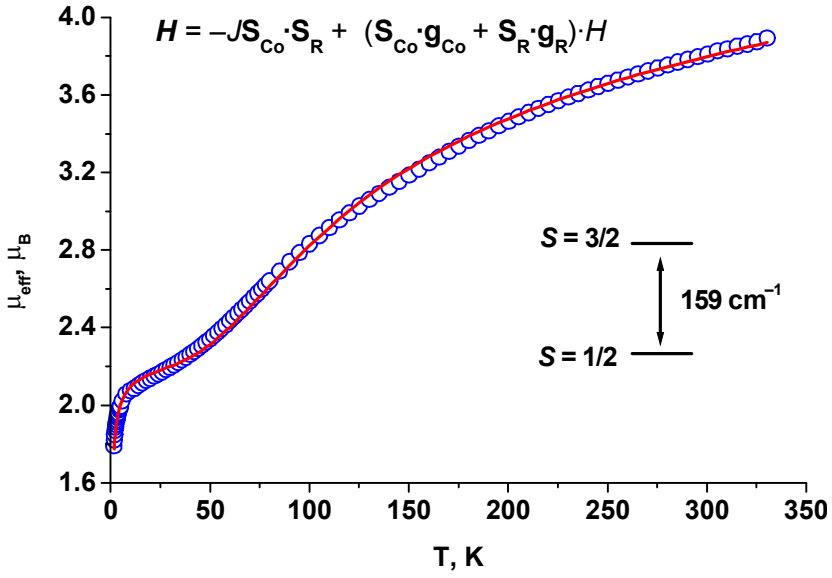

Figure 6. Temperature dependence of the effective magnetic moment of **11.**

EPR spectroscopy reveals that complex **11** undergoes partial dissociation in solution according to

$$[Co(BIAN)_3] \rightleftharpoons [Co(BIAN)_2] + BIAN$$

Electronic structures of $[Ni^{II}(^{F}DAD)_2]$ and $[Ni^{II}(^{F}BIAN)_2]$, as well as electronic structures of $[Ni(DAD)_2]$ complexes characterized previously by X-ray analysis were shown to consist of a divalent nickel d^8 ion and a pair of monoanionic radical ligands. Since the distorted tetrahedral geometry of these complexes imply a high-spin Ni^{II} (S_{Ni} = 1) center, observed diamagnetism is ascribed to antiferromagnetic intramolecular coupling of metal spins with spins of two π-radical ligands.

Chapter IV.

Four new complexes of iron and copper with bulky BIAN ligands were synthesized.

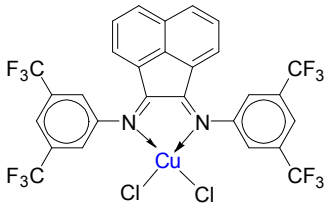

$[Cu^{II}(^{F}BIAN)Cl_2]$ **12**

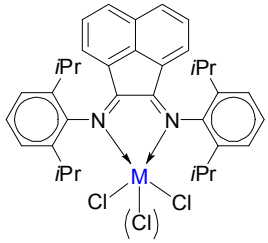

$[Cu^{II}(Dip\text{-}BIAN)Cl_2]$ **13**

$[Fe^{II}(Dip\text{-}BIAN)Cl_2]$ **14**

$[Fe^{III}(Dip\text{-}BIAN)Cl_3]$ **15**

Complexes **12** – **15** were thoroughly characterized by mass spectrometry, UV-vis, IR spectroscopies, and elemental analysis. The high-spin states of iron complexes $[Fe^{II}(Dip\text{-}BIAN)Cl_2]$ (S = 2) and $[Fe^{III}(Dip\text{-}BIAN)Cl_3]$ (S = 5/2) were established by means of magnetic susceptibility measurements in solution (Evans method). The crystal structure of $[Cu^{II}(Dip\text{-}BIAN)Cl_2]$ was determined. Hydrogen atoms of two chloroform molecules are in close H…Cl contact with two chlorine atoms of the complex in the cell, as shown in Figure 7.

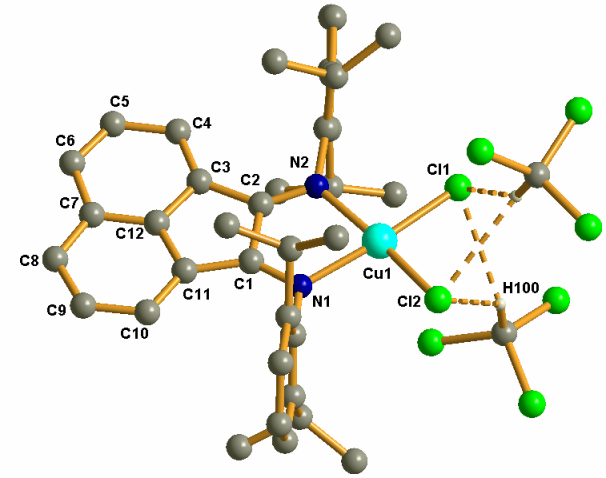

Figure 7. Molecular structure of **13** with two chloroform molecules. All hydrogen atoms except those of chloroform molecules are not shown.

The complexes, after activation with MAO, were tested in ethylene polymerization. The iron complexes **14** and **15** are able to polymerize ethylene with low (~3 kg PE/mol_{cat}·h·atm) activity, while copper complexes **12** and **13** are no catalysts for ethylene polymerization. Low activity of iron complexes **14** and **15** and inactivity of copper complexes **12** and **13** in ethylene polymerization is more likely due to electronic than steric reasons. None of active centers proposed for complexes **12** – **15** follows the "14 electrons rule" postulated by Gibson for highly active catalysts for polymerization of α-olefins.

Chapter V.

Three alkaline earth phthalocyanines [PcM] (M = Ca, Sr, Ba) **16** – **18** and two complexes with crown ethers [PcBa(18-CR-6)] **19** and [PcBa(DB18-CR-6)] **20** were synthesized. The latter two reveal improved solubility compared to the parent complex **18**.

Two routes are available for synthesis of **16**, namely, starting from metallic calcium or form water-free $CaCl_2$. In contrast, only the use of metallic strontium and barium resulted in formation of target complexes **17** and **18**, respectively. The use of chlorides of strontium and barium as starting materials did not lead to the metallophthalocyanines. This was ascribed to low solubility of $SrCl_2$ and $BaCl_2$ in the reaction medium – boiling 1-pentanol. The low concentration of Ba^{2+} and Sr^{2+} dications in alcoholic solution predominantly leads to the formation of metal-free PcH_2.

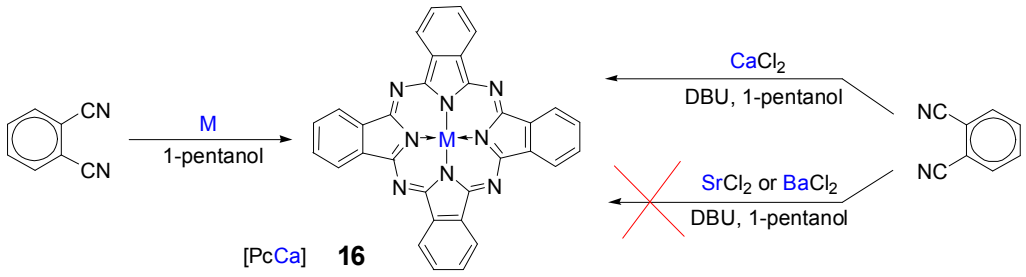

Although some references regarding [PcCa] and [PcBa] were found in the older literature, these complexes have never been prepared and characterized in pure form. In this work, all complexes **16** – **20** were thoroughly characterized by means of mass spectrometry, NMR, IR, UV-vis spectroscopies and elemental analysis. In the MALDI-TOF spectra of **16** – **18**, signals corresponding to $[PcM_2]^+$ ions were detected. This may point out to the formation of chain arrangement in crystal structures of these complexes.

Preliminary results on the investigation of the packing structure of **16**–**18** by single crystal X-ray crystallography reveal that two molecules of [PcBa] form a dimer subunit $[PcBa]_2$ in columnar stacked array. The double-deckers $[PcBa]_2$ being strictly aligned along *c* axis in the crystal do not form an infinite one-dimensional chain structure. Thus, the crystal packing of **18** is

best described as a "broken chain" shown in Figure 8. Further attempts to obtain the infinite chain structure by crystallization are tempting.

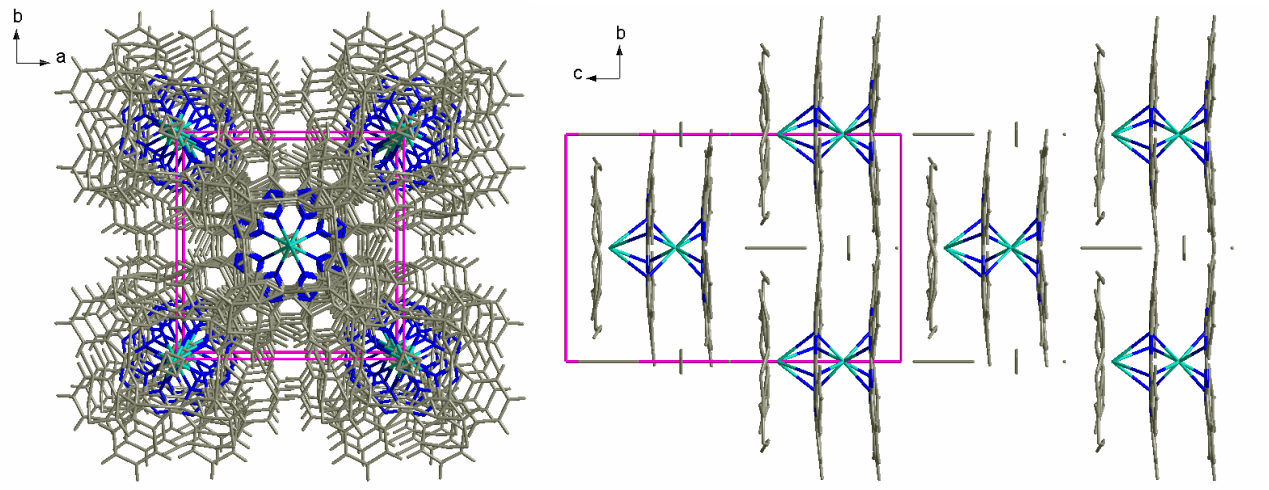

Figure 8. Crystal packing of **18** showing a "broken chain" arrangement of $[BaPc]_2$ subunits; disordered atoms of coordinated solvent molecules terminate as third coordination plane each columnar subunit.

Complexes **19** and **20** are 1:1 complexes of corresponding crown ether with phthalocyaninatobarium **18** as was judged by ^{1}H NMR spectroscopy. Double-decker (sandwich-like) structures are proposed for complexes **19** and **20**.

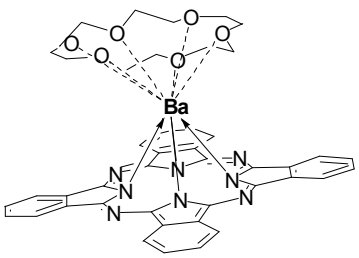

[PcBa(18-CR-6)] **19**

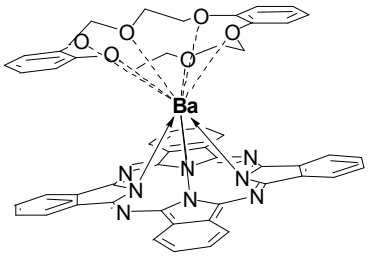

[PcBa(DB18-CR-6)] **20**

Further investigation of physicochemical properties of complexes **16** – **18** is promising in view of their potential in pseudo-one-dimensional semi-/conducting materials.

☙ Crystallographic Data ❧

All crystal structures reported in this work were determined by Dr. Klaus Harms (Marburg University).

[Ni^{II}(BPPD)$_2$] **1**·hexane

CCDC _

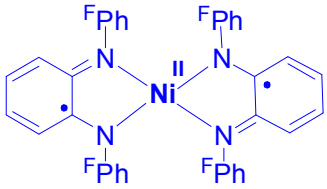

Identification code	mk01	
Habitus, color	irregular, dark (black green)	
Crystal size	0.22 x 0.15 x 0.14 mm^3	
Crystal system	Monoclinic	
Space group	C 2/c	Z = 8
Unit cell dimensions	a = 58.619(3) Å	α= 90°.
	b = 15.3293(6) Å	β= 97.288(3)°.
	c = 8.6322(4) Å	γ = 90°.
Volume	7694.1(6) $Å^3$	
Cell determination	35506 peaks with Theta 1.35 to 25.5°.	
Empirical formula	C_{42} H_{22} F_{20} N_4 Ni	
Formula weight	1021.35	
Density (calculated)	1.763 Mg/m^3	
Absorption coefficient	0.642 mm^{-1}	
F(000)	4080	

Data collection:

Diffractometer type	IPDS2
Wavelength	0.71073 Å
Temperature	193(2) K
Theta range for data collection	1.69 to 25.00°.
Index ranges	-69<=h<=69, -18<=k<=18, -10<=l<=10
Data collection software	STOE WinXpose (X-Area)
Cell refinement software	STOE WinCell (X-Area)
Data reduction software	STOE WinIntegrate (X-Area)

Solution and refinement:

Reflections collected	42127
Independent reflections	6752 [R(int) = 0.0911]
Completeness to theta = 25.00°	99.4 %
Observed reflections	4779[I>2sigma(I)]
Reflections used for refinement	6752
Absorption correction	Semi-empirical from equivalents
Max. and min. transmission	1.1395 and 0.8182
Largest diff. peak and hole	1.128 and -0.494 e.$Å^{-3}$
Solution	Direct methods
Refinement	Full-matrix least-squares on F^2
Treatment of hydrogen atoms	Calculated, fixed isotr. U'S
Programs used	SHELXS-97 (Sheldrick, 1997)
	SHELXL-97 (Sheldrick, 1997)
	WinGX, Diamond 2.1, STOE IPDS2 software
Data / restraints / parameters	6752 / 1 / 636
Goodness-of-fit on F^2	1.064
R index (all data)	wR2 = 0.1477
R index conventional [I>2sigma(I)]	R1 = 0.0576

[Pd^{II}(BPPD)$_2$] **2**·*4*(C_4H_8O)

CCDC _

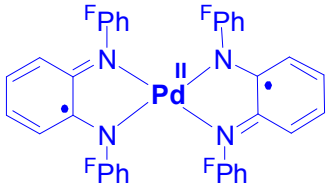

Identification code	mk2	
Habitus, color	trapeze, brownish	
Crystal size	0.27 x 0.15 x 0.02 mm^3	
Crystal system	Orthorhombic	
Space group	F d d d	Z = 8
Unit cell dimensions	a = 15.0923(14) Å	α= 90°.
	b = 19.2020(14) Å	β= 90°.
	c = 35.566(3) Å	γ = 90°.
Volume	10307.1(15) $Å^3$	
Cell determination	9087 peaks with Theta 2 to 26°.	
Empirical formula	C_{52} H_{40} F_{20} N_4 O_4 Pd	
Formula weight	1271.28	
Density (calculated)	1.638 Mg/m^3	
Absorption coefficient	0.483 mm^{-1}	
F(000)	5104	

Data collection:

Diffractometer type	IPDS2
Wavelength	0.71073 Å
Temperature	193(2) K
Theta range for data collection	1.81 to 24.99°.
Index ranges	-17<=h<=17, -20<=k<=21, -42<=l<=42
Data collection software	STOE WinXpose (X-Area)
Cell refinement software	STOE WinCell (X-Area)
Data reduction software	STOE WinIntegrate (X-Area)

Solution and refinement:

Reflections collected	16959
Independent reflections	2200 [R(int) = 0.1010]
Completeness to theta = 24.99°	96.5 %
Observed reflections	1643[I>2sigma(I)]
Reflections used for refinement	2200
Extinction coefficient	X = 0.00020(4)
Absorption correction	Semi-empirical from equivalents
Max. and min. transmission	1.1316 and 0.8581
Largest diff. peak and hole	0.635 and -0.927 $e.Å^{-3}$
Solution	Patterson (SHELXS-86)
Refinement	Full-matrix least-squares on F^2
Treatment of hydrogen atoms	Located, solvent-H's calculated
Programs used	SHELXS-86 (Sheldrick, 1986)
	SHELXL-97 (Sheldrick, 1997)
	SHELXTL, STOE IPDS2 software
Data / restraints / parameters	2200 / 0 / 193
Goodness-of-fit on F^2	1.005
R index (all data)	wR2 = 0.1189
R index conventional [I>2sigma(I)]	R1 = 0.0496

[Co(BPPD)$_2$] 3·*2*(C_4H_8O)

CCDC _

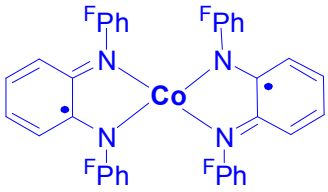

Identification code	co44a
Habitus, color	plate, dark
Crystal size	0.34 x 0.18 x 0.07 mm^3
Crystal system	Monoclinic
Space group	C 2/c Z = 8
Unit cell dimensions	a = 59.292(3) Å α= 90°.
	b = 15.3580(4) Å β= 97.952(9)°.
	c = 8.6688(3) Å γ = 90°.
Volume	7818.0(5) Å^3
Cell determination	33737 peaks with Theta 1.3 to 25°.
Empirical formula	C_{44} H_{24} Co F_{20} N_4 O_2
Formula weight	1079.60
Density (calculated)	1.834 Mg/m^3
Absorption coefficient	0.584 mm^{-1}
F(000)	4312

Data collection:

Diffractometer type	IPDS2
Wavelength	0.71069 Å
Temperature	193(2) K
Theta range for data collection	1.37 to 25.00°.
Index ranges	-70<=h<=70, -18<=k<=18, -9<=l<=10
Data collection software	STOE WinXpose (X-Area)
Cell refinement software	STOE WinCell (X-Area)
Data reduction software	STOE WinIntegrate (X-Area)

Solution and refinement:

Reflections collected	48100
Independent reflections	6888 [R(int) = 0.1086]
Completeness to theta = 25.00°	99.9 %
Observed reflections	4681[I>2sigma(I)]
Reflections used for refinement	6888
Extinction coefficient	X = 0.00084(10)
Absorption correction	None
Largest diff. peak and hole	0.481 and -0.409 e.Å^{-3}
Solution	Direct methods
Refinement	Full-matrix least-squares on F^2
Treatment of hydrogen atoms	Located, isotropic refinement
Programs used	SHELXS-97 (Sheldrick, 1997)
	SHELXL-97 (Sheldrick, 1997)
	Diamond 2.1, STOE IPDS2 software
	Platon
Data / restraints / parameters	6888 / 0 / 583
Goodness-of-fit on F^2	0.942
R index (all data)	wR2 = 0.1218
R index conventional [I>2sigma(I)]	R1 = 0.0454

[Cu^{II}(BPPD)$_2$] **4**·hexane

CCDC _

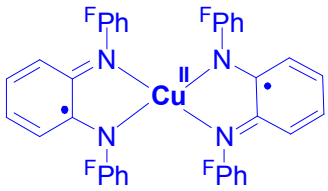

Identification code	khus01a	
Habitus, color	Plate, dark	
Crystal size	0.14 x 0.11 x 0.05 mm^3	
Crystal system	Monoclinic	
Space group	C 2/c	Z = 8
Unit cell dimensions	a = 59.219(3) Å	α= 90°.
	b = 15.3696(8) Å	β= 97.394(4)°.
	c = 8.5864(5) Å	γ = 90°.
Volume	7750.1(8) $Å^3$	
Cell determination	19977 peaks with Theta 1.5 to 24.9°.	
Empirical formula	C_{42} H_{22} Cu F_{20} N_4	
Formula weight	1026.18	
Density (calculated)	1.759 Mg/m^3	
Absorption coefficient	0.700 mm^{-1}	
F(000)	4088	

Data collection:

Diffractometer type	IPDS2
Wavelength	0.71073 Å
Temperature	193(2) K
Theta range for data collection	2.08 to 24.94°.
Index ranges	-69<=h<=70, -18<=k<=18, -10<=l<=10
Data collection software	STOE WinXpose (X-Area)
Cell refinement software	STOE WinCell (X-Area)
Data reduction software	STOE WinIntegrate (X-Area)

Solution and refinement:

Reflections collected	39191
Independent reflections	6754 [R(int) = 0.0697]
Completeness to theta = 24.94°	99.6 %
Observed reflections	4456[I>2sigma(I)]
Reflections used for refinement	6754
Absorption correction	None
Largest diff. peak and hole	0.339 and -0.440 $e.Å^{-3}$
Solution	Coordinates of the isostructural Ni compound
Refinement	Full-matrix least-squares on F^2
Treatment of hydrogen atoms	Calculated, fixed isotropic U's
Programs used	SHELXL-97 (Sheldrick, 1997)
	Diamond 2.1, STOE IPDS2 software
Data / restraints / parameters	6754 / 61 / 641
Goodness-of-fit on F^2	0.928
R index (all data)	wR2 = 0.0996
R index conventional [I>2sigma(I)]	R1 = 0.0398

[Fe^{III}(BPPD)$_2$] 5·(C_4H_8O)

CCDC _

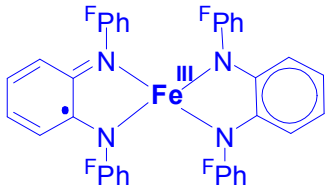

Identification code	mar170_2
Habitus, color	prism, dark
Crystal size	0.33 x 0.21 x 0.02 mm^3
Crystal system	Monoclinic
Space group	P $2_1/n$ Z = 4
Unit cell dimensions	a = 8.6433(11) Å α= 90°.
	b = 28.148(2) Å β= 92.910(9)°.
	c = 15.3298(18) Å γ = 90°.
Volume	3724.8(7) $Å^3$
Cell determination	12131 peaks with Theta 1.4 to 25°.
Empirical formula	C_{40} H_{18} F_{20} Fe N_4 O
Formula weight	1006.43
Density (calculated)	1.795 Mg/m^3
Absorption coefficient	0.548 mm^{-1}
F(000)	2000

Data collection:

Diffractometer type	IPDS2
Wavelength	0.71073 Å
Temperature	123(2) K
Theta range for data collection	1.45 to 23.00°.
Index ranges	-9<=h<=9, -30<=k<=28, -16<=l<=16
Data collection software	STOE WinXpose (X-Area)
Cell refinement software	STOE WinCell (X-Area)
Data reduction software	STOE WinIntegrate (X-Area)

Solution and refinement:

Reflections collected	32048
Independent reflections	5181 [R(int) = 0.1889]
Completeness to theta = 23.00°	99.9 %
Observed reflections	2937[I>2sigma(I)]
Reflections used for refinement	5181
Absorption correction	None
Largest diff. peak and hole	0.399 and -0.376 e.$Å^{-3}$
Solution	Direct methods
Refinement	Full-matrix least-squares on F^2
Treatment of hydrogen atoms	Calculated, fixed isotropic U's
Programs used	SIR2004 (Giacovazzo et al, 2004)
	SHELXL-97 (Sheldrick, 1997)
	Diamond 2.1, STOE IPDS2 software
Data / restraints / parameters	5181 / 0 / 597
Goodness-of-fit on F^2	0.990
R index (all data)	wR2 = 0.1283
R index conventional [I>2sigma(I)]	R1 = 0.0672

1,2,2,3,4-pentafluoro-10-(2,3,4,5,6-pentafluorophenyl)-2,10-dihydrophenazine 6

CCDC 278836

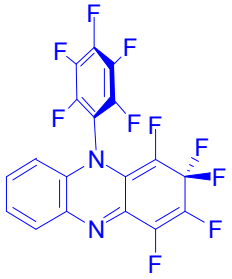

Identification code	mar143	
Habitus, color	prism, colorless	
Crystal size	0.27 x 0.15 x 0.03 mm^3	
Crystal system	Triclinic	
Space group	P -1	Z = 2
Unit cell dimensions	a = 7.3050(12) Å	α= 110.261(12)°.
	b = 9.8882(15) Å	β= 93.019(13)°.
	c = 11.6230(19) Å	γ = 90.223(13)°.
Volume	786.3(2) $Å^3$	
Cell determination	5281 peaks with Theta 1.4 to 26.2°.	
Empirical formula	C_{18} H_4 F_{10} N_2	
Formula weight	438.23	
Density (calculated)	1.851 Mg/m^3	
Absorption coefficient	0.194 mm^{-1}	
F(000)	432	

Data collection:

Diffractometer type	IPDS2
Wavelength	0.71073 Å
Temperature	293(2) K
Theta range for data collection	1.87 to 25.00°.
Index ranges	-8<=h<=8, -11<=k<=11, -13<=l<=13
Data collection software	STOE WinXpose (X-Area)
Cell refinement software	STOE WinCell (X-Area)
Data reduction software	STOE WinIntegrate (X-Area)

Solution and refinement:

Reflections collected	5372
Independent reflections	2619 [R(int) = 0.0221]
Completeness to theta = 25.00°	94.6 %
Observed reflections	1791[I>2sigma(I)]
Reflections used for refinement	2619
Extinction coefficient	X = 0.023(4)
Absorption correction	None
Largest diff. peak and hole	0.155 and -0.138 e.$Å^{-3}$
Solution	Direct methods
Refinement	Full-matrix least-squares on F^2
Treatment of hydrogen atoms	Located, isotropic refinement
Programs used	SIR-2002
	SHELXL-97 (Sheldrick, 1997)
	Diamond 2.1, STOE IPDS2 software
Data / restraints / parameters	2619 / 0 / 288
Goodness-of-fit on F^2	0.932
R index (all data)	wR2 = 0.0789
R index conventional [I>2sigma(I)]	R1 = 0.0305

1,3,4-trifluoro-10-(2,3,4,5,6-pentafluorophenyl)-2(10H)-phenazinone **7**· ½(C_7H_8)

CCDC 278837

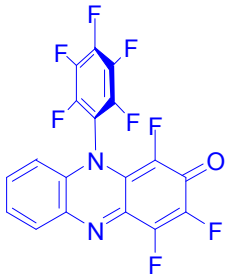

Identification code	mar155	
Habitus, color	prism, red	
Crystal size	0.30 x 0.21 x 0.02 mm^3	
Crystal system	Monoclinic	
Space group	C 2/c	Z = 8
Unit cell dimensions	a = 22.0360(18) Å	α= 90°.
	b = 7.3998(8) Å	β= 104.016(10)°.
	c = 23.335(2) Å	γ = 90°.
Volume	3691.8(6) $Å^3$	
Cell determination	10201 peaks with Theta 1.8 to 25°.	
Empirical formula	$C_{21.50}$ H_8 F_8 N_2 O	
Formula weight	462.30	
Density (calculated)	1.664 Mg/m^3	
Absorption coefficient	0.159 mm^{-1}	
F(000)	1848	

Data collection:

Diffractometer type	IPDS2
Wavelength	0.71073 Å
Temperature	193(2) K
Theta range for data collection	1.80 to 25.00°.
Index ranges	-26<=h<=26, -8<=k<=8, -27<=l<=27
Data collection software	STOE WinXpose (X-Area)
Cell refinement software	STOE WinCell (X-Area)
Data reduction software	STOE WinIntegrate (X-Area)

Solution and refinement:

Reflections collected	19404
Independent reflections	3249 [R(int) = 0.0701]
Completeness to theta = 25.00°	99.9 %
Observed reflections	1946[I>2sigma(I)]
Reflections used for refinement	3249
Extinction coefficient	X = 0.0004(2)
Absorption correction	Semi-empirical from equivalents
Max. and min. transmission	0.9794 and 0.9035
Largest diff. peak and hole	0.302 and -0.156 $e.Å^{-3}$
Solution	Direct methods
Refinement	Full-matrix least-squares on F^2
Treatment of hydrogen atoms	Located, isotropic refinement
Programs used	SHELXS-97 (Sheldrick, 1997)
	SHELXL-97 (Sheldrick, 1997)
	Diamond 2.1, STOE IPDS2 software
Data / restraints / parameters	3249 / 72 / 328
Goodness-of-fit on F^2	0.931
R index (all data)	wR2 = 0.1097
R index conventional [I>2sigma(I)]	R1 = 0.0444

[Ni^{II}(^{F}DAD)$_2$] 8·(C_7H_8)

CCDC 290299

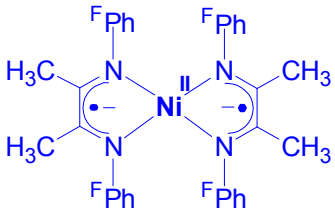

Identification code	mk93
Habitus, color	plate, dark red
Crystal size	0.45 x 0.12 x 0.06 mm^3
Crystal system	Orthorhombic
Space group	P b c n Z = 4
Unit cell dimensions	a = 20.0534(10) Å α= 90°.
	b = 12.9233(7) Å β= 90°.
	c = 14.2875(10) Å γ = 90°.
Volume	3702.7(4) $Å^3$
Cell determination	17148 peaks with Theta 1.8 to 26.2°.
Empirical formula	C_{39} H_{20} F_{20} N_4 Ni
Formula weight	983.30
Density (calculated)	1.764 Mg/m^3
Absorption coefficient	0.663 mm^{-1}
F(000)	1960

Data collection:

Diffractometer type	IPDS2
Wavelength	0.71073 Å
Temperature	193(2) K
Theta range for data collection	1.87 to 26.24°.
Index ranges	-24<=h<=24, -16<=k<=16, -17<=l<=17
Data collection software	STOE WinXpose (X-Area)
Cell refinement software	STOE WinCell (X-Area)
Data reduction software	STOE WinIntegrate (X-Area)

Solution and refinement:

Reflections collected	33387
Independent reflections	3719 [R(int) = 0.0505]
Completeness to theta = 25.00°	100.0 %
Observed reflections	2536[I>2sigma(I)]
Reflections used for refinement	3719
Extinction coefficient	X = 0.0010(2)
Absorption correction	Gaussian
Max. and min. transmission	0.9534 and 0.8047
Largest diff. peak and hole	0.304 and -0.190 $e.Å^{-3}$
Solution	Direct methods
Refinement	Full-matrix least-squares on F^2
Treatment of hydrogen atoms	Located, isotropic refinement
Programs used	SHELXS-97 (Sheldrick, 1997)
	SHELXL-97 (Sheldrick, 1997)
	Diamond 2.1, Stoe X-Area
Data / restraints / parameters	3719 / 0 / 328
Goodness-of-fit on F^2	0.896
R index (all data)	wR2 = 0.0810
R index conventional [I>2sigma(I)]	R1 = 0.0315

[Co^{II}(^{F}DAD)$_2$] 9·(C_7H_8)

CCDC 290300

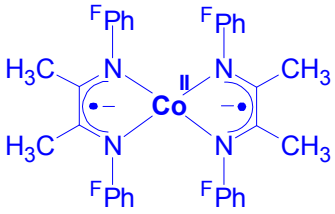

Identification code	co114
Habitus, color	needle, brown
Crystal size	0.28 x 0.06 x 0.04 mm^3
Crystal system	Orthorhombic
Space group	P b c n Z = 4
Unit cell dimensions	a = 20.077(2) Å α= 90°.
	b = 12.9232(14) Å β= 90°.
	c = 14.3559(12) Å γ = 90°.
Volume	3724.8(6) Å^3
Cell determination	7584 peaks with Theta 1.4 to 23.7°.
Empirical formula	C_{39} H_{20} Co F_{20} N_4
Formula weight	983.52
Density (calculated)	1.754 Mg/m^3
Absorption coefficient	0.599 mm^{-1}
F(000)	1956

Data collection:

Diffractometer type	IPDS2
Wavelength	0.71073 Å
Temperature	193(2) K
Theta range for data collection	1.87 to 26.26°.
Index ranges	-24<=h<=24, -16<=k<=15, -17<=l<=16
Data collection software	STOE WinXpose (X-Area)
Cell refinement software	STOE WinCell (X-Area)
Data reduction software	STOE WinIntegrate (X-Area)

Solution and refinement:

Reflections collected	28558
Independent reflections	3744 [R(int) = 0.1666]
Completeness to theta = 25.00°	100.0 %
Observed reflections	1825[I>2sigma(I)]
Reflections used for refinement	3744
Absorption correction	None
Largest diff. peak and hole	0.272 and -0.348 e.Å^{-3}
Solution	Direct methods
Refinement	Full-matrix least-squares on F^2
Treatment of hydrogen atoms	Calculated, riding
Programs used	Sir-92
	SHELXL-97 (Sheldrick, 1997)
	Diamond 2.1, STOE IPDS2 software
Data / restraints / parameters	3744 / 0 / 312
Goodness-of-fit on F^2	0.910
R index (all data)	wR2 = 0.0916
R index conventional [I>2sigma(I)]	R1 = 0.0527

$[Ni^{II}(^{F}BIAN)_2]$ 10

CCDC 290301

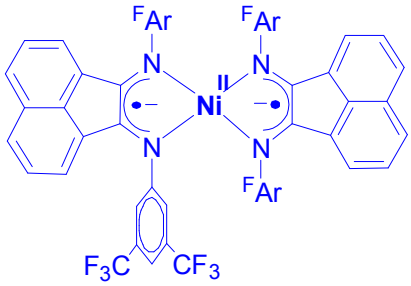

Identification code	mar_75	
Habitus, color	plate, dark	
Crystal size	0.28 x 0.27 x 0.05 mm^3	
Crystal system	Monoclinic	
Space group	C 1 2/c 1	Z = 4
Unit cell dimensions	a = 18.3645(19) Å	α= 90°.
	b = 18.1763(14) Å	β= 113.622(12)°.
	c = 16.7383(18) Å	γ = 90°.
Volume	5119.1(9) $Å^3$	
Cell determination	8000 peaks with Theta 1.7 to 26°.	
Empirical formula	C_{56} H_{24} F_{24} N_4 Ni	
Formula weight	1267.50	
Density (calculated)	1.645 Mg/m^3	
Absorption coefficient	0.511 mm^{-1}	
F(000)	2528	

Data collection:

Diffractometer type	IPDS1
Wavelength	0.71073 Å
Temperature	193(2) K
Theta range for data collection	1.65 to 26.01°.
Index ranges	-22<=h<=22, -22<=k<=22, -20<=l<=20
Data collection software	STOE Expose
Cell refinement software	STOE Cell
Data reduction software	STOE Integrate

Solution and refinement:

Reflections collected	25039
Independent reflections	4890 [R(int) = 0.0496]
Completeness to theta = 25.00°	98.1 %
Observed reflections	3355[I>2sigma(I)]
Reflections used for refinement	4890
Absorption correction	Gaussian
Max. and min. transmission	0.9673 and 0.8733
Largest diff. peak and hole	0.258 and -0.254 $e.Å^{-3}$
Solution	Direct methods
Refinement	Full-matrix least-squares on F^2
Treatment of hydrogen atoms	Riding on calculated positions
Programs used	SHELXS-97 (Sheldrick, 1997)
	SHELXL-97 (Sheldrick, 1997)
	Diamond 2.1, STOE IPDS1 software
Data / restraints / parameters	4890 / 204 / 544
Goodness-of-fit on F^2	0.876
R index (all data)	wR2 = 0.0714
R index conventional [I>2sigma(I)]	R1 = 0.0330

[Co^{I}(^{F}BIAN)$_3$] 11·*2*(C_7H_8)

CCDC 290302

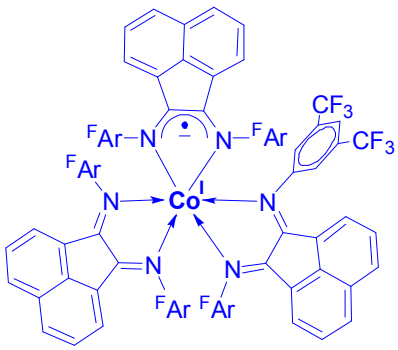

Identification code	mar144
Habitus, color	prism, dark
Crystal size	0.40 x 0.14 x 0.04 mm^3
Crystal system	Triclinic
Space group	C 2/c Z = 4
Unit cell dimensions	a = 28.843(2) Å α= 90°.
	b = 13.3691(9) Å β= 101.695(6)°.
	c = 23.2949(19) Å γ = 90°.
Volume	8796.3(11) Å^3
Cell determination	21722 peaks with Theta 1.4 to 25°.
Empirical formula	C_{98} H_{52} Co F_{36} N_6
Formula weight	2056.39
Density (calculated)	1.553 Mg/m^3
Absorption coefficient	0.325 mm^{-1}
F(000)	4132

Data collection:

Diffractometer type	IPDS2
Wavelength	0.71073 Å
Temperature	193(2) K
Theta range for data collection	1.44 to 26.20°.
Index ranges	-35<=h<=35, -16<=k<=16, -28<=l<=28
Data collection software	STOE WinXpose (X-Area)
Cell refinement software	STOE WinCell (X-Area)
Data reduction software	STOE WinIntegrate (X-Area)

Solution and refinement:

Reflections collected	62074
Independent reflections	8806 [R(int) = 0.1020]
Completeness to theta = 25.00°	100.0 %
Observed reflections	4840[I>2sigma(I)]
Reflections used for refinement	8806
Absorption correction	Semi-empirical from equivalents
Max. and min. transmission	0.9514 and 0.9103
Largest diff. peak and hole	0.516 and -0.379 e.Å^{-3}
Solution	Direct methods
Refinement	Full-matrix least-squares on F^2
Treatment of hydrogen atoms	Riding on calculated positions
Programs used	SHELXS-97 (Sheldrick, 1997)
	SHELXL-97 (Sheldrick, 1997)
	Diamond 2.1, STOE IPDS2 software
Data / restraints / parameters	8806 / 0 / 790
Goodness-of-fit on F^2	0.908
R index (all data)	wR2 = 0.1139
R index conventional [I>2sigma(I)]	R1 = 0.0507

[Cu^{II}(Dip-BIAN)Cl_2] 13·*4*($CHCl_3$)

CCDC _

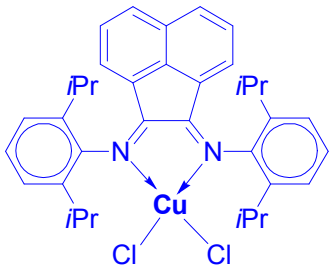

Identification code	mar193_2	
Habitus, color	prism, dark	
Crystal size	0.36 x 0.18 x 0.12 mm^3	
Crystal system	Orthorhombic	
Space group	P 2_1 2_1 2_1	Z = 4
Unit cell dimensions	a = 11.5571(5) Å	α= 90°.
	b = 20.1850(13) Å	β= 90°.
	c = 21.8028(10) Å	γ = 90°.
Volume	5086.2(5) $Å^3$	
Cell determination	0 peaks with Theta 0 to 0°.	
Empirical formula	C_{40} H_{44} Cl_{14} Cu N_2	
Formula weight	1112.61	
Density (calculated)	1.453 Mg/m^3	
Absorption coefficient	1.195 mm^{-1}	
F(000)	2260	

Data collection:

Diffractometer type	IPDS2
Wavelength	0.71073 Å
Temperature	173(2) K
Theta range for data collection	1.37 to 26.01°.
Index ranges	-12<=h<=14, -24<=k<=24, -26<=l<=26
Data collection software	STOE WinXpose (X-Area)
Cell refinement software	STOE WinCell (X-Area)
Data reduction software	STOE WinIntegrate (X-Area)

Solution and refinement:

Reflections collected	36081
Independent reflections	9892 [R(int) = 0.0387]
Completeness to theta = 25.00°	99.9 %
Observed reflections	8052[I>2sigma(I)]
Reflections used for refinement	9892
Absorption correction	Semi-empirical from equivalents
Max. and min. transmission	0.7881 and 0.7382
Flack parameter (absolute struct.)	0.116(12)
Largest diff. peak and hole	0.376 and -0.400 $e.Å^{-3}$
Solution	Direct methods
Refinement	Full-matrix least-squares on F^2
Treatment of hydrogen atoms	Calculated positions, riding
Programs used	SIR-92
	SHELXL-97 (Sheldrick, 1997)
	Diamond 3.1, STOE IPDS2 software
Data / restraints / parameters	9892 / 10 / 541
Goodness-of-fit on F^2	0.995
R index (all data)	wR2 = 0.0919
R index conventional [I>2sigma(I)]	R1 = 0.0378